

RIGA TECHNICAL UNIVERSITY
Faculty of Electrical and Environmental Engineering
Institute of Power Engineering

Ivars Zālītis

Doctoral Student of the Study Programme “Power Engineering”

**APPLICATION OF ESTIMATION OF MODEL
PARAMETERS FOR PROTECTIVE
AUTOMATION OF TRANSMISSION LINES**

Doctoral Thesis

Scientific supervisor
Associate Professor Dr. sc. ing.
ALEKSANDRS DOLGICERS

RTU Press
Riga 2020

Zālītis, I. Application of Estimation of Model Parameters for Protective Automation of Transmission Lines. Doctoral Thesis. Riga: RTU Press, 2020. 179 p.

Published in accordance with the decision of the Promotion Council “RTU P-05” of 16 July, 2020, Minutes No. 75/20.

This research has been supported by the Latvian Council of Science, project: Management and Operation of an Intelligent Power System (I-POWER) (No. lzp-2018/1-0066) and by National Research Programme project: Innovative Intelligent Network Technologies and their Optimization (INGRIDO). 2018 – 2021.

This research was funded by the Ministry of Economics of the Republic of Latvia, project “Trends, Challenges and Solutions of Latvian Gas Infrastructure Development (LAGAS)”, project No. VPP-EM-INFRA-2018/1-0003.

The logo for I-POWER, featuring the letters 'I-POWER' in a stylized, orange, blocky font.

ACKNOWLEDGEMENTS

The author wishes to express his gratitude to the scientific supervisor, Associate Professor of the Riga Technical University Institute of Power Engineering **Aleksandrs Dolgicers**, for his advice and support provided during the doctoral studies, and the Head of the Institute of Power Engineering, **Antans Saulus Sauhats**, for the encouragement to start doctoral studies.

Finally, a huge thanks to my family for their support and understanding during these years of doctoral studies and writing of the Thesis.

ABSTRACT

Transmission lines are indispensable part of power transmission system, which are highly exposed to fault risk factors of environmental and anthropogenic nature. Therefore, protection and control have to be robust and reliable as possible. Distance protection and some of fault location methods, used today for transmission lines, operate within a limited scope of available information that can result in errors and incorrect operation, especially when faults have high transient resistance.

In order to overcome these drawbacks of one-terminal-based distance protection and fault locations methods it is proposed to use a technique of estimation of unknown power system model parameters, solving these problems as an optimisation tasks. The scope of available information is extended by incorporation of all measurements, available from the controlled substation, thus eliminating necessity of long-distance communication networks, and by a separate stage of parameter estimation during the pre-fault regime, which is similar to estimation of fault parameters but operates with a nonlinear model reflecting the influence of governors. The Thesis provides modelling tools for both pre-fault and different fault regimes based on symmetrical component and topological modelling methods to accommodate the increased measurement scope. The proposed method was extensively tested considering two different strategies for selection of measured parameters used by the optimisation. The proposed method and its results is not limited to the fault location or distance protection, as the developed technique was also used to create a new method of an adaptive single-phase automatic reclosing algorithm.

The proposed method can be used as a base for creation of robust algorithms and devices for the fault location, distance protection and single-phase automatic reclosing. It can also be modified or directly implemented for different transmission line automation and protection problems. The modelling tools described in the Thesis can be used for a further analysis and development of relay protection and automation.

The Doctoral Thesis consists of an Introduction; 8 chapters; Conclusions; appendices; the Bibliography. The total number of pages is 179 including appendices. The Doctoral Thesis contains 25 tables; 85 figures; 75 equations; 163 cited sources of information; 3 appendices.

ANOTĀCIJA

Pārvades līnijas ir neatņemama pārvades tīkla sastāvdaļa, kura ir nemitīgi pakļauta antropogēnas un dabīgas izcelsmes bojājumu riska faktoriem. Līdz ar to pārvades līniju aizsardzībai un automātikai jābūt maksimāli robustai un drošai. Mūsdienās pārvades līnijām pielietotā distantaizsardzība un daļa no bojājuma vietas noteikšanas metodēm izmanto nepilnīgu mērījumu kopu, kas var novest pie to kļūdainas vai nekorektas darbības, ja bojājumam ir liela pārejas pretestība.

Minēto distantaizsardzības un bojājuma vietas noteicēju, kuri izmanto vienus mērījumus, trūkumu novēršanai piedāvāts pielietot modeļa parametru identifikāciju, realizējot šīs funkcijas ar optimizācijas palīdzību. Pieejamās informācijas apjoma palielinājums panākts izmantojot visus pieejamos mērījumus no kontrolētās apakšstacijas, tādā veidā izvairoties no tālsakaru tīklu nepieciešamības, un otru parametru identifikācijas posmu pirmsavārijas režīma laikā, kas ir līdzīgs bojājuma režīma parametru identifikācijas posmam, bet izmanto nelineāru tīkla modeli, lai ievērotu regulatoru ietekmi. Disertācijā aprakstīti arī uz simetrisko sastāvdaļu un topoloģiskās modelēšanas metodēm balstīti pirmsavārijas un avārijas režīmu modelēšanas paņēmieni, kas dod iespēju izmantot paplašināto mērījumu kopu. Piedāvātā metode tika plaši testēta dažādos scenārijos, vienlaikus salīdzinot divas dažādas optimizācijā izmantoto mērījumu izvēles stratēģijas. Darbā piedāvāto metodi un tās rezultātus iespējams izmantot arī citām aizsardzības un automātikas funkcijām, kā tas parādīts, izstrādājot adaptīvu vienfāzes automātiskās atkalieslēgšanas algoritmu.

Piedāvāto metodi var izmantot, izstrādājot robustus bojājuma vietas noteikšanas, distantaizsardzības un vienfāzes automātiskās atkalieslēgšanas algoritmus un ierīces. Šo metodi iespējams arī tālāk modificēt vai tiešā veidā pielietot citu pārvades līniju automātikas un aizsardzības funkciju attīstīšanai. Papildus dotie modelēšanas paņēmieni izmantojami esošo relejaizsardzības un automātikas metožu analīzei un pilnveidei.

Promocijas darbā ir ievads, astoņas nodaļas, secinājumi, pielikumi un informācijas avotu saraksts ar kopējo apjomu 179 lappuse. Promocijas darbs satur 25 tabulas, 85 attēlus, 75 vienādojumus, 163 informācijas avotus un trīs pielikumus.

TABLE OF CONTENTS

LIST OF ABBREVIATIONS.....	8
INTRODUCTION.....	9
1. FAULT LOCATION, DISTANCE PROTECTION AND ADAPTIVE AUTOMATIC RECLOSING AS PARTS OF THE POWER SYSTEM CONTROL	15
1.1. Mathematical statement of the protective automation problem	15
1.2. Fault location, distance protection and automatic reclosing functions.....	19
1.3. The general approach of the proposed method.....	21
1.4. Conclusions	22
2. TECHNICAL BACKGROUND OF FAULT LOCATION, DISTANCE PROTECTION AND ADAPTIVE AUTOMATIC RECLOSING METHODS.....	23
2.1. Existing fault location methods	23
2.2. Existing distance protection methods.....	30
2.3. Existing adaptive single-pole automatic reclosing methods	45
2.4. Conclusions	46
3. MODELLING OF ASYMMETRICAL REGIMES OF A POWER SYSTEM.....	48
3.1. A single transverse asymmetry.....	48
3.2. A single longitudinal asymmetry.....	54
3.3. Multiple simultaneous asymmetries	59
3.4. Conclusions	67
4. APPLICATIONS OF TOPOLOGICAL METHODS FOR MODELLING OF POWER SYSTEM REGIMES.....	68
4.1. Nodal potential method in matrix form	68
4.2. Modelling of steady-state fault regimes	69
4.3. Modelling of steady-state pre-fault regimes.....	70
4.4. Modelling of transient regimes using a numerical inverse Laplace transform	71
4.5. Modern distance protection terminal under scrutiny – testing experience.....	75
4.6. Conclusions	82
5. APPLICATION OF THE ESTIMATION OF POWER SYSTEM MODEL PARAMETERS FOR FAULT LOCATION AND DISTANCE PROTECTION	83
5.1. The framework of the model parameter estimation method	83
5.2. Modified randomised search initially tested for estimation of model parameters	85

5.3. Modified genetic algorithm applied for estimation of model parameters	92
5.4. Conclusions	99
6. SYNTHESIS OF OPTIMAL OBJECTIVE FUNCTION FOR ESTIMATION OF MODEL PARAMETERS	100
6.1. Fault parameter selection strategies.....	101
6.2. Development of future strategies of parameter-selection-based analysis of objective function	103
6.3. Conclusions	108
7. TESTING OF THE PROPOSED PARAMETER ESTIMATION METHOD AND PARAMETER SELECTION STRATEGIES	109
7.1. The power system used for the case studies	109
7.2. Results of parameter selection.....	111
7.3. Testing results for the proposed method	121
7.4. Conclusions	132
8. APPLICATION OF THE MODEL PARAMETER ESTIMATION AND TOPOLOGICAL MODELLING APPROACH FOR THE DEVELOPMENT OF AN ADAPTIVE SINGLE-POLE AUTOMATIC RECLOSING	133
8.1. Modelling of high-voltage transmission line in phase coordinates	133
8.2. Dynamic arc model used for development and testing of the adaptive automatic reclosing method	139
8.3. The proposed adaptive single pole automatic reclosing method.....	143
8.4. Testing of the proposed adaptive automatic reclosing method	147
8.5. Conclusions	152
CONCLUSIONS.....	154
APPENDICES	157
REFERENCES	168

LIST OF ABBREVIATIONS

Sequence number	Abbreviation	Explanation
1.	HV	High-Voltage
2.	L-E	Phase-to-Earth
3.	DP	Distance Protection
4.	FL	Fault Location
5.	CB	Circuit Breaker
6.	EHV	Extra-High-Voltage
7.	ZS	Zero-Sequence
8.	AR	Automatic Reclosing
9.	ASPAR	Adaptive Single-Pole Automatic Reclosing
10.	GA	Genetic Algorithm
11.	SPAR	Single-Pole Automatic Reclosing
12.	OHTL	Overhead Transmission Line
13.	EMF	Electromotive Force
14.	FI	Fault Indicator
15.	CT	Current Transformer
16.	TW	Travelling Wave
17.	DC	Direct Current
18.	HVDC	High-Voltage Direct Current
19.	AC	Alternating Current
20.	GPS	Global Positioning System
21.	ANN	Artificial Neural Network
22.	PS	Positive-Sequence
23.	NS	Negative-Sequence
24.	PMU	Phasor Measurement Unit
25.	DFT	Discrete Fourier Transform
26.	ANN	Artificial Neural Networks
27.	L-L	Phase-to-Phase
28.	VT	Voltage Transformer
29.	FD	Fault Detector
30.	L-L-E	Phase-to-Phase-to-Earth
31.	SCADA	Supervisory Control and Data Acquisition
32.	RMS	Root Mean Square

Note: Throughout the Thesis superscript indexes (1, 2, 0) right after an electric parameter (voltage, current, apparent power, impedance, capacitance etc.) denote positive-, negative- and zero-sequence quantities, if not specified otherwise.

INTRODUCTION

The topicality of the subject of the Doctoral Thesis

Transmission lines are highly exposed to fault risk factors of environmental and anthropogenic nature. The fault statistics [1] confirm this as between 60 % and 70 % of faults in the high-voltage (hereafter – HV) grids of the Baltic region were transmission line faults. It can also be seen that on average 60.2 % and 67.6 % of these are phase-to-earth (hereafter – L-E) faults for 100–150 kV and 220–330 kV lines, respectively, in the Baltic region. These faults are known to result in poor performance of many of the existing distance protection (hereafter – DP) and fault location (hereafter – FL) algorithms that use the measurement data of only one terminal. This is due to the presence of the fault path resistance and fault current infeed from the other end of the line as well as the simplifications used for the model of the power system. One solution to this problem is application of communication networks between the substations. This allows implementing fast and accurate algorithms but they often require precise synchronisation of the measurement data. Additionally, there is a risk of loss of communication due to the damage caused by the fault or for other reasons. Considering the above, it remains desirable to develop a method that could accurately determine the fault distance if the scope of information on the faulted line is limited to data available at the “own” substation, at least as a backup measure to communication-related methods.

The fault statistics [1] also show that on average only 19.8 % and 29.5 % of the transmission line faults are permanent faults for 100–150 kV and 220–330 kV lines, respectively, in the Baltic region. Thus, in most cases, a transmission line can be successfully re-energised for operation after the deionisation of an electric arc channel at the fault point. As most of the faults involve one phase, it is usually possible to disconnect and reconnect only the faulted phase if separate control of the phase circuit breakers (hereafter – CB) is available. This is beneficial, as power transmission is retained via the healthy phases, resulting in less impact on the dynamic stability of the power system during the isolation of the fault and the reclosing procedure, especially in HV and extra-high-voltage (hereafter – EHV) networks. Often a conventional application of a fixed time setting determined based on the maximum possible arc deionisation time is still used. The use of a fixed time setting can result in a larger impact on the system stability and a longer flow of undesirable zero-sequence (hereafter – ZS) current in power transformer neutral line if the arc extinction is rapid. Therefore, it can be useful to obtain an adaptive automatic reclosing (hereafter – AR) method.

The hypothesis of the Doctoral Thesis

One-terminal-measurement-based approaches of FL and DP prove unreliable when a fault has a high fault path resistance and the network topology is more complicated; such an approach can be replaced by a technique based on the estimation of unknown power system model parameters, solving the problem as an optimisation task with the aim to achieve independence from large-distance communication networks and better performance compared with existing methods using one-terminal measurements. It is beneficial to divide this task into the estimation of pre-fault and fault regime parameters to decrease the number of

unknown parameters for each particular stage. This method or its results can be used for other power system automation tasks.

The aim of the Doctoral Thesis

The aim of the doctoral thesis is to develop a novel method of two-stage estimation of unknown power system model parameters and lay the foundation for the solution of FL, DP, adaptive AR and similar problems via optimisation procedures, thus increasing the reliability and robustness of the power system.

The tasks of the Doctoral Thesis

In order to achieve the aim of the doctoral thesis, the following tasks have been set.

1. Investigation of the performance of existing fault location, distance protection and adaptive automatic reclosing methods and devices.
2. Description and development of modelling tools for pre-fault and fault regimes of the power system necessary for the implementation of the model parameter estimation method.
3. Creation of a framework for two-stage estimation of unknown power system model parameters.
4. Implementation of the created framework with optimisation tools for fault location and distance protection.
5. Investigation of the objective function of the optimisation and synthesis of an optimal objective function.
6. Testing of the developed fault location and distance protection algorithms and comparison with existing methods.
7. Development of an adaptive single-pole automatic reclosing algorithm, using the described modelling tools and the proposed model parameter estimation method.

Methods and tools of research

The results presented in the Thesis were obtained by applying the following methods and tools.

1. Topological power system modelling methods.
2. The nodal potential (admittance) and the Gauss-Seidel method.
3. The symmetrical component method.
4. The model parameter estimation method.
5. The genetic algorithm.
6. Computations, simulations and data processing in MATLAB©, MATLAB SimPowerSystems©.
7. ISA DRTS 64 signal generator using waveform playback from COMTRADE files of ISA TDMS 7.0.4©.
8. High-voltage 110–220 kV transmission line protection terminal REDI.
9. Smoky, a program for reading fault recordings.

The scientific novelty of the Doctoral Thesis

1. A novel numerical method of topological modelling of multiple simultaneous asymmetrical power system faults.
2. A novel method of hybrid (symmetrical components and per-phase integration) topological modelling of a high-voltage line.
3. Two-stage optimisation based estimation of unknown model parameters and its implementation for fault location, distance protection and adaptive automatic reclosing.
4. Development of parameter selection strategies for the synthesis of an optimal objective function used by the proposed parameter estimation method.
5. Application of numerical inversion of the Laplace transform in conjunction with topological network analysis.
6. The technique of mixed virtual/real testing of a distance protection terminal in cases of faults with a nonstationary fault path resistance such as faults caused by fallen trees.

The practical significance of the Doctoral Thesis

1. The proposed modelling methods can be used for future analysis and development of relay protection and automation.
2. The proposed method can be used as a basis for the development of highly-robust fault location and distance protection devices that are immune to fault path resistance and capable to operate without data communication.
3. The developed adaptive automatic reclosing algorithm can be implemented into a corresponding device, which would offer a significant contribution to system stability.

The personal contribution of the author to the research performed

The modelling methods for power system stationary and transient regimes as well as the framework for the model parameter estimation method were developed under the supervision of Associate Professor Aleksandrs Dolgicers. The literature analysis, modelling implementations into program codes, simulation and testing results, applications of the proposed method for the fault location, distance protection and adaptive single-pole automatic reclosing and the Conclusions belong personally to the author.

Volume and structure of the Doctoral Thesis

The Doctoral Thesis is written in English. It comprises an introduction, 8 chapters with 34 sections, conclusions and a list of references with 163 cited sources of information. The Thesis contains 75 equations, 25 tables, 85 figures and 3 appendices. The total volume of the Thesis is 181 pages including appendices.

The first chapter describes interaction of external factors and control systems with the power system as a controlled object. The role of modelling and optimisation in power system control is also indicated. Next, simplifications used for control systems and the proposed method are discussed and descriptions of power system control subtasks of FL, DP and AR are given. Finally, description of an application of the proposed method for FL is introduced.

The second chapter provides extensive technical background of FL and DP methods and devices as well as technical background of adaptive single-pole automatic reclosing (hereafter – ASPAR).

The third chapter describes general principles of modelling of stationary asymmetrical power system faults including both shunt and series (usually short circuits and open phase) faults according to the method of symmetrical components. The most commonly used complex equivalent circuits for these faults are also presented. Additionally, descriptions of two numerical calculation methods for multiple stationary simultaneous asymmetric faults are given.

The fourth chapter is dedicated to mathematical methods suitable for the calculation of stationary pre-fault and fault regime state parameters on the basis of topological modelling, particularly the nodal potential (admittance) method in conjunction with the Gauss-Seidel method as a numerical solver. A numerical inverse Laplace transform in combination with topological analysis of the power system is also presented for calculation of the free component of transient current and voltage waveforms or for use in control systems with models in Laplace space. Additionally, the results of the testing of an existing DP terminal using a virtual-real laboratory for faults with nonstationary fault path resistance are presented.

The fifth chapter includes a general framework of the proposed model parameter estimation method. Next, the general framework in combination with different optimisation tools is implemented for FL and DP. The chapter also presents some of the results obtained by the initially used modified randomised search as the optimisation core.

The sixth chapter presents the possible parameter selection strategies as a means to obtain an optimal objective function for the model parameter estimation method. In-depth analysis of objective function surfaces created by single parameters and the principles of their interaction that should minimise the presence of false extrema are presented.

The seventh chapter is dedicated to the testing of the performance of the implementation of the proposed method with the genetic algorithm (hereafter – GA) for FL. After a description of the case study network, parameter groups obtained by the conservative and opportunistic strategies described in Chapter 6 are presented. Chapter 7 also shows the effects of using different parameter group sizes and selection strategies on the surfaces of the objective function. Then, the results and analysis of an extensive testing of the FL using the proposed method and a comparison with existing one-terminal- and two-terminal-measurement-based FL methods are given.

The eighth chapter demonstrates an approach to detailed modelling of a transmission line during the dead time of single-pole automatic reclosing (hereafter – SPAR). The described approach is used to analyse the changes of line-side faulted phase voltage during the dead time for various fault distances and equivalent fault path resistances. Next, dynamic arc models are implemented to represent the nonlinear character of both the primary and secondary arc and the elongation as well as the extinction of the fault secondary arc. Based on the analysis of both steady-state and dynamic simulation results, an ASPAR algorithm with a dedicated logic block was developed and tested in scenarios of transient faults with different fault arc elongation speeds and permanent faults.

Finally, the main results of the thesis are summarised in Conclusions.

The approbation of the Doctoral Thesis

The results of the research have been presented at international scientific conferences in Latvia and abroad.

1. The 4th Workshop on Advances in Information, Electronic and Electrical Engineering (AIEEE'2016), Vilnius, Lithuania, 10–12 November 2016.
2. 2017 17th IEEE International Conference on Environment and Electrical Engineering and 2017 IEEE Industrial and Commercial Power System Europe (EEEIC / I&CPS Europe), Milan, Italy, 6–9 June 2017.
3. 12th IEEE PES Powertech Conference Towards and Beyond Sustainable Energy Systems, Manchester, United Kingdom, 18–22 June 2017.
4. 2017 IEEE 58th International Scientific Conference on Power and Electrical Engineering of Riga Technical University (RTUCON 2017), Riga, Latvia, 12–13 October 2017.
5. The 5th Workshop on Advances in Information, Electronic and Electrical Engineering (AIEEE'2017), Riga, Latvia, 24–25 November 2017.
6. The 6th IEEE Workshop on Advances in Information, Electronic and Electrical Engineering (AIEEE'2018), Vilnius, Lithuania, 8–10 November 2018.

The results of the research have been published in the proceedings of scientific conferences and a scientific journal.

1. A. Dolgicers, **I. Zalitis**, and J. Kozadajevs. The Modified Seidel Method as a Tool for the Evaluation of the Stability of a Power System. In: *2016 IEEE 4th Workshop on Advances in Information, Electronic and Electrical Engineering (AIEEE'2016)*, Vilnius, Lithuania, 10–12 November 2016. Piscataway: IEEE, 2017, pp. 27–33, ISBN: 978-1-5090-4474-0. Available from: DOI: 10.1109/AIEEE.2016.7821806.
2. **I. Zalitis**, A. Dolgicers, and J. Kozadajevs. A power transmission line fault locator based on the estimation of system model parameters. In: *Proceedings 2017 IEEE International Conference on Environment and Electrical Engineering*, Milan, Italy, 6–9 June 2017. Piscataway: IEEE, 2017, pp. 1–6, ISBN: 978-1-5386-3918-4. Available from: DOI: 10.1109/EEEIC.2017.7977459.
3. **I. Zalitis**, A. Dolgicers, and J. Kozadajevs. A distance protection based on the estimation of system model parameters. In: *Proceedings 2017 IEEE Manchester PowerTech*, Manchester, UK, 18–22 June 2017. Piscataway: IEEE, 2017, pp. 1–6, ISBN: 978-1-5090-4238-8. Available from: DOI: 10.1109/PTC.2017.7981277.
4. A. Dolgicers and **I. Zalitis**. Numerical calculation method for symmetrical component analysis of multiple simultaneous asymmetrical faults. In: *Proceedings 2017 IEEE 58th International Scientific Conference on Power and Electrical Engineering of Riga Technical University*, Riga, Latvia, 12–13 October 2017. Piscataway: IEEE, 2017, pp. 1–7, ISBN: 978-1-5386-3847-7. Available from: DOI: 10.1109/RTUCON.2017.8124748.
5. **I. Zalitis**, A. Dolgicers, and J. Kozadajevs. Experimental testing of distance protection performance in transient fault path resistance environment. In: *Proceedings 2017 5th IEEE Workshop on Advances in Information, Electronic and Electrical Engineering*, Riga, Latvia, 24–25 November 2017. Piscataway: IEEE, 2018, pp. 1–6, ISBN: 978-1-5386-4138-5. Available from: DOI: 10.1109/AIEEE.2017.8270526.

6. **I. Zalitis**, A. Dolgicers, and J. Kozadajevs. Influence Analysis of Mutual Coupling Effects between a High-Voltage Transmission Line and a Fiber-optic Cable with a Conductive Support Element. In: *2018 IEEE 6th Workshop on Advances in Information, Electronic and Electrical Engineering (AIEEE'2018)*, Vilnius, Lithuania, 8–10 November 2018. Piscataway: IEEE, 2018, pp. 1–7, ISBN: 978-1-7281-2000-3. Available from: DOI: 10.1109/AIEEE.2018.8592447.
7. **I. Zalitis**, A. Dolgicers, and J. Kozadajevs. An adaptive single-pole automatic reclosing method for uncompensated high-voltage transmission lines. *Electric Power Systems Research*, vol. 166, pp. 210–222, Jan. 2019. ISSN: 0378-7796. Available from: <https://doi.org/10.1016/j.epsr.2018.10.012>.

One patent has been obtained.

1. Riga Technical University. *Transmission line single-phase-to-ground fault locator method*. A. Dolgicers, **I. Zalitis** and J. Kozadajevs (inventors). Int. Cl.: H02H7/26. LV Patent 15207, issued May 20, 2017. 20 p. Available from: https://worldwide.espacenet.com/publicationDetails/originalDocument?FT=D&date=20170520&DB=&locale=en_EP&CC=LV&NR=15207B&KC=B&ND=4#.

1. FAULT LOCATION, DISTANCE PROTECTION AND ADAPTIVE AUTOMATIC RECLOSING AS PARTS OF THE POWER SYSTEM CONTROL

Automation is widely used in the modern world starting from everyday household appliances to large power systems. This is especially important for the protection and automation of power system elements that sometimes have to operate in a fraction of a second, exceeding human reaction time, such as transmission line protection. Most of these power system automation and protection devices can be described by considering a more general problem – power system control.

1.1. Mathematical statement of the protective automation problem

Power system operation is affected by parameters of the systems elements $P(t)$, such as electrical impedances and admittances, external known or observable parameters $X(t)$, such as electricity price and ambient temperature, external unknown and only partially predictable stochastic parameters $S(t)$, such as faults of the power system elements and random changes in loading of the power system and control processes and actions $C(t)$, such as disconnection of the power system elements, regulation of transformer or generator voltage etc. These processes and parameters of the power system determine the values of controlled state parameters $Y(t)$, such as node voltages, branch currents, active and reactive powers and frequency. Both known or observed parameters $X(t)$ and controlled parameters $Y(t)$ are determined with some degree of errors $\varepsilon(t)$. Based on the available measurements ($X(t)$ and $Y(t)$) and system parameters $P(t)$, a control system has to perform control operations $C(t)$, which ensure optimal operation of the power system, adherence to imposed limitations of controlled parameters $Y(t)$, and provide necessary information $I(t)$ about the power system, such as system loading level, warnings, fault type and fault distance indications etc. to the personnel [2]. The described interactions between external factors, the power system and the control system can be depicted in a generalised closed loop control system [3]–[6] (Fig. 1.1).

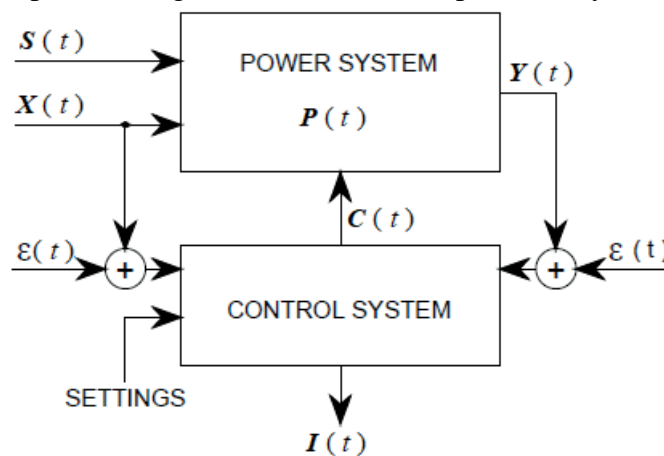


Fig. 1.1. Generalised closed-loop system for control of the power system.

Considering that the control system has to ensure optimal operation of the power system it also has to directly and/or indirectly maximise or minimise some kind of an objective function *OBF*, such as energy losses in the power system or profit of the power system operator [7]. This optimisation taking into account limitations of controlled parameters $\mathbf{Y}(t)$ can be defined as follows:

$$\mathbf{C}(t) \rightarrow \min(OBF) \text{ or } \max(OBF), \quad (1.1)$$

where

$$OBF = f(\mathbf{X}(t), \mathbf{S}(t), \mathbf{Y}(t), \mathbf{P}(t)), \quad (1.2)$$

with limitations

$$\mathbf{Y}_{\min i} \leq \mathbf{Y}_i \leq \mathbf{Y}_{\max i}, i = 1, \dots, n, \quad (1.3)$$

where \mathbf{Y}_i – i -th element from vector of controlled parameters and processes;

$\mathbf{Y}_{\min i}$ and $\mathbf{Y}_{\max i}$ – the minimum and maximum permissible values of \mathbf{Y}_i ;

n – is the number of controlled parameters.

As control operations $\mathbf{C}(t)$ may possibly lead to changes in $\mathbf{Y}(t)$, such that limits (1.3) are not met because these changes are observed with time delay due to electromechanical, electromagnetic inertia of the power system and observation errors $\varepsilon(t)$ it is advisable, in addition to limitations of $\mathbf{Y}(t)$, impose direct limitations on control operations:

$$\mathbf{C}_{\min i} \leq \mathbf{C}_i \leq \mathbf{C}_{\max i}, i = 1, \dots, m, \quad (1.4)$$

where \mathbf{C}_i – i -th element from vector of possible control operations;

$\mathbf{C}_{\min i}$ and $\mathbf{C}_{\max i}$ – the minimum and maximum permissible quantities of regulation or other control actions, m is the number of elements in the control operation vector $\mathbf{C}(t)$.

Some of the control system subtasks can be solved using statistical analysis, pattern recognition algorithms or expert systems such as prediction of system loads or determination of the fault type, but most of automation and protection systems directly or indirectly utilises models of the power system and/or its parts. Some of these systems issue control actions $\mathbf{C}(t)$ based on logic that only tests if measured parameters $\mathbf{X}(t)$ and/or $\mathbf{Y}(t)$ are within pre-defined limitations, which are input as settings (Fig. 1.1). Usually this applies to systems with high-speed operation requirement for example: relay protection. Settings are determined using the power system model, which simultaneously works as an a priori optimisation achieving the optimal operation overall. However, when operation time is less restricted or the a priori optimisation is not possible, the control system often incorporates a model of the power system in order to perform the optimisation online. Such systems can either have some general definition of the optimal operation condition integrated within the optimisation itself, such as minimum total energy losses, or use pre-defined desired values of the controlled parameters $\mathbf{Y}_D(t)$ input by user, which the optimisation has to achieve by synthesis of optimal control operations $\mathbf{C}(t)$. This involves minimisation of difference between model output $\mathbf{Y}_M(t)$ and the desired values of controlled parameters $\mathbf{Y}_D(t)$:

$$\Delta = \mathbf{Y}_D - \mathbf{Y}_M, \quad (1.5)$$

where Δ – a vector of differences between the desired and modeled values of controlled parameters;

Y_D – a vector of desired values of the controlled parameters;

Y_M – a vector of model outputs corresponding to Y_D .

In this case additional logic block might be necessary to transform the control operations implemented for the model $C'(t)$ to their equivalents necessary for the real power system $C(t)$. Such control systems can be further improved by adding additional feedback loop that updates the power system model parameters $P'(t)$ if the control actions taken resulted in controlled parameters $Y(t)$ different from the desired ones $Y_D(t)$ (Fig. 1.2).

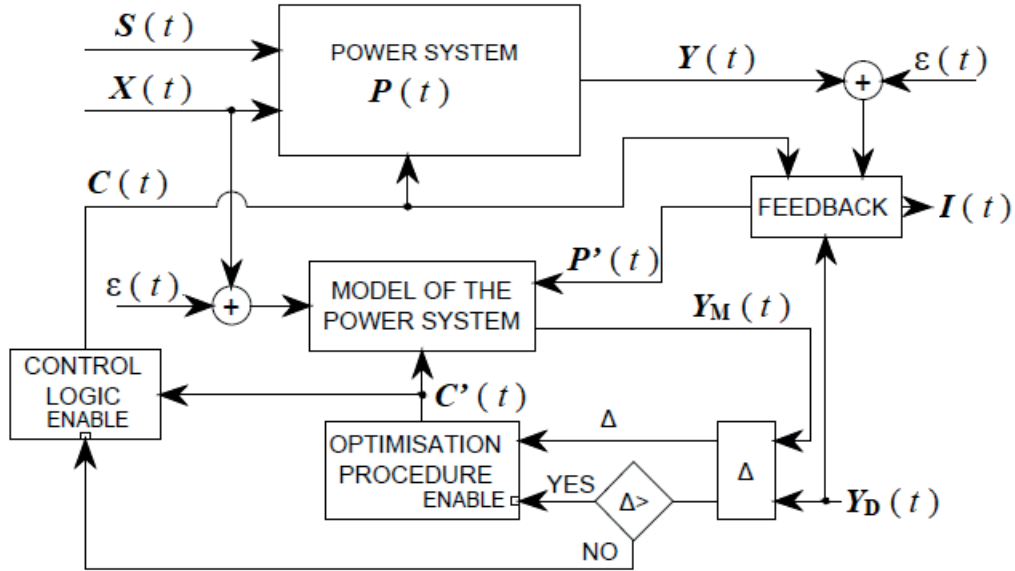


Fig. 1.2. Closed-loop control system with online synthesis of optimal control operations.

In case of a high computational capacity being available, the control system should also predict the future state of the system based on measurement data and known dynamic characteristics of the system and use this prediction to generate optimal control actions (similarly to automatic synchronisation or automatic frequency load shedding [2]–[4], [7]).

In some cases, either due to lack of measurement data or external influences such as faults, the control system might be required to estimate real system parameters $P(t)$ and/or the unknown stochastic parameters $S(t)$ or values of unavailable controlled state parameters $Y(t)$. One approach to this task is to directly estimate unknown data from available measurements ($X(t)$ and/or $Y(t)$) by using equations derived from state equations that constitutes the model of the power system. This approach often involve significant level of simplifications mainly due to insufficient amount of measurement data to solve the inverse problem to calculation of state parameters $Y(t)$ with known power system element data $P(t)$ for a large system or in some cases simply due to low computational capabilities of the device used for implementation. This problem could be solved by use of more measurements, which requires a reliable communication infrastructure, but there is also possibility to use optimisation tools in order to obtain estimates of unknown parameters necessary for determination control actions even in case of limited scope of measurement data, which is also the approach adopted for the proposed method. Often these tools estimate the unknown system parameters by diminishing the difference between the model output $Y_M(t)$ and corresponding available

measurements $Y(t)$ from the real power system (example for estimation of $P(t)$ and $S(t)$ is given in Fig. 1.3) or estimate part of these parameters and replace others with probability distributions [8], [9].

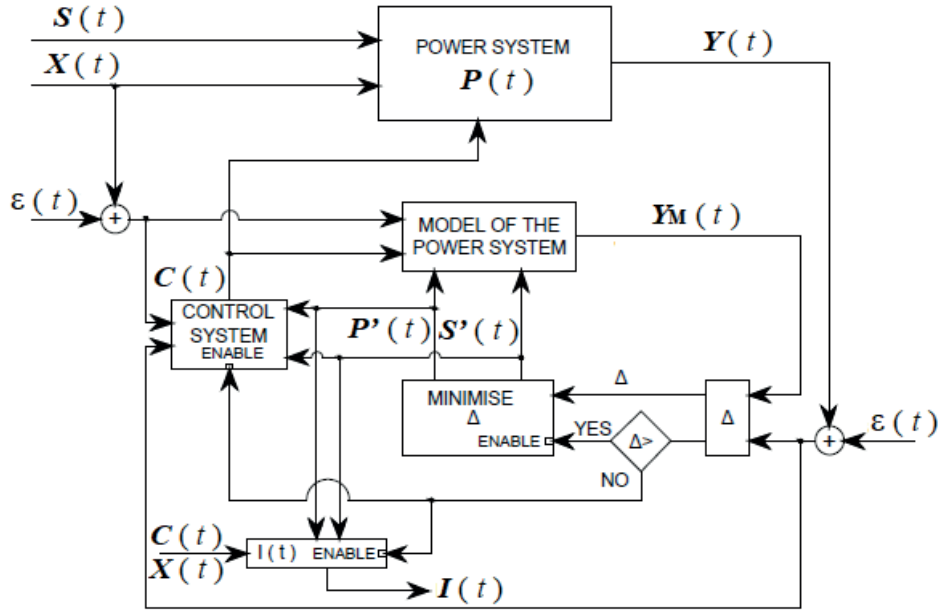


Fig.1.3. Closed-loop control system incorporating an estimation of unknown system parameters $P(t)$ and stochastic external processes $S(t)$ with an optimisation tool.

The whole control system problem defined by (1.1)–(1.4) is nonlinear, stochastic, multi-criterial and it includes many state and optimisation variables, and as such this problem cannot be solved without some simplifications. Main type of simplifications used in practice is decomposition, which can be geographic or element wise, meaning that control system is divided in subsystems or subtasks that are responsible for only separate elements or parts of the power system. Another decomposition can be according to control operation types (regulation, protection and other automation actions). Besides decomposition of the control system in smaller parts, there are different simplifications regarding the model used, which can include representation of the structure of the power system, parameters of power system elements (distributed or lumped, nonlinear or linear), external influences (deterministic or stochastic) and type of state equations (differential equations for transients or algebraic equations for steady-state) etc.

In this Thesis, only part of the control system – protective automation – will be considered with particular focus on the FL, DP and AR used for transmission lines that are created by applying the parameter estimation. Regarding the model simplifications the element parameters used will be lumped and linear and only the fundamental harmonic components of the measured signals will be considered. While performing the parameter estimation it will be assumed that their maximum and minimum possible values are known and the values between those limits are uniformly distributed. Measurement errors will be disregarded when testing both the proposed method and existing methods for comparison so that errors arise only from the deficiencies or the limitations of the methods themselves.

1.2. Fault location, distance protection and automatic reclosing functions

As this Thesis focuses on FL, DP and AR methods used for overhead transmission lines (hereafter – OHTL), a brief description of these protection and automation functions should be given.

The main task of the FL methods and devices is determination of the distance of fault from the substation where the FL device is installed, but they may be required to also determine the faulted line and fault type if this information is not provided by relay protection [10], [11]. In case of the example network below (Fig. 1.4) the FL should determine that the fault distance from substation busbars B2 is α kilometres or per unit and that the faulted line is L1, and the fault type if required. The main requirement to the FL is accuracy, as length of OHTL can reach hundreds of kilometres and they may cross hard to access terrain such as swamps. Additionally some of the faults are not obvious even during visual inspection (usually transient faults). Therefore, an accurate fault distance estimate reduces the time necessary for the identification and the repair of the fault resulting in improved resilience of the power system.

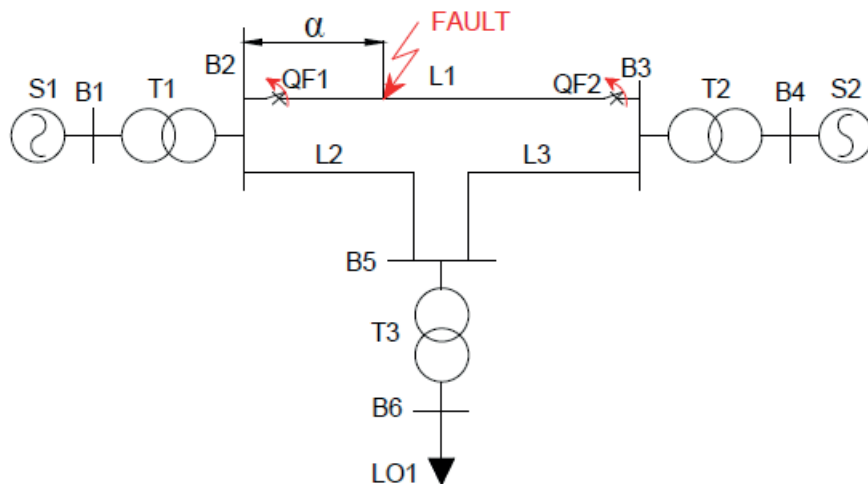


Fig. 1.4. An example network for the description of FL and DP.

DP is closely related to FL, as one of main operations it has to perform is to estimate the fault distance, but here this estimate is expressed as an apparent impedance determined by a DP relay $Z_{rel} = f(\alpha)$. In most cases it is calculated using busbar voltages and faulted line phase current measurements from only one substation (for example: in Fig. 1.4 busbar B2 voltages and line L1 currents may be used). The primary task of DP is to determine if there is a fault in the line protected by the relay (in Fig. 1.4 for DP controlling CB QF1 or QF2 it is line L1) based on the apparent impedance, and to open the controlled CB (indicated by red arrows in Fig. 1.4) if the line is faulted. The presence of a fault is registered if the apparent impedance is within a special operation regions defined in the complex $R-X$ impedance plane (Fig. 5.5). High-speed operation is one of main requirements for DP in order to reduce damage to the protected elements due to thermal and electromechanical impact of the fault and to reduce the potential risk of losing the dynamic stability of the power system in case of HV and EHV OHTL faults. Thus the available computation time for estimation of apparent impedance is

limited and hence the accuracy of this estimation is often not as strictly enforced, but remains desirable. One reason to improve the accuracy is to adhere to DP requirement of sensitivity – capability to operate for all faults in elements protected by DP at most unfavourable operation conditions such as low current short-circuits that differs little from high loading regimes. As the DP often protects not only its controlled line, but also serves as a reserve protection to next lines after it (in Fig. 1.4: line L2 and L3) or other elements after the controlled line it has to adhere also to a critical requirement of selectivity – to operate only for intended fault scenarios prioritising protection devices that are closest to the fault in order to minimise loss of loads. This is achieved by combination of time delays before trip signal is issued and increasing sizes of operation regions [5], [12]–[15].

As mentioned in the introduction, permanent faults constitute lesser part of all OHTL faults and after relay protection, such as DP, clears the fault by opening the CB it is possible to re-energised the line after some time delay called “dead time” necessary for the deionisation and restoration of insulation strength of an electric arc channel at the fault point. This is the main task of AR. Often the OHTL are double-fed having sources at both ends of the line (in Fig. 1.5: systems S1 and S2), which means that synchronisation between both sources is necessary before re-establishment of the line connection to avoid potential damage to the line. Due to this reason and in order to provide better operation conditions for relay protection in case of a permanent fault, the AR first tests the line condition by closing only one of the CB, and closes the second one after synchronisation only if the fault was transient in nature as indicated in Fig. 1.5: first closing QF1 and then QF2. The main requirement of AR is to minimise the dead time necessary before the reclosing, because during this time power system resilience is decreased (in some cases this also is the down-time of loads), while retaining sufficient time for restoration of insulation strength to avoid resumption of the fault. Typically by referring to AR a simultaneous reclosing of all three phases is understood, but in cases of L-E faults an AR subtype disconnecting and reclosing only one phase – SPAR – can be used. In this Thesis a further subtype of SPAR that in stead of using constant setting changes the dead time – ASPAR – will be considered [3], [4], [6], [15].

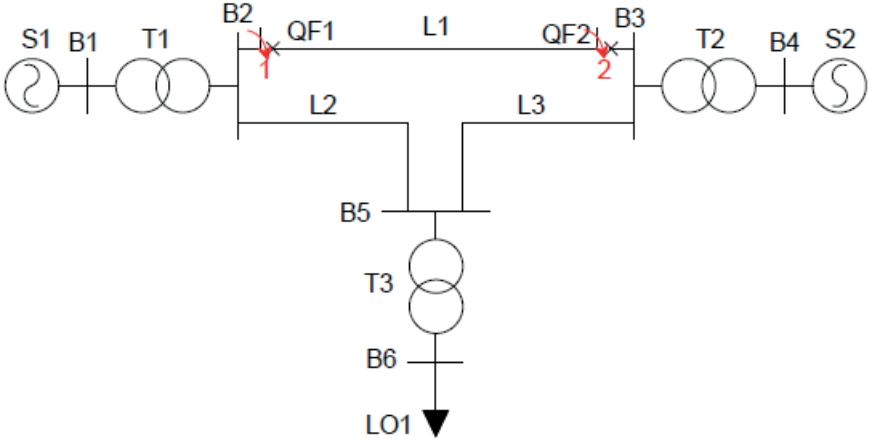


Fig. 1.5. An example network for the description of AR of transmission lines.

1.3. The general approach of the proposed method

The base structure of the proposed method is similar to one shown while discussing power system control (Fig. 1.3). However, in order to achieve the estimation of unknown power system fault parameters (most importantly distance to the fault α and the equivalent fault path resistance R_F), the use of optimisation is further supplemented, first, by an additional estimation of pre-fault parameters of the system (mainly loading and generation connected to system nodes, which makes this mostly a state estimation). This increases the information available before the estimation of aforementioned system parameters for the fault regime (operation mode) allowing to determine equivalent electromotive forces (hereafter – EMF) of nearby generators and impedances of loads (if these are considered), which one would otherwise have to either assume leading to errors in some pre-fault cases or to estimate simultaneously with α and R_F , significantly increasing the computational cost and risk of estimation errors. Secondly, in contrast to two-terminal-measurement-based methods that extend their scope of available information seeking measurements from the other end of the line with long distance communication networks, the proposed method extends available measurements to other system elements within the controlled substation with easy to secure and synchronise communication. The difference in available information can be described by using the example network shown in Fig. 1.4. One-terminal-measurement-based FL methods would only have measurements of busbar B2 L-E voltages and line L1 phase currents, but two-terminal-measurement-based FL methods would also have busbar B3 L-E voltage and line L1 phase current measurements from the other end of the line. Additionally, as it will be shown by the analysis of existing FL and DP methods in Chapter 2 the pre-fault values of these measurements are often considered only when the fault distance is estimated using superimposed fault components. On the other hand the proposed method would use busbar B2 L-E voltage, line L1 and L2 phase current as well as transformer T1 phase current measurements during both pre-fault and fault regimes. To accommodate the increased measurement scope, the models used for the parameter estimation must exceed the two-machine network applied often or an isolated model of the line [16], [17]. The flexible pre-fault and fault regime modelling approaches necessary for this task will be addressed in Chapters 3 and 4. More details of the proposed method and optimisation tools applied for its implementation will be given in the Chapter 5. The results obtainable during the parameter estimation used for FL can be further implemented for other power system automation and protection functions (represented in Fig. 1.3 in general as control system), which in this Thesis will be DP and ASPAR. The expanded scope of measurement data opens another question of how many and which measured parameters are beneficial to use for the proposed method. This question will be discussed in Chapter 6 of the Thesis.

1.4. Conclusions

1. FL, DP and AR are subtasks of a more general problem – power system control – that aims to sustain and optimise the operation of the system.
2. Most often both an apriori optimisation implemented in devices as settings and online optimisation utilised by the control system to generate optimal control operations requires modelling of the power system or its elements to some degree of detail.
3. Some of the automation and protection functions have to additionally estimate unknown parameters of the power system elements due to lack of measurement data or changes of the system caused by external influences such as faults.
4. The main task of the FL is estimation of the fault distance from the substation, but it may be required to determine the faulted line and the fault type.
5. The main requirement to FL is accuracy as it is crucial to reduction of time necessary for fault identification and repair of the line.
6. DP is used to clear faults in power system elements it protects by opening the CB it controls.
7. The most important requirements to DP is sensitivity to ensure intended operation even in unfavourable fault scenarios, selectivity to restrain from premature or unintended operation and operation speed to limit damage caused by a fault to the line and power system as a whole.
8. The main task of AR is to re-energise a transmission line after a fault in it is cleared and reconnect the second end of the line if the fault has been transient in nature.
9. The main requirement to AR is the minimisation of the time before the line is re-energised and reconnected while ensuring restoration of insulation strength at the fault point and synchronisation between both ends of the line if necessary.

2. TECHNICAL BACKGROUND OF FAULT LOCATION, DISTANCE PROTECTION AND ADAPTIVE AUTOMATIC RECLOSING METHODS

DP has been used for almost 100 years and the principle behind it could have been introduced even earlier with one of the first publications on the existing relays dating back to 1923 [18]. Likewise the FL problem on OHTL has attracted the interest of electrical engineers for at least 110 years [19]. The AR of OHTL on the other hand is relatively new power system automation function with publications found dating back to 1963 [20], but most probably its applications were tested even earlier. Since then, numerous modifications and improvements of methods and devices used for these automation and protection functions have been introduced, which will be discussed in this chapter of the Thesis.

2.1. Existing fault location methods

There are numerous FL methods and modifications of these. Here, they will be described in few larger groups according to their type.

First, different topological or inspection methods will be considered. The simplest one and one of the first approaches to FL was to sectionalise the line with disconnection switches. After the CB cleared the fault, the first disconnection switch would be opened and the section of the line re-energised. If no fault was present, the line was disconnected, the first disconnection switch was closed and the repair team proceeded to the next switch and the procedure was repeated until the protection was tripped, which identified the line section between this and the previous switch as faulted, reducing the time required to locate the fault [19]. This method is time-consuming, it requires additional investments for installation of the disconnection switches and the accuracy of this method is limited by the number of switches.

First fault indicators (hereafter – FI) called tower targets were invented by 1949, and these operated when the lightning or fault current flowing through the tower burned a fuse of gunpowder cartridge that released an indicator target [21], [22]. These indicators are cheaper than sectionalising switches and could be installed at every tower, but they require manual resetting and a new gunpowder cartridge after each operation. Another inspection-based FL method described in [21], [22] was use of a tracer signal of fifth harmonic, easily detectable with a portable detection device, that decreased as the repair team approached the location of the fault. Similar approaches with detection of EMF induced from a higher-harmonic tracer signal signals are used till this day to pinpoint the exact location of faults in power cable networks [23].

Field sensing or so-called electromagnetic applications FI initially did not have automatic resetting either, but their operation did not require gunpowder. However, these devices had to be set to operate before the relay protection disconnected the line. Later, several FI devices with automatic resetting were developed. One of these had a reset function activated when the L-E voltage exceeded 5 kV for 5 min. Another example is current-activated reset; when the current through a single-winding current transformer (hereafter – CT) of the FI had decreased

below the fault regime threshold but was still above minimal expected load regime current. These FI had little operation time and their coordination with relay protection was easy, but they were ineffective for cases of transient faults [24].

In 1989, a paper presented an approach where FI are used for measurements of the earth wire current and the measurement data for the positive half-wave are sent to a control central by a fibre optic channel in optical power ground wire. The fault can be located by determining the maximum change in the magnitude and angle of the earth wire current, which was achieved with fuzzy logic [25]. This approach does not require checking the operation of every FI on the way but immediately determines the faulted section; however, it still is limited by and requires the installation of FI.

Today, FI are more often used in distribution networks and more research is dedicated to the problem of optimal placement of the FI [26], [27]. The usage of such indicators in the area of HV networks is limited, mostly due to their inability to pinpoint the distance to the fault (only the faulted section between FI is indicated) and relatively large investments required for implementation.

The second large group uses transient waves of current or voltage, usually referred to as the travelling wave (hereafter – TW) method. The TW method applications have been reported since 1931 [28] whereas the use of direct current (hereafter – DC) voltage pulses for FL on cables has been proposed at least since 1946 [29]. Both methods determine the fault distance by the time a transient wave or a pulse travels along the line, but the pulse method injects external pulses with a pulse generator while the TW method uses the current or voltage transients created by the fault. Initially, these methods used recordings of oscilloscopes for calculations [29]–[31]. The authors of [30], [31] presented two types of TW FL: type A, which measures the time that is necessary for the first voltage collapse wave reflection from the substation to travel to the fault and back to this substation, and type B, which measures the time difference between wave arrivals at both ends of the line. The authors also proposed using electronic time counters instead of the oscilloscopes. Papers [21], [22] also described type C and type F FL that are essentially pulse radar methods, which use DC or radio-frequency pulses, with the only difference that type C FL injects a single pulse and measures the time of the reflection whereas type F uses successive pulses. Type D FL is also described, which, similarly to type B, detects the arriving waves at both substations, but the measurements are performed at both ends by synchronised timers. These papers report that the errors of these approaches were below 1 % for the TW methods developed by 1957, but at the time of their development there were open questions regarding the sufficiency of the reflection coefficient, especially for the type A method, since it required reflections both from the busbars and the fault and because of effects of attenuation to wave decay along the line [31].

By 1985, research had turned to FL with TW methods for high-voltage direct current (hereafter – HVDC) lines [32], [33]. This method takes advantage of the fact that the transient current waves of a HVDC line fault travelling to both line ends have different signs and therefore a type A TW FL device could be developed that measures time between the arrival of the first wave and the next wave that has the same polarity as the first one. The reported

error of FL is below 0.12 %. It should be mentioned that the authors of [32], [33] introduced a setting of 100 A after the differentiator-smoother to determine if the transient is fault-induced, not an alternating current (hereafter – AC) side disturbance, but an oscillogram from the publication also showed that the amplitude of the second wave was not significantly larger than the setting. This could lead to inability to detect the second wave front for more distant faults.

An interesting approach labelled as the TW method was presented in 1986 [34]. Here, measurements of instantaneous current and voltage were recorded for 5 ms from one terminal of an OHTL. Next, the transient curves were estimated for various points along the line based on line model equations. These curves were then used to calculate the energy expended at these points on the line as integrals of current, voltage squares or product of their squares. As the voltage drop and the current increase is the largest at the fault point, the fault distance can be determined by finding the point where the acceleration of change in expended energy is the largest. This method is capable of determining the fault distance for three-terminal (tapped) lines, but the error is above 1 % even for a two-terminal lines and it introduces an additional computation burden compared to other TW methods that have at least the same accuracy for regular lines.

In 1996, a paper reported an approach that combines type D TW FL with the global positioning system (hereafter – GPS) for time-stamping the arrival of the TW, which is determined by a minimum amplitude and signal rise time setting. This provided an opportunity for more precise time measurements, which beneficial since the speed of the wave is close to the speed of light and even small errors can result in significant distance estimation errors. It was reported that the accuracy was within one tower span and in most cases it was also possible to determine the locations of both direct and indirect lightning strikes, except in cases of almost simultaneous strikes [35].

One paper from 1999 combined artificial neural networks (hereafter – ANN) with the Prony method for signal processing of the TW to fit nonlinear time signal to linear model that has a set of damped sinusoidal components (modes) [36]. Considering the scale of the higher-frequency components of the TW that are analysed and provided to the ANN, the measurements have to be extremely accurate to obtain correct information of multiple modes. Additionally, a significant database has to be generated to train the ANN.

By 1998, continuous wavelet transformation was introduced combined with modal transformation for a TW FL [37]. The paper also suggested use of dominant frequencies of the aerial mode (mode 2 and mode 3) instead of earth mode due to a lower attenuation coefficient and reported accuracy of ± 300 m. However, all reflected waves were neglected and the method of choosing the optimal dilation parameter and frequencies used was not clearly explained.

Recently, the research of this type of FL targets specific line types and fault types such as hybrid lines (OHTL with cable sections) [38] and TW FL in case of simultaneous faults [39].

It should be mentioned that most TW methods require high time resolution, which can make the FL equipment for these methods more expensive.

The last significant group discussed will be FL methods that use electrical measurements (most often in steady-state quantities of the fault regime) with a model of the line to determine the fault distance. Initially, these measurements were carried out after de-energising of the line using low-voltage DC with a resistance and galvanometer bridge derived from Wheatstone design (the Murray and Varley loop tests). These could fail due to insufficient voltage for repeated breakdown of the HV insulation. Later, in 1907, it was proposed to connect an AC generator, an HV step-up transformer and a current-limiting resistor before the CTs of the disconnected line and to create a loop from one healthy phase and a phase with an L-E fault at both ends of the line. That way, the ratio of currents measured in these two phases is determined by the ratio of the impedances of two current paths to the fault point. This method requires disconnection of the line, creation of an artificial loop and an external AC source. The reported errors of this FL method are below 0.01 % [19].

Another early approach to FL task with measurement of electrical quantities was the use of automatic oscilloscopes, which were triggered by instantaneous undervoltage and overcurrent relays at several substations of the power system. Then the recorded oscillograms were used to determine the magnitudes of current of the faulted line and healthy parallel lines as well as their proportion, which was then compared with pre-computed curves $I_{\text{FAULTED}} = f(\alpha)$, $I_{\text{HEALTHY}} = f(\alpha)$ and $I_{\text{HEALTHY}}/I_{\text{FAULTED}} = f(\alpha)$ to determine the distance to the fault α . The error of this FL method could reach 10 % [21], [22], [40]. This approach required time-consuming computations to produce the curves necessary; additional time was necessary to retrieve the oscillograms from different substations. However, this method provides additional data for further analysis and it can be used for transient faults.

A similar method using magnetic links that “recorded” current or voltage measurements with the residual magnetism of a metal core of a coil as well as current and voltage curves for FL has been reported [21], [22], but their error may reach 20 %.

Several devices called annunciator ammeters were used, mostly for L-E faults. They applied pre-calculated curves of proportions of ZS current to total fault current or total fault ZS current ($I^0/I_F = f(\alpha)$ or $I^0/I_F^0 = f(\alpha)$). This method required manual acquisition of ZS current measurements from both terminals at the line ends. These devices often presented this measurement as a number of overcurrent coils that tripped resulting in a large discretisation step and errors up to 20 % [21], [22], [41].

In 1977, a paper presented a FL method that first calculates a Thevenin’s equivalent of the receiving end of the line during the pre-fault regime and then solves a system of nonlinear equations derived from Kirchhoff’s laws and earth fault loops with the Newton-Raphson method. Additionally, the authors describe extraction of steady-state values from the transient signal [42]. It would be desirable to prove that this system of nonlinear equations provides only one feasible root.

Around this time period (from the 1970s to the 1980s), the use of various digital devices for FL began and a wide range of concurrent design was introduced. One of the first of these applications is digital FL that uses one-terminal measurements and determines the fault distance as the ratio of calculated fault reactance to the reactance of the whole line [16]. This

approach could compensate changes in apparent reactance due to fault path resistance and remote-end infeed (the reactance effect [12]) only for fault path resistances up to 36 Ω .

In 1983, a microprocessor FL method was introduced that also used one-terminal measurements, but the currents used were superimposed components of the fault regime (the difference between a measured fault and a pre-fault values) [17]. In the paper, it was assumed that the angle of the total fault current and the superimposed current of the sending end of the line is equal, which is not true in cases of high line pre-fault loading [11], [43] and the algorithm of this device failed to converge to a solution if simultaneous faults occurred.

In 1985, another FL method using superimposed fault parameters was presented. However, here the fault current was expressed with positive-sequence (hereafter – PS) and negative-sequence (hereafter – NS) currents and their current distribution coefficients, and then this equation was inserted into the faulted phase voltage equation. After the division of the resulting quadratic equation into real and imaginary parts it was possible to obtain an equation with only the fault distance as the unknown parameter [44]. Here, similarly to [42], the question arises regarding multiple possible roots of the solution.

In 1989, a microprocessor FL using measurements from both ends of the line and modal transformation was introduced [45]. In this paper, the transfer of measurements data from the other end of the line is done manually and therefore requires the presence of personnel at both substations.

Since at least 1999, GPS systems have been applied also to this category of FL methods. Papers [46]–[48] combine GPS and phasor measuring units (hereafter – PMU) to obtain synchronised measurements from both ends of the line and apply Clarke transformation. The pre-fault measurements are used to estimate online the modal line propagation constants and surge impedances and an additional Discrete Fourier Transform (hereafter – DFT) modification is used to avoid errors due to nonnominal power frequency.

Another approach that has been reported at least since 1996 is the use of artificial neural networks (hereafter – ANN) for this type of FL methods [36]. Usually, for this type of FL, the ANNs are provided with a DC component, a fundamental frequency component, a 100–350 Hz frequency range component and a 400–1000 Hz frequency range component obtained from the instantaneous voltage and current signals of all the phases. One of these papers from 2000 also proposed using a simplified ANN for fault type recognition before the ANN-based FL [49]. As mentioned before, applications of ANNs require a significant database for training. Additionally, use of several higher frequency components may increase errors due to measurement noise.

In 2001, a FL method was described that applied the idea of [44] to parallel lines, but without pre-fault measurements and with compensation for line shunt capacitances [50]. In this paper, besides the question of possible additional roots of the quadratic equation, the fault current from the remote-end system is neglected.

A 2005 paper proposed that the FL task could be solved as an optimisation, which minimises the difference of the fault point voltage calculated separately from two-terminal measurements plus the imaginary part of the calculated fault path impedance. In addition, it is proposed that in case of CT saturation, the real and imaginary parts of the current of that

phase are added as an unknown parameter to be determined by the optimisation [51]. This approach could obtain the fault distance even if all of the CTs at one substation were saturated, but this method is highly dependent on the operation of the communication network and synchronisation of the measurements.

In 2005, a FL technique based on the Monte-Carlo method was reported. This technique substitutes the unknown impedance of the remote-end power system equivalent impedance with a probability distribution; it also assumes purely active character of apparent power at the fault point. This makes it possible to formulate an optimisation task: to find the parameters of a transmission line four-port equivalent, which ensures that the imaginary part of the sum of symmetrical components of the apparent power is equal to zero, and then solve it using the Monte-Carlo method [8], [9]. This approach has a high computation cost.

In 2011 and 2012, two similar papers presented the idea to use the GA to solve a similar minimisation task as in [51], but only considering the difference of calculated voltage at the fault point. The 2011 paper [52] is interesting because it considers the possible synchronisation shift angle as an additional unknown parameter for optimisation. The only risk here is that the estimated angle will be shifted by a period, which could introduce error if the fault path resistance value is not stationary as discussed in Section 4.5. The 2012 paper uses almost the same objective function, but in a time domain, and the fault distance is derived from the time of arrival of the voltage wave, which is determined using an optimisation [53].

In a 2017 paper, the Whale optimisation algorithm was proposed and compared with GA with the same base principle as in [53], achieving similar accuracy [54].

Recently, further improvements to ANN methods have been proposed combining ANNs with other intelligent algorithms to include not only the FL, but also fault type identification and selection of the optimal FL method [55], [56]. Another interesting paper about a pattern recognition method similar in application to ANNs should be mentioned. It is based on the k-nearest neighbour [57], which only uses voltage signal measurements from one terminal, obtains the harmonic spectrum of this signal and then uses a database of similarly processed recordings to recognise the fault distance. This allows avoiding problems associated with communication networks and CT saturation, but this method requires a high sampling frequency and a sufficient database of fault recordings.

Lastly, a FL method, which is hard to pin to the previous groups – the resonance or standing wave method – can be described. This method works on de-energised lines. A standing wave signal generator with variable frequency is connected to the line and, as the injected waves are summed with reflected waves, maximum and minimum voltage points can be observed for various frequencies. The fault distance can be calculated from the frequency difference between two neighbouring minimum and maximum points [21], [22], [58].

As can be seen, a significant number of FL methods have been developed, from which methods using measurements from terminals at both ends of the line can be considered fast and accurate, yet they have a significant dependency on safe communication networks and often precise synchronisation is also required. Additionally, initial approaches to use of extended measurements was slow because of the manual data acquisition and limited

computational capacities and sometimes reduced accuracy because of large discretisation steps of measurement devices or model simplifications to reduce computational time. Other methods using one-terminal measurements have a limited scope of available information that often lead to use of simplified line models or introduction of assumptions, which were applicable only in part of possible fault scenarios. TW methods are well recognised as one of the solutions in case of this limited measurement data environment and in theory it is very accurate, but these methods have to distinguish the correct wave fronts, consider wave decay, measurement noise, additional reflections and they require a significant sampling frequency. There are methods that can express the fault distance with nonlinear equations using Kirchhoff's laws and current distribution coefficients to approximate the influence of the remote-end power system, but this approach only partially compensates for the remote-end infeed and there is also a risk that there will be several feasible roots obtained by solving the developed equations. Another approach that can partially compensate for the limitations of available measurements is to use pattern recognition such as ANNs, but application of these approaches requires training data across a large space of possible scenarios. The probabilistic approach to values of unknown parameters with the Monte-Carlo method is also oriented towards compensation for limited information, but this is only an approximate representation of remote-end infeed and it requires a large number of simulation trials. Considering the possibility of loss of communications between the substations during the fault and the aforementioned drawbacks of FL methods using one-terminal measurements, it was concluded that an algorithm capable of solving the FL task in such an incomplete information environment, especially in case of complicated line configurations (parallel lines, nonuniform structure etc.), based only on one-terminal measurements, would prove to be beneficial.

As the primary implementation of the method proposed in this Thesis is FL, and the types of FL methods are so various with different measurements used and fault distance estimation approaches taken as shown by literature analysis above, it would be useful to show them graphically (Fig. 2.1). In the Fig. 2.1 FL type, which the proposed method is part of is indicated by red lines and a red frame.

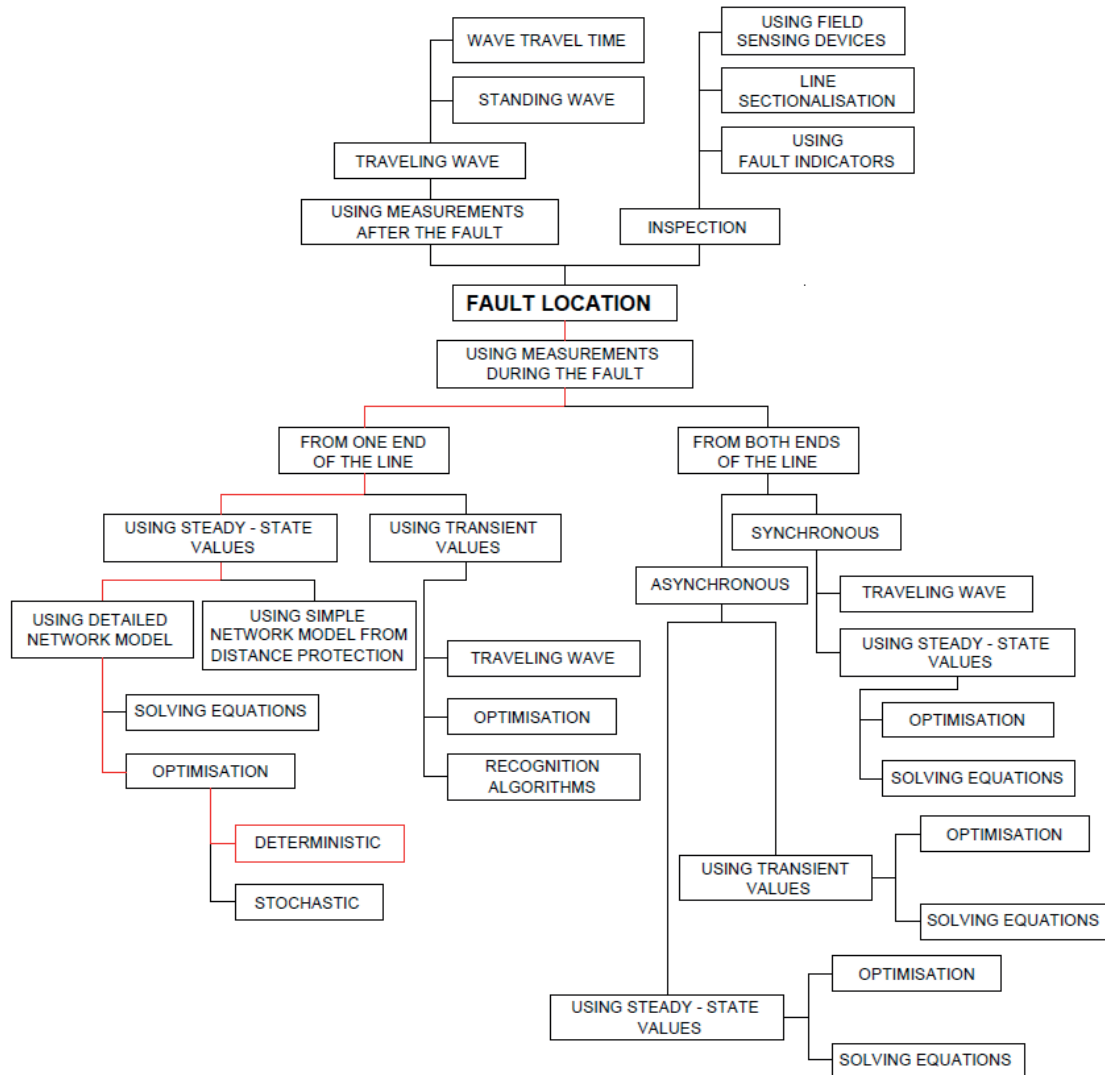


Fig. 2.1. Types of FL methods.

2.2. Existing distance protection methods

Most of the research on the DP was made for methods based on electrical fault regime measurements from one terminal of the line, therefore the following analysis will be more chronological in nature rather than about groups of solutions.

The earliest type of DP is the so-called balanced-beam-type DP relay. This type of relay is the most primitive electromagnetic relay that operates based on Ohm's law (the fault loop impedance measurement). Two coils affect a balanced beam that is pivoted in the centre. The relay current flows through one coil creating operation torque proportional to the ampere-turn square $M_{OP} = K_{OP} \cdot (w_{OP} \cdot I_{REL})^2$, but the voltage measured by the relay is connected to the second coil creating the restraining torque $M_{RES} = K_{RES} \cdot (w_{RES} \cdot I_{RES})^2$, where K_{OP} , K_{RES} are constant mechanical coefficients of operation and restraining coils, w_{OP} , w_{RES} are the number of windings in operation and restraining coils, $I_{RES} = U_{REL}/Z_{RES}$ is the current of the restraining coil determined by relay voltage and the impedance of the restraining circuit (the second coil and additional resistance R_{RES} if added). The number of windings w_{OP} , w_{RES} and the additional resistor R_{RES} then could be used to determine the "balance point" or operation

setting $|Z_{\text{SET}}| = R_{\text{RES}} \cdot w_{\text{OP}}/w_{\text{RES}}$. If a fault occurs closer than the predefined setting ($\alpha Z^1_{\text{L}} < |Z_{\text{SET}}|$), then the faulted phase voltage would be lower than at the “balance point” and the phase current higher, resulting in operation coil connecting the trip contacts attached to the balanced beam. This produces a nondirectional circle trip zone in the R - X diagram that is hard to coordinate [59]–[62].

Direct implementation of balanced-beam-type DP in practice was not found, but since 1923, a functional combination of an induction disc overcurrent relay with the voltage restraint coil and the balanced-beam operation mechanism has been reported (a C-Z type DP relay). This relay automatically incorporated a time delay with a spring, which is tightened by the disc, allowing for time coordination between DPs at different substations [63]. The use of a DP or impedance relay rapidly intensified during the 1920s because the DP was easier to apply for more complex, interconnected systems compared to directional overcurrent relays. During this time, applications of DP for both phase-to-phase (hereafter – L-L) and L-E faults were developed. Additional compensators were presented in [64] to account for a possible neutral shift of voltage transformer (hereafter – VT) secondary windings. Both the balanced-beam relay and the C-Z type relay described are nondirectional, requiring an additional relay for the determination of the fault direction. In the papers, neither fault path resistance nor load impedance that could result in incorrect operation were considered.

A 1930 paper presented the stepped coordination principle for selectivity with back-up protection, a combination of DP with carrier protection to send a trip signal to the other end of the line in case of zone I trip. The paper is one of the first to describe the influence of fault path resistance, which was considered of importance mainly for L-E faults, and the idea of creation of a reactance relay is therefore proposed. It is also mentioned that by 1930, research had begun on electronic DP and directional elements using thermionic and gas-filled tubes, however, the initially developed relays were no more effective than electromechanical relays [65]. The change in apparent reactance (the reactance effect) for particularly unfavourable cases – fallen tree faults – can be seen from results of a digital DP testing in Section 4.5.

By 1931, the inability of C-Z type relays to compensate for the voltage drop caused by the ZS currents of the protected and parallel healthy line was recognised as well. Therefore, an impedance relay with an either current or voltage drop compensation using a ZS current filter was introduced [66]. Building upon this work, the reactance relay with the same ZS compensation was created to partially decrease the influence of the fault path resistance. This was achieved by adding one more operation coil connected to the relay voltage (U_{REL}) with a capacitor to achieve a 90° shift angle between the new operational voltage and the relay voltage [67]. Both of these relays were more precise for L-E faults than the C-Z type relays previously used, but only the reactance-type relay could partially reduce the impact of fault path resistance if this resistance or the angle between the fault and the relay current was small (low pre-fault loading).

A more practical application of DP and carrier-pilot protection discussed in [65] was presented in 1938 using the already widespread DP relays containing all three zones in one device. Zone III is used as a fault detector (hereafter – FD) that initiates the carrier signal transmission. When directional relays have operated, Zone I is tripped on one side of the line

and the carrier signal transmission is stopped that de-energises the carrier receiver relay and its normally closed contacts shunt Zone II time relay contacts, allowing for faster DP trip on the other side of the line [68]. This approach is convenient incorporation of existing DP relays if the installation of carrier-pilot protection equipment was justified and performed.

Based on the idea of applying selector relays in an earlier study, a 1943 paper presented a DP with a selector relay system that was more economical and could be used for sub-transmission or distribution networks, which was usually protected by cheaper directional overcurrent relays. Instead of using three DP relays for L-L faults and three for L-E faults, only two reactance-type relays were to be used (one for each fault type) and two selector relays. In case of L-L faults, the selector relay consisted of four overcurrent relays and several auxiliary relays providing the necessary L-L voltages and delta currents as well as indication of faulted phases. In case of L-E faults, three undervoltage relays and several auxiliary relays were used to provide the necessary phase voltage and current to the reactance relay (including ZS current compensation) as well as indication of the faulted phase [69]. Even though it is not as cost-efficient as modern digital phase-selection methods, such applications of the selector relays made DP more economical and widely used. It can be noted that other ways of optimisation of electromechanical DP relaying systems, such as reduction of starting elements, were also researched in this time period [70].

Later in 1943, a paper discussed three possible methods of protection for three-terminal lines. The first approach was to increase/decrease the DP setting based on the presence of either load or generators at the tapped line as well as the expected infeed/outfeed current values. The setting strategy is for Zone I to cover 90 % of line up to the closest substation, providing less coverage for the line section to the furthest substation. Zone II is to be set beyond the furthest substation, which in some cases could exceed the line after the closest substation. The second idea presented is essentially to extend the carrier-pilot combination with DP described in [68] for three substations. The last method is using pilot-wires for implementation of differential current protection [71]. The carrier-pilot and differential method are more reliable in this case but require additional investments.

A more universal modification of the balanced-beam-type relay compared to the reactance relay was proposed in 1944. The restraint voltage was made proportional to the vector sum of the relay voltage and the voltage drop caused by the relay (operating) current across variable impedance. In this way, by modifying the variable impedance and the auxiliary transformer setting, which provides the relay voltage, it was possible to change the diameter of the circle operation region, shift the centre of the region along a certain axis and to rotate this axis $\pm 30^\circ$ from the reactance axis [72]. This provides an opportunity to shift the operation regions forward along the line impedance for zones II and III instead of increasing the diameter of the region with the same centre as Zone I, decreasing the risk of unwanted operation during high loading of the line or during a power swing.

The interest in analysis of DP operation during power swings started at least from 1937, as referenced in a 1945 paper describing an already refined analytical approach to the determination of the apparent impedance measured by a DP relay during a power swing without and with faults. If the equivalent circuit elements were linear and both systems could

be represented with Thevenin's equivalents, then this impedance could be determined based on a PS network diagram, the proportion of EMFs and the angle of their phase shift for power swings as well as three-phase faults during the power swing. However, by using the Clarke transform, it was made possible to consider also asymmetrical faults during a power swing [73]. Later, a 1949 paper introduced a simplified graphical approach to constructing impedance diagrams for power swings and phase faults during them. This last paper also described convenient methods for graphically obtaining the apparent impedance of all phase and earth fault distance relays during faults with different fault distances and fault path resistances. It was also shown that in case of L-L and phase-to-phase-to-earth (hereafter – L-L-E) faults, the earth fault DP relays of the faulted phases can be tripped, and similarly for L-E faults one of the phase fault DP relays can be tripped. This could lead to confusion when compared with separate faulted phase indicators such as described in [69], therefore it was proposed to introduce blocking according to the detected number of faulted phases [74]. The methods described above had to use various simplifications for their analysis due to limited computational capabilities at the time, but they did provide more practical tools to analyse and improve the operation of DP.

A 1948 paper proposed using the reactance type relay in order to avoid time delays for faults on short lines with fault path resistance and use an MHO type relay as a directional starting element (with a capacitor for faster operation in case of three-phase faults next to a substation) [75]. This directional element was more sensitive than the previous starting elements, but it would be cheaper and more reliable to have an inherent fault detection and directional operation due to the corresponding operation region of DP than in the case of introduction of additional relays.

Around 1950, some of the first practical electronic relays based on high-vacuum tubes were presented, including the MHO DP relay as referenced in a 1954 paper. The electronic relay described in the paper consists of two diodes and one high-vacuum tube. It is connected so that the negative half-wave of the relay instantaneous voltage has to be in phase with the instantaneous voltage drop across an R-L replica of the line impedance caused by the relay current in order for the relay to operate. As a result, operation is restricted to the fault closer than the setting distance. The operation region can be MHO or sectors of a circle with setting impedance as the chord [76]. There is a slight possibility of trip for metallic faults just behind the relay and the operation time depends on the fault inception angle (0.5–1.0 cycles). Also, as the replica impedance must have the same R/X ratio as the fault, the fault path resistance and the power system impedance might further deter the relay's operation.

The next significant step in the development of DP was the introduction of transistors into DP relays by 1956. Two application methods were described: the pulse relay and direct-phase-comparison. Both methods first derive two voltages from the relay voltage and current, using auxiliary transformers and replica impedances. The pulse relay creates pulses from the second voltage when it is at the positive maximum. Then the first voltage and these pulses are applied to a coincidence circuit, which trip the protection only if the first voltage is positive while the pulse is present. Essentially, the operation criterion is that the angle between both voltages has to be $\pm 90^\circ$. The direct-phase-comparison relay applies both voltages directly to

the coincidence circuit. As a result, the output is a voltage signal while both input voltages coincide. This output is applied to an integrating circuit and then the output of last circuit is compared with a setting, which determines if the both initial voltages coincidence angle is at least 90° . By modifying the auxiliary transformer ratios and the replica impedances, it is possible to implement directional relay, impedance, reactance, resistance, MHO and different offset impedance operation regions [77]. Additionally, a polarising voltage is introduced from a healthy phase to secure correct operation for directional and MHO relay operation in case of a metallic fault next to the substation, but this also can cause significant transient overreach (unintended operation during electrical transients).

Introduction of electronics to DP did not deter further development of electromechanical relays, as shown by a 1958 paper that introduced a single phase DP relay for the protection of all L-L and L-L-E faults. This relay was constructed as a four-pole cylinder unit connected in an open delta and operates as an induction motor. This relay has only voltage coils, therefore operation current is introduced before the relay terminals as voltage drops across replica impedances by using single-air-gap transformer-type compensators. The relay operates if the phase sequence of the resulting voltages changes from a positive to a negative one, which happens for faults within the protection zone (the voltage drop across the replica impedance exceeds the voltage measured by the relay). The introduction of these auxiliary-transformer-type compensators damps the DC offset of the relay current and reduces the transient overreach, but can lead to a small additional time delay before operation. Another interesting feature described in this paper is the blocking of the DP in case of power swings using sequential operation of DP relays, which, although with slight modifications, remains widely used. In the paper, a separate DP relay with a shifted circle operation region enclosing Zone II of a three-phase fault DP with a safety margin is used in combination with a slow pick-up auxiliary time relay. This limits the time in which the impedance locus must reach Zone II of the three-phase fault DP in order for the protection to trip [78], [79]. Besides the possible time delay due to current DC offset, this type of relay could not be applied to L-E fault protection, but it does reduce the number of relays necessary for the phase fault protection.

By 1966, the first DP operation region close to quadrilateral ones was proposed for phase fault protection. First, signals U_{REL} , $U_{RELE}^{-j90^\circ}$, $I_{REL}R_{Fmax} - U_{REL}$ and negative sampling pulses of voltage drop across replica impedance $I_{REL}Z_{REP}$ are provided to a variable-phase comparator, which operates according to the criterion of impedance angles: $\arg(Z_{REL} - R_{Fmax}) > \arg(Z_{REP}) > \arg(Z_{REL})$, where R_{Fmax} is the maximum possible fault path resistance. If the phase detector operates, then the output of it is connected to the logical AND gate with signals $(KU_{REL} - I_{REL}R_{REP})e^{j90^\circ}$ (K being different coefficient for zones I–III). This AND gate provides both discrimination of internal/external fault and discrimination of zone that has to operate with additional time delays for zones II and III. This paper also described a method of faulted phase identification using differentiating elements (d/dt) with phase currents and application of a synchronous motor for corresponding automatic switching that provides phase and earth fault DP relays with the necessary voltage and current [80]. The use of a synchronous motor is undesirable due to the heavy reliance on moving parts.

A DP relay with a different quadrilateral operation region was proposed in a 1970 paper. This relay performs two phase sequence tests, which can be achieved with ferrite-core logic or semiconductor flip-flop logic (semiconductor logic requires an external power source, but it provides a more refined operation region). Voltage drop signals in replica impedances $I_{REL}Z_{REP1}$, $I_{REL}Z_{REP2}$, $I_{REL}Z_{REP1} - I_{REL}Z_{REP3}$ and $I_{REL}Z_{REP2} - I_{REL}Z_{REP3}$ define the DP relay operation region and signals U_{REL} and $U_{REL} - I_{REL}Z_{REP3}$ are used to indicate that the apparent impedance is within the operation region. When there is an internal fault, both determination sequence blocks operate, causing logical AND gate operation that sends a trip signal [81]. The operation region of this relay seems to cover potential R_F values only in case of close faults and there is a notable transient overreach.

Around 1967–1969, the first proposals of computer- (microprocessor-) based relay protection were published as described in a 1971 paper. This paper presented an algorithm for digital estimation of peak values of voltage and current signals as well as their phase shift angle using the instantaneous current, voltage measurement values and instantaneous derivative values of these measurements. The estimated peak and phase shift values are then used to calculate the apparent impedance seen by a DP relay. The DC offset is reduced by using mimic impedances in CT secondary winding with X/R ratio set same as for a fault at the Zone I boundary and in order to decrease the effects of measurement noise, three-point smoothing is applied to the calculated modulus of apparent impedance. This approach could obtain the modulus of impedance with an accuracy of $\pm 10\%$ and argument $\pm 15^\circ$ 5 ms after fault inception [82]. However, as sinusoidal character of current and voltage are assumed, the accuracy of this algorithm is questionable when current and voltage distortions are present in HV OHTLs due to TW.

A more practical implementation was demonstrated in a different 1972 paper. Here, the relay algorithm first checks if there are indications of a developing power swing and in that case it greatly desensitizes the DP (except L-E fault protection). If no power swing is detected, a detector of phase faults is activated, which uses present current measurements as well as their rates of change to predict current values 6 samples later and compares actual measurements to previously predicted values. In case the difference exceeds an adapting limit for any phase, a fault occurrence is detected. After that, a fault type analysis block is activated, which can issue an instant trip in case of severe overcurrent or activate L-L or L-E DP based on excessive phase, ZS currents and low voltage indications. The impedance is calculated similarly to the algorithm in [82], but using first and second divided differences, which are described as less susceptible to errors caused by current and voltage signal distortions. As the authors of the publication note, the adaption of computers to DP provides very convenient means to obtain any operation region desired in the form of tables of impedance modulus and argument [83], [84]. The described algorithm did not include compensation of parallel line ZS current and in case the fault type analysis block cannot immediately determine fault type, the relay requires an additional test using Zone III of both L-L and L-E fault algorithms before permitting operation of Zone I or II for one of the algorithms. This introduces an additional delay compared to direct testing of all three zones.

A 1972 paper demonstrated that for any asymmetrical fault the phase sequence of ZS compensated L-E voltages will change. This conclusion was used to develop a single phase-sequence determination relay using three sine comparators, three AND gates and one OR gate for the DP for all L-L, L-L-E and L-E faults [85]. The proposed method does provide a compact solution for both phase and earth faults, but it is unclear if this phase sequence change is not affected by the fault path resistance or current and voltage signal distortions.

An electronic DP relay with an operation region more resembling modern quadrilateral ones was proposed in 1974. This relay used four signals: U_{REL} and three signals $U_{REL}-I_{REL}Z_{REP}$ with different replica impedances, which together defined the boundaries of the quadrilateral operation region. It was shown that in case of an external fault, the maximum angle between any two phasors of these signals did not exceed 180° , whereas in case of internal fault it did. A coincidence block was presented that creates pulses if this maximum angle is less than 180° , but if the fault is internal no pulses are generated and the auxiliary relay is deenergised. The normally closed contacts of the auxiliary relay perform the trip command [86]. This relay does not consider the reactance effect and the transient overreach is still considerable. Later, in 1976, a different phase-sequence relay was proposed. It was mentioned that previous similar type DP relays could not operate correctly in case of arcing faults due to the narrow operation region and it was proposed to implement a six-input phase-sequence comparator that used regular L-E voltages and voltages after ZS compensation. It was demonstrated that only one phase sequence of these signals is not characteristic to fault regimes and can be used as a criterion. This achievement also resulted in an expanded operation region [87], but this might require external blocking for power swings and result in a decreased safety margin to heavy loading apparent impedance.

The use of computers for DP also lead to research in digital filtering applications in DP relaying. A 1975 paper presented a simple method for calculation of fundamental frequency orthogonal components of voltage and current phasors using the Fourier series – DFT. The approximate values A, B of orthogonal components a, b are as follows:

$$A = \frac{2}{N} \sum_{k=0}^N \left[f \left(t - \frac{kT}{N} \right) \cos \left(\frac{\omega kT}{N} \right) \right], \quad (2.1)$$

$$B = \frac{2}{N} \sum_{k=0}^N \left[f \left(t - \frac{kT}{N} \right) \sin \left(\frac{\omega kT}{N} \right) \right], \quad (2.2)$$

where $f(t)$ – a periodic function;

T – the period of $f(t)$, s;

A and B – the approximate values of orthogonal components a, b of the function $f(t)$;

k – the index of the harmonic component;

N – the number of measured samples during this period (as $N \rightarrow \infty, A \rightarrow a$ and $B \rightarrow b$).

This made it possible to create DP algorithms more immune to errors caused by higher frequency distortions, and the use of voltage drop $I_{REL}Z_{REP}$ instead of I_{REL} decreased the DC offset, but only partially, and some error due to the fundamental frequency component of the DC offset remained [88]. Also the basic version of DFT can produce inaccurate results in the

presence of subharmonic interference caused by capacitor VTs and in case of fundamental frequency deviations from the nominal one.

A 1976 paper presented an electronic relay that, depending on eccentricity, can have a hyperbolic, circular (impedance), MHO, elliptical and parabolic operation region in the $R-X$ diagram. The operation setting also depends on the difference of the Z_{REL} and Z_{REP} angles [89]. This would reduce the requirements for operation in case of a significant fault path resistance, but it could lead to overreach if the system impedance has a different angle and is significantly larger than the line impedance represented by the replica impedance.

In 1977, a paper dedicated to DP for high-resistance L-E faults was published, which was possibly the first of online adaptive DP methods. This protection has an operation region similar to a quadrilateral one. It is highly extended along the resistance axis and it can be rotated $\pm 15^\circ$ relative to the point of a replica setting impedance. This angle is changed depending on the pre-fault line loading in order to account for the reactance effect. A minimal ZS current setting has to be exceeded for this DP to operate with the intention to prevent unintended trip during heavy loading conditions and symmetrical power swings [90]. This approach is one of the first to start transition from use of simplified model considering only one side of the line in the device and partially accounting for this with settings to method that tries to estimate influence of the power system equivalent on the other end of the line online (in essence implementing the two-machine network model). However, there is a possibility that in case of heavy pre-fault loading the rotation of the operation region by -15° can result in loss of sensitivity for faults at the setting distance. Also, if power flows in the protected and the next line are opposite due to network interconnections, the zones I of the DP of these lines could overlap in high-resistance fault regions.

Further developments of the DFT and symmetrical component applications for DP were described in a 1979 paper. The DFT in this paper was changed so that it did not provide the orthogonal components but the complex phasor directly. After incorporating the symmetrical component method in the numerical DFT calculation, a recursive calculation method for both the phase quantity phasors and the symmetrical component phasors was presented. Additionally, a transient control function was described that used an inverse DFT to obtain a vector of instantaneous current values representing only the fundamental frequency, which is then subtracted from a vector of corresponding measurement points. The one-norm of the obtained difference vector over $\frac{1}{2}$ cycle measurement points can be used as a FD or as in the paper to block the DP, reducing the risk of transient overreach [91]. This does introduce an additional time delay before the DP is allowed to operate and the problems of frequency deviations and subharmonic signal distortions are also relevant for this application.

A 1983 paper was one of the first to introduce TW method application for DP. This algorithm first obtained two signals by using instantaneous relay current and voltage values and replica impedance. The second signal has a peak when the TW is moving towards the line after being reflected from a source behind the relay and the first signal has peak when this reflected signal returns to the relay location after being reflected from the fault point. The fault distance is then obtained by the time difference between the detection of the second and first signal peaks. Additionally, a cross-correlation function is used to recognise these peaks

and modal transformation is used for three-phase line implementation [92]. It can be noticed from the results that the value of the cross-correlation function was low for L-E faults and low fault incidence angles. Also, if there are several significant power sources behind the relay, multiple peaks of the second and possibly the first signal could be detected, leading to incorrect distance estimation.

In 1990, a paper introduced a digital DP using NS and ZS currents. The operation of this DP required the operation of a directional element, a NS overcurrent element and a NS and ZS-current-based distance element with a corresponding phase selection element. The NS overcurrent element operated when this current exceeded a setting that depends on phase current values. The distance element calculates the apparent impedance from L-L or L-E voltages and NS and ZS currents as well as PS and ZS current distribution coefficients. The use of NS and ZS currents is intended to decrease the influence of the pre-fault loading especially for Zone II and III applications. The phase selection element determines the calculation phase for sequence currents by the angle between NS and ZS current phasors. If the angle is within $\pm 60^\circ$ or the ZS current is below 400 A, this element operates. This allows operation in case of L-L faults for all of L-E or L-L zones to operate. Additionally, the paper presents a new ZS calculation formula using L-L delta currents, which decreases errors caused by frequency deviations [93]. The use of the directional element seems unnecessary when the operation region of the DP could be made inherently directional, and if significant fault path resistance results in a small ZS current, the phase-selection element may operate for all phases.

From 1991, adaptive DP algorithms started to attract even more interest from researchers. One paper started by introducing compensation of the apparent reactance setting in case of frequency deviations. The deviation was calculated using the difference between the proportions of a current sample before a zero-crossing to the difference of the samples before and after the zero-crossing that are one cycle apart. A rotation of the operation region boundary similar to the one in the 1977 paper, but affecting only the upper boundary of the quadrilateral region, was presented. Here, the rotation angle was calculated by means of the ZS current of the relay, the compensated phase current of the relay and the phase angle difference between equivalent ZS impedances from both line ends in case of fault at the limit of the zone setting. In order to avoid operation during power swings, the rate of change of relay current must exceed the maximum value expected during the load regime or the power swings, which is calculated from the peak value of load current [94]. It seems that frequency deviation compensation could be performed at least once in every $\frac{1}{2}$ cycle, which also includes zero-crossing, and it may be affected by current distortions that are partially negated by a digital narrow band-pass filter. Soon afterwards, in 1994, a paper presented a fully adaptive operation region. This region is an approximation of an ideal operation region, which is obtained by considering faults at the zone limit with all considered fault path resistances and all distances with maximum considered fault path resistance for known impedances of power systems, the proportion of their EMFs E_{S1}/E_{S2} and the angle between them, δ , with linear sections. These known values are updated during the pre-fault regime. The operation region is further divided into sections and the DP trip can be issued if the apparent impedance

is within any of these sections. This new algorithm works in parallel to a simpler digital DP with a quadrilateral operation region because it is blocked for one cycle to avoid transient overreach [95]. Even considering the additional delay, the setting of 95 % of the line for the adaptive algorithm still presents a higher risk of unwanted overreach due to measurement errors. The high coverage of the line could also lead to coordination issues in case of different power flows in neighbouring lines due to system interconnections between them that would lead to the orientation of the adaptive zones towards each other.

In a 1995 paper, a directional element based on superimposed PS components for DP is described. This element uses superimposed PS components of relay current and voltage measurements to calculate apparent superimposed impedance. For faults in the forward direction, this impedance is within the third quadrant of the $R-X$ impedance plane and for reverse faults – in the first quadrant. The superimposed components are calculated using the pre-fault values recorded five cycles before. The proposed directional element was introduced to allow easier setting for series-compensated lines and the DP with this directional element was tested using a real-time digital simulator [96], which might be the first DP testing with this technology. The directional element might be useful for the particular problem, but the DP used with it is a fairly simple one without consideration of fault path resistance or power swings.

By 1996, ANNs were being introduced for DP algorithms. One such application was oriented towards better measurement filtering. This DP first uses a second order Butterworth filter to remove higher frequency distortions, then uses ANNs to determine the correct fundamental harmonic orthogonal component values, essentially performing the functions of a DC offset and Fourier filters. The paper also described a DC offset removing algorithm that was used to process the training data [97]. This approach can help with transient overreach and higher harmonic distortions, but it does not address any other shortcomings of the DP itself. The algorithm also uses 12 different ANNs for the real and imaginary parts of each phase and unless a very limited training data base is sufficient to guarantee accurate results, the training process could be very time consuming.

A different paper published in 1996 addressed the problem of DP coordination. Coordination rules for zones II and III of different relay pairs were described based on the impedances of adjacent lines. These rules were used to derive several coordination properties, which together were implemented into a program for automatic coordination testing of the whole network [98]. This approach allows faster testing of possible DP coordination issues across larger power systems, but this can only partially decrease the issues of the typical DP.

Later, in 1997, a different setting strategy for DP close to multiple power generation units with a probabilistic approach was presented. First, using simulation results, the apparent impedance is calculated in case of fault at the end of the next line with a nominal or average number of active generators and their generation profiles. Then the same fault simulation and impedance calculation is repeated with only one generation unit being active. After that, the fault simulation with nominal or average generation, except disconnection of one generator in one of the source branches, is repeated for all generation branches between both lines and the difference of apparent impedance compared with nominal generation is calculated, creating a

sensitivity matrix. This sensitivity matrix was then combined with statistical data on generation profiles and fault probabilities to obtain the probability of different changes in apparent impedance due to current infeed from generation units. This, in turn, combined with CT, VT errors, provides an opportunity to calculate the probability that the relay will obtain a particular apparent impedance value for faults in the next line. These probabilities can then be used to calculate the probability that the DP will ensure necessary operation or restraint for an unwanted operation, and if both requirements cannot be met simultaneously it is proposed to use smaller coordination time intervals to ensure selectivity [99]. This method does provide the opportunity to consider such current infeed and obtain the necessary DP settings with a defined certainty, but this opens the question of the necessary statistic data quantity to have a sufficiently representative data collection. Also, the paper ignored the fault path resistance and with it, the influence of a potential power source at the end of the second line that could shift the probabilities of the apparent impedance.

A 1999 paper proposed combination of digital versions of MHO and reactance type DP, which results in a “bowl”-shaped operation region. The operation region of zones I and II for L-L faults is defined by the variable MHO region of Zone III limited by the reactance relay settings, but Zone III is defined only by the aforementioned MHO characteristic. DP for L-E faults has a more complex operation region, which is a combination of a variable MHO, a ZS reactance relay and a half MHO half straight-line relay. Additionally, the limiting line of the reactance relays is made adaptive with rotation as described in [94]. This relay is said to be easily adapted to different loading and line lengths and it can operate for faults with a higher fault path resistance compared to a simple MHO [100]. This greater coverage of higher resistance faults increases the necessity for power swing blocking and testing of heavy loading conditions to avoid unwanted operations. In addition, the described relay does not seem more practical or easier to implement compared to quadrilateral operation region relays, especially when compared with the solution for L-E faults.

A different 1999 paper presented DP that obtained fault distance and fault path resistance as a result of an optimisation that minimises the difference between measured voltage samples and ones calculated from current measurements based on line differential equations. It was proposed to solve this optimisation problem with a recursive least-square procedure that would reduce the computational burden compared with a previously used classical batch least-square method [101]. This approach represented the remote-end of the line by using the current distribution coefficient, which does not fully represent the influence of the remote-end power system, which is also why the results presented had notable errors. As this fast-operating DP algorithm uses instantaneous values, it might have larger errors in the presence of various current and voltage signal distortions.

An interesting directional element for digital DP was also proposed in 1999. The algorithm first calculates superimposed relay voltages and currents for all phases. Next, they are compared with pre-defined settings for fault detection. Then, three-phase power is calculated, using the same superimposed current and voltage values, and summed for five consecutive samples. As the polarities of the superimposed currents and voltages are opposite for a forward fault, the obtained power will be negative, which is the criterion for the

directional element [102]. This approach is considered to be less affected by parallel line mutual induction and series compensation because it does not use a polarising phase or a symmetrical component quantity that might be significantly affected by such lines.

A paper published in 2000 found a different application of an ANN for the DP as compared to [97]. The idea of the ideal trip or operation region from [95] was used in this paper, but instead of online recalculation of the adaptive operation region and then separate testing of the operation criterion, the ANN uses the last pre-fault power flow measurement and apparent impedance value calculated from fault regime measurements to issue the trip signal. Essentially, after the training, the ANN within itself adapts the operation region and checks if the apparent impedance is within this region [103]. In the paper, a three-source ring network model was used, which provides flexibility for a different system configuration, such as representation of a parallel line. However, besides the amount of training data that ANNs require, there remains the question of selectivity for such adaptive zone solutions.

A different paper from 2000 presented a study of different linear dynamic operators, which were used to define equations for the estimation of relay apparent resistance depending on the difference between measured and calculated current samples. In addition, several parametric resolution techniques were considered: the least-square estimate, the least-square method with a moving data window, the forgetting factor algorithm (which exponentially decreases the influence of older sample points) and the Kalman filter. These were tested with electromagnetic transients in current and voltage signals, frequency deviations, CT saturation, data corruption, harmonic distortions etc. The results were presented as time in which the apparent impedance was within $\pm 5\%$ of the expected value. It was shown that methods based on line differential equations operate faster than DFT and are more resilient against frequency deviations, but they are more susceptible to higher harmonic distortions [104]. This study provides valuable insight in the dynamic response of various DP algorithms and their reliability, but it addresses only the problems of signal processing for DP.

Another version of an adaptive DP based on the ideal trip region from [95] was published in 2001. This paper proposed dividing the operation region into a fixed part and an adaptive one. The fixed part is common for all considered faults whereas the adaptive part is recalculated based on system parameters delivered by a supervisory control and data acquisition (hereafter – SCADA) system. This results in less calculation necessary compared to the original 1994 paper [105]. In case communication with SCADA is lost the fixed part of the operation region remains active, but this DP could fail to operate, or operate with a delay, for faults that should fall within the adaptive part.

A paper from 2006 mentions how DFT suffers both from DC offset and slow operation if a classic full-cycle DFT is used. Faster operation may be achieved with half-cycle DFT, but this approach is less stable. First, the proposed DP detects fault inception based on a modified version of a fault detection index calculated by modal measurement values and line parameters obtained by Clarke transformation. Then, using an initial data window size of $\frac{1}{2}$ or $\frac{1}{4}$ of the cycle, three measurements are made. When three consecutive measurements are available, it is possible to use a DFT with a variable data window size and the recursive DC offset compensation outlined in the paper. After that, with every following measurement, the

window size is increased by one measurement point until the number of available samples corresponds to a full cycle. Then, a DFT with recursive DC offset is used, but the size of the data window remains fixed. Taking into account that the initial data window of $\frac{1}{4}$ of the cycle will obtain phasor values faster but with an increased error, the reach for the DP algorithm with this window size is restricted to 65 % of the line. Also, it is used in parallel to the algorithm that implements an initial window size of $\frac{1}{2}$ cycle and has a setting of 80 % of the line [106]. The described DP had faster and more precise operation than the classic full- or half-cycle DFT with mimic circuits, but it only considered faults with a low fault path resistance and ignored other difficulties the DFT algorithms face (frequency deviations, subharmonic distortions etc.).

A different paper from 2006 presented a DP algorithm based on the Monte-Carlo method. The algorithm does not use calculated impedance, but instead calculates the apparent power at the fault point. As the fault is resistive in nature, it is possible to define a boundary condition function that states that the reactive power of the fault must be zero, which was shown to depend on the fault distance and remote-end impedance. Instead of directly calculating the fault distance from this condition with some fixed remote-end impedance value, the described algorithm performs Monte-Carlo simulations assuming normal distribution of remote-end impedance. Then, it calculates the corresponding fault distances, and resistances and compares them and the assumed impedances to physical limitations, saving only the results that correspond to physical limitations and the defined boundary condition. The operation of DP is based on the estimated fault distance, resistance and their standard deviation [107]. This approach provides flexible means to consider remote-end infeed and measurement errors, but it requires a significant number of simulated trials resulting in a heavy computational burden. This algorithm resulted in decreased errors and dispersion of apparent impedances (compared to the conventional algorithm) for various simulated pre-fault and fault cases, but the algorithm could not completely eliminate them as the remote-end EMF was not taken into consideration.

A 2011 paper used probability theory to define the optimal reach of a conventional DP algorithm similarly to [99]. As the main problems of the DP are loss of sensitivity (no operation for faults within set reach) and loss of selectivity (operation for faults beyond the set reach), the authors of the paper propose minimising the function that is a sum of the probabilities of loss of selectivity and sensitivity weighted by a priority coefficient (the importance of selectivity over sensitivity). Both probabilities are functions of chosen resistance and reactance settings, known system parameters and several random parameters. Here, the probabilities of various random parameters (fault distance, resistance, measurement error etc.) are considered by known or assumed distributions. For each setting, they are calculated as sums of probabilities for faults that result in either loss of selectivity or loss of sensitivity, which are in turn determined as the product of the probabilities of each random parameter describing the particular fault case since these parameters are considered independent [108]. This approach provides a quantitative way to evaluate the DP performance and determine the optimal DP settings, considering both selectivity and sensitivity simultaneously and the random nature of several parameters. However, obtaining or assuming

adequate probability distributions for these parameters may be difficult and it is possible that lower probability of loss of sensitivity may be acquired by retaining minimal probability of loss of selectivity, if the option of smaller coordination time intervals were considered.

Several papers have been dedicated to the determination of fault path resistance using two-terminal measurements. This is done in order to either improve the DP settings by analysis of real fault recordings and determination of the probabilities of various fault path resistance values [109], [110] or subtract the estimated resistance from the apparent impedance [111]. The obtained data about fault path resistance values may be useful for the development or setting of one-terminal-measurement-based DP methods, but if reliable communications between substations are available, the differential protection may be more effective.

In 2015, a paper dedicated to earth fault DP on parallel OHTLs was published considering both L-E fault and cross-country faults that are L-L-E faults with one faulted phase in each line. The fault distance is calculated based on the consideration that the phasors of voltage and current symmetrical components have the same angle and known current distribution coefficients. Additionally, a parallel line ZS compensation is described in case the actual measurements from the parallel line are not available. For cross-country faults, a similar approach is used but in terms of six-sequence components: PS, NS and ZS for forward and reverse directions (forward current components have the same direction in parallel lines, reverse ones are opposite) [112]. The assumption used in the paper that current distribution coefficients are real numbers only applies if the equivalent system impedances are ignored. The proposed DP for cross-country faults requires additional calculations to distinguish the correct fault distance from two roots and it determines accurate distance values only for fault path resistances up to 10 Ω . A similar DP task was also discussed for untransposed lines in a 2016 paper, but in this paper, instead of current distribution coefficients and six-sequence components, a matrix with precise self- and mutual impedances and measurements from both lines was used [113]. As the current distribution coefficients are replaced only with the particular impedances of the line, the impact of various power system regimes might have an influence on the accuracy of this algorithm.

Another probabilistic approach to DP setting was discussed in a 2015 paper. In this paper, the probability of a particular fault distance determined by the relay is assumed to be a Gaussian function of the fault distance determined by the relay, the actual fault distance and the standard deviation of the error of the fault distance determined by the relay under various fault scenarios. Assuming uniform probability density of possible fault distances, it is possible to determine the probabilities of a correct trip and restraint (sensitivity and selectivity) by integration of the Gaussian function. Zone I is set so that the probability of a correct trip is maximal while the probability of correct restraint to trip is 1. Zone II is set so that the probability of a correct trip is 1 for the whole of the first line, there is no overlap with Zone II of the next line DP and the probability of a correct restraint is maximal. Zone III is set so that the probability of a correct trip is 1 for the first line and the longest next line [114]. The setting rules for Zone III should include at least coordination with Zone III of the next line.

Additionally, the determination of the standard deviation value for errors of the DP algorithm for the Gaussian function might be complicated.

A different paper from 2015 described a FL algorithm that could be directly applied to DP as well. By multiplying the fault loop voltage equation by conjugated value of the fault current and considering only imaginary parts, it was possible to remove the necessity to consider fault path resistance. Then the obtained equation was modified to create an iterative solution for accurate fault loop reactance and resistance calculation, using one-terminal phase quantity measurements and the fault distance estimate from the previous step to recalculate the current distribution coefficients and load decoupled compensation current. For asymmetrical faults, this current was the NS or ZS current component whereas for three-phase faults superimposed phase current was used [115]. This method requires a communication network, but, as it is used only to acquire updated remote-end power system impedance, measurement synchronisation is not a necessity.

A paper from 2018 described typical methods for blocking DP in case of power swings, the most common being limitation of time in which the apparent impedance locus must travel between special concentric outer impedance zones and control of phase shift angle between current and voltage, which fluctuate significantly during power swings. The method proposed in this paper is for unblocking DP in case a fault has occurred during the power swing. The fault occurrence is detected by sudden change in the frequency composition of the current waveform. In order to achieve this, the Fisher asymmetry coefficient is used for one cycle of absolute instantaneous current values. The value of this coefficient must exceed the maximum value possible in case of a power swing for unblocking to be performed [116]. In some cases, if the fault occurs near the electrical centre, this method cannot distinguish the fault from a power swing. Development of better DP blocking methods and possible correct operation of DP during power swings remain topical subjects for research to this day [117], [118].

From the foregoing analysis, it can be seen that most of the DP research has been more oriented towards various implementations of DP itself in electromechanical, electronic or digital devices, obtaining new operation regions to better cover potential values of the apparent impedance and different signal processing techniques and approaches to achieve cheaper and more compact DP relaying for both phase and earth faults. Starting from 1977, DP with online adaptation to pre-fault loading was introduced to ensure sensitivity for DP being one of few approaches that extends the model implemented in the DP relay itself outside the controlled substation, but these methods do present an increased risk for loss of selectivity due to extended operation regions and their rotation. This can be partially evaluated and minimised by using probabilistic approaches to the setting of the DP, but these require adequate probability distributions of various random fault parameters and usually do not consider the adaptive operation zones. One implementation of the TW method for DP was found, but the accuracy of this approach may be reduced by reflections from several close generation sources and the cross-correlation function used had a small sensitivity reserve in case of L-E faults. This illustrates that compared to FL the creators of DP applications have paid even less attention to compensations of problems caused by the limited scope of measurement data and have been more interested in adapting the operation criterion to these

drawbacks, which only partially can be attributed to high-speed operation requirement. The only DP methods found that attempted to better account for remote-end infeed was a Monte-Carlo approach similar to the one from FL analysis and a simple parameter estimation algorithm that minimised the difference between the measured voltage and the voltage drop obtained from the relay current and a replica impedance [101]. Both methods used current distribution coefficients, but the Monte-Carlo approach allowed flexibility of remote-end impedance by using probability distribution instead of exact value. The parameter estimation approach allowed more adaptability as it aimed to estimate not only the fault distance, but also the fault path resistance and used optimisation instead of directly applied equations. The parameter estimation approach might be more robust and accurate if a wider scope of one substation measurements were used, as it is done for the proposed method, and at least the remote-end EMF were considered.

2.3. Existing adaptive single-pole automatic reclosing methods

As one of the applications of the parameter estimation in this Thesis is ASPAR a brief review of the technical background for this type of power system automation will also be presented.

Wide-spread interest and development of ASPAR can be observed since the 1990s. Several ASPAR methods were provided in [119], starting from the use of the absolute value of faulted phase voltage. It is shown that depending on the compensation of PS capacitance with shunt reactors, the faulted phase voltage would reach about 0.5–1.0 p.u. if the compensation coefficient was above 0.7 p.u. after the complete deionisation of the arc channel. This value is significantly higher than during the arcing process and provides a sufficient difference to ensure sensitivity, but such an approach would be unsuitable when the line is uncompensated or the compensation coefficient is below 0.7 p.u. For uncompensated lines, a different approach is needed; one possible proposed solution is to use the angle between the faulted phase voltage and the ZS current, which would decrease after the extinction of the fault arc [119]. However, the setting chosen is driven by a hard compromise and would in most cases be between the angle values when the arc is present and the one when the arc has been quenched. Therefore, an additional delay would be required not only after arc extinction to ensure full deionisation of the arc channel, but also between operation and actual arc extinction. The third method discussed in [119] is to control the period of the faulted phase voltage signal and it is proposed for cases with a partial compensation of line capacitance (up to 0.6 p.u.). The idea behind this approach is that when the arc is extinguished, a free voltage component with a lower frequency (defined by the number of the capacitance-shunt reactor circuits) will be present and by applying superposition it was calculated that the resulting faulted phase voltage frequency could be 0.5–0.94 p.u. of the fundamental one depending on the compensation level. However, the decrease process of the measured faulted phase voltage frequency often has fluctuations, which may lead to a premature or delayed determination of arc extinction. Another approach was proposed in [120], where the time of arc extinction was determined by comparing a measured voltage

signal with a modelled voltage sine signal with a DC offset. However, in order to evaluate the difference of the voltage signal introduced by higher-harmonic distortions, the ASPAR device would require a high sampling frequency and some additional voltage waveform distortions can be expected that are caused by the transient process triggered by the arc extinction. An approach using ANNs for ASPAR is known, where the DC component and the 1st–4th harmonic components of recordings were used to train the ANN to recognise the moment when a full deionisation has occurred [121]. ANNs require recordings for training and they are not guaranteed to be universal, meaning that different sets of training data might be necessary for different power systems. Another method recognises the moment when the arc is extinguished by an abrupt change in the faulted phase voltage root mean square (hereafter – RMS) value calculated over a running window [122]. This method considers disconnection of the healthy phases to quench the secondary arc, which may adversely affect the system stability and the presence of a sufficiently abrupt change of this RMS value should be tested for different fault and line loading conditions. The next method identifies two events of a voltage drop (the outset of the fault and the disconnection of the CBs) followed by a voltage increase at the moment when the secondary arc has been quenched [123]. This approach may fail if the fault is located close to the substation and with a small fault path resistance, because after the disconnection of the CBs the voltage drop would be insignificant or the algorithm would determine an increase in voltage because of the overvoltage wave after the fault disconnection. A method that detects the presence of a voltage DC component to determine the moment when the fault arc has been extinguished is known [124]. A significant DC component surge is also present during the transient after the disconnection of the CBs and that requires an additional delay in order to prevent undesirable, premature operation of SPAR. A method implementing the Karrenbauer transformation in matrix form is also known, which is used to determine the change in the oscillation frequencies of the line-side voltage when the fault arc is extinguished [125]. Another method considers a sudden rise of second- and fourth-harmonic content in the current of the shunt reactor [126]. These methods are suitable only for lines with a high degree of compensation.

2.4. Conclusions

1. Measurements from both terminals of the line provide opportunities for fast and accurate FL but their operation can be critically affected in case of loss of communication between substations or loss of synchronisation of these measurements.
2. Existing FL methods using one-terminal measurements operate with a limited scope of available information and try to create algorithms that are independent from the influence of the remote-end power system such as TW methods, or to approximate this influence or errors caused by it using methods such as ANN and Monte-Carlo. The TW methods can be affected by different wave distortions, additional reflections and they require a high sampling frequency, but the methods that try to approximate the remote-end influence often introduce significant model simplifications and sometimes completely ignore pre-fault loading or require a large amount of fault data, or presents a significant computational burden.

3. Most of the research on DP was more oriented towards various implementations of the DP itself in electromechanical, electronic or digital devices, obtaining new operation regions to better cover potential values of the apparent impedance and different signal processing techniques and approaches to achieve cheaper and more compact DP relaying for both phase and earth faults.
4. The loss of sensitivity due to the remote-end infeed can be partially compensated with adaptive DP operation regions, but this increases the risk of loss of selectivity. Both sensitivity and selectivity can be simultaneously optimised, considering the drawbacks of the DP using probabilistic approaches, but these do not guarantee certainty for both of the criteria as it does not solve the original drawbacks of the DP but only minimises their influence and the probability distributions of apparent impedance errors can be difficult to obtain.
5. Some of the existing ASPAR methods control changes in the value of faulted phase voltage or try to detect the presence of either voltage signal distortions or DC offset. Others are developed specifically for lines with shunt reactors and these methods operate based on resulting higher-harmonic components of either voltage or current signals. Most of these ignore the influence of healthy-phase power flow or they are highly dependent on accurate measurements of higher-harmonic components or DC offset, requiring a higher sampling frequency and resulting in more expensive devices.

3. MODELLING OF ASYMMETRICAL REGIMES OF A POWER SYSTEM

As mentioned before in the introduction most of the OHTL faults are asymmetrical with L-E short circuits being the most common. The method of symmetrical components is widely used to calculate steady-state parameters for these faults [59]–[62], [127], which is also necessary for the proposed method. These faults require special equivalent circuits and in some cases even modified calculation processes.

3.1. A single transverse asymmetry

First, a single transverse asymmetry or shunt faults can be discussed. These regimes of the power system are caused by either short circuits or asymmetrical load of the phases. Therefore, power system points where such an asymmetry is present can in general be represented with different phase shunt impedances ($\dot{Z}_{KA}, \dot{Z}_{KB}, \dot{Z}_{KC}$) and a common neutral impedance to earth, \dot{Z}_{KN} (Fig. 3.1).

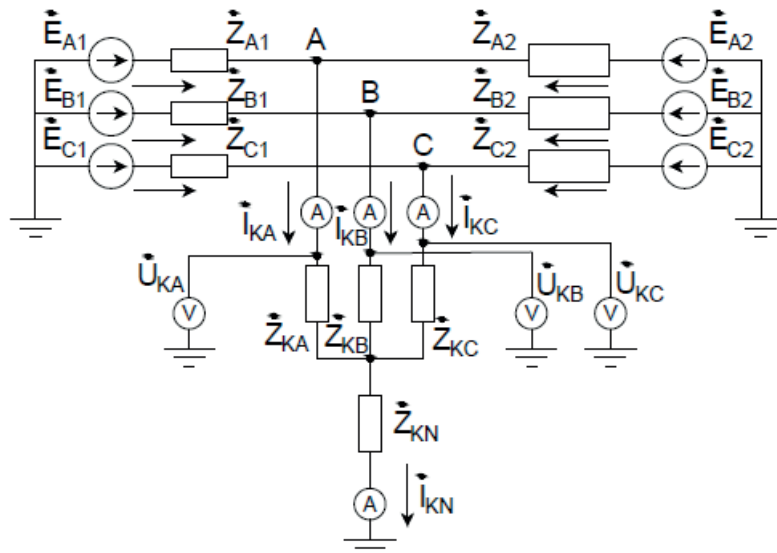


Fig. 3.1. The equivalent circuit of a single transverse asymmetry between two power systems in phase coordinates.

The asymmetry present in the power system is usually described separately from the rest of the power system, which is considered symmetrical, and the solution to the regime calculation problem is obtained by a unification of equations describing the symmetrical and asymmetrical parts of the whole power system or by interconnecting the sequence networks of the symmetrical part of the system according to the particular type of asymmetry. The hardest to describe and to calculate is the regime of the general asymmetry when all of the phase impedances are different ($0 \leq \dot{Z}_{KA} \neq \dot{Z}_{KB} \neq \dot{Z}_{KC} < \infty \Omega$). This particular case is difficult because the complex equivalent circuit of this regime cannot be created with electrical interconnections between sequence networks but instead it must use ideal transformers with complex transformation ratios defined by operators: $\dot{a} = e^{i120^\circ}$ $\dot{a}^2 = e^{-i120^\circ}$ (see Fig. 3.2

where K1, K2 and K0 represent point of transverse asymmetry and N1, N2 and N0 represent neutral of sequence networks).

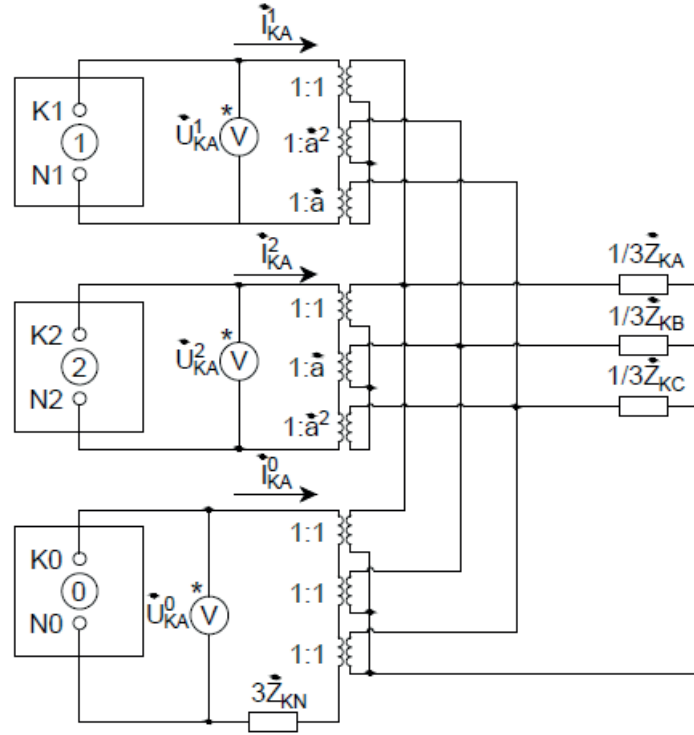


Fig. 3.2. The complex equivalent circuit of a general single transverse asymmetry in symmetrical component coordinates.

The problem here is that the ideal transformers are defined as lossless, without the magnetic leakage and with infinite inductance, which is hard to accurately represent in both a physical model and a numerical one [128], [129]. Therefore, it is suggested that the general equation system should be used, which allows calculating the symmetrical components of the special phase voltage based on impedances \dot{Z}_{KA} , \dot{Z}_{KB} , \dot{Z}_{KC} in combination with a simultaneous numerical regime calculation of separate sequence networks of the symmetrical part of the power system. In cases where these sequence networks are small, it is also possible to use matrix solutions with Thevenin's equivalents of the sequence networks. In order to use any of these approaches, the general equation system must be defined. This is achieved by first expressing the symmetrical components of the special phase (here, Phase A) from the phase voltages of the fault:

$$\begin{cases} \dot{U}_{KA}^1 = \frac{1}{3}(\dot{U}_{KA} + a\dot{U}_{KB} + a^2\dot{U}_{KC}), \\ \dot{U}_{KA}^2 = \frac{1}{3}(\dot{U}_{KA} + a^2\dot{U}_{KB} + a\dot{U}_{KC}), \\ \dot{U}_{KA}^0 = \frac{1}{3}(\dot{U}_{KA} + \dot{U}_{KB} + \dot{U}_{KC}), \end{cases} \quad (3.1)$$

where \dot{U}_{KA}^1 , \dot{U}_{KA}^2 , \dot{U}_{KA}^0 – phasors of PS, NS and ZS quantities of Phase A voltage at the fault point, V;

\dot{U}_{KA} , \dot{U}_{KB} , \dot{U}_{KC} – phasors of Phase A, Phase B and Phase C voltages at the fault point, V.

Simultaneously, these fault voltages can be defined by voltage drops across fault impedances:

$$\begin{cases} \dot{U}_{KA} = \dot{I}_{KA}\dot{Z}_{KA} + \dot{I}_{KN}\dot{Z}_{KN}, \\ \dot{U}_{KB} = \dot{I}_{KB}\dot{Z}_{KB} + \dot{I}_{KN}\dot{Z}_{KN}, \\ \dot{U}_{KC} = \dot{I}_{KC}\dot{Z}_{KC} + \dot{I}_{KN}\dot{Z}_{KN}, \end{cases} \quad (3.2)$$

where $\dot{I}_{KA}, \dot{I}_{KB}, \dot{I}_{KC}$ – phasors of Phase A, Phase B and Phase C fault currents, A;

\dot{I}_{KN} – the phasor of the neutral current at the fault point, A;

$\dot{Z}_{KA}, \dot{Z}_{KB}, \dot{Z}_{KC}$ – fault impedances of Phase A, Phase B and Phase C, Ω ;

\dot{Z}_{KN} – the neutral impedance at the fault point, Ω .

By substitution of the phase voltages of the fault from (3.2) into (3.1), further substitution of the phase currents of the fault with the symmetrical components analogically to (3.1) and substitution

$$\dot{I}_{KN} = \dot{I}_{KA} + \dot{I}_{KB} + \dot{I}_{KC} = 3\dot{i}_{KA}^0, \quad (3.3)$$

it is possible to obtain an equation system that links the symmetrical components of the special phase fault voltage to the symmetrical components of the special phase fault current only by the fault path impedances of the phases and the common neutral:

$$\begin{cases} \dot{U}_{KA}^1 = \frac{1}{3}[\dot{i}_{KA}^1(\dot{Z}_{KA} + \dot{Z}_{KB} + \dot{Z}_{KC}) + \dot{i}_{KA}^2(\dot{Z}_{KA} + \dot{a}^2\dot{Z}_{KB} + \dot{a}\dot{Z}_{KC}) \\ \dot{U}_{KA}^2 = \frac{1}{3}[\dot{i}_{KA}^1(\dot{Z}_{KA} + \dot{a}\dot{Z}_{KB} + \dot{a}^2\dot{Z}_{KC}) + \dot{i}_{KA}^2(\dot{Z}_{KA} + \dot{Z}_{KB} + \dot{Z}_{KC}) \\ \dot{U}_{KA}^0 = \frac{1}{3}[\dot{i}_{KA}^1(\dot{Z}_{KA} + \dot{a}^2\dot{Z}_{KB} + \dot{a}\dot{Z}_{KC}) + \dot{i}_{KA}^2(\dot{Z}_{KA} + \dot{a}\dot{Z}_{KB} + \dot{a}^2\dot{Z}_{KC}) \\ \quad + \dot{i}_{KA}^0(\dot{Z}_{KA} + \dot{a}\dot{Z}_{KB} + \dot{a}^2\dot{Z}_{KC})], \\ \quad + \dot{i}_{KA}^0(\dot{Z}_{KA} + \dot{a}^2\dot{Z}_{KB} + \dot{a}\dot{Z}_{KC})], \\ \quad + \dot{i}_{KA}^0(\dot{Z}_{KA} + \dot{Z}_{KB} + \dot{Z}_{KC} + 9\dot{Z}_{KN})], \end{cases} \quad (3.4)$$

where $\dot{i}_{KA}^1, \dot{i}_{KA}^2, \dot{i}_{KA}^0$ – phasors of PS, NS and ZS quantities of Phase A current at the fault point, A.

The equation system (3.4) can now be used in combination with separate sequence networks (similarly to [130]) by representing the symmetrical components of the fault point voltage $\dot{U}_{KA}^1, \dot{U}_{KA}^2, \dot{U}_{KA}^0$ shown in Fig. 3.2 with EMF sources. These sources are updated during a sequential numerical calculations of separate sequence networks using the sequence current obtained in the approximation step $k + 1$ and other two sequence current values obtained in the previous approximation steps k and $k - 1$ (for example: the EMF source for the PS network regime calculation of the approximation step $k + 2$ $\dot{U}_{KA}^{1\ k+2}$ is obtained from the symmetrical components of fault current: $\dot{i}_{KA}^{0\ k+1}, \dot{i}_{KA}^{2\ k}, \dot{i}_{KA}^{1\ k-1}$). As mentioned before, if sequence networks are simple, an analytical matrix solution can be used. This approach requires the sequence networks to be transformed into Thevenin's equivalents with EMFs $\dot{E}_{K\Sigma}^1, \dot{E}_{K\Sigma}^2, \dot{E}_{K\Sigma}^0$ and impedances $\dot{Z}_{K\Sigma}^1, \dot{Z}_{K\Sigma}^2, \dot{Z}_{K\Sigma}^0$ of the special phase. Taking into an account that typically $\dot{E}_{K\Sigma}^2 = \dot{E}_{K\Sigma}^0 = 0$ V it is possible to show the sequence networks with the Thevenin's equivalents and EMF sources representing the symmetrical components of the fault point voltage (Fig. 3.3).

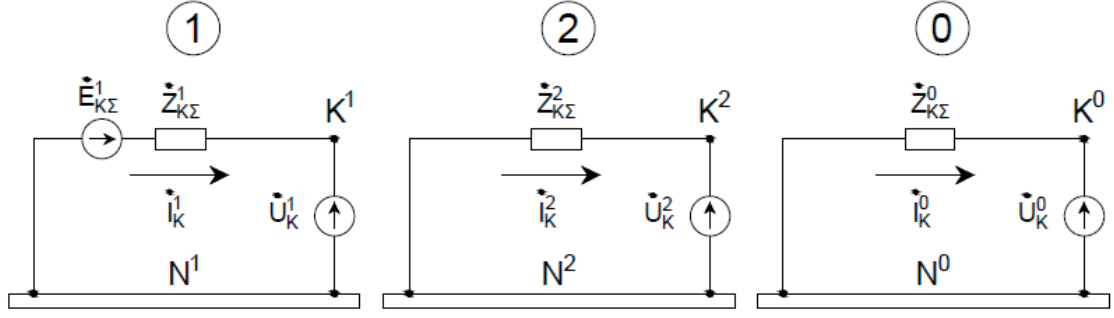


Fig. 3.3. The Thevenin's equivalents of sequence networks representing the symmetrical part of the power system and EMF sources representing the transverse asymmetry.

These sequence networks provide the equations that link the symmetrical part and the asymmetrical part of the power system:

$$\begin{cases} \dot{U}_{KA}^1 = \dot{E}_{KA\Sigma}^1 - i_{KA}^1 \dot{Z}_{K\Sigma}^1, \\ \dot{U}_{KA}^2 = 0 - i_{KA}^2 \dot{Z}_{K\Sigma}^2, \\ \dot{U}_{KA}^0 = 0 - i_{KA}^0 \dot{Z}_{K\Sigma}^0, \end{cases} \quad (3.5)$$

where $\dot{E}_{K\Sigma}^1$ – the phasor of the EMF of the Thevenin's equivalent of the PS network, V;

$\dot{Z}_{K\Sigma}^1, \dot{Z}_{K\Sigma}^2, \dot{Z}_{K\Sigma}^0$ – impedances of Thevenin's equivalents of PS, NS, ZS networks, Ω .

It is possible to obtain the equation system for calculation of symmetrical components of fault current by combining equations (3.4) and (3.5):

$$A_K \mathbf{I}_K^S = \mathbf{E}_K, \quad (3.6)$$

where \mathbf{I}_K^S – the vector of the symmetrical components of the fault current of the special or calculation phase, A;

\mathbf{E}_K – the vector of the EMFs of the Thevenin's equivalents, V;

A_K – a coefficient matrix defined by both fault path impedances and impedances of the Thevenin's equivalents, Ω .

The vectors and the matrix used in (3.6) can be presented as follows:

$$\mathbf{I}_K^S = \begin{bmatrix} i_{KA}^1 \\ i_{KA}^2 \\ i_{KA}^0 \end{bmatrix}, \quad (3.7)$$

$$\mathbf{E}_K = \begin{bmatrix} \dot{E}_{KA\Sigma}^1 \\ \dot{E}_{KA\Sigma}^2 \\ \dot{E}_{KA\Sigma}^0 \end{bmatrix}, \text{ typically } \begin{bmatrix} \dot{E}_{KA\Sigma}^1 \\ 0 \\ 0 \end{bmatrix}, \quad (3.8)$$

$$A_K = \frac{1}{3} \begin{bmatrix} \dot{Z}_{KABC1} + 3\dot{Z}_{K\Sigma}^1 & \dot{Z}_{KABC3} & \dot{Z}_{KABC2} \\ \dot{Z}_{KABC2} & \dot{Z}_{KABC1} + 3\dot{Z}_{K\Sigma}^2 & \dot{Z}_{KABC3} \\ \dot{Z}_{KABC3} & \dot{Z}_{KABC2} & \dot{Z}_{KABC1} + 3\dot{Z}_{K\Sigma}^0 + 9\dot{Z}_{KN} \end{bmatrix}, \quad (3.9)$$

where $\dot{Z}_{KABC1}, \dot{Z}_{KABC2}, \dot{Z}_{KABC3}$ – combinations of the fault path impedances ($\dot{Z}_{KABC1} = \dot{Z}_{KA} + \dot{Z}_{KB} + \dot{Z}_{KC}$, $\dot{Z}_{KABC2} = \dot{Z}_{KA} + a\dot{Z}_{KB} + a^2\dot{Z}_{KC}$, $\dot{Z}_{KABC3} = \dot{Z}_{KA} + a^2\dot{Z}_{KB} + a\dot{Z}_{KC}$), Ω .

When the calculation of the Thevenin's equivalents of the symmetrical part of the power system is reasonably easy, either the equation system (3.6) with modifications of matrix (3.9)

or other equations for particular fault types can be used. They provide the symmetrical components of the current and voltage of the special phase with the help of (3.5). However, if currents or voltages in other parts of the power system are required, additional calculations are necessary.

In cases when the fault path impedances of at least two phases are equal, it is possible to use a complex equivalent circuit of electrically interconnected sequence networks to obtain the symmetrical components of currents and voltages of the whole system with one calculation of a network regime. This allows to accommodate the extended measurement scope for the proposed method and adapt it to different network configurations. One of such cases is an asymmetrical load or a three-phase short circuit with equal fault path impedances in two phases. As an example, a case with a shunt asymmetry between two systems S1 and S2 where Phase B and Phase C impedances are equal ($0 \leq \dot{Z}_{KA} \neq \dot{Z}_{KB} = \dot{Z}_{KC} < \infty \Omega$) can be considered (Fig. 3.4). In this particular case, the special or calculation phase is Phase A and the complex equivalent circuit would provide the symmetrical components of this phase. It can also be noted that this complex equivalent circuit can be easily modified to fit different three-phase fault types by modifying the fault path impedances or removing network of a particular sequence entirely in cases such as short circuits without contact with earth $\dot{Z}_{KN} = \infty \Omega$. One such modification can be shown for an L-L-E short circuit, which has a total fault path impedance $0 \leq \dot{Z}_F < \infty \Omega$ between the faulted phases, but the third phase remains healthy (Fig. 3.5).

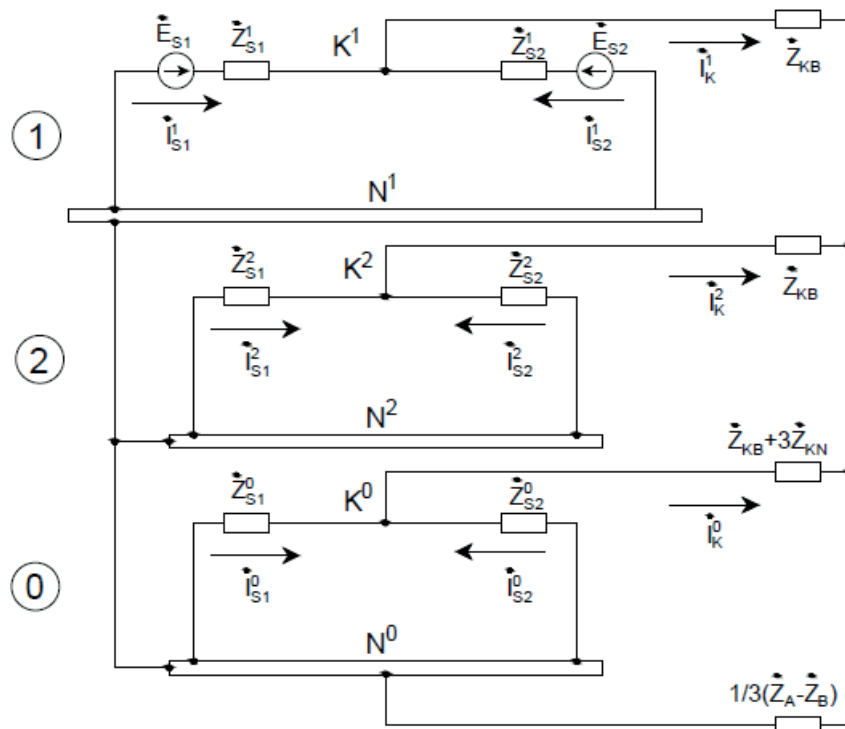


Fig. 3.4. The complex equivalent circuit for a three-phase short circuit or an asymmetrical load with identical impedances in Phase B and C.

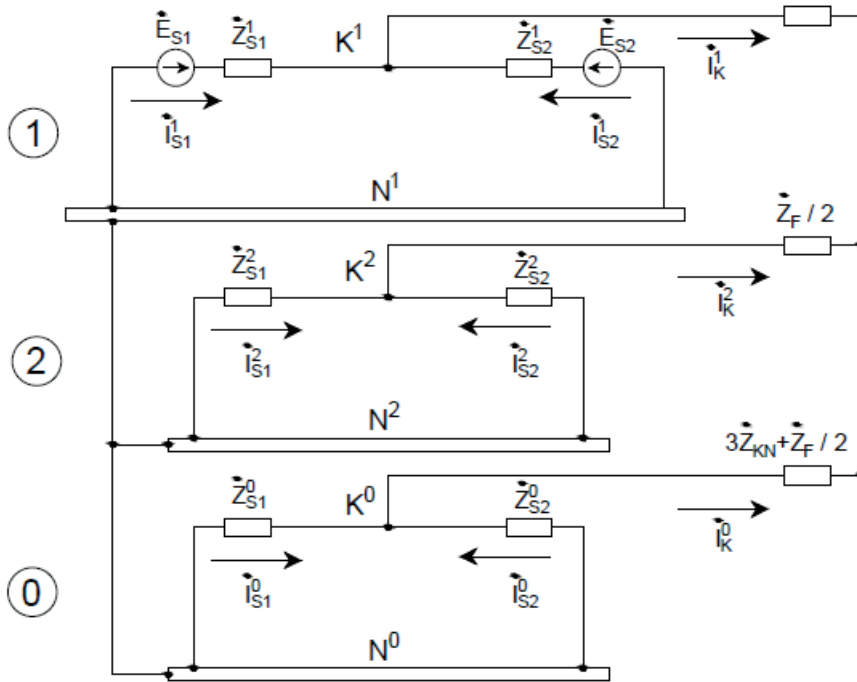


Fig. 3.5. The complex equivalent circuit for an L-L short circuit to earth with fault path impedance between the faulted phases

One complex equivalent circuit, which cannot be obtained from Fig. 3.4, is the L-E short circuit (for example: $0 \leq \dot{Z}_{KA} < \infty \Omega$, $\dot{Z}_{KB} = \dot{Z}_{KC} = \infty \Omega$, $\dot{Z}_{KN} = 0 \Omega$), because the boundary conditions ($\dot{I}_{KB} = \dot{I}_{KC} = 0 \text{ A}$) require the sequence networks to be connected in series (Fig. 3.6).

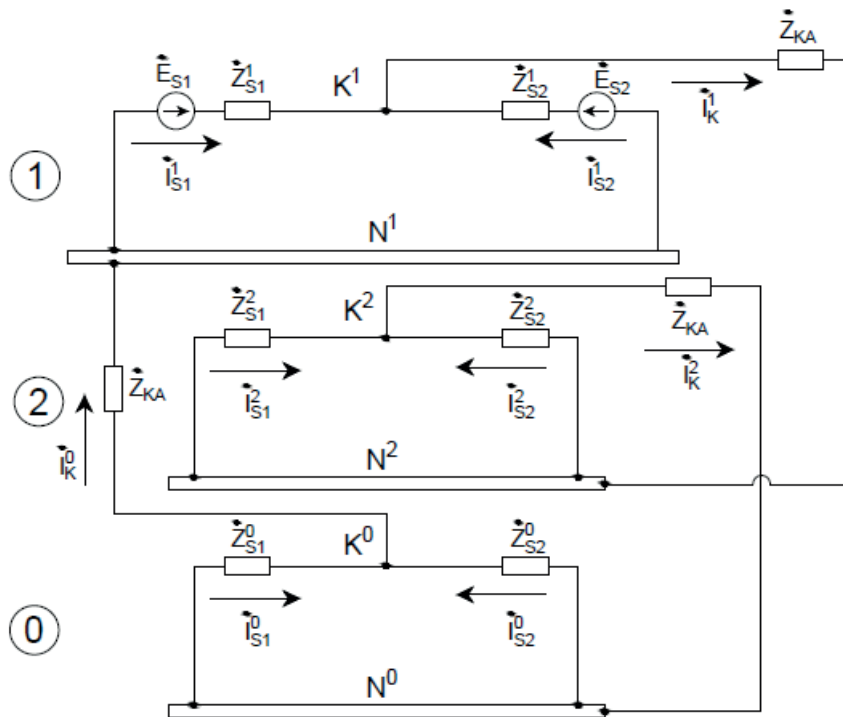


Fig. 3.6. The complex equivalent circuit for an L-E short circuit in Phase A with fault path impedance.

3.2. A single longitudinal asymmetry

Next, a single longitudinal asymmetry or series faults can be discussed. These regimes of the power system are caused by asymmetry of phase series impedances or open-phase faults that can be also used to analyse OHTL operation during AR. This type of asymmetry can be represented by series impedances in phases (Fig. 3.7).

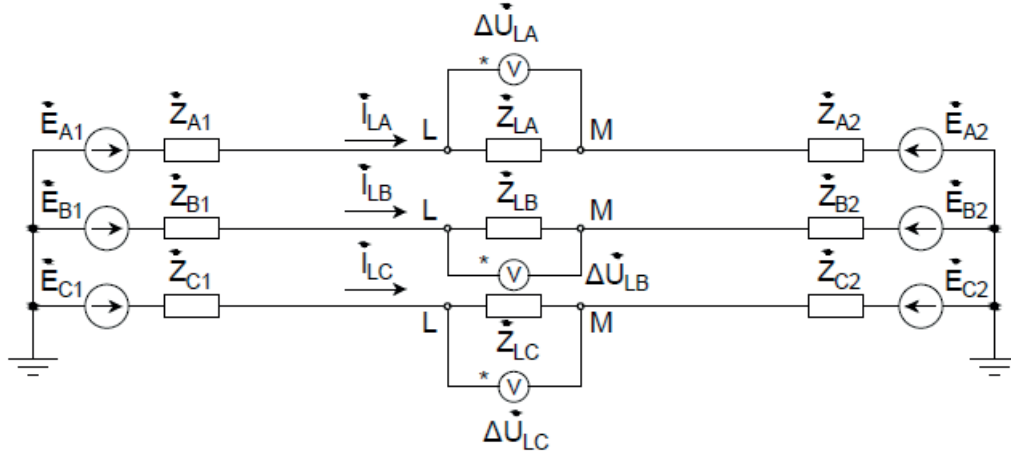


Fig. 3.7. The equivalent circuit of a single longitudinal asymmetry between two power systems in phase coordinates.

Similarly to the transverse asymmetry, general longitudinal asymmetry ($0 \leq \dot{Z}_{LA} \neq \dot{Z}_{LB} \neq \dot{Z}_{LC} < \infty \Omega$) can be theoretically represented with a complex equivalent circuit where sequence networks are interconnected only with ideal transformers (Fig. 3.8).

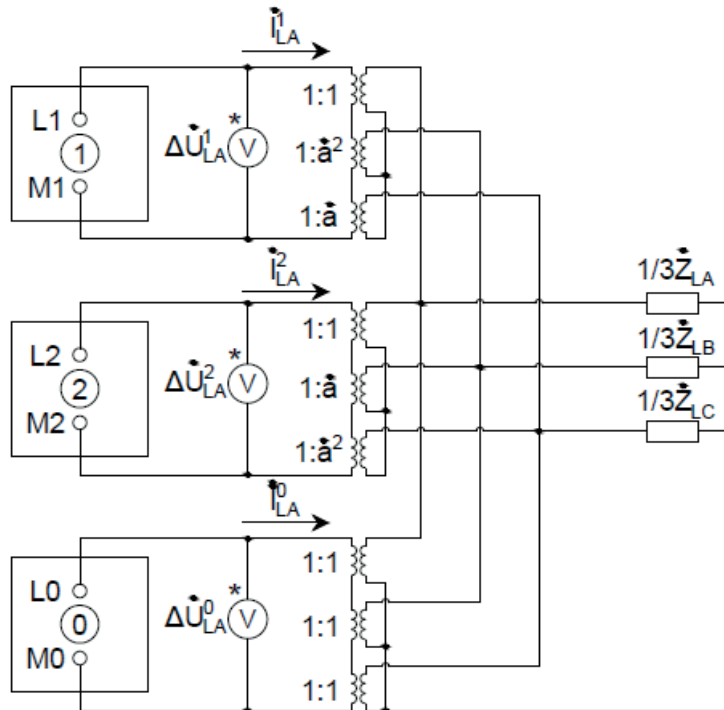


Fig. 3.8. The complex equivalent circuit of a single longitudinal asymmetry in symmetrical component coordinates.

This equivalent circuit, similarly to transverse asymmetry, is more theoretical due to the presence of ideal transformers, and other approaches are advised for practical calculations. As before, it is possible to devise an equation system that describes the asymmetry point, but this time these equations must be made for symmetrical components of the special phase voltage drop across longitudinal impedances. First, these components can be expressed from voltage drops across impedances of different phases:

$$\begin{cases} \Delta\dot{U}_{LA}^1 = \frac{1}{3}(\Delta\dot{U}_{LA} + \dot{a}\Delta\dot{U}_{LB} + \dot{a}^2\Delta\dot{U}_{LC}), \\ \Delta\dot{U}_{LA}^2 = \frac{1}{3}(\Delta\dot{U}_{LA} + \dot{a}^2\Delta\dot{U}_{LB} + \dot{a}\Delta\dot{U}_{LC}), \\ \Delta\dot{U}_{LA}^0 = \frac{1}{3}(\Delta\dot{U}_{LA} + \Delta\dot{U}_{LB} + \Delta\dot{U}_{LC}), \end{cases} \quad (3.10)$$

where $\Delta\dot{U}_{LA}^1, \Delta\dot{U}_{LA}^2, \Delta\dot{U}_{LA}^0$ – phasors of PS, NS and ZS quantities of Phase A voltage drop at the fault point, V;

$\Delta\dot{U}_{LA}, \Delta\dot{U}_{LB}, \Delta\dot{U}_{LC}$ – phasors of Phase A, Phase B and Phase C voltage drops at the fault point, V.

The voltage drops across impedances of different phases can be expressed as follows:

$$\begin{cases} \Delta\dot{U}_{LA} = \dot{I}_{LA}\dot{Z}_{LA}, \\ \Delta\dot{U}_{LB} = \dot{I}_{LB}\dot{Z}_{LB}, \\ \Delta\dot{U}_{LC} = \dot{I}_{LC}\dot{Z}_{LC}, \end{cases} \quad (3.11)$$

where $\dot{I}_{LA}, \dot{I}_{LB}, \dot{I}_{LC}$ – phasors of Phase A, Phase B and Phase C fault currents, A;

$\dot{Z}_{LA}, \dot{Z}_{LB}, \dot{Z}_{LC}$ – fault impedances of Phase A, Phase B and Phase C, Ω .

By substitution of the voltage drops of different phases from (3.11) into (3.10) and further substitution of the phase currents of the fault with the symmetrical components similarly to (3.10), it is possible to obtain an equation system that allows calculating the symmetrical components of the special phase voltage drop from the symmetrical components of the special phase current and the series impedances of different phases:

$$\begin{cases} \Delta\dot{U}_{LA}^1 = \frac{1}{3}[\dot{I}_{LA}^1(\dot{Z}_{LA} + \dot{Z}_{LB} + \dot{Z}_{LC}) + \dot{I}_{LA}^2(\dot{Z}_{LA} + \dot{a}^2\dot{Z}_{LB} + \dot{a}\dot{Z}_{LC}) \\ \Delta\dot{U}_{LA}^2 = \frac{1}{3}[\dot{I}_{LA}^1(\dot{Z}_{LA} + \dot{a}\dot{Z}_{LB} + \dot{a}^2\dot{Z}_{LC}) + \dot{I}_{LA}^2(\dot{Z}_{LA} + \dot{Z}_{LB} + \dot{Z}_{LC}) \\ \Delta\dot{U}_{LA}^0 = \frac{1}{3}[\dot{I}_{LA}^1(\dot{Z}_{LA} + \dot{a}^2\dot{Z}_{LB} + \dot{a}\dot{Z}_{LC}) + \dot{I}_{LA}^2(\dot{Z}_{LA} + \dot{a}\dot{Z}_{LB} + \dot{a}^2\dot{Z}_{LC}) \\ \quad + \dot{I}_{LA}^0(\dot{Z}_{LA} + \dot{a}\dot{Z}_{LB} + \dot{a}^2\dot{Z}_{LC})], \\ \quad + \dot{I}_{LA}^0(\dot{Z}_{LA} + \dot{a}^2\dot{Z}_{LB} + \dot{a}\dot{Z}_{LC})], \\ \quad + \dot{I}_{LA}^0(\dot{Z}_{LA} + \dot{Z}_{LB} + \dot{Z}_{LC})], \end{cases} \quad (3.12)$$

where $\dot{I}_{LA}^1, \dot{I}_{LA}^2, \dot{I}_{LA}^0$ – phasors of PS, NS and ZS quantities of Phase A current at the fault point, A.

The equation system (3.12) can be used with separate sequence networks in a numerical regime calculation process, which constantly updates the values of EMFs in the same manner as described in Section 3.1 after the equation (3.4), but this time the EMF sources will be connected in series with other elements between corresponding points of asymmetry (L1, L2, L0 and M1, M2, M0). It is also possible to obtain Thevenin's equivalents of the sequence

networks for a longitudinal asymmetry by obtaining EMFs $\dot{E}_{L\Sigma}^1, \dot{E}_{L\Sigma}^2, \dot{E}_{L\Sigma}^0$ and impedances $\dot{Z}_{L\Sigma}^1, \dot{Z}_{L\Sigma}^2, \dot{Z}_{L\Sigma}^0$ of the special phase. Taking into an account that typically $\dot{E}_{L\Sigma}^2 = \dot{E}_{L\Sigma}^0 = 0$ V, it is possible to show the Thevenin's equivalents of sequence networks representing the symmetrical part of the network and EMFs between points L1, L2, L0 and M1, M2, M0 equal to symmetrical components of the voltage drop of the special phase representing the asymmetry (Fig. 3.9).

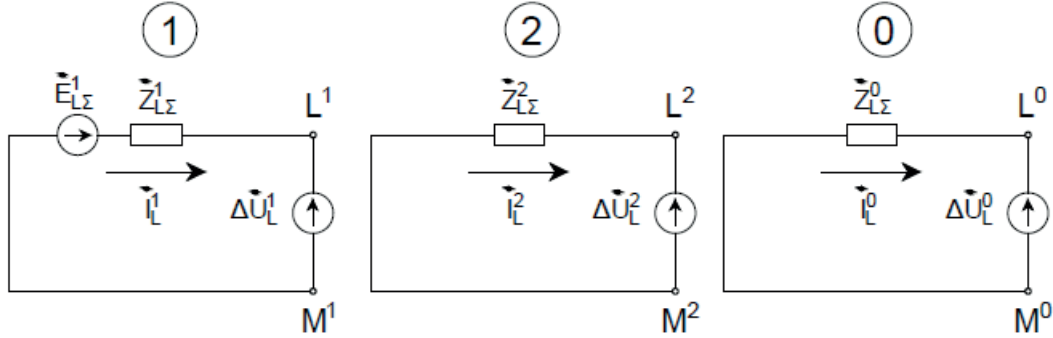


Fig. 3.9. The Thevenin's equivalents of sequence networks representing the symmetrical part of the power system and EMF sources representing the longitudinal asymmetry.

These sequence networks provide the equations that link the symmetrical part and the asymmetrical part of the power system:

$$\begin{cases} \Delta\dot{U}_{LA}^1 = \dot{E}_{LA\Sigma}^1 - \dot{i}_{LA}^1 \dot{Z}_{L\Sigma}^1, \\ \Delta\dot{U}_{LA}^2 = 0 - \dot{i}_{LA}^2 \dot{Z}_{L\Sigma}^2, \\ \Delta\dot{U}_{LA}^0 = 0 - \dot{i}_{LA}^0 \dot{Z}_{L\Sigma}^0, \end{cases} \quad (3.13)$$

where $\dot{E}_{L\Sigma}^1$ – the phasor of the EMF of the Thevenin's equivalent of the PS network, V;

$\dot{Z}_{L\Sigma}^1, \dot{Z}_{L\Sigma}^2, \dot{Z}_{L\Sigma}^0$ – impedances of Thevenin's equivalents of PS, NS, ZS networks, Ω .

It is possible to obtain the equation system for the calculation of the symmetrical components of fault current by combining equations (3.12) and (3.13):

$$A_L \mathbf{I}_L^S = \mathbf{E}_L, \quad (3.14)$$

where \mathbf{I}_L^S – the vector of the symmetrical components of the current of the special or calculation phase, A;

\mathbf{E}_L – the vector of the EMFs of Thevenin's equivalents, V;

A_L – a coefficient matrix defined by the phase impedances and the impedances of Thevenin's equivalents, Ω .

The vectors and the matrix used in (3.14) can be presented as follows:

$$\mathbf{I}_L^S = \begin{bmatrix} \dot{i}_{LA}^1 \\ \dot{i}_{LA}^2 \\ \dot{i}_{LA}^0 \end{bmatrix}, \quad (3.15)$$

$$\mathbf{E}_L = \begin{bmatrix} \dot{E}_{LA\Sigma}^1 \\ \dot{E}_{LA\Sigma}^2 \\ \dot{E}_{LA\Sigma}^0 \end{bmatrix}, \text{ typically } \begin{bmatrix} \dot{E}_{LA\Sigma}^1 \\ 0 \\ 0 \end{bmatrix}, \quad (3.16)$$

$$A_L = \frac{1}{3} \begin{bmatrix} \dot{Z}_{LABC1} + 3\dot{Z}_{L\Sigma}^1 & \dot{Z}_{LABC3} & \dot{Z}_{LABC2} \\ \dot{Z}_{LABC2} & \dot{Z}_{LABC1} + 3\dot{Z}_{L\Sigma}^2 & \dot{Z}_{LABC3} \\ \dot{Z}_{LABC3} & \dot{Z}_{LABC2} & \dot{Z}_{LABC1} + 3\dot{Z}_{L\Sigma}^0 \end{bmatrix}, \quad (3.17)$$

where $\dot{Z}_{LABC1}, \dot{Z}_{LABC2}, \dot{Z}_{LABC3}$ – combinations of the phase impedances ($\dot{Z}_{LABC1} = \dot{Z}_{LA} + \dot{Z}_{LB} + \dot{Z}_{LC}$, $\dot{Z}_{LABC2} = \dot{Z}_{LA} + \dot{a}\dot{Z}_{LB} + \dot{a}^2\dot{Z}_{LC}$, $\dot{Z}_{LABC3} = \dot{Z}_{LA} + \dot{a}^2\dot{Z}_{LB} + \dot{a}\dot{Z}_{LC}$), Ω .

When the calculation of Thevenin's equivalents of the symmetrical part of the power system is not excessively time-consuming, either the equation system (3.16) with modifications of matrix (3.17) or other standardised equations for particular fault types can be used. However, as before in case of one transverse asymmetry, these approaches only provide the symmetrical components of the current and voltage drop of the special phase at the point of asymmetry.

In cases when the series phase impedances of at least two phases are equal, it is possible to use a complex equivalent circuit of electrically interconnected sequence networks to obtain symmetrical components of currents and voltages of the whole system with one calculation of a network regime. One of these cases is when there are two identical phase impedances and one phase where the series impedance differs from the other two (for example: $0 \leq \dot{Z}_{LB} = \dot{Z}_{LC} = \dot{Z}_{LF} < \infty \Omega$, $0 \leq \dot{Z}_{LA} \neq \dot{Z}_{LF} < \infty \Omega$). The complex equivalent circuit for this type is presented in Fig. 3.10. It can be noted that this complex equivalent circuit can be easily modified to fit different longitudinal asymmetry types, for example: by removing the branch $(1/3)(\dot{Z}_{LA} - \dot{Z}_{LF})$, one can obtain the complex equivalent circuit for the one open-phase fault with or without impedances in other phases.

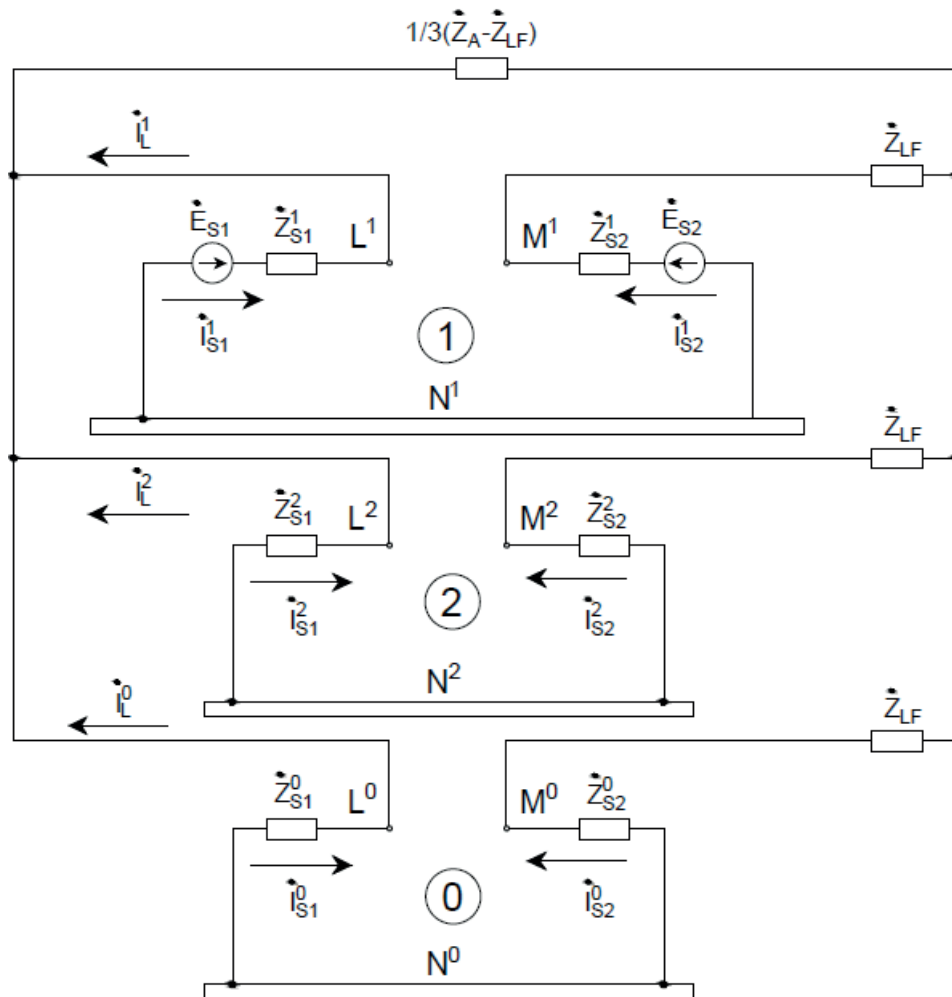


Fig. 3.10. The complex equivalent circuit for a longitudinal asymmetry with identical impedances in Phase B and C.

One complex equivalent circuit, which cannot be obtained from Fig. 3.10, is the two-open-phase fault (for example: $0 \leq \dot{Z}_{LA} = \dot{Z}_{LF} < \infty \Omega$, $\dot{Z}_{LB} = \dot{Z}_{LC} = \infty \Omega$), because the boundary conditions ($\dot{I}_{LB} = \dot{I}_{LC} = 0 \text{ A}$), similarly to L-E short circuit, require the sequence networks to be connected in series (Fig. 3.11). It can be noticed how the asymmetry points, which are used for interconnections of sequence networks, differ for transverse asymmetry (Fig. 3.2–3.6) and longitudinal asymmetry (Fig. 3.8–3.11).

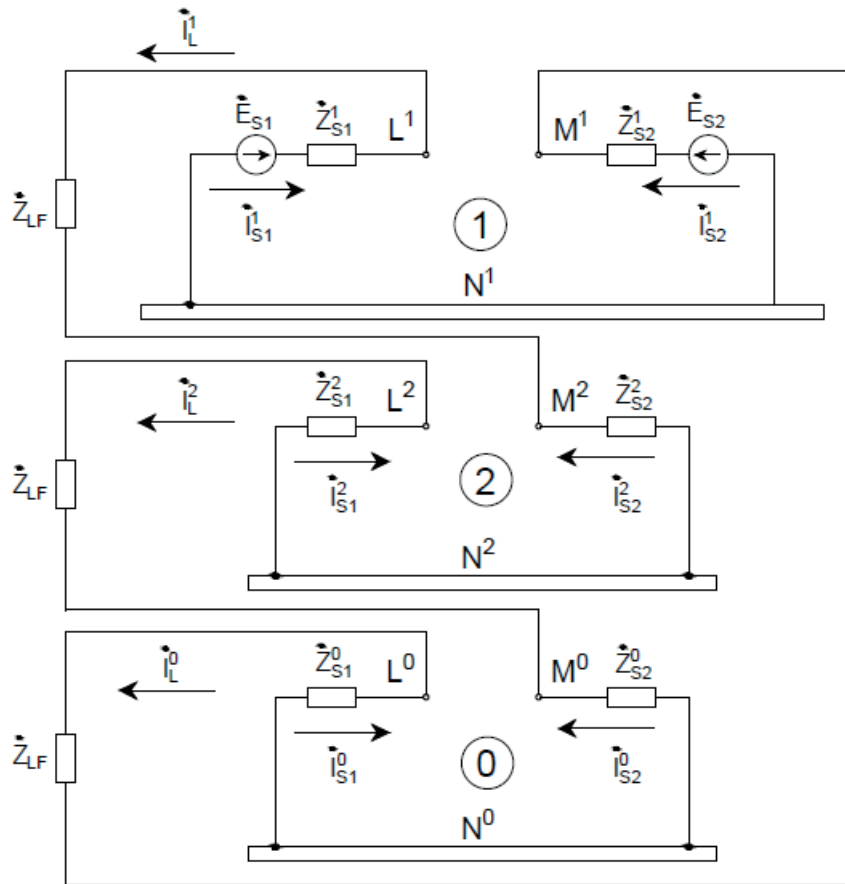


Fig. 3.11. The complex equivalent circuit for two open-phase faults with series impedance in the third phase.

3.3. Multiple simultaneous asymmetries

In most cases, only one asymmetric fault has to be modelled, but there are still regimes of the power system when either multiple asymmetries of the same type or multiple asymmetries of different types are present simultaneously. These regimes often are either short circuits, which have triggered overvoltages that in turn caused other short circuits, combinations of short circuits and open phase “faults”, which are present during the operation of SPAR, and combinations of faults with other asymmetries caused by asymmetrical load, asymmetrical power system elements (for example: different phase resistances of CB contacts due to malfunction) etc. In this Thesis, the main application for the calculation approaches used for simultaneous asymmetries is determination of regime of healthy phases during ASPAR necessary for detailed modelling of the line in phase coordinates (see Chapter 8).

Analytical solutions for these faults are possible and can be achieved in a reasonable time frame if the power system is small and simple. However, even then the equation system for calculation of symmetrical components of currents of faults or asymmetry points will increase by 3 for every additional asymmetry and an additional Thevenin’s equivalent will have to be obtained in respect to the additional asymmetry points to take into account the interaction of multiple asymmetries. As analytical solutions can easily become exceedingly time-consuming and due to various combinations of different asymmetries being possible, only a more general

topological approach will be presented in this Thesis for calculations of power system regimes with multiple simultaneous asymmetries.

In theory, for most of regimes with multiple simultaneous asymmetries it is possible to create one complex equivalent circuit, but only one of the asymmetries can be represented with direct electrical interconnections between sequence networks. The links between sequence networks of other asymmetries have to be represented by ideal transformers (same as Fig. 3.2 for transverse asymmetries and Fig. 3.8 for longitudinal asymmetries) [128], [131]. Few exceptions to the necessity to use ideal transformers were found where direct electrical interconnections could be used, but it requires that at least one point representing each of the two asymmetries is the same and therefore their potentials are equal and the special or calculation phase for the two asymmetries is the same [128]. As an example, a case of two simultaneous metallic L-L-E short circuits in Phase B and Phase C can be shown (Fig. 3.12).

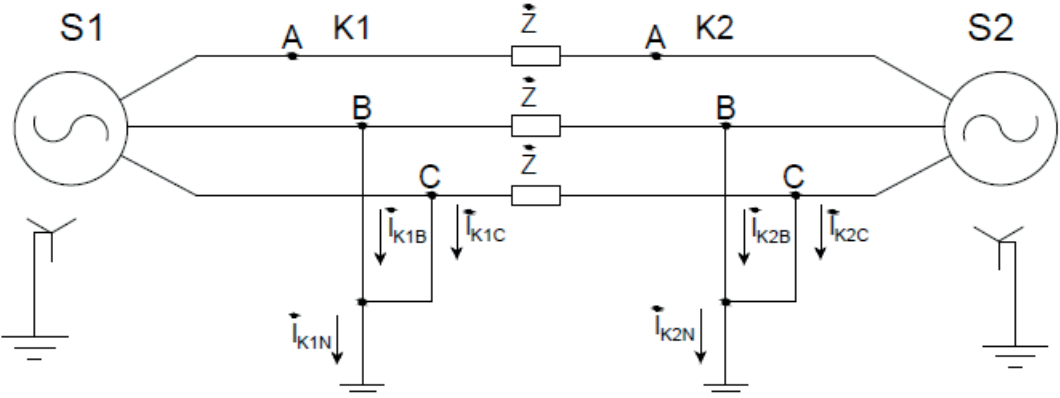


Fig. 3.12. Two simultaneous metallic L-L-E short circuits in Phase B and Phase C at different points of the power system.

In this case for both asymmetries the special phase is Phase A and the common point is the earthed neutrals of the sequence networks (Fig. 3.13).

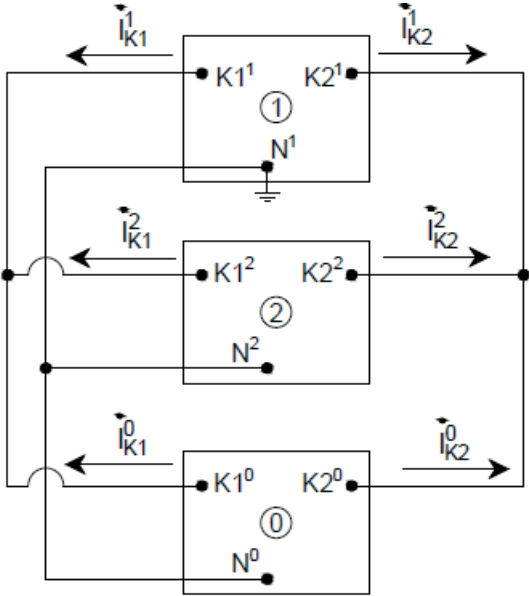


Fig. 3.13. The complex equivalent circuit for two simultaneous metallic L-L-E short circuits in Phase B and Phase C at different points of the power system.

The idea of a topological modelling approach to calculation of power system regimes with multiple simultaneous asymmetries by substitution of interconnections using ideal transformers with adaptable EMF sources, which should enforce the boundary conditions, was presented in theory in [129], but no practical implementation of this idea was presented. Two different numerical adaptations of this idea were developed by the author for calculation of the power system regime when multiple simultaneous asymmetries are present and will be presented here. The first adaptation uses only one complex equivalent circuit or one set of sequence networks. When all of the asymmetries are general (all of the shunt and/or series phase impedances are different), none of them can be represented with direct electrical connections, but the representation with EMF sources can be used if the values of these EMFs are updated during the regime calculation process according to the equation systems (3.4) and/or (3.12) as described after (3.4). This approach is convenient because the general forms of asymmetries provide opportunities to analyse different particular types of these asymmetries just by changing the impedances of the phases and for each of the sequence networks the regime calculation is performed separately, which is faster compared to the calculation of a regime of a whole complex equivalent circuit, but this approach tends to be numerically unstable for larger values of these impedances. As an example for these situations, it is possible to consider a regime of simultaneous general transverse ($0 \leq \dot{Z}_{KA} \neq \dot{Z}_{KB} \neq \dot{Z}_{KC} < \infty \Omega$) and general longitudinal ($0 \leq \dot{Z}_{LA} \neq \dot{Z}_{LB} \neq \dot{Z}_{LC} < \infty \Omega$) asymmetries (Fig. 3.14).

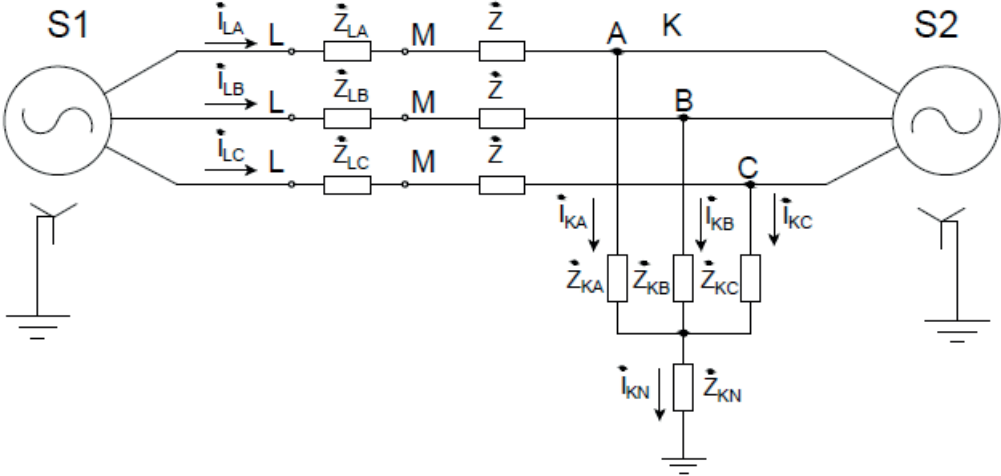


Fig. 3.14. Simultaneous general transverse and general longitudinal asymmetry at different points of the power system.

The set of sequence networks with the additional EMF sources representing the asymmetries, which would be updated based on (3.4) and (3.12), are shown in Fig. 3.15.

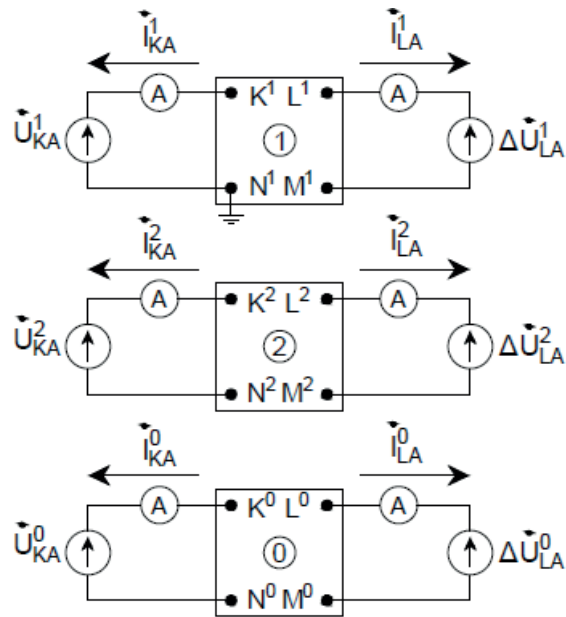


Fig. 3.15. The set of sequence networks for calculations of a regime with simultaneous general transverse and general longitudinal asymmetry in different points of the power system.

Due to the aforementioned possible numerical instability, if possible, it is advised to utilise approaches where at least one of the asymmetries is represented with direct electrical interconnections, because then the sequence networks are directly bound together with links that are unaffected by adaptations between approximation steps. This results in a more stable numerical calculation process for a larger fault path or phase series impedances. For both of these approaches, the same algorithm can be used (Fig. 3.16) with the only difference being that instead of one inner calculation cycle for a complex equivalent circuit one must use three consecutive cycles for separate sequence networks if only the general forms of the asymmetries are present.

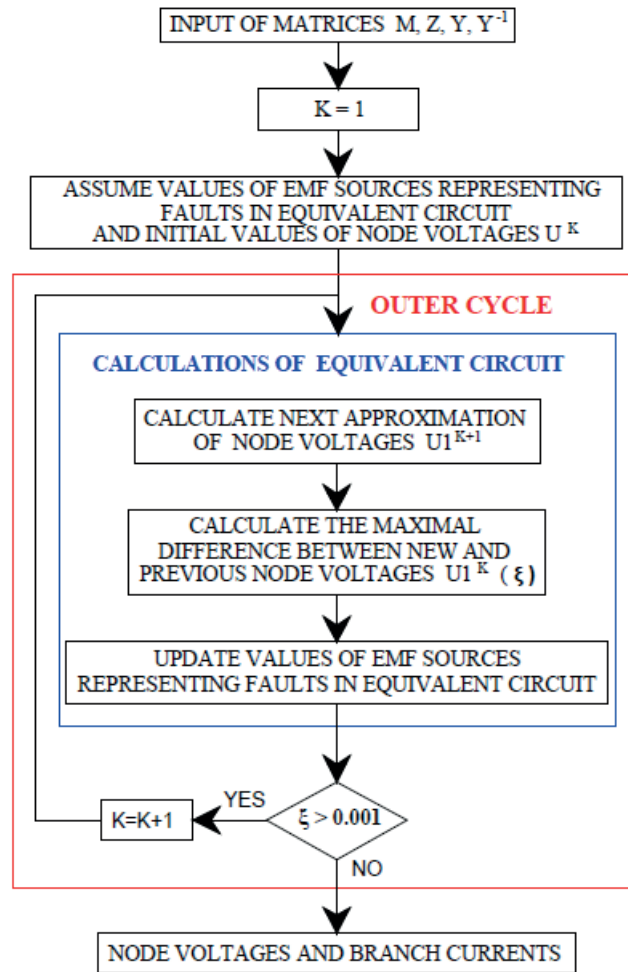


Fig. 3.16. The flowchart of the numerical calculation method for regimes of power system with multiple asymmetries when the values of additional EMF sources are updated analytically.

The second adaptation requires that all of the asymmetries present can be represented with direct electrical interconnections because for this approach the added EMF sources are updated between approximation steps, based on values obtained directly from additional complex equivalent circuits. Accordingly, this approach requires one complex equivalent circuit for every asymmetry present. Each of these complex equivalent circuits has one of the asymmetries represented with direct electrical interconnections between the sequence networks and all other asymmetries are represented with additional EMF sources [130]. As an example, it is possible to consider a longitudinal asymmetry with two identical series impedances \dot{Z}_{L2} and a simultaneous transverse asymmetry with two identical fault path impedances \dot{Z}_{K2} (Fig. 3.17).

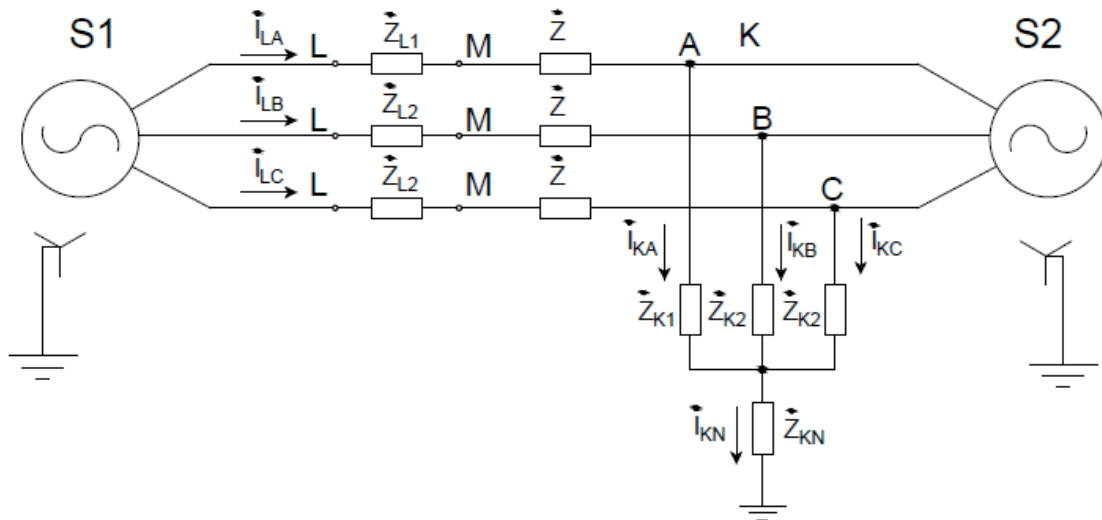


Fig. 3.17. Simultaneous longitudinal and transverse asymmetries that have two identical fault path impedances and two identical series impedances.

The corresponding complex equivalent circuits for the regime in Fig. 3.17 can be seen in Fig. 3.18 and 3.19.

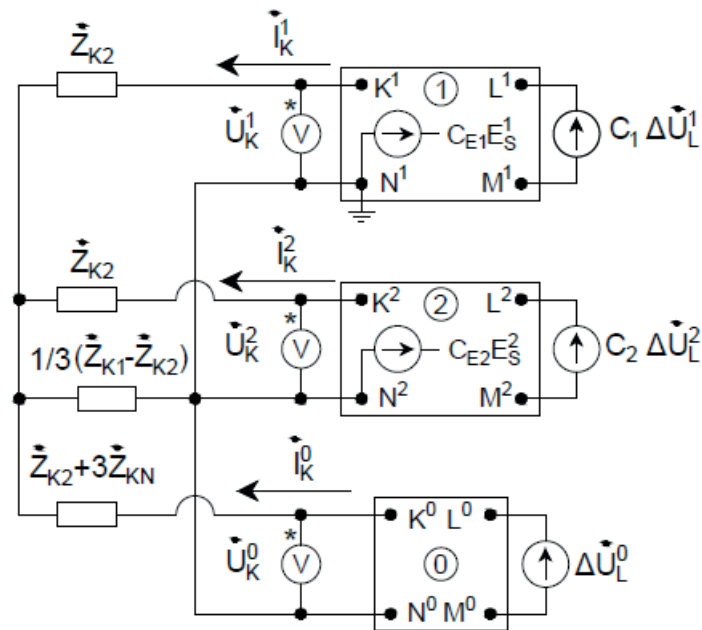


Fig. 3.18. The complex equivalent circuit for simultaneous longitudinal and transverse asymmetries that have two identical fault path impedances and two identical series impedances with electrical interconnections representing the transverse asymmetry.

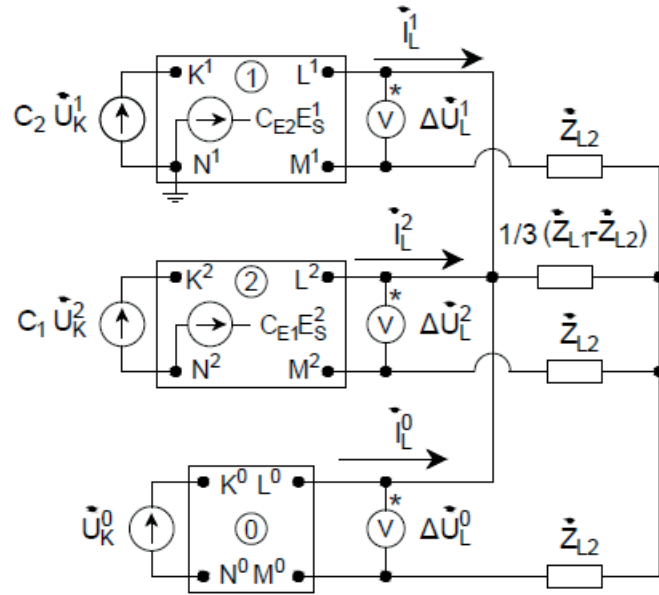


Fig. 3.19. The complex equivalent circuit for simultaneous longitudinal and transverse asymmetries that have two identical fault path impedances and two identical series impedances with electrical interconnections representing the longitudinal asymmetry.

It can be noted how the voltages “measured” from one equivalent circuit are introduced into the other one as EMF sources and additional coefficients C_1 , C_2 are used to account for a possible difference of the special (calculation) phase. The coefficients C_{E1} , C_{E2} , C_{E3} , C_{E4} are added if the EMFs of generators and other sources of the power system are only known for Phase A and the special phases of asymmetries are Phase B and/or Phase C. The combinations of coefficient values defined by operators \dot{a} and \dot{a}^2 for different special phases are presented in Table 3.1.

Table 3.1.
Coefficients for Calculations of Simultaneous Asymmetries with Different Special Phases

Special phase of Circuit 1	Special phase of Circuit 2	C_1	C_2	C_{E1}	C_{E2}	C_{E3}	C_{E4}
A	A	1	1	1	1	1	1
A	B	\dot{a}	\dot{a}^2	1	1	\dot{a}^2	\dot{a}
A	C	\dot{a}^2	\dot{a}	1	1	\dot{a}	\dot{a}^2
B	A	\dot{a}^2	\dot{a}	\dot{a}^2	\dot{a}	1	1
B	B	1	1	\dot{a}^2	\dot{a}	\dot{a}^2	\dot{a}
B	C	\dot{a}	\dot{a}^2	\dot{a}^2	\dot{a}	\dot{a}	\dot{a}^2
C	A	\dot{a}	\dot{a}^2	\dot{a}	\dot{a}^2	1	1
C	B	\dot{a}^2	\dot{a}	\dot{a}	\dot{a}^2	\dot{a}^2	\dot{a}
C	C	1	1	\dot{a}	\dot{a}^2	\dot{a}	\dot{a}^2

The flowchart for the numerical calculation process of a regime with two simultaneous asymmetries when multiple complex equivalent circuits are used is presented in Fig. 3.20. Matrices B1 and B2 in the flowchart are equal to all of the right part of equation system (4.1) for the particular equivalent circuit.

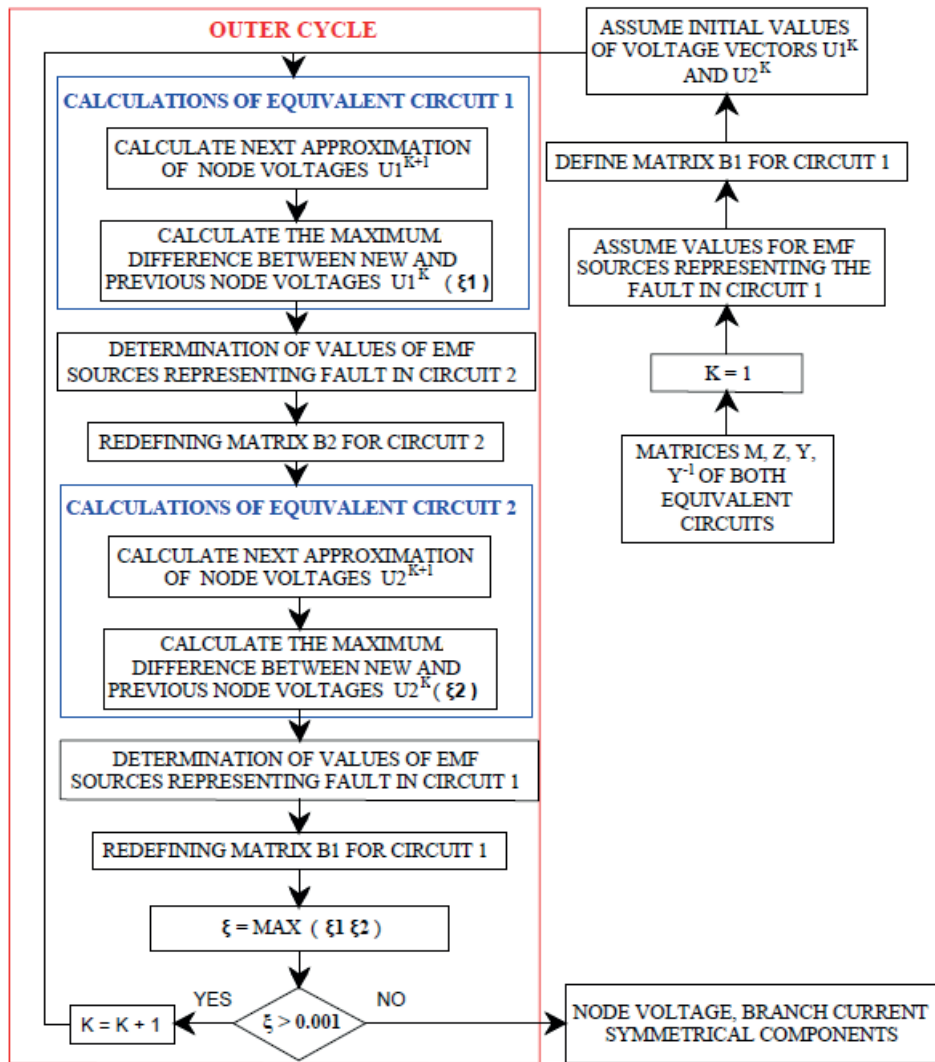


Fig. 3.20. The flowchart of the numerical calculation method for regimes of power system with multiple asymmetries when the values of additional EMF sources are updated based on calculations of additional complex equivalent circuits.

One can notice that the second approach with a simultaneous calculations of regimes of multiple complex equivalent circuits require more preparation, but it was also noticed during the testing of this method that it was numerically stable even when the values of fault path or series impedances of phases were significant.

In the face of intended extension of measurement scope used for the proposed method as described in Section 1.3, calculation of additional Thevenin's equivalents of sequence networks demonstrated in Fig. 3.3 and 3.9 and analytical derivation of controlled parameter values from their counterparts at the points of asymmetry would be overly case specific and impractical. Therefore application of topological modelling methods for extended equivalent circuits of the power system that could calculate currents and voltages of multiple power system elements simultaneously would be desirable. The symmetrical-component-based modelling approaches described in this chapter mainly provides ways to represent various asymmetries with equivalent circuits and the manner in which their node voltages and branch currents should be calculated. The mathematical description of these equivalent circuits and

numerical solution methods necessary to solve equation systems obtained will be provided in Chapter 4.

3.4. Conclusions

1. Asymmetrical regimes of the power system, which include most common faults, can be modelled using the symmetrical component method. This is implemented by separation of the point of the asymmetry and the remaining symmetrical part of the power system.
2. Regime calculation for a single point of asymmetry can be performed by iteratively recalculating the values of the EMF sources representing the asymmetry in separate sequence networks according to the boundary conditions of this asymmetry or by using one complex equivalent circuit if at least two phases have the same impedance at the point of the asymmetry.
3. Fault regimes with multiple simultaneous asymmetries can be modelled by one complex equivalent circuit with electrical interconnections representing one of the asymmetries and iteratively recalculated EMF sources representing the other asymmetries or by interchanging calculation of regimes for two or more of such complex equivalent circuits where each circuit represents a different asymmetry with electrical interconnections.

4. APPLICATIONS OF TOPOLOGICAL METHODS FOR MODELLING OF POWER SYSTEM REGIMES

In order to accommodate the necessity for calculation of currents and voltages of multiple power system elements corresponding to extended measurement scope within the controlled substation topological modelling methods with state equations in matrix form can be applied to the equivalent circuits developed in the previous chapter. Therefore, this chapter will be dedicated to compilation of state equation systems and their solution methods.

4.1. Nodal potential method in matrix form

In order to calculate the currents and voltages of the power system necessary for further analysis, one can manually compose equations according to Kirchhoff's and Ohm's laws applied to the equivalent circuit of the power system and solve them [132], [133]. However, this process can easily become excessively time-consuming if performed in such a straightforward manner for larger complex network configurations. Taking into account also that the proposed method requires integration of power system regime calculations into a larger optimisation algorithm, a more computer-friendly topological nodal potential (admittance) method in matrix form was chosen. The nodal potential method is derived from Ohm's law and Kirchhoff's first law, and it allows calculating the voltages of the nodes of the equivalent circuit in respect to a chosen base node. The equation system of the nodal potential method in matrix form is as follows [134]:

$$YU = I - MZ^{-1}E + Y_B U_B, \quad (4.1)$$

where Y – the matrix of the nodal admittances ($Y = MZ^{-1}M^T$), s;

U – the vector of the node voltages, V;

I – the vector of the current sources, A;

M – the first-incidence matrix of the network topology graph;

Z – the matrix of the network impedances, Ω ;

E – the vector of the branch EMFs, V;

Y_B – the base node admittance vector, s;

U_B – the base node voltage, V.

In order to compose the equation system for a particular equivalent circuit (4.1), certain input matrices have to be created according to this circuit:

- the first incidence matrix M represents the structure of the equivalent circuit by showing which branches connect different nodes and the assumed directions of the branch currents. An element M_{ij} of matrix M assumes value -1 if a current of branch j flows into node i , value 1 if the current of branch j flows out of node i and value 0 if branch j is not connected to node i ;
- an element I_i of the vector of current sources I assumes value J if there is a current source of J A connected to and directed towards node i , value $-J$ if the current sources is connected to and directed away from node i and value 0 if there are no current sources connected to node i ;

- an element E_j of the vector of the branch EMFs E assumes value E_1 if an EMF source of E_1 V is present in branch j and its direction matches the assumed current direction, value $-E_1$ if the EMF source is present and its direction is opposite to the assumed current direction and value 0 V if there are no EMF sources present in branch j ;
- the creation of the network impedance matrix Z can be separated into the defining of diagonal elements Z_{jk} ($k = j$), which assume the values of the impedance of branch j , and the defining of non-diagonal elements Z_{jk} ($k \neq j$), which assumes the values of the impedance of the mutual induction between branches k and j Z_{Mkj} if both of the assumed current flow directions simultaneously “enter” or “leave” the dotted terminals of branch j and k coils, values $-Z_{Mkj}$ if one of the branch currents “enters” the dotted terminal of its respective coil while the second current “leaves” the dotted terminal of its respective coil, and value 0 Ω if branches j and k are not linked with mutual inductance;
- an element Y_{Bi} of the base node admittance vector Y_B assumes a value of the total admittance of the branches connecting the base node and node i if it is connected to the base node, and value 0 s if node i is not electrically connected to the base node.

The described creation of input matrices for the equation system of the nodal potential method is more systematic and easier applied for computer-based calculations than separate equations. In order to obtain the unknown node voltages, one must then solve the linear equation system (4.1), which can be done in multiple ways: by Cramer’s rule, by multiplication with an inverse matrix, factorisation or different numerical methods. In this Thesis, either inbuilt functions of the simulation environment or the Gauss-Seidel method will be used to solve the equation system of the nodal potential method.

4.2. Modelling of steady-state fault regimes

When modelling the fault regimes, it will be assumed that the base node (the neutral of the PS network) is earthed ($U_B = 0$ V) for solutions in both phase coordinates and symmetrical component coordinates. Therefore a slightly simplified version of the equation system (4.1) is used, which does not require the creation of base node admittance vector Y_B . In this case, the numerical solution of the equation system $YU = I - MZ^{-1}E$ can be obtained by implementing the Gauss-Seidel method [134]:

$$U_i^{k+1} = \sum_{j=1}^{i-1} C_{ij} U_j^{k+1} + \sum_{m=i+1}^n C_{im} U_m^k + D_i, \quad (4.2)$$

where n – the number of nodes in the equivalent circuit except the base node;

k – the number of the approximation step of the Gauss-Seidel method;

C – a coefficient matrix obtained from the matrix of nodal admittances ($C_{ij} = -Y_{ij}/Y_{ii}$, $C_{ii} = 0$);

D – a vector obtained from the matrix of nodal admittances and the vector of constant terms ($B = I - MZ^{-1}E$, $D_i = -B_i/Y_{ii}$).

The implementation of (4.2) is repeated for all nodes $i = 1, \dots, n$ until the maximum difference between the node voltages of approximation step $k + 1$ and step k has been reduced

below an accuracy setting ε chosen by the user (while $\varepsilon \leq \max_i (|\mathbf{U}_i^{k+1} - \mathbf{U}_i^k|)$). Then, the branch currents can be calculated by Ohm's law in matrix form [134]:

$$\mathbf{I}_Z = \mathbf{Z}^{-1}(\mathbf{E} + \mathbf{M}^T(\mathbf{U} - \mathbf{U}_B)), \quad (4.3)$$

where the values of the EMFs (vector \mathbf{E}) and the node voltages used are L-E values.

It is easy to see that the topological modelling technique combined with the nodal potential (admittance) method in the matrix form and the use of complex equivalent circuits obtained using the method of symmetrical components provides a means that is convenient to implement in computer-based calculations, for representation of both single and multiple simultaneous asymmetries as demonstrated by the examples in Appendices 1–3.

4.3. Modelling of steady-state pre-fault regimes

The main goal of the modelling of the pre-fault regime for this Thesis is to estimate the pre-fault regime EMFs. However, the pre-fault (usually, load) regime is mostly determined by the apparent powers of sources and loads, which themselves can be nonlinear functions of node voltages. This means that the regime calculations would require the solution of nonlinear equation system, but an approximate linear solution can also be used, which represents the sources and loads of the power system as current sources (injections). The aforementioned current sources are determined by the constant apparent power of the node and the L-L voltage:

$$\mathbf{J} = \mathbf{I} = \hat{\mathbf{S}} / (\sqrt{3}\hat{\mathbf{U}}), \quad (4.4)$$

where $\hat{\mathbf{S}}$ – the conjugated three-phase apparent power, VA;

$\hat{\mathbf{U}}$ – the conjugated L-L voltage, V.

This substitution can be justified because of the voltage regulation used in transmission networks and typically applied generator control strategies (constant active and reactive power P_G , $Q_G = \text{const}$ or constant active power and voltage P_G , $|U| = \text{const}$). Since all of the sources and loads will be depicted with their respective current injections, the branch EMF vector $\mathbf{E} = 0$ V, and the equation system of the nodal potential method can be modified into

$$\mathbf{Y}\mathbf{U} = \mathbf{I} + \mathbf{Y}_B\mathbf{U}_B = \hat{\mathbf{D}}_S\hat{\mathbf{U}}^{-1} + \mathbf{Y}_B\mathbf{U}_B, \quad (4.5)$$

where $\hat{\mathbf{U}}^{-1}$ – a vector of inverse conjugated L-L nodal voltages ($\hat{\mathbf{U}}_i^{-1} = 1/\hat{\mathbf{U}}_i$), V^{-1} ;

$\hat{\mathbf{D}}_S$ – a diagonal matrix of conjugated apparent powers connected to the power system nodes ($\hat{D}_{Sij} = \hat{\mathbf{S}}_i/\sqrt{3}$ if $i = j$ and $\hat{D}_{Sij} = 0$ if $i \neq j$), VA.

It can be seen that for this approach, an additional vector of apparent node powers \mathbf{S} has to be created. An element S_i of the vector of apparent node powers \mathbf{S} assumes the value of S_S if a source of S_S VA is connected to node i , value $-S_L$ if a load of S_L VA is connected to the node i and value 0 VA if there are no sources or loads connected to node i . The corresponding implementation of a numerical solution of equation system (4.5) is

$$\mathbf{U}_i^{k+1} = \sum_{j=1}^{i-1} C_{ij}\mathbf{U}_j^{k+1} + \sum_{m=i+1}^n C_{im}\mathbf{U}_m^k + \frac{1}{Y_{ii}}(\hat{D}_{Sii}\hat{\mathbf{U}}_i^{-1k} + \mathbf{Y}_{Bi}\mathbf{U}_B). \quad (4.6)$$

In case of convergence issues of (4.6) a numerical implementation of inverse matrix method solution to (4.5) ($\mathbf{U} = \mathbf{Y}^{-1}\widehat{\mathbf{D}}_S\widehat{\mathbf{U}}^{-1} + U_B$) can be used instead:

$$\mathbf{U}_i^{k+1} = \sum_{j=1}^{i-1} Y_{ij}^{-1}\widehat{\mathbf{D}}_{Sjj}\widehat{\mathbf{U}}_j^{-1k+1} + \sum_{m=i+1}^n Y_{im}^{-1}\widehat{\mathbf{D}}_{Smm}\widehat{\mathbf{U}}_m^{-1k} + U_B. \quad (4.7)$$

When the node L-L voltages are estimated, the branch currents can be calculated by (4.3), taking into account that EMF vector $\mathbf{E} = 0$ V and dividing voltage vector \mathbf{U} and base node voltage U_B by $\sqrt{3}$ to obtain phase currents. Then the pre-fault EMF of the generator can be calculated from the busbar L-E voltage of the generator by adding the voltage drop in the stator winding.

4.4. Modelling of transient regimes using a numerical inverse Laplace transform

The methods presented in Sections 4.2 and 4.3 are intended for calculations of steady-state, or so-called enforced, power system regimes, but in some cases the transient response of the power system is also necessary. The base approach to the task of calculating the power system transients is to compose the differential equations, which can be Kirchhoff's laws of instantaneous currents and voltages for static linear circuits or include mechanical processes, and then solve the obtained equation system. When the equivalent circuit is simple, an analytical solution can be obtained by solving the characteristic equations and by using the initial conditions of the reactive elements. However, in most cases the power system will have a more complex structure or nature, and numerical methods are used to calculate the transient processes. The methods used vary, but some of the most common ones are the trapezoidal rule, Euler's and Runge-Kutta methods [135], [136].

In this study, a different approach will be described based on a numerical inverse Laplace transform. The Laplace transform has long been applied for description of electrical circuit transients and in the control theory. In essence, the Laplace transform is a transition from the time domain to the Laplace domain. The Laplace transform from a time domain function $f(t)$ to a Laplace domain function $F(s)$ is performed by integration:

$$F(s) = \int_0^{\infty} f(t)e^{-st} dt, \quad (4.8)$$

where $f(t)$ – the original time domain function;

$F(s)$ – the Laplace domain equivalent of the original time domain function $f(t)$;

s – a complex parameter of the Laplace domain ($s = c + i\omega$, $i = \sqrt{-1}$).

This transform is also depicted as $f(t) \doteq F(s)$ or $L[f(t)] = F(s)$. The Laplace transform is useful because in the Laplace domain the differential equations are represented by algebraic equations, and the roots of this equation also represent the solution to the original problem in the Laplace domain. Therefore, by performing an inverse Laplace transform ($F(s) \doteq f(t)$ or $L^{-1}[F(s)] = f(t)$) of the obtained roots, one can obtain the original time domain transients. The inverse Laplace transform is represented by an integration of the Laplace domain function $F(s)$ across all the possible values of parameter ω :

$$f(t) = \frac{1}{2\pi i} \int_{c-i\infty}^{c+i\infty} F(s)e^{st} ds. \quad (4.9)$$

The inverse transform as shown in (4.9) is usually replaced by a sum of residues over the essential points (most often singularities or poles):

$$f(t) = \frac{1}{2\pi i} \int_{c-i\infty}^{c+i\infty} F(s)e^{st} ds = \sum_{k=1}^n \text{Res}(F(s), s_k)e^{st}, \quad (4.10)$$

where k – the number of the essential points of the function $F(s)$.

For simple ordinary differential equations with low order poles in the Laplace domain, this analytical solution is workable, but with the increase of the number and order of poles the calculation process of residues becomes very time-consuming. Again, it is possible to use approximate numerical methods to obtain values of the time domain function. One of such methods is based on decomposition into Fourier series. This method obtains the time domain function using the values of the Laplace domain function $F(s)$ calculated for equally distributed values of the real part axis $\text{Re}(s) = c$ [137], [138]. It assumes that the function in the Laplace domain $F(s)$ exists if $\text{Re}(s) > 0$, which can be achieved by using $F(s + a)$ instead of $F(s)$ (this is equivalent to multiplication of the function $f(t)$ by e^{-at}) and $f(0) = 0$.

First, this method replaces the exponent in the Laplace transform in (4.8) with a cosine:

$$e^{-\sigma t} = \cos(x), \quad (4.11)$$

where σ – a positive real number;

x – a substitution parameter;

The number σ can be freely chosen according to the theory [137], but after some testing it was found that a relatively optimal value of this parameter can be calculated as follows:

$$\sigma = \frac{K_\sigma \pi}{2T_{\max}}, \quad (4.12)$$

where T_{\max} – the time for which $f(t)$ is to be plotted, s;

K_σ – a proportionality coefficient freely chosen from approximate interval 1–20 (higher values are advised for regimes where oscillations can be expected).

This substitution leads to a change from time to x :

$$t = \frac{1}{\sigma} \ln(\cos(x)), \quad (4.13)$$

and to a modification of the original time domain function:

$$f(t) = f\left(\frac{1}{\sigma} \ln(\cos(x))\right) = \phi(x), \quad 0 \leq x \leq \pi/2. \quad (4.14)$$

Now the Laplace transform in (4.8) can be shown in the following form:

$$F(s) = \frac{1}{\sigma} \int_0^{\pi/2} (\cos(x))^{((s/\sigma)-1)} \sin(x) \phi(x) dx. \quad (4.15)$$

Next the function $\phi(x)$ can be replaced by a Fourier series of an odd function in sine series:

$$\phi(x) = \sum_{k=0}^{\infty} S_k \sin((2k+1)x), \quad (4.16)$$

where S_k – the coefficients of the sine series:

$$S_k = \frac{4}{\pi} \int_0^{\pi/2} \phi(x) \sin((2k+1)x) dx. \quad (4.17)$$

At the same time, the coefficients of sine series S_k can be determined from the values of the function in the Laplace domain $F(s)$ calculated for equally distributed points on the real axis of $s_m = (2m + 1)\sigma$ ($m = 1, 2, \dots, \infty$):

$$\sigma F((2m + 1)\sigma) = \int_0^{\pi/2} (\cos(x))^{2m} \sin(x) \phi(x) dx. \quad (4.18)$$

The first two elements of the integral can be expressed as linear combinations of $\sin((2m + 1)x)$:

$$(\cos(x))^{2m} \sin(x) = 2^{-2m} \sum_{i=0}^m \left(\binom{2m}{i} - \binom{2m}{i-1} \right) \sin((2(m-i) + 1)x), \quad (4.19)$$

where $\binom{2m}{i} = \frac{(2m)!}{i!(2m-i)!}$ - i combinations of $2m$.

Taking into an account (4.16), (4.19) and that

$$\int_0^{\pi/2} \sin((2\alpha + 1)x) \sin((2\beta + 1)x) dx = \begin{cases} 0, & \alpha \neq \beta \\ \pi/4, & \alpha = \beta \end{cases} \quad (4.20)$$

as well as that for a particular point m the sine series will have only elements $\beta = m - i$ ($i = 0, 1, 2, \dots, m$), the equation (4.18) can be modified:

$$\sigma F((2m + 1)\sigma) = 2^{-2m} \frac{\pi}{4} \sum_{i=0}^m \left(\binom{2m}{i} - \binom{2m}{i-1} \right) S_{m-i}, \quad (4.21)$$

or

$$\sum_{i=0}^m \left(\binom{2m}{i} - \binom{2m}{i-1} \right) S_{m-i} = \frac{4^{m+1}}{\pi} \sigma F((2m + 1)\sigma). \quad (4.22)$$

Equation (4.22) provides the link between the coefficients of the sine series and the values of the function in the Laplace domain. Now it is possible to determine the coefficients based on these values and previously calculated coefficient values: $S_0 = \frac{4}{\pi} \sigma F(\sigma)$, $S_1 + S_0 = \frac{4^2}{\pi} \sigma F(3\sigma)$, $S_2 + 3S_1 + 2S_0 = \frac{4^3}{\pi} \sigma F(5\sigma)$ and so on until the m -th element is determined according to (4.22). These coefficients can then be used to obtain the function $\phi(x)$ according to (4.16), which provides the original time domain function if x is substituted with t expressed from (4.11):

$$f(t) = \sum_{i=0}^m (S_i \sin((2i + 1) \arccos(e^{-\sigma t}))). \quad (4.23)$$

As mentioned before, the demonstrated solution assumes that $f(0) = 0$, but if this is false, then a modification can be made by obtaining a substitute function $f_2(t) = f(t) - f(0)$ first. This can be achieved by using $F_2(s) = F(s) - f(0)/s$ instead of $F(s)$ and then the original function in the time domain can be calculated: $f(t) = f_2(t) + f(0)$.

One can notice that for a more precise approximation of the function $\phi(x)$ with the sine series and therefore also the function $f(t)$ in the time domain, a higher number of calculation nodes m is desirable as they define the number of obtainable coefficients for the sine series (see (4.22)). However, as m increases, the elements defining the multiplier by the coefficient S_0 ($i = m$) $\binom{2m}{m} - \binom{2m}{m-1}$ also increase, which can reach the maximum numerical value of a computer with a 32- or 64-bit system ($2^{32} - 1$ or $2^{64} - 1$). It is advised to use values $m > 16$

with caution [138] (values above 24 often result in numerical oscillations and large errors). Also after the testing of the described approach it was noticed that the substitution of the function $F(s)$ with $F(s + a)$ to meet the requirement $Re(s) > 0$ often results in an incorrect time domain function if the equivalent circuit contains AC sources. Therefore, the presented method is useful mainly to calculate the transients of DC circuits or to separately calculate the DC component of the transients of an AC circuit (in these cases, direct use of the function $F(s)$ instead of the substitute function $F(s + a)$ does not result in major errors). The flowchart of the presented method can be seen in Fig. 4.1.

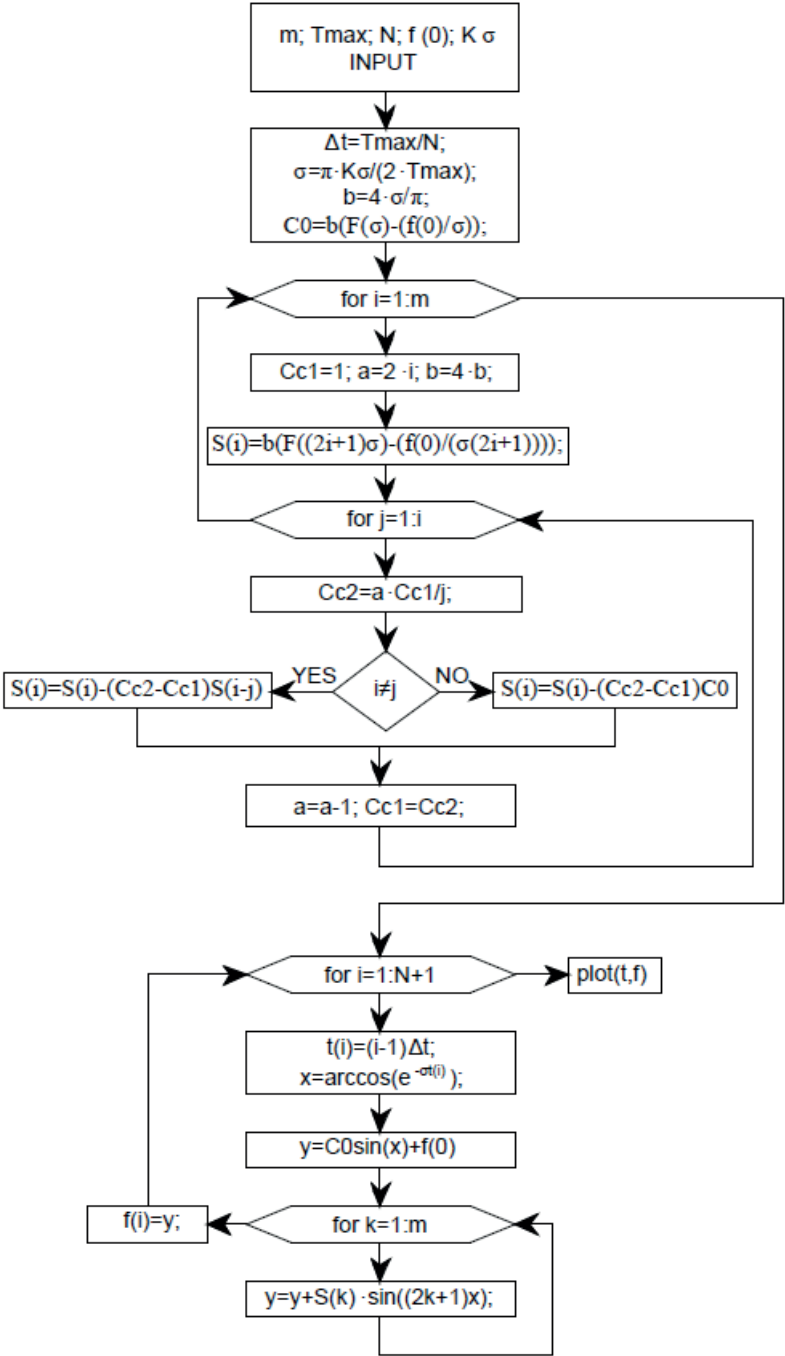


Fig. 4.1. The flowchart of the presented numerical inverse Laplace transform method

This algorithm can also be used in combination with topological representation of the power system to simultaneously calculate the DC components of several voltages or currents. This can be achieved by using the topological nodal potential method (4.1) and Ohm's law (4.3) (assuming a base voltage of 0 V) in Laplace space:

$$Y(s)U(s) = I(s) - MZ^{-1}(s)E(s), \quad (4.24)$$

$$I_Z(s) = Z^{-1}(s)(E(s) + M^T U(s)), \quad (4.25)$$

where $Y(s)$, $U(s)$, $I(s)$, $Z(s)$, $E(s)$, $I_Z(s)$ – vectors and matrices Y , U , I , Z , E , I_Z from (4.1) and (4.3) transformed into Laplace domain.

In this case the main differences are in the elements that make up the branch impedance vector (such as $R_{LINE} + sL_{LINE}$, $1/(sC_{LINE})$ representing the longitudinal resistance, inductance and shunt capacitance of an OHTL π -section) and the EMF vector (such as $i_{DCL}(0) L_{LINE}$ representing the DC component created by an energy change in line inductance at the moment of commutation).

The presented numerical inverse Laplace transform could also be useful for control systems that use power system dynamics described by a model in Laplace space $W(s)$ for their optimisation. In this case the inverse Laplace transform would be used at least for obtaining control actions in time domain $L^{-1}[C'(s)] = C'(t)$, but could be applied to transform model output $L^{-1}[Y_M(s)] = Y_M(t)$ for comparison with desired values $Y_D(t)$ if these are not transformed to Laplace space by DFT (Fig. 4.2).

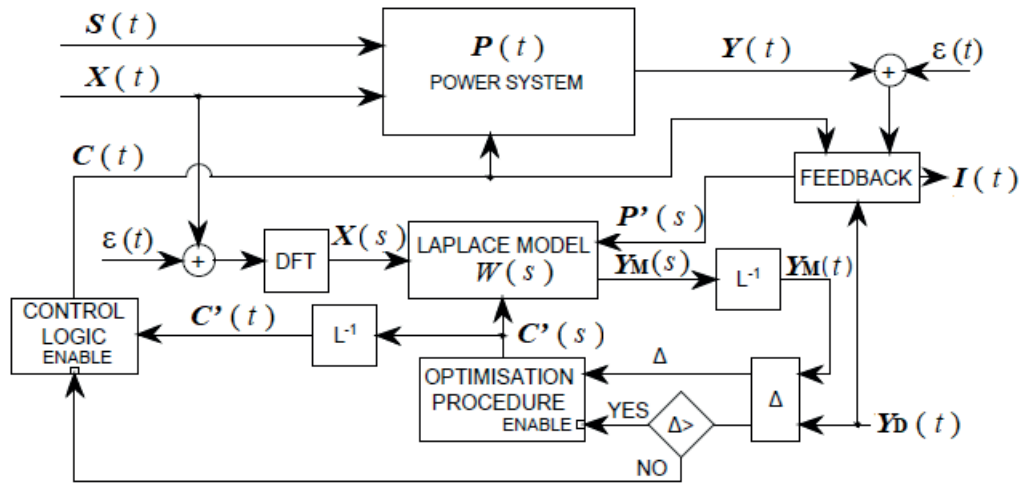


Fig.4.2. Control system using model in Laplace space for optimisation.

Application of this or other numerical topological modelling approach for calculation of fault transients used for the model parameter estimation could be another direction for future research. In this respect, one interesting option might be the use of the Hilbert-Huang transform [139].

4.5. Modern distance protection terminal under scrutiny – testing experience

Modelling approaches such as described in previous sections can then be used to simulate various fault cases and evaluate performance of protection and automation devices that either

have to clear these faults or provide information regarding them. One of the main reasons for research and development of the proposed fault distance estimation method was to consider the influence of the remote-end power system infeed through fault path resistance that resulted in inaccurate results and impaired performance of many FL and DP methods as described in Sections 2.1 and 2.2. This is done for comparison between existing one-terminal based DP and FL methods and the proposed method further into the Thesis (Fig. 5.4–5.7 and Fig. 7.8–7.11). However, there is a special but fairly common type of L-E faults in the Baltic region – fallen-tree faults [1], [140]. These require additional modelling tools for analysis, but their influence should also be highlighted. The fallen-tree faults can have additional nonstationary resistance to earth during the burnout and flashover of the trunk of the tree as indicated from previous analysis of field recordings of fallen-tree faults [141]. These recordings of oscillograms of DP apparent impedance modulus, apparent resistance and reactance showed that both rapid burnout with a fast decline of apparent impedance and a slow burnout with a delayed fall of the apparent impedance exist (Fig. 4.3–4.5).

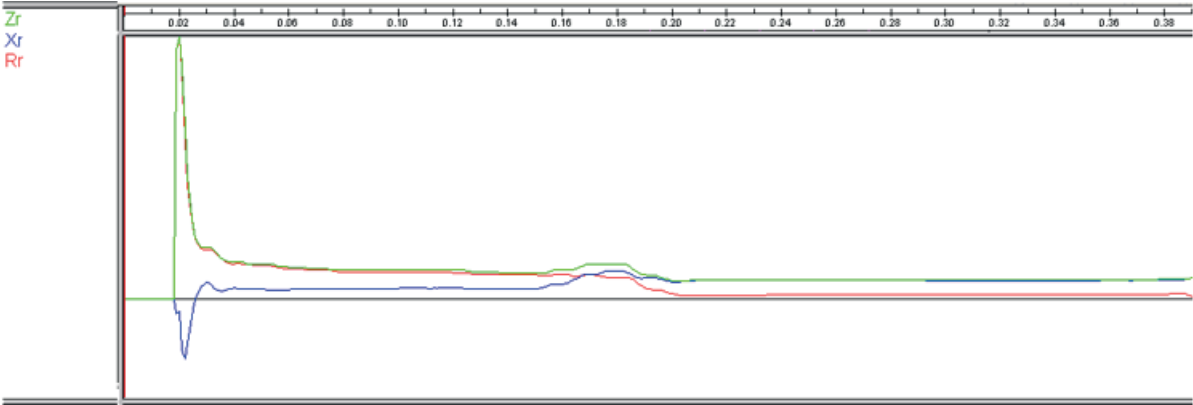


Fig. 4.3. Oscillogram of DP relay apparent resistance R_r , reactance X_r and impedance modulus Z_r during an L-E fault with a rapid tree burnout [141].

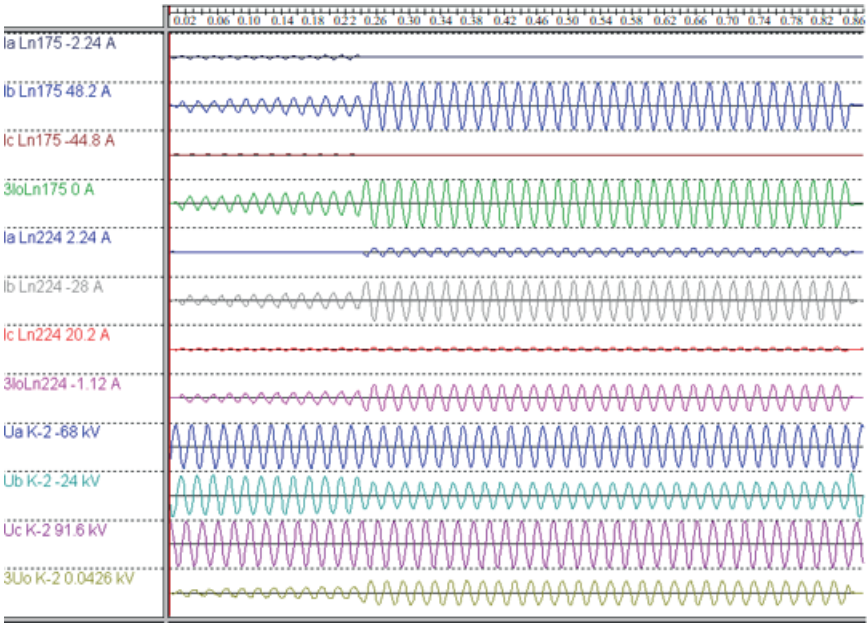


Fig. 4.4. Phase current I_a , I_b , I_c and phase voltage U_a , U_b , U_c oscillograms during an L-E fault with a slow tree burnout [141].

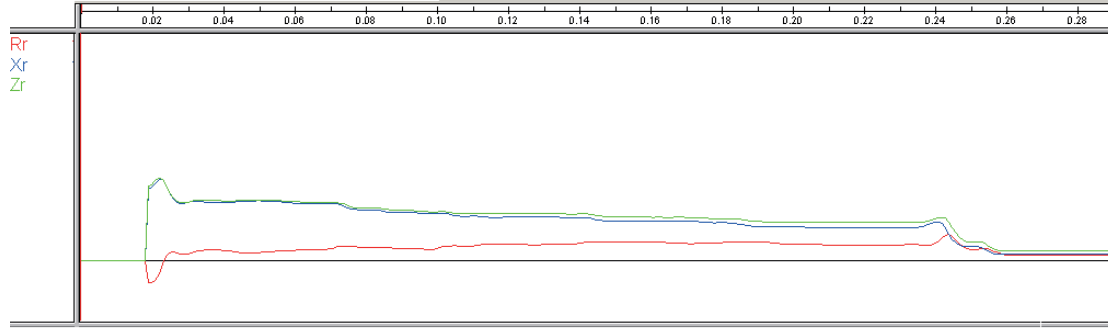


Fig. 4.5. Oscillogram of DP relay apparent resistance R_r , reactance X_r and impedance modulus Z_r during an L-E fault with a slow tree burnout [141].

Considering that the total earth path resistance could be divided in a stationary part R_E that represents the state after the burnout with a well established arc channel and a transient part $R_E(t)$ representing additional resistance present during the burnout of the tree, it is possible to describe the apparent impedance including both parts separately [142]:

$$\dot{Z}_{DP} = \left(\alpha \dot{Z}_L^1 + (R_E + R_E(t))(1 + \dot{I}_{S1}/\dot{I}_{S2}) \right) / \left(1 + K_0(3\dot{I}_{S1}^0/\dot{I}_{S1}) \right), \quad (4.26)$$

where α – the fault distance, p.u.;

\dot{Z}_L^1 – the PS impedance of the protected line, Ω ;

R_E and $R_E(t)$ – the stationary and transient parts of the earth path resistance, Ω ;

\dot{I}_{S1} and \dot{I}_{S2} – the phasors of phase current of the faulted phase from the close and remote-end power systems, A;

\dot{I}_{S1}^0 – the phasor of ZS current from the close end power system, A;

K_0 – the ZS compensation coefficient calculated from the ZS and PS impedances of the protected line.

Taking into an account the reactance effect caused by the stationary fault path resistance mentioned in Section 2.2, equation (4.26) and Fig. 4.5, it can be expected that for fallen-tree faults the apparent impedance locus may enter the correct operation region with additional delays due to the transient component $R_E(t)$. This would further degrade the performance of the DP, which already could have an apparent impedance greater than the setting of DP due to the stationary component R_E of the fault path resistance.

In order to test the influence of such faults on DP performance, a modern digital transmission line protection and automation terminal with DP function based on [143] was tested using a virtual-real laboratory. First, the fault was simulated in MATLAB SimPowerSystems environment and a COMTRADE file was created from the obtained current and voltage transient waveforms. Then the waveforms were generated using an ISA DRTS 64 signal generator that was connected to the 110–220 kilovolt transmission line protection and automation terminal mentioned earlier. The testing included metallic faults (no fault path resistance), faults with a stationary earth path resistance and faults with both a stationary resistance and a transient one and considered relays on both sides of the protected line (Q1 and Q2 in the tables below). The main results of this experimental testing are

summarised in Tables 4.1 and 4.2. For more details about simulations and the numbers of fault scenarios in Tables 4.1 and 4.2, please see [142].

Table 4.1.

Results of DP Testing for L-L-E Faults [142]

Fault		Q1			Q2		
		Zone	<i>t</i> _{TRIG} , s	<i>t</i> _{TRIP} , s	Zone	<i>t</i> _{TRIG} , s	<i>t</i> _{TRIP} , s
Metallic	1	I	0.015	0.215	I	0.02	0.22
	2	I	0.015	0.215	I	0.02	0.22
	3	I	0.02	0.22	I	0.015	0.215
	4	II	0.01	0.71	V	0.02	0.47
	5	II	0.02	0.72	-	-	-
	6	III	0.01	1.21	-	-	-
	7	-	-	-	-	-	-
	8	V	0.02	0.47	II	0.02	0.72
	9	-	-	-	II	0.02	0.72
	10	-	-	-	III	0.02	1.22
	11	-	-	-	III	0.02	1.22
Constant earth path and fault resistance between phases	1	I	0.02	0.22	I	0.02	0.22
	2	I	0.02	0.22	I	0.02	0.22
	3	I	0.02	0.22	I	0.02	0.22
	4	II	0.02	0.72	-	-	-
	5	III	0.02	1.22	-	-	-
	6	IV	0.02	1.72	-	-	-
	7	-	-	-	-	-	-
	8	V	0.02	0.47	II	0.02	0.72
	9	-	-	-	II	0.02	0.72
	10	-	-	-	III	0.02	1.22
	11	-	-	-	III	0.02	1.22
Transient earth path and constant fault resistance between phases	1	I	0.02	0.22	I	0.02	0.22
	2	I	0.02	0.22	I	0.02	0.22
	3	I	0.02	0.22	I	0.02	0.22
	4	II	0.02	0.72	-	-	-
	5	III	0.02	1.22	-	-	-
	6	IV	0.02	1.72	-	-	-
	7	-	-	-	-	-	-
	8	V	0.02	0.47	II	0.02	0.72
	9	-	-	-	II	0.02	0.72
	10	-	-	-	III	0.02	1.22
	11	-	-	-	III	0.02	1.22

Table 4.2.

Results of DP Testing for L-E Faults [142]

Fault		Q1			Q2		
		Zone	$t_{TRIG, S}$	$t_{TRIP, S}$	Zone	$t_{TRIG, S}$	$t_{TRIP, S}$
Metallic	1	I	0.015	0.215	I	0.02	0.22
	2	I	0.015	0.215	I	0.015	0.215
	3	I	0.02	0.22	I	0.02	0.22
	4	II	0.01	0.71	V	0.02	0.47
	5	II	0.02	0.72	-	-	-
	6	III	0.02	1.22	-	-	-
	7	-	-	-	-	-	-
	8	V	0.02	0.47	II	0.015	0.715
	9	-	-	-	II	0.02	0.72
	10	-	-	-	III	0.02	1.22
	11	-	-	-	III	0.02	1.22
Constant earth path resistance	1	I	0.02	0.22	I	0.02	0.22
	2	I	0.02	0.22	I	0.02	0.22
	3	II	0.02	0.72	I	0.02	0.22
	4	III	0.01	1.21	-	-	-
	5	III	0.02	1.22	-	-	-
	6	IV	0.02	1.72	-	-	-
	7	-	-	-	-	-	-
	8	V	0.02	0.47	II	0.02	0.72
	9	-	-	-	II	0.02	0.72
	10	-	-	-	III	0.02	1.22
	11	-	-	-	III	0.02	1.22
Transient earth path resistance	1	I	0.41	0.61	I	0.31	0.51
	2	I	0.64	0.84	I	0.26	0.46
	3	II	0.51	1.21	I	0.23	0.43
	4	III	0.27	1.47	-	-	-
	5	III	0.52	1.72	-	-	-
	6	IV	0.63	1.9	-	-	-
	7	-	-	-	-	-	-
	8	V	0.38	0.83	II	0.22	0.92
	9	-	-	-	II	0.28	0.98
	10	-	-	-	III	0.3	1.5
	11	-	-	-	III	0.4	1.6

The results summarised in Tables 4.1 and 4.2 show that the presence of a stationary fault resistance could result in a failure to operate for a backwards-directed reservation zone for one of the relays for both L-L-E and L-E faults. The presence of stationary resistance also resulted in operation of an incorrect zone for one of the relays, which added a time delay of one selectivity time interval before the DP trip, but did not significantly affect the time the zone of operation was triggered (apparent impedance locus entered the zone). As can be seen from Table 4.1, addition of transient earth path resistance did not result in further delays for the operation of the DP L-L loop algorithm as it determines apparent impedance between the phases. However, the results for L-E faults from Table 4.2 show that the presence of the

transient resistance component can result in time delays before the zone that operated is triggered both in case of correct zone of operation and incorrect one. This can also be illustrated by differences in apparent impedance locus oscillograms (Fig. 4.6 and 4.7).

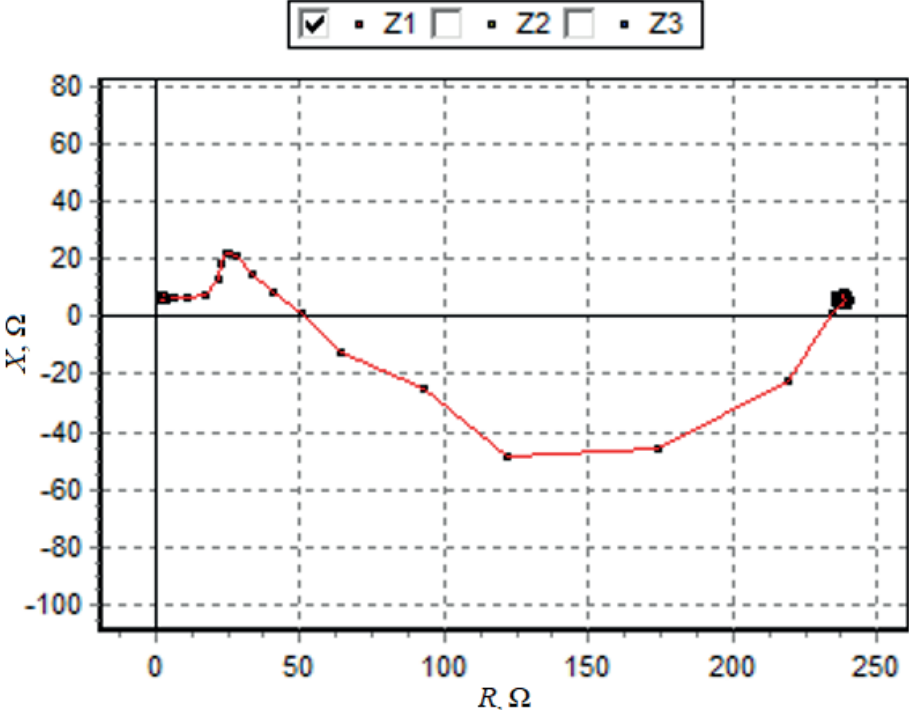


Fig. 4.6. The relay Q1 apparent impedance locus in primary ohms in case of a metallic L-E fault in scenario 2.

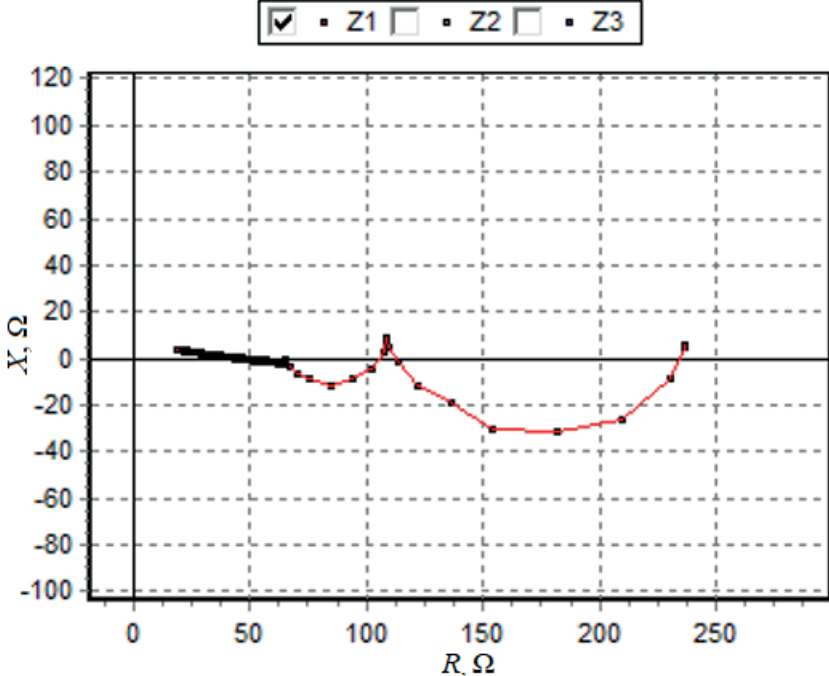


Fig. 4.7. Relay Q1 apparent impedance locus in primary ohms in case of a L-E fault in scenario 2 with stationary and transient earth path resistance present.

The comparison of Fig. 4.6 and 4.7 already indicates that an additional time delay will be present before triggering of Zone I as the number of measurement points necessary for the

apparent impedance locus to move from load conditions (small pre-fault time was considered in the simulations) of about 240 Ω to stationary apparent fault impedance. The impact of this delayed change in apparent impedance can be clearly seen in oscillograms of DP zone triggering times shown in Fig. 4.8 and 4.9.

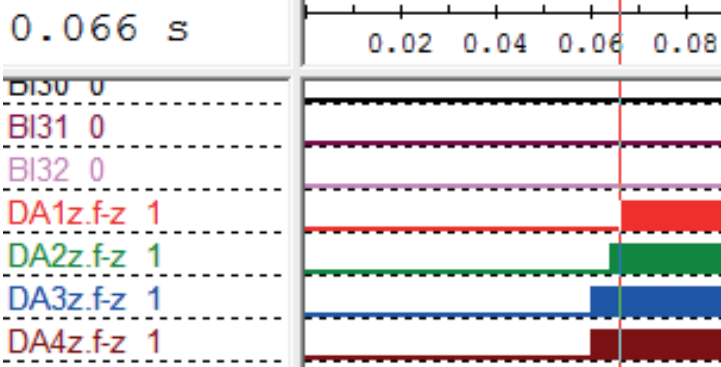


Fig. 4.8. Trigger times of relay Q1 L-E DP zones DA1z, DA2z, DA3z and DA4z in case of a metallic fault in fault scenario 2.

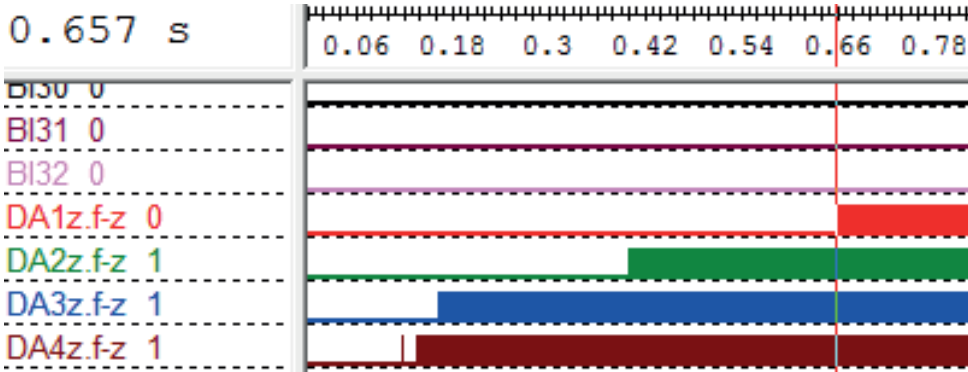


Fig. 4.9. Trigger times of relay Q1 L-E DP zones DA1z, DA2z, DA3z and DA4z for the fault scenario 2 when a stationary and transient earth path resistance is present.

These oscillograms clearly show that after a 50 ms recording of the pre-fault regime in case of presence of stationary and transient earth path resistance there will be a slightly larger time delay even before Zones III and IV are triggered, but the most of the added time delay before operation of Zone I is while the impedance locus slowly enters zones I and II. This might differ a little for a different setting strategy of Zone III, but it is clear that the impedance locus will enter Zone IV relatively fast as it is set closer to pre-fault loading impedance with a safety margin, but it will enter the zones defined by the line impedances significantly slower during a slow tree burnout as indicated by the results above. This negative effect of both the stationary fault path resistance and especially the transient earth path resistance for L-E faults can be avoided by using the proposed method because it considers and even estimates the value of equivalent fault path resistance. Additionally, it uses steady-state phasor values determined after signal processing, which allows diminishing the effect of electric transients and estimating the value of the equivalent fault resistance as the mean value over the data window of the measurement.

4.6. Conclusions

1. Topological modelling of power system equivalent circuits that represent asymmetrical power system regimes combined with the nodal potential (admittance) method in the matrix form result in flexible and easy-to-implement modelling means for computer-based fault analysis and the estimation of unknown power system parameters.
2. The obtained equation systems describing the steady-state of the power system can be solved numerically by methods such as the Gauss-Seidel method.
3. Numerical solver of inverse Laplace transform could be considered for future use for estimation of unknown power system parameters using instantaneous measurement values.
4. The presence of fault path resistance negatively affects the performance of the existing digital DP terminal both for L-E and L-L-E faults, resulting in additional time delays due to operation with an incorrect zone. In case of fallen-tree faults, which are known to happen in the Baltic region and in Northern Europe, even larger time delays can be observed for L-E faults due to a slower decrease in the apparent impedance during the burnout of the tree.

5. APPLICATION OF THE ESTIMATION OF POWER SYSTEM MODEL PARAMETERS FOR FAULT LOCATION AND DISTANCE PROTECTION

5.1. The framework of the model parameter estimation method

As mentioned before in Section 1.3 the proposed parameter estimation method is defined as an optimisation task, which minimises the difference between the measurements from the controlled substation and the corresponding outputs of the mathematical model of the power system. The extension of available measurements to include different branches of the same substation provides more information about the state of the closest power system elements with minimal investments and risk for loss of communication. The proposed method is performed in two separate stages: an estimation of unknown model parameters of the pre-fault regime and then the fault regime. This separation is created to decrease the number of unknown parameters for each individual stage compared to use of only one stage.

The first stage is the estimation of the pre-fault regime parameters, which should be performed online at regular time intervals or after detecting a significant change of any of the measured parameters, which is not caused by a fault. This estimation process uses measurements of the controlled substation bus voltage and current, power flows of the branches connected to the substation buses (lines, power transformers etc.). These values are compared with the output of a mathematical model of the pre-fault regime, and the difference Δ (Fig. 5.1), which is also the objective function f_{OBJ} for the optimisation algorithm, is calculated:

$$f_{OBJ} = \sum_{i=1}^{N_{MEA}} (K_{Wi} \cdot ((y_i - y_{mi})/y_i)^2), \quad (5.1)$$

where K_{Wi} – the weight coefficient of the i -th parameter;

N_{MEA} – the number of measurements used for the estimation process;

y_i and y_{mi} – the measured value of the i -th parameter and the corresponding model output.

Then this value and its change between the steps of the optimisation is used for testing of a combination of convergence criteria of the optimisation. If these criteria are not met, then the values of the parameters being estimated are adjusted and the model output is recalculated. This is repeated until the convergence criteria are met, which ensures that the difference Δ has reached the value of its global minimum or a value in vicinity of the global minimum. The parameters estimated for the pre-fault regime, are the real and imaginary powers of the main generation and load nodes of the power system that are not directly controlled and if simplifications of the power system model are used then the PS resistance and reactance of links to the controlled branches are also estimated. Therefore, if no simplifications are used the first estimation stage can be considered to be state estimation. When the estimation of parameters of the pre-fault regime is concluded (the convergence criteria are met), the last model output is used to calculate the equivalent EMFs of the generation nodes of the pre-fault regime and the equivalent impedances of

the load nodes if these impedances are taken into account in the model of the fault regime. These results are then saved in a memory block updating the previous values (Fig. 5.1).

The second stage of the estimation of unknown parameters used for the fault regime is initiated by an additional start or an existing relay protection logic, which determines the fault type and the moment of fault occurrence. The voltage and current measurements from the elements at the controlled substation are recorded (after processing) and then used to determine the difference Δ compared with the corresponding outputs of the fault regime model using the same equation (5.1). Parameters estimated during the second estimation stage are the fault distance α , the equivalent fault path resistance R_F and if necessary NS and ZS equivalent resistance and reactance of links to the controlled branches when simplifications of the network topology are used. This model uses values of equivalent source EMFs and impedances of loads if they are taken into account and the estimated equivalent impedances of the external power system saved from the last estimation of the pre-fault regime parameters. An optimisation iteratively adjusts the values of the fault parameters, which are being estimated, until the convergence criteria for this stage are met as well. The last values, which satisfied the convergence criteria, are then saved and the fault distance is extracted from this group of parameters (see Fig. 5.1). Both estimation stages use the same optimisation method.

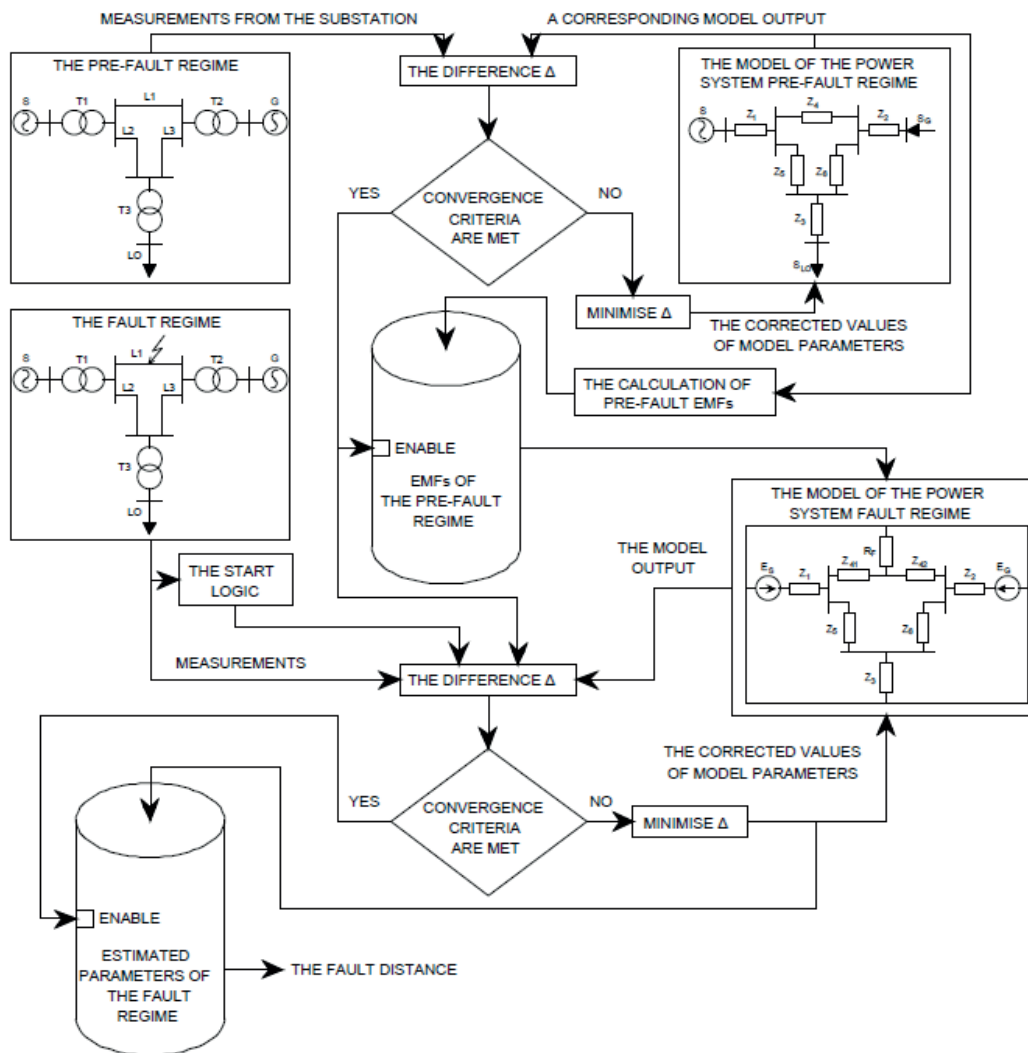


Fig. 5.1. The flowchart of the two-stage parameter estimation.

Next, the optimisation tools used to achieve the estimation process can be described.

5.2. Modified randomised search initially tested for estimation of model parameters

As mentioned in the previous section, the estimation of unknown parameters is defined as an optimisation task with the aim to minimise the difference between measured and modelled quantities. Considering that the objective (difference) function uses multiple parameters, which will in most cases be nonlinear functions of the estimated parameters (for an example Fig. 6.1), it can be suspected that this function can have false extrema. Therefore, in order to avoid potential convergence towards these false extrema, the first tested method of optimisation was a randomised search with a constriction procedure similar to the bisection method applied to search space limitations. This method starts by generating a vector of unknown parameter values \mathbf{X} within the given search space limitations from a uniform distribution with a random number generator using the following equation for each estimated parameter:

$$\mathbf{X} = \mathbf{X}_{\min} + (\mathbf{X}_{\max} - \mathbf{X}_{\min})R, \quad (5.2)$$

where \mathbf{X} – a vector of unknown parameter values;

\mathbf{X}_{\min} and \mathbf{X}_{\max} – vectors of minimum and maximum possible \mathbf{X} values ;

R – a randomly generated number from 0 to 1.

When the values of the vector \mathbf{X} have been generated, they are introduced into the model and the calculation of node voltages and branch currents is performed according to the methods given in Chapter 3 and 4. Then, the model outputs are compared with the measurement data as described in the previous section. This process is repeated until a certain number of improvements (N_{IMPR}) is reached, when the recalculated value of difference Δ is smaller than the previous best one. Each time an improvement is made, the smallest Δ value and the corresponding vector \mathbf{X}_B of the best estimates is updated. When the number of improvements (N_{IMPR}) has been reached, the limits of vector \mathbf{X} imposed on random number generator are reduced:

$$\mathbf{X}_{\max}, \mathbf{X}_{\min} = \mathbf{X}_B \pm \mathbf{X}_N (\mathbf{K}_{\%} / (200s)), \quad (5.3)$$

where \mathbf{X}_B – the vector \mathbf{X} with the currently smallest value of the objective function;

$\mathbf{K}_{\%}$ – the maximum difference from the nominal or average values of \mathbf{X} elements, %;

\mathbf{X}_N – a vector of the nominal or average values of \mathbf{X} elements;

s – the step number of the parameter estimation process.

The described process of generation of the unknown parameter vector \mathbf{X} , recalculation of the objective function (the difference), reduction of the search space limits for a random number generator based on the best values of model parameters is repeated until the convergence criteria are met. Taking into account that for different network configurations and fault scenarios the absolute value of the f_{OBJ} minima may differ, but the decrease in the rate of change of this difference df_{OBJ} will remain similar during the convergence process, the end criterion for the parameter estimation was chosen: $df_{\text{OBJ}} \leq 0.001$. The general block

diagram of the proposed parameter estimation algorithm implemented with modified randomised search described above is presented in Fig. 5.2.

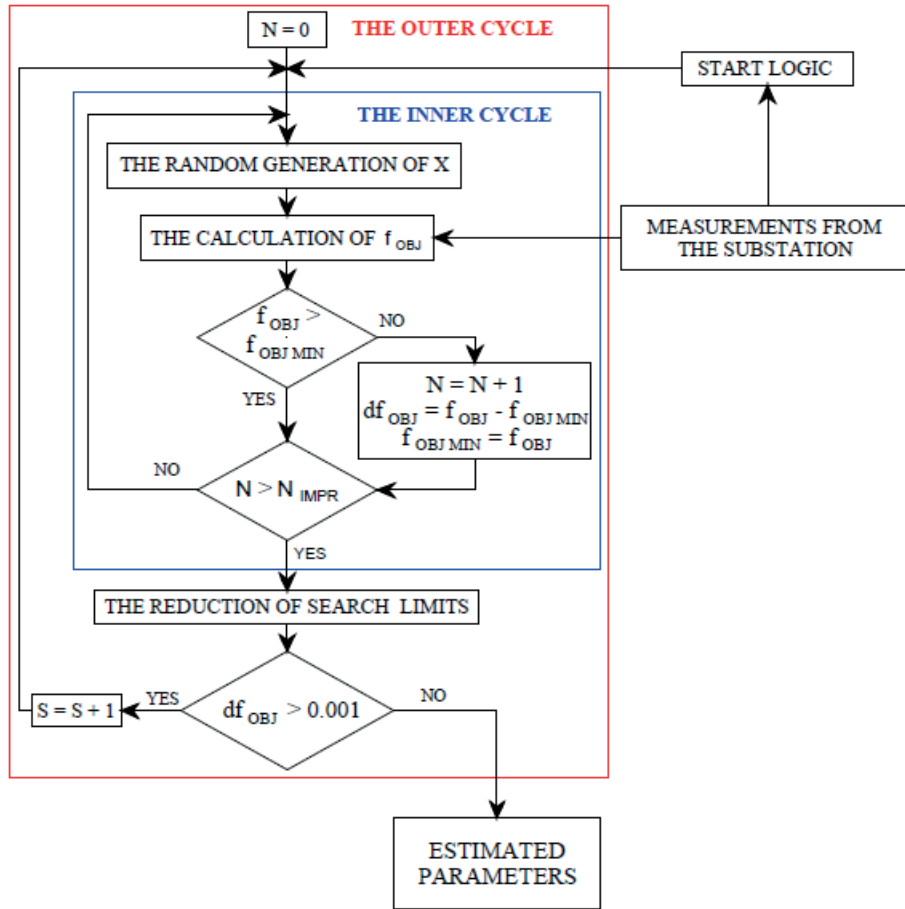


Fig. 5.2. The flowchart of unknown parameter estimation algorithm implemented using a modified randomised search algorithm.

This optimisation method in combination with the estimation of model parameters described in Section 5.1 was first tested for the DP. The fault distance obtained was used to calculate apparent impedance from the PS impedance of the line for easier comparison with the classical DP algorithm using the following formula for L-E faults in one-circuit lines [12], [70]:

$$\dot{Z}_{REL} = \dot{U}_{Ph} / (\dot{I}_{Ph} + \dot{K}i^0), \quad (5.4)$$

and formula for L-E faults in double-circuit line [12], [70]:

$$\dot{Z}_{REL} = \dot{U}_{Ph} / (\dot{I}_{Ph} + \dot{K}i^0 + \dot{K}_M i_P^0), \quad (5.5)$$

where \dot{Z}_{REL} – the apparent impedance determined by DP relay, Ω ;

\dot{U}_{Ph} – the phasor of the faulted phase voltage, V;

\dot{I}_{Ph} – the phasor of the faulted phase current, A;

i^0 and i_P^0 – phasors of the ZS currents of the faulted and healthy parallel line, A;

\dot{K} – a ZS compensation coefficient determined by the ZS and PS impedances of the faulted line ($\dot{K} = (\dot{Z}_L^0 - \dot{Z}_L^1) / \dot{Z}_L^1$);

\dot{K}_M – a ZS mutual coupling compensation coefficient determined by impedance of ZS mutual coupling between both lines and the PS impedance of the faulted line ($\dot{K}_M = \dot{Z}_M^0 / \dot{Z}_L^1$).

During the testing of this application, the results for the pre-fault estimation stage were also saved, and they showed that for this optimisation method, the powers of the two generators (P_{G1}, P_{G2}) and two loads (P_A, P_B) were estimated with errors within 2 % (Fig. 5.3). For more details about the testing scenarios and the power system used for the testing of DP, please see [144].

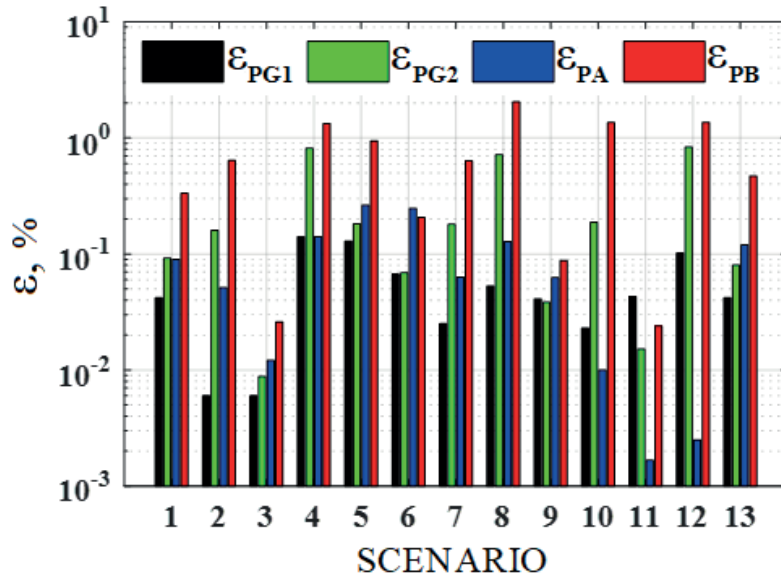


Fig. 5.3. Errors of the pre-fault power estimates from the testing of the application of the model parameter estimation method with modified randomised search for DP [144].

The results from testing of the fault estimation stage of the proposed method and the classical DP relay algorithm showed that the fault path resistance does not have to be extraordinarily large (it did not exceed 36Ω in these scenarios) for the apparent impedance to result in significant errors, but the proposed algorithm was able to successfully determine the fault distance with comparatively miniscule errors (Fig. 5.4).

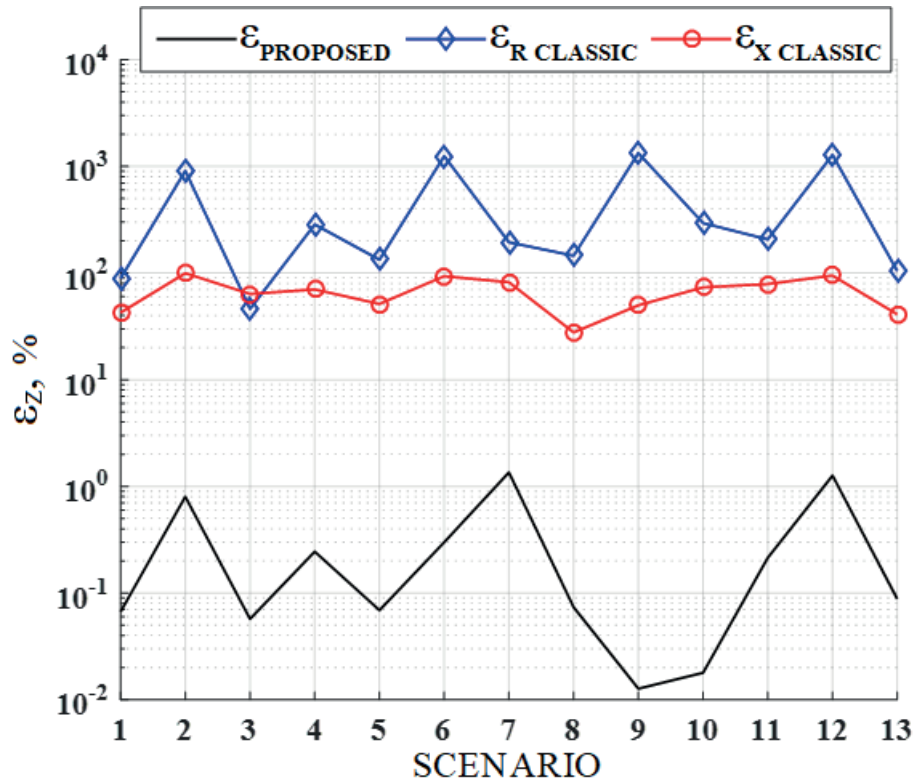


Fig. 5.4. Errors of the apparent impedance estimates obtained by the proposed method with modified randomised search and apparent resistance and reactance obtained by the classical DP relay relative to impedance of the line to the fault point [144].

The effects of these errors on the performance of the DP can also be demonstrated using zone operation regions in an R - X diagram (see Fig. 5.5 where the blue circles depict precise fault impedances, the red triangles close to them are the impedances obtained by the proposed method using the modified randomised search algorithm and the black quadrangles are the results obtained by the classic relay algorithm).

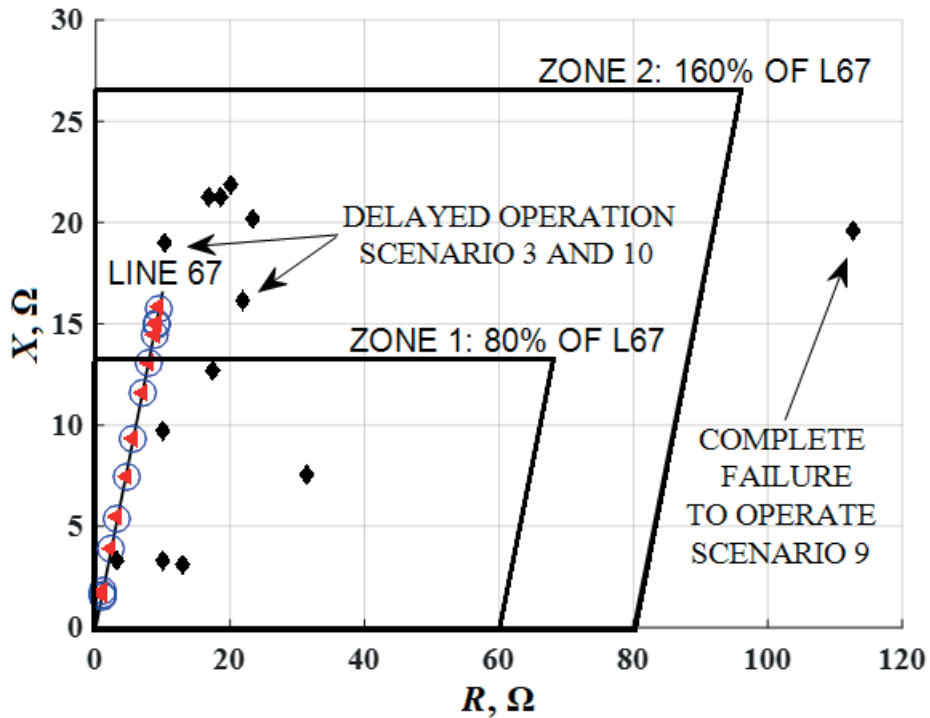


Fig. 5.5. Comparison of apparent impedances obtained by the classical DP relay algorithm and the proposed method in the R - X plane and their impact on the performance of DP [144].

The R - X diagram in Fig. 5.5 shows that the presence of the fault path resistance resulted in an apparent impedance shift from Zone I to Zone II and consequently an additional time delay for scenarios 3 and 10 (similarly to the results obtained in the DP testing in Section 4.5). Scenario 9, which considered the highest fault path resistance of 35.7Ω , resulted in an apparent impedance shift from just inside Zone I to beyond Zone II for the classical DP relay algorithm, which in that particular study would have resulted in failure to operate as only 2 zones were considered. Most probably this apparent impedance shift would result in a trip of the next reserving zone III or IV, but this would still result in a significant time delay. Meanwhile, the accuracy of the proposed method allowed the DP to operate correctly for faults inside and outside Zone I and Zone II.

A different study performed later tested the accuracy of FL based on the proposed method with the modified randomised search in comparison of the one-terminal-measurement-based FL method incorporated in the existing digital OHTL protection and automation terminal tested in Section 4.5. This study aimed not only to demonstrate the overall accuracy of the proposed method, but also to directly show how the accuracy of the existing method was unaffected by the fault path resistance, the fault distance and the pre-fault loading of the line (Fig. 5.6).

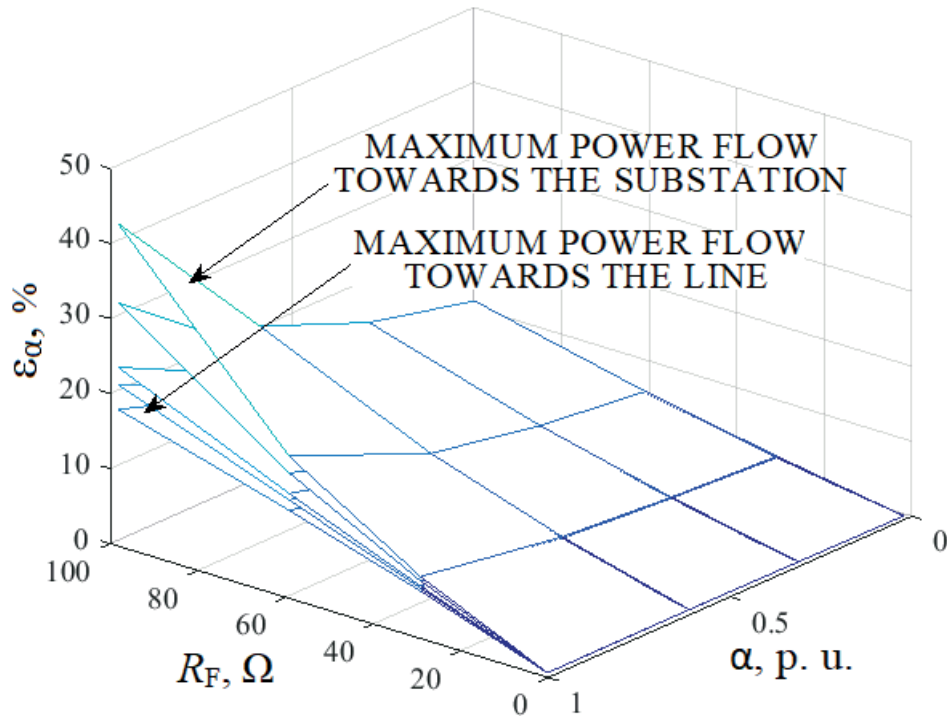


Fig. 5.6. Errors of fault distances determined by an existing fault locator using one-terminal measurements in different cases of pre-fault power flows, fault distances and fault path resistances.

The results shown in Fig. 5.6 indicate that not only does the error of the existing FL increase for faults further in the line with larger fault path resistance, but also that in case of pre-fault power flow towards the substation where the FL is installed the obtained fault distance error will be larger than in case of larger pre-fault power flow towards the line. On the other hand, the proposed method with the modified randomised search provided more accurate results that did not show any distinct dependency on the pre-fault power flow in the line (see Fig. 5.7 where the surface with white sections represents the accuracy of the existing FL and the surface with coloured sections depicts the accuracy of the proposed method and Fig. 5.8). For more details on this study, please see [145].

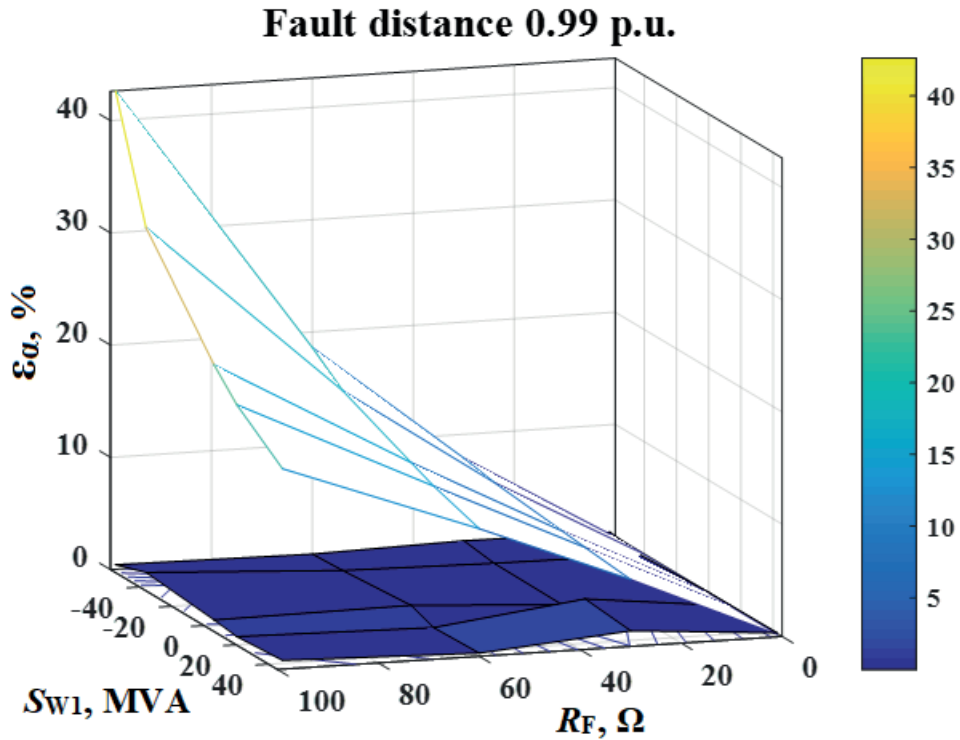


Fig. 5.7. Fault distance estimation errors ϵ_α of an existing fault locator using one-terminal measurements and the proposed method with the modified randomised search algorithm in different cases of pre-fault power flows S_{W1} , fault path resistances R_F and a fixed fault distance of 99 % [145].

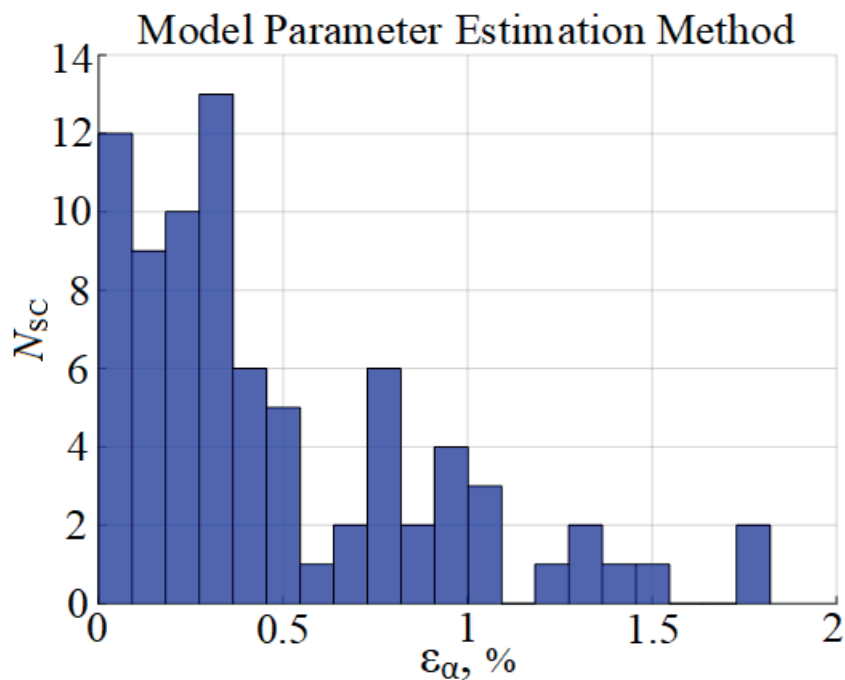


Fig. 5.8. Histogram of fault distance estimation errors ϵ_α of the proposed method with the modified randomised search algorithm [145].

As can be seen from the foregoing analysis, the proposed algorithm was able to provide more accurate and adaptive means for estimation of the fault distance compared with the existing one-terminal-measurement-based DP and FL, by applying the described randomised

search algorithm. However, this approach did require significant calculation time and an even higher accuracy could be desired, which prompted the search for a different optimisation tool that could decrease computation time and improve accuracy while retaining the capability to avoid false extrema.

5.3. Modified genetic algorithm applied for estimation of model parameters

The GA was chosen because it is a versatile and has been shown to be useful in similar technical tasks [54], [146], [147]. This method is also relatively easy to implement and with some safety mechanisms it can avoid convergence to local extrema if they are present in the objective function [148], [149].

The GA is based on the natural selection leading to a group of genomes that correspond to individuals which are most adapted to a particular environment. The optimisation is created by assuming the individuals of a population as particular solutions of the optimisation problem and the objective function values as a measure of fitness or the adaptability of these individuals. The GA can be represented by a chain of several typically used steps or operators:

- pairing of parent individuals;
- recombination (reproduction);
- mutation of offspring individuals;
- determination of the adaptability of parent and offspring individuals;
- selection of population members for the next generation.

Several different types of these GA operators and GA algorithm structures are known and used [27], [147]–[149] from which only the ones used in this Thesis will be described in further detail.

During the parameter estimation with the GA, the values of unknown parameters will be defined as follows:

$$\mathbf{X}_i = \mathbf{X}_{\min i} + \mathbf{K}_{\mathbf{X}_i} \cdot \Delta \mathbf{X}_i, i = 1, \dots, N_{\text{PAR}}, \quad (5.6)$$

where \mathbf{X}_i – the i -th parameter to be estimated;

$\mathbf{X}_{\min i}$ – the minimum considered value of the parameter \mathbf{X}_i ;

$\mathbf{K}_{\mathbf{X}_i}$ – a natural number that determines the estimated value of the parameter \mathbf{X}_i ;

$\Delta \mathbf{X}_i$ – the discretisation step of the result of the parameter \mathbf{X}_i ;

N_{PAR} – the number of parameters to be estimated.

The GA will operate with binary values of $\mathbf{K}_{\mathbf{X}_i}$, the decimal values of which are restricted by the physical limitations of the i -th parameter $0 \leq \mathbf{K}_{\mathbf{X}_i} \leq (\mathbf{X}_{\max i} - \mathbf{X}_{\min i})/\Delta \mathbf{X}_i$, where $\mathbf{X}_{\max i}$ is the maximum considered value of the parameter \mathbf{X}_i . It should also be mentioned that for the GA, each individual or solution is represented by a chromosome, which is a consequent chain of $\mathbf{K}_{\mathbf{X}_i}$ values in binary form and each binary number in this chain is correspondingly called a gene.

The first step of the GA used in this Thesis is the creation of the first population. Typically, this step is performed by randomly generating the values of individuals across the search space until a predefined number of population members $POPsize$ are created. This approach in essence provides the diversity of the gene pool (different starting points on the objective function), which should suffice for GA to converge to a global extremum. However, after some testing of the GA on standard testing functions (axis parallel hyper-ellipsoid function and Schwefel's or sine root function) and on the FL task, it was noticed that for the usually suggested population size $POPsize$ of 20 [26], [148], [149], the speed of the convergence process (number of generations N_{GEN}) and to some degree the accuracy, varied between several identical tests. Additionally, significant differences in the mean values of the objective function of the first generation for repeated tests were observed. Therefore, the different adaptabilities of the randomly generated first-generation individuals were suspected to cause part of the observed variations of the convergence speed and accuracy. In order to make the performance of GA more stable and more dependent on the composition of the objective function than the quality of the first generation members, it was decided to first randomly generate a group of individuals several times larger than $POPsize$. The size of this group was assumed 3000. Then the fitness (the value of the objective function) of the members of this group is calculated using (5.1) and a separate selection is performed to create the first generation for the main GA cycle. This procedure increases the adaptability of the first generation and, as a consequence, it will limit the range of differences between the mean fitness of the first generation, making the convergence process less random. A similar result could be achieved by increasing the $POPsize$, but it would increase the computation cost for every generation and it would significantly prolong the time necessary to meet the convergence criteria. The selection method used to assemble the first generation is the same one that is used in the main GA cycle (described further below). Before entering the main GA cycle, the generation number N_{GEN} is set to 1 and the number of stagnating generations N_{STAG} is set to 0.

The main GA cycle begins with the pairing of the parent individuals, which will be performed by the "outbreeding" approach. According to this approach, one of the two parent individuals is chosen at random from the existing population, but the second parent individual is chosen such that it has the largest Hamming distance (number of different genes) between it and the first parent individual. This approach was chosen because it results in the creation of offspring individuals, which are positioned between the parent individuals in the search space and therefore this decreases the probability of convergence to a local extremum. After the pairing, the probability of occurrence of any mutation of the chromosome of offspring individuals P_{MUT} for these pairs of parent individuals is calculated according to the "incest" approach. This approach increases the probability of chromosome mutations P_{MUT} for offspring individuals created by genetically similar parents:

$$P_{MUT} = P_{MUTmax}(1 - (d_{HAMM}/N_{GENE})) \quad (5.7)$$

where P_{MUTmax} – the maximum probability of mutations of the chromosome of the offspring individuals;

d_{HAMM} – the Hamming distance between the chromosomes of the parent individuals;;

N_{GENE} – the gene count in the chromosomes.

The “incest” mechanic increases the mutations of offspring individuals when the GA converges towards a particular solution, which also decreases the probability of missing the global extremum. The maximum probability of a mutation of an offspring’s chromosome P_{MUTmax} is used in order to prevent the mutation operator from completely blocking the fulfilment of the convergence criterion of the population genetic similarity. Here this value was assumed 90 % as advised in [149].

The second step in the main GA cycle is recombination or reproduction, in which a group of chromosomes sized $POPsize$ is created from chromosomes of parent individuals. In this Thesis, an approach similar to the “triadic crossover” was used. The recombination approach used generates a mask gene of 0 or 1 at random with some probability defined by the user (here, 50 % was chosen) for each gene of a chromosome. Then the genes of the first parent individual from a pair are compared with the corresponding values of the mask. If a gene coincides with the mask, this particular gene is copied to the first offspring individual and the corresponding gene of the second parent individual is copied to the second offspring individual. However, if this gene differs from the mask, the first offspring obtains the gene of the second parent and the second offspring obtains the corresponding gene from the first parent. This approach creates offspring chromosomes as combination from both parents, but it achieves a much higher degree of gene diversity in the offspring individuals than a “single-” or “multi-point crossover” [148], [149] and therefore it provides the opportunity for the GA to test more points in the search space.

The third step in the main GA cycle is the mutation, which can change some genes of the offspring individuals. The approach of “density mutation” was used in this Thesis. This approach first compares a randomly generated value within the boundaries [0, 1] with the probability of chromosome mutations P_{MUT} , calculated after the pairing of parents, for each offspring, and if this random number is smaller than P_{MUT} , then for each gene of this offspring a second random number is generated (also within the boundaries [0, 1]) and compared with the probability of a gene mutation P_{GENEMUT} . When the second random number is smaller than P_{GENEMUT} , this gene is inverted. The value of P_{GENEMUT} was assumed 25 % in order to further stimulate the genetic diversity of the offspring individuals. After the recombination and mutation, the values of the fitness (the objective function) of the offspring individuals are calculated.

The fourth step in the main GA cycle is the selection process that determines which parent and offspring or randomly generated individuals should be allowed to form the next generation according to their adaptability or fitness (the value of the objective function). The selection process applied here consists first of the “Elite selection” approach where 10 % (at least 1 member) of next generation members are directly chosen from a selection group consisting according to their adaptability, but for all the remaining positions to the next generation, the “roulette-wheel selection” is applied where the probability of “winning” a position into the next generation is determined by the value of the objective function of an individual (for the minimisation task):

$$P_k = 1 - (f_{OBJk} / \sum_{m=1}^{N_{REM}} f_{OBJm}), \quad (5.8)$$

where P_k – the probability of “winning” in the roulette-wheel selection for the k -th individual;
 f_{OBJk} – the value of the objective function of the k -th individual;
 N_{REM} – the number of remaining individuals from the selection group which were not chosen for the next generation by the “Elite selection”.

When the selection process is finished, several parameters are calculated. First, the difference between the maximum and minimum fitness values and the maximum Hamming distance of the obtained population for the next generation are calculated for convergence criteria tests:

$$\Delta f_{OBJ} = \left| (\max(\mathbf{F}_{OBJ}) - \min(\mathbf{F}_{OBJ})) / \max(\mathbf{F}_{OBJ}) \right|, \quad (5.9)$$

$$\max d_{HAMM} = \max(D_{HAMM}) / N_{GENE}, \quad (5.10)$$

where Δf_{OBJ} – the difference between the maximum and minimum values of the objective function, p.u.;

\mathbf{F}_{OBJ} – the vector of the objective function values corresponding to the individuals of the obtained population;

$\max d_{HAMM}$ – the maximum value of the Hamming distance between individuals of the obtained population, p.u.;

D_{HAMM} – the matrix of Hamming distances between all of the individuals of the obtained population;

Then, the differences of the maximum and minimum values of the objective function between the current generation and the previous one are calculated:

$$\Delta \max f_{OBJ} = \left| (\max(\mathbf{F}_{OBJ}) - \max f_{OBJ\ MEM}) / \max f_{OBJ\ MEM} \right|, \quad (5.11)$$

$$\Delta \min f_{OBJ} = \left| (\min(\mathbf{F}_{OBJ}) - \min f_{OBJ\ MEM}) / \min f_{OBJ\ MEM} \right|, \quad (5.12)$$

where $\Delta \max f_{OBJ}$ and $\Delta \min f_{OBJ}$ – the differences of the maximum and minimum values of the objective function between the current generation and the previous one, p.u.;

$\max f_{OBJ\ MEM}$ and $\min f_{OBJ\ MEM}$ – the maximum and minimum values of the objective function of the previous generation.

The values of $\Delta \max f_{OBJ}$ and $\Delta \min f_{OBJ}$ are then compared with a user-defined stagnation margin (here, 0.001 p.u. was used) to test if either of the boundaries of the population had any noticeable changes. If both of them are below this setting, it is considered that the GA is stagnating and the number of stagnating generations N_{STAG} is increased by 1; otherwise, this counter is reset to 0. Next, N_{STAG} is compared with a user-defined number of permissible stagnations. The value assumed here is 20 generations, which showed a minimal influence if the convergence process was stable during the testing of the algorithm. When the number of stagnating generations N_{STAG} exceeds the number of permissible stagnations, an additional group of individuals is randomly generated (here, 1000 individuals). In comparison to the generation of the initial selection group before the main GA cycle, the limitation of the random generator for these individuals does not cover the whole search space. The limitations used for the generation of these individuals are obtained by first using the current best

solution in the last obtained population as the centre point and the boundaries around this point are defined by the Hamming distance:

$$\mathbf{K}_{X_i} \in [\mathbf{K}_{XBEST_i} - \Delta\mathbf{K}_{X_i}; \mathbf{K}_{XBEST_i} + \Delta\mathbf{K}_{X_i}], \quad (5.13)$$

where \mathbf{K}_{XBEST_i} – the value of coefficient \mathbf{K}_{X_i} of the i -th parameter of the most adapted individual of the current population;

$\Delta\mathbf{K}_{X_i}$ – the radius of the search space for the additionally generated random individuals determined by the maximum Hamming distance of the current population ($\Delta\mathbf{K}_{X_i} = \max d_{\text{HAMM}}(\mathbf{X}_{\text{maxi}} - \mathbf{X}_{\text{mini}})/(4 \cdot \Delta\mathbf{X}_i)$).

This approach to the setting of limitations for the random generator was chosen so that the diameter of the search space should not exceed 50 % of the total search space defined by \mathbf{X}_i limitations, which allows decreasing the number of random individuals generated and retaining sufficient coverage of random points within these limitations. The main reason of this additional procedure is to manually increase genetic diversity available to GA when the natural selection process yields no results and to test if the current best solution is not a local minimum. It can also be seen that, as the population converges towards a solution, these limitations decrease, which can potentially generate solutions similar to the best one helping the convergence if the recombination and mutations yield only offspring individuals with a low adaptability, stalling the convergence. As before, the values of objective functions for these randomly generated individuals are then calculated and another selection process is performed between the current population and the additional group of individuals. After the selection process, the number of stagnating generations N_{STAG} is reset to 0.

The last step in the main cycle of the GA is the test of convergence criteria. These can be defined by the values of the Hamming distance or the difference of the objective function values between members of the population obtained after the selection process and/or they can be defined by changes of these criteria between the current generation and the previous one. In this Thesis, the criteria of minimal difference between maximum and minimum values of the objective function $\min \Delta f_{\text{OBJ}}$ and the minimal Hamming distance $\min d_{\text{HAMM}}$ in p.u., and an additional minimal generation count $\min N_{\text{GEN}}$ was used. After some testing of the GA, the values of $\min \Delta f_{\text{OBJ}} = 0.05$ p.u. and $\min d_{\text{HAMM}} = 0.05$ p.u., and $\min N_{\text{GEN}} = 50$ were chosen because they ensured a sufficient accuracy while not prolonging the convergence process. If any of the convergence criteria are not met, then the steps of the main GA cycle are repeated. The flowchart of the GA used for the FL can be seen in Fig. 5.9. The convergence of this approach is presented in Fig. 5.10 and 5.11. The case study results obtained with the estimation of the model parameters with the modified GA will be presented separately in Chapter 7 of the Thesis.

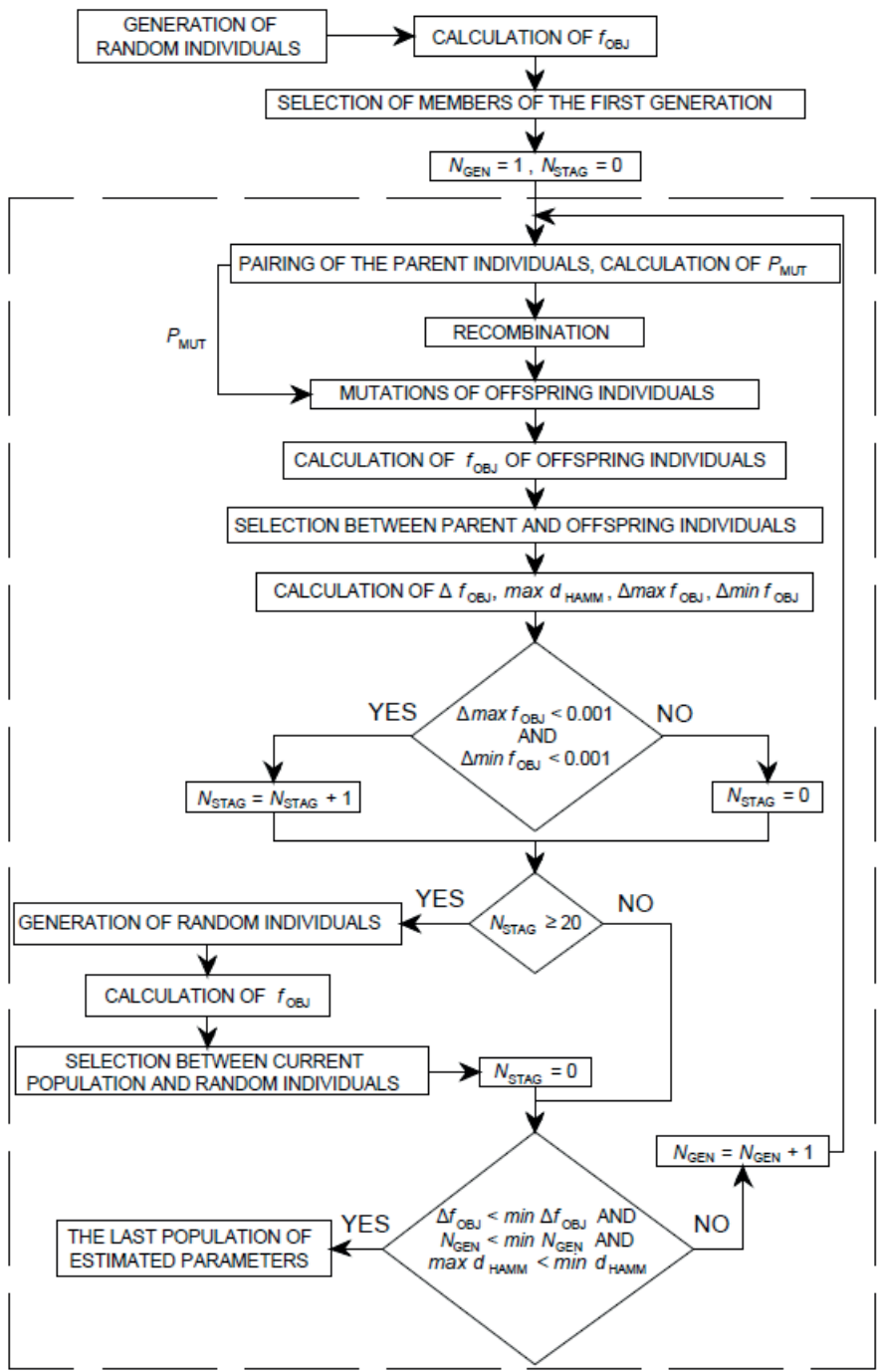


Fig. 5.9. The flowchart of GA used for estimation of unknown model parameters.

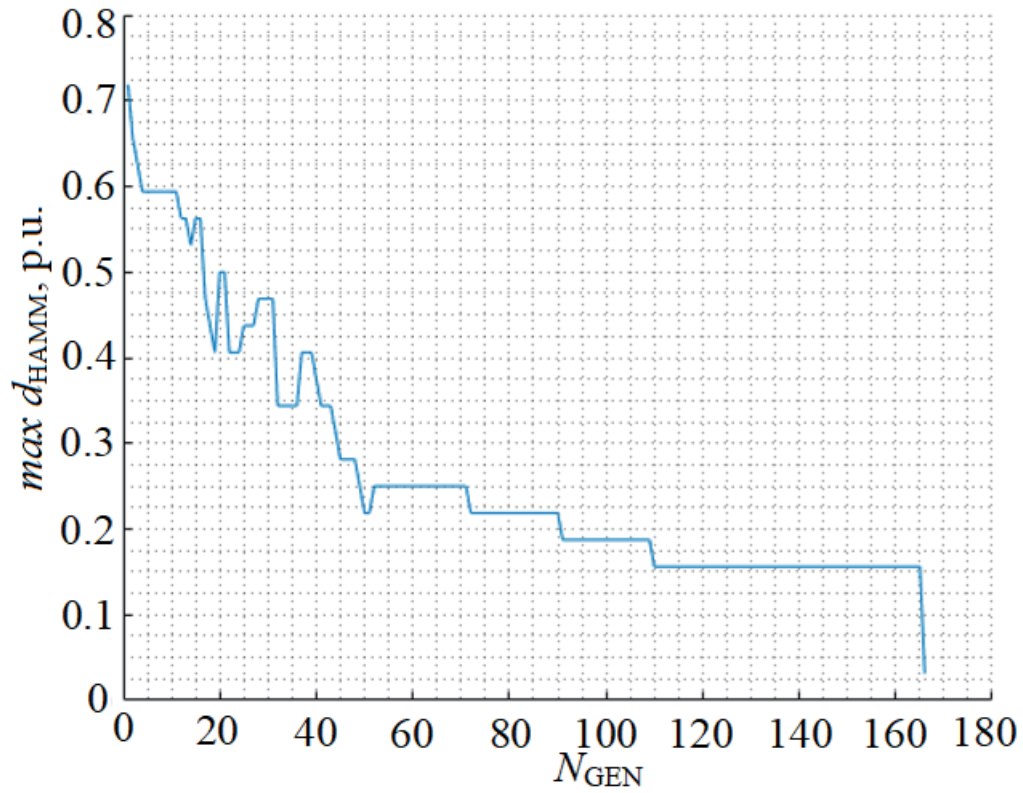


Fig. 5.10. GA convergence towards one solution shown by maximum genetic difference of the population.

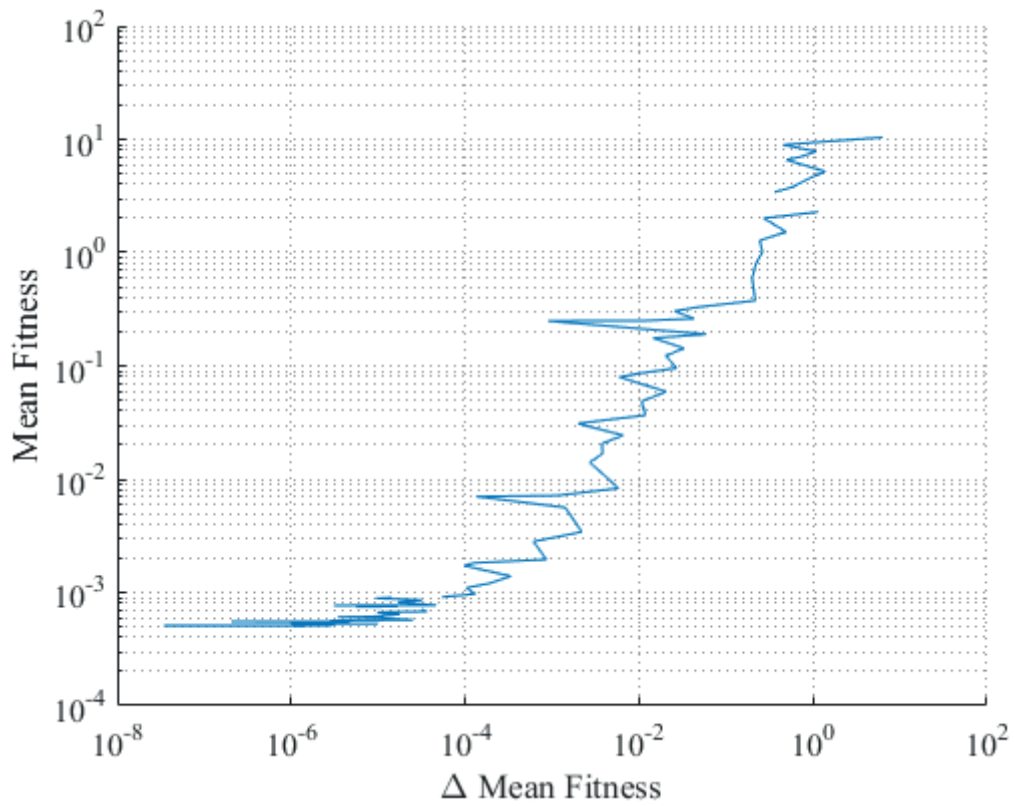


Fig. 5.11. The convergence path of GA used for estimation of unknown model parameters shown by the mean population fitness and its change between generations.

5.4. Conclusions

1. The division of the model parameter estimation into two stages reduces the amount of unknown data that have to be determined after fault inception, thus making the second stage more feasible.
2. Since the objective function for the estimation of unknown parameters can have distortions and false extrema, an optimisation tool that can find the global extremum in such conditions is necessary.
3. The accuracy of the existing digital FL using one-terminal measurements has a high degree of dependence on the pre-fault power flow, especially if it is oriented towards the substation. The proposed applications of parameter estimation for DP and FL do not have this dependence as both the equivalent fault path resistance and the pre-fault loading of the power system are also estimated.
4. The proposed method provided a sufficient accuracy for both estimation stages, when tested with the modified randomised search as an optimisation tool, and in terms of accuracy it outperformed DP and FL algorithms implemented in an existing OHTL protection and automation terminal.
5. The initially tested modification of a randomised search provided satisfactory results, but it did require significant computation time, which led to the adoption of the GA.

6. SYNTHESIS OF OPTIMAL OBJECTIVE FUNCTION FOR ESTIMATION OF MODEL PARAMETERS

The framework of the parameter estimation for FL and DP described in Chapter 5 of this Thesis is universal in nature, but the question of the synthesis of an optimal version of the objective function (5.1) remains. This can include the use of optimal weight coefficient K_{w_i} values and a selection of optimal parameter group Y . In case of the pre-fault regime, the parameter group Y used for (5.1) should include at least voltage, current and apparent power measurements from the controlled substation. Taking into an account that the pre-fault regime in a transmission system will be practically symmetrical [150], [151], this parameter group size will not be exceedingly large. The faults, on the other hand, can be expected to be mainly asymmetrical [62], [152], [153] with the most common ones being the L-E faults in the Northern-European region [1]. Therefore the parameter group Y could include real and imaginary parts or magnitudes and angles of phase quantities, symmetrical component quantities of busbar voltages and branch currents, apparent power for each branch connected to the substation as well as combinations of these parameters. This could easily result in an unnecessarily large and hard to manage parameter group. Considering this, the main focus of the synthesis of the optimal objective function in this Thesis was on the objective function for the estimation of the fault regime parameters.

Initially, the task of selecting the optimal parameter group and weight coefficients was merged by applying an additional outer GA that used the accuracy of the proposed method and the necessary generation count for its objective function. The idea was that this algorithm would be provided with a larger already sorted parameter group and the outer GA algorithm could choose the larger weights for “useful” parameters and exclude “harmful” parameters that negatively affect the objective function of the proposed method by choosing a weight coefficient close to zero. However, this required performing numerous FL tests for each possible combination of weight coefficients for the mean results of these tests to be more dependent on the particular combination of weights. Therefore, the convergence of this outer GA was slow and in most cases identical attempts of this optimisation randomly selected high coefficient values for most of the parameters and low ones for the remaining ones. This result indicated that almost every parameter selected by the parameter selection strategies described in Section 6.1 below could be part of one of many potentially successful parameter groups Y and that more probably the number of available parameters has a greater impact than the particular values of the weight coefficients. Based on these results, it was decided to assume K_{w_i} for all the parameters used for the estimation of fault parameters 100 to slightly magnify the sensitivity of all parameters, and instead test different parameter selection strategies and the effect that the number of parameters used has on the accuracy. The weight coefficients could also have an impact on pre-fault parameter estimation stage, but this remains a subject for future studies.

6.1. Fault parameter selection strategies

As the main purpose of the proposed method is to determine a correct fault distance, the accuracy of estimation of this parameter can be prioritised. Considering that the fitness or objective function is defined as the difference between measured and modelled parameter values, one can expect that the sensitivity of the parameter to changes in the fault distance α is vital since if there are no changes of the parameter, the optimisation can randomly select any α and still find no difference to the model output. However, after examining the graphs of different parameters, it can be seen that even those parameters that are highly dependent on α in most cases also retain significant dependence on the fault path resistance R_F . The R_F often changes not only the parameter value for a fixed α , but also the rate of change of the parameter when changing α (see Fig. 6.1 and Section 7.1 for description on the case study).

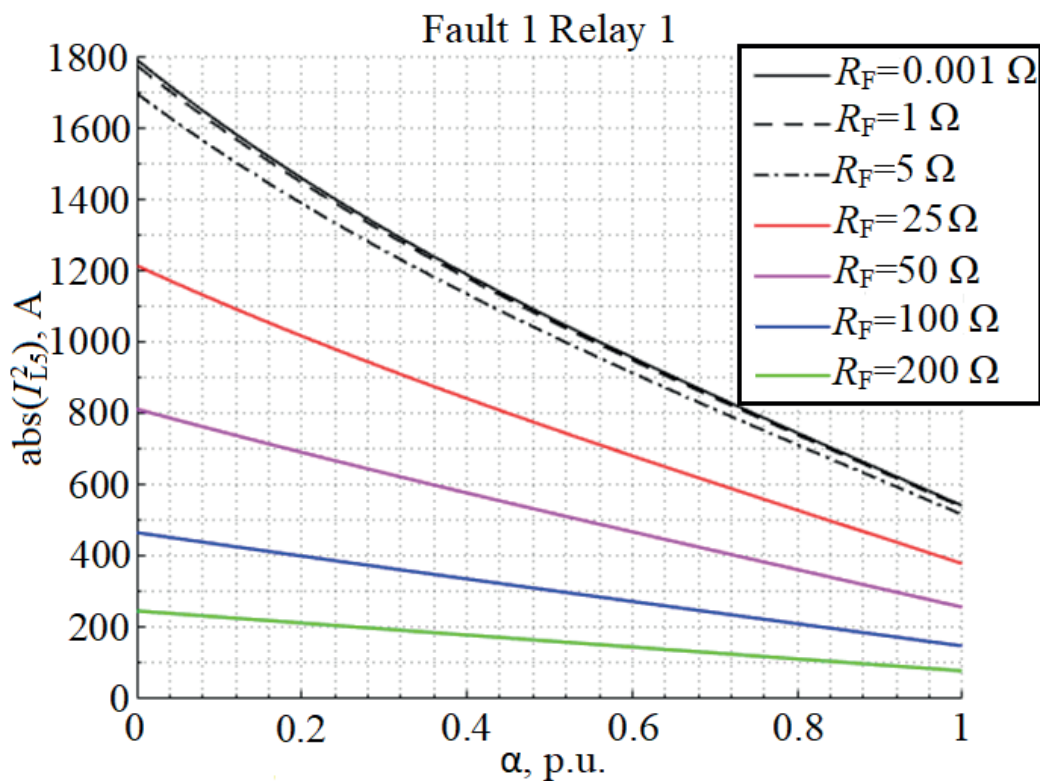


Fig. 6.1. The graph of the absolute value of the NS current of line L5 for the FAULT1 of the case study power system.

Based on the previous considerations, two parameter selection strategies were proposed: a conservative strategy and an opportunistic one. The idea behind the opportunistic strategy is to sort all the available measured or derived parameters at the controlled substation only according to their maximum sensitivity aiming to select the parameters that would result in an objective function with a sufficient difference if the assumed fault distance α differs from the real one α^* to limit the impact of assuming incorrect R_F . The conservative strategy first tests if the minimum sensitivity of an available parameter $\min(\Delta y_i)$ (most often when the true fault path resistance R_F^* is maximum considered value R_{Fmax}) reaches a certain minimum limit and if the change of the parameter is monotonic. This is done to ensure that for all of the considered α and R_F the parameter would yield at least some level of change in its value for

the optimisation to operate with. The monotonic character criterion was put forward to ensure that at least for a correctly determined R_F^* the parameter graph would represent an unambiguous function. After reviewing the results of parameter analysis, the baseline setting of $\min(\Delta y_i) \geq 0.01\%$ was chosen because this limit still allowed to obtain a sufficiently large group of parameters for testing.

In order to compare the sensitivity of the measured parameters, the derivatives of these parameters in respect to α could be used, but for larger power systems obtaining an analytical equation of every parameter $y_i(\alpha)$ and its derivative $dy_i/d\alpha$ is very time-consuming. Therefore, numerical calculations of fault regimes with different fault distances α for several different fault path resistances R_F were performed and then discrete differences $(\Delta y_i/\Delta\alpha) \approx dy_i/d\alpha$ were calculated. Additionally, fixed fault distance intervals of $\Delta\alpha = 0.05$ p.u. of the faulted line were assumed in order to focus on differences of the analysed parameter Δy_i caused by this change in the fault distance.

Taking into an account that the proposed parameter estimation should be accurate for any pre-fault and fault regime, it was decided that before the evaluation and selection of an optimal parameter group, a separate search would be conducted across various loading and generation scenarios to obtain the minimum values of the differences Δy_i for each 5% section of the line of a particular R_F value assumed, ensuring that in any other pre-fault regime the dependency of y_i on α would be even more profound compared to the one used for parameter selection. This search was performed by simulations with randomised pre-fault regimes with R_F values of 0.001 Ω , 1 Ω , 5 Ω , 25 Ω , 50 Ω , 100 Ω and 200 Ω until the decrease of all Δy_i between search steps k and $k + 1$ was below 1% and a minimum of 2000 steps had been carried out. Next, the minimum difference $\min(\Delta y_i)$ (typically when $R_F = 200 \Omega$) and maximum difference $\max(\Delta y_i)$ (typically when $R_F = 0.001 \Omega$) was determined for all of the available parameters. The parameters considered in the initial search were:

- the magnitudes, real and imaginary parts of faulted phase voltage from substation busbars and its PS, NS, ZS quantities;
- the magnitudes, real and imaginary parts of faulted phase current from all the branches connected to the substation and their PS, NS, ZS quantities;
- the magnitudes, real and imaginary parts of faulted phase apparent power from all branches connected to the substation and their PS, NS, ZS quantities;
- the fault distance calculated by an existing FL algorithm [143].

In order to adequately compare the available parameters, which have different numerical values y_i and differences Δy_i , adaptive base quantities of these parameters are necessary. The base quantities adopted in this Thesis can be obtained by first assuming the nominal pre-fault regime. Then the values of faulted phase current magnitude and the faulted phase apparent power magnitude for the particular fault and branch (faulted or healthy) were calculated for all of the analysed α and R_F values, and the maximum value of these was chosen. These were used as a base for parameters corresponding to the faulted phase current, the apparent power or their symmetrical components, but for the voltage parameters, the maximum of the faulted phase voltage magnitude was determined (here, also nominal voltage could be used). These base quantities were chosen because they represent the parameters, which will or can be

directly measured and impact possible measurement errors, which means that the higher in percent is the parameter difference Δy_i caused by difference between the actual fault distance and an assumed one in reference to these base quantities, the lower the possibility that an error in measurements will compromise the results of parameter estimation. The base quantity used for the fault distance obtained by the existing FL algorithm was the line length.

An example of parameter group selection for both strategies and analysis of the results obtained by using these strategies with the GA-based parameter estimation is presented in Chapter 7 of the Thesis.

6.2. Development of future strategies of parameter-selection-based analysis of objective function

The analysis of the surfaces of the objective function in Section 7.2 of this Thesis shows that the tested parameter selection strategies will in some cases yield surfaces of the objective function with distortions and false extrema. In some cases, these extrema will be oriented around the true fault distance α^* , which could cause only minor errors, but in other cases these can be oriented around the true fault path resistance R_F^* value, such as depicted in Fig. 6.2, or in other configurations (Fig. 7.2–7.4). The last two cases can cause more significant fault distance estimation errors if the optimisation algorithm fails to distinguish the true global minimum. Therefore, it was decided to conduct further analysis on the surfaces of the objective function created by individual parameters and their interaction when several parameters are used simultaneously.

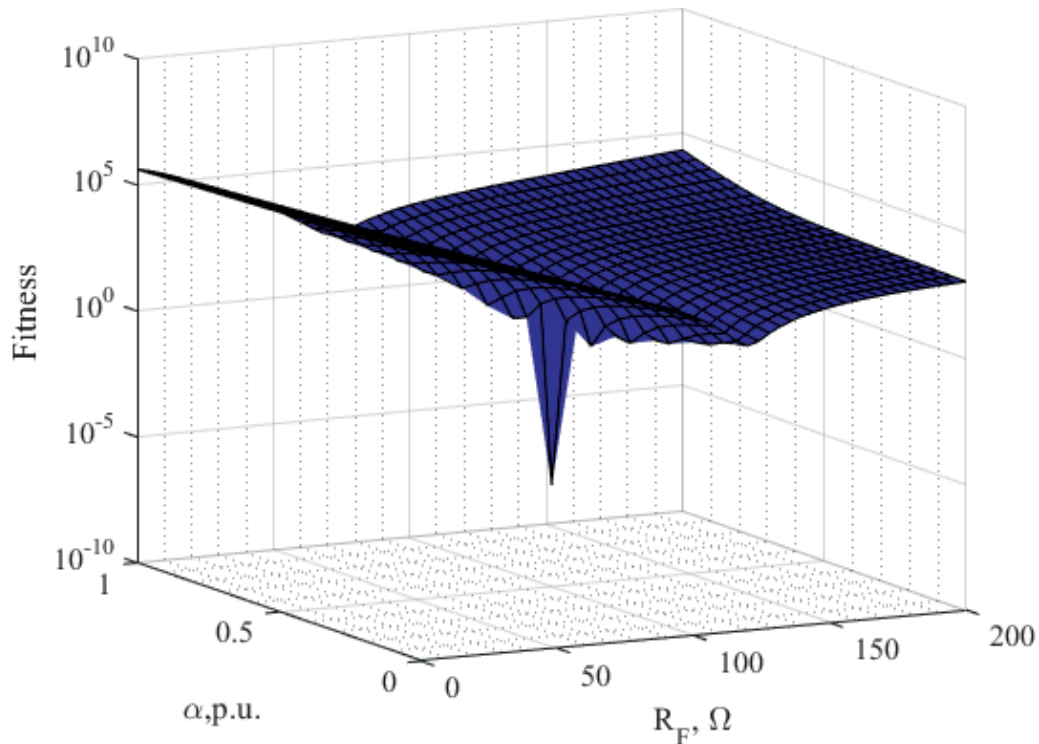


Fig. 6.2. An example of the surface of the objective function (fitness) obtained with the opportunistic parameter selection strategy.

As equation (5.1) shows, for a single parameter y any point in the search space (possible values of at least α and R_F), which has parameter value $y = y^* = y(\alpha^*, R_F^*)$, will yield the lowest possible value of the objective function $f_{OBJ} = 0$. This means that in theory, if only one parameter is used the optimisation can determine the fault distance accurately with certainty only if the measured parameter does not depend on fault path resistance, and function $y(\alpha)$ is monotonic. Otherwise, the surface of the objective function will have value 0 at all points where the surface of the parameter values $y = y(\alpha, R_F)$ crosses a horizontal plane determined by the measured value $y = y(\alpha^*, R_F^*)$, and the optimisation could choose any of these points at random. The orientation of the lines created by these points can be partially assessed with 2D depictions such as Fig. 6.1. A significant number of parameters analysed for the case study power system were monotonic and the characteristics for different fault path resistances were in consequent order (Fig. 6.1), but even for these types of parameters there was a difference in the orientation of lines where $f_{OBJ} = 0$ (hereafter – minimum ravines). Some of these parameters have minimum ravines that are limited by certain fault distance intervals for all of the potential true fault distances and fault path resistances (Fig. 6.3). It should be noted that in the analysis below linearised versions of the true minimum ravines will be depicted as these figures are intended only to approximately illustrate the orientation of the minimum ravines and their interaction.

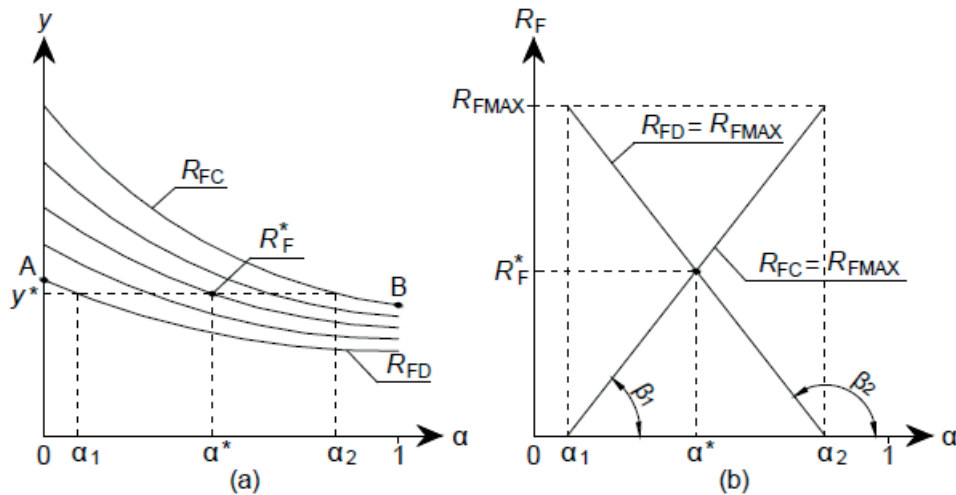


Fig. 6.3. A monotonic graph of the values of parameter y (a) and orientation of minimum points of the objective function (b) when these point are within a limited fault distance interval.

This is true when the maximum point of the characteristic, which has the lowest absolute values $y(A)$, is above the minimum point of the characteristic, which has the highest absolute values $y(B)$, as shown in Fig. 6.3 (a). As can be seen in Fig. 6.3, the smaller the distance between characteristics with different fault path resistances, the closer the orientation of the minimum ravine is to 90° from the α axis (angle β). Most often, the current parameters had the highest values when the fault path resistance was 0Ω and the lowest values when it was the maximum considered value R_{Fmax} , as can be expected and seen in Fig. 6.1, whereas for voltage parameters the opposite tended to be true. This determines whether the angle of ravine β is acute or obtuse as shown in Fig. 6.3 (b). For these parameters, the angle of minimum ravine β can be calculated as follows:

$$\beta_1 = \arctg((R_{FC} - R_{FD}) / (R_{Fmax}(\alpha_2 - \alpha_1))) \text{ if } R_{FC} > R_{FD}, \quad (6.1)$$

$$\beta_2 = 90^\circ + \arctg(R_{Fmax}(\alpha_2 - \alpha_1) / (R_{FC} - R_{FD})) \text{ if } R_{FC} < R_{FD}, \quad (6.2)$$

where R_{FC} and R_{FD} – the boundary fault path resistances of parameter value characteristics that still cross the line $y = y^*$, Ω ;

R_{Fmax} – the maximum fault path resistance considered in the analysis, Ω ;

α_1 and α_2 – the fault distance limits for which there is at least one point from the line $y = y^*$, p.u.

If the value $y(A) < y(B)$, any point (α, R_F) that has parameter value within the zone between lines $y = y(A)$ and $y = y(B)$ will have a ravine with limited fault path resistance and all of the potential fault distance values (Fig. 6.4).

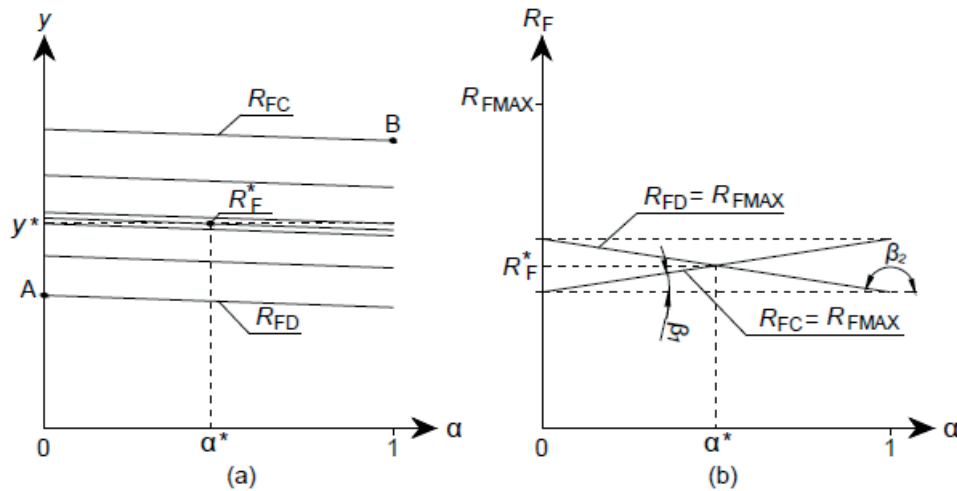


Fig. 6.4. A monotonic graph of the values of parameter y (a) and orientation of minimum points of the objective function (b) when these points are within limited fault path resistance interval.

One can see that the distance between the characteristics of different R_F values in Fig. 6.4 (a) is larger than in Fig. 6.3 (a) and therefore the angles in Fig. 6.4 (b) are either smaller or larger than in Fig. 6.3 (b) depending on β being acute or obtuse. The equations for determination of the angle of ravine β are the same as before, only in most cases the difference $\alpha_2 - \alpha_1$ is equal to 1 p.u. and R_{FC} and R_{FD} are different from both 0 Ω and R_{Fmax} .

There are also parameters with mixed order of characteristics, and other parameters, which result in multiple minimum ravines simultaneously (function $y(\alpha)$ is ambiguous). One type of these parameters has V-shape characteristics (typical for NS and ZS current of a healthy parallel line) that yield one ravine with an acute angle and another one with an obtuse angle (see Fig. 6.5).

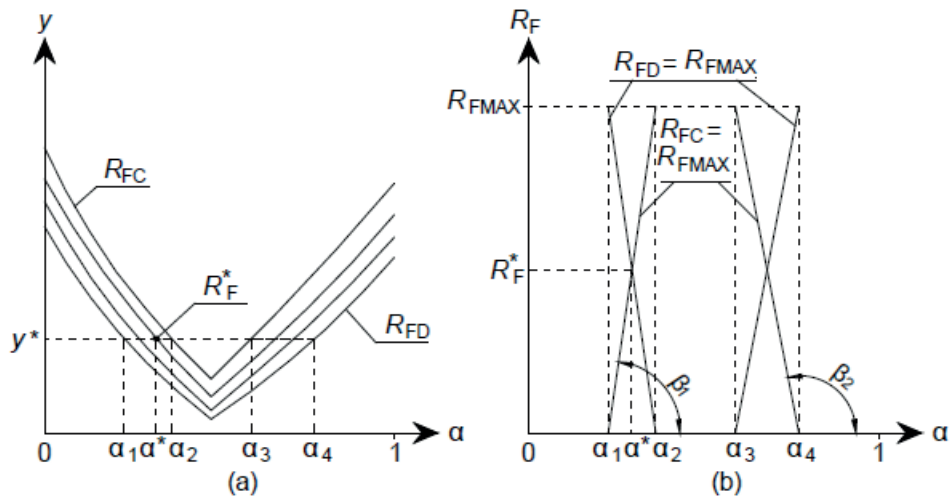


Fig. 6.5. A V-shape graph of the values of parameter y (a) and orientation of the minimum points of the objective function (b).

In theory, these parameters can be used as well, because the ravines of different parameters will cross each other at point (α^*, R_F^*) and the false minimum ravines should be compensated by the surfaces of other parameters, given that the orientation of the minimum ravines for these parameters are sufficiently different from each other. However, the use of the aforementioned parameters also presents difficulties to possible grouping of parameters since the character of the minimum ravines they yield changes for different true fault parameters (α^*, R_F^*) . The crossing of these minimum ravines and the evaluation of their difference can be easily described for linearised versions of the ravines from Fig. 6.3 (b) and Fig. 6.4 (b). This crossing can happen between minimum ravines that have an obtuse angle and an obtuse angle, an acute angle and an obtuse angle as well as an acute angle and an obtuse one (Fig. 6.6).

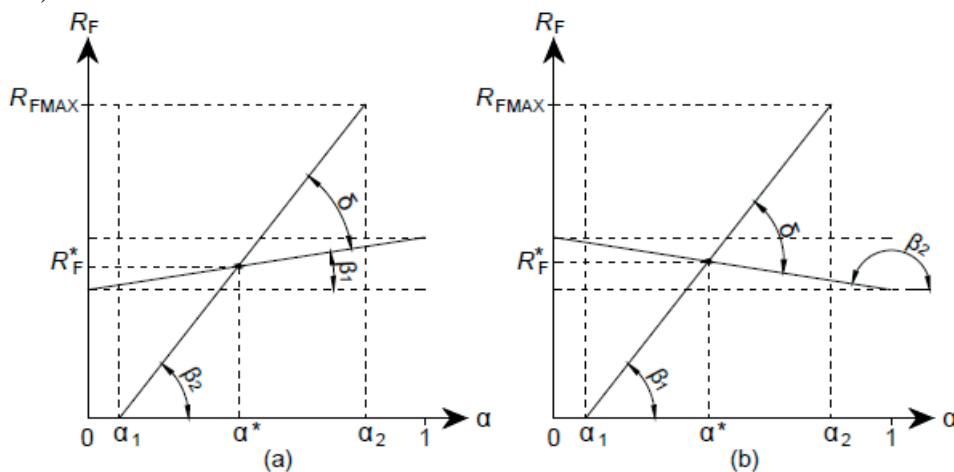


Fig. 6.6. Crossing of two linearised minimum ravines with acute angles (a) and one ravine with an acute angle and a second ravine with an obtuse angle (b).

The difference between the minimum ravines determines how well defined is the objective function for optimisation to locate the true fault distance and the fault path resistance. The closer the ravines are, the less distinct the global minimum will be. This distance can be described by using the smallest angle created at the crossing point (α^*, R_F^*)

by the ravines denoted δ in Fig. 6.6. This angle can be calculated using the angles of each of the ravines. For crossing of two ravines with obtuse or acute angles:

$$\delta = \beta_2 - \beta_1; \beta_2 > \beta_1, \quad (6.3)$$

and for the crossing of one ravine with an acute angle and a second ravine with an obtuse angle:

$$\delta = 180^\circ + \beta_1 - \beta_2; \beta_2 > \beta_1, \quad (6.4)$$

where δ – the smallest angle created by two crossing ravines, $^\circ$;

β_1 and β_2 – the angles of the minimum ravines in reference to the α axis, $^\circ$.

After some testing of combinations of two parameters with varying difference angles δ , it was noticed that starting from values $\delta \approx 10\text{--}20^\circ$, the crossing point of the combined objective function already becomes distinct. Therefore it should be possible to group parameters according to the angle of their linearised minimum ravines while ensuring that the difference angle δ of ravines of individual parameters from two groups remains in the aforementioned interval. Parameter analysis showed that assembling a group of parameters with either a distinctly acute or a distinctly obtuse angle, which are more sensitive to R_F (Fig. 6.4), was relatively easy. The second group should therefore be more sensitive to difference of α (the angle of the ravine should be as close to 90° as possible). These considerations allow formulating approximate criteria to two parameter groups based on the potential angles of their minimum ravines (Fig. 6.7).

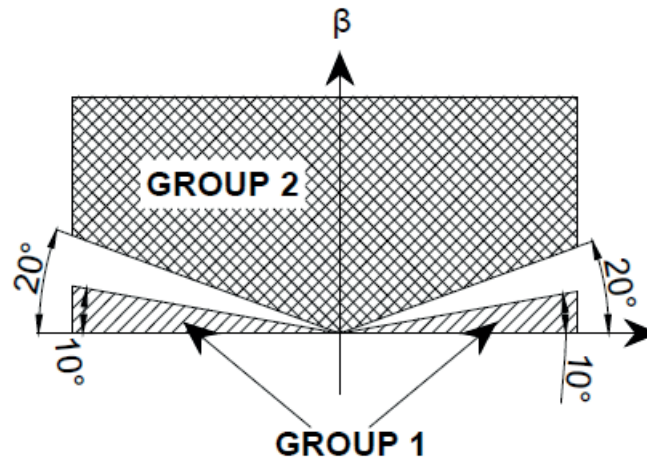


Fig. 6.7. Potential criteria for parameter grouping according to the angle of their minimum ravines.

According to equations (6.3) and (6.4), the division between parameter groups in Fig. 6.7 ensures that $\delta \geq 10^\circ$ if both ravines have either an acute angle or an obtuse one and that $\delta \geq 20^\circ$ if one has an acute angle but the second one has an obtuse angle. If the number of parameters with high dependency on fault distance allows it, the margins of group 2 can be shifted to $30^\circ \leq \beta \leq 150^\circ$ ensuring $\delta \geq 20^\circ$. In this case, the parameter group used for the objective function Y would be created by taking parameters from GROUP1 and GROUP2 in interchanging manner according to their ranking within those subgroups. The ranking could be done by first finding the fault scenario (α , R_F) that has the ravine angle closest to the margins of the particular subgroup. Then the parameters which have the largest angle reserve

to the margins in the “worst” scenario are ranked first. This would allow further increasing the δ for the resulting objective function, assuming that the impact of neither of the subgroups would severely outweigh the other one. This idea could be tested as an individual parameter selection strategy, or combination with the already tested strategies could be used in the future.

6.3. Conclusions

1. One approach to the selection of measured parameters for use in the objective function is to sort them only by their sensitivity to changes in the fault distance. However, it often results in objective functions with surface distortions and false extrema, which increases the risk of inaccurate fault distance estimation.
2. Analysis of measurable parameter curves for different fault distance and resistance values can also be used to obtain parameter groups that would result in fewer distortions in the surface of the objective function and a more distinct global extremum.

7. TESTING OF THE PROPOSED PARAMETER ESTIMATION METHOD AND PARAMETER SELECTION STRATEGIES

7.1. The power system used for the case studies

The power system used for studying the characteristics of the available parameters and the testing of the implementation of the proposed method for FL using GA is presented in Fig. 7.1.

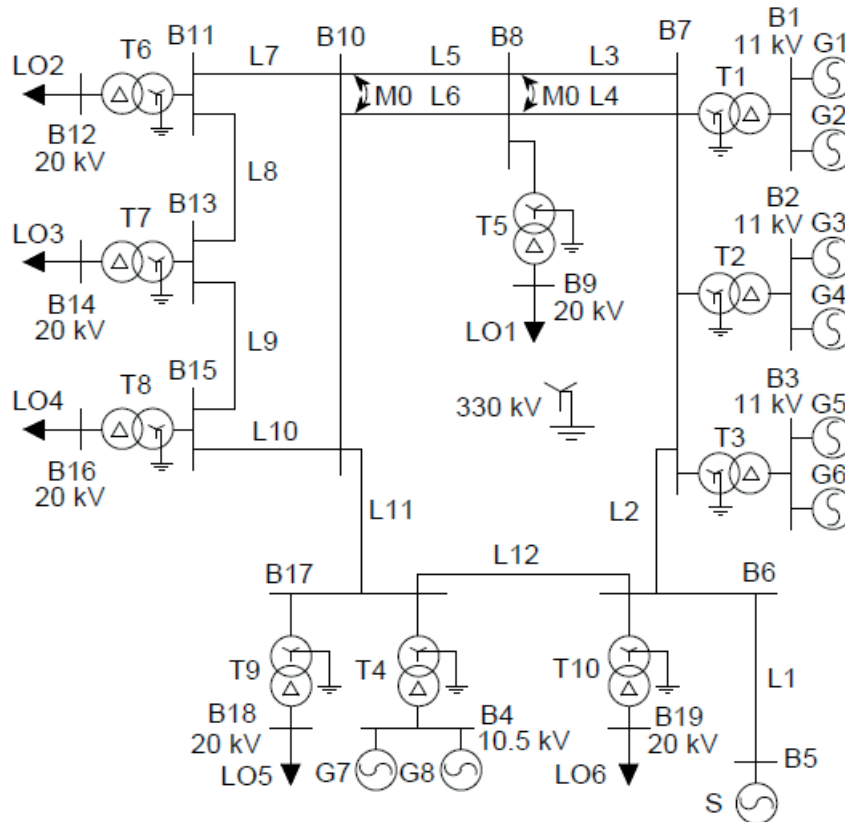


Fig. 7.1. The case study power system.

The data of the case study power system are provided in Tables 7.1–7.4.

Table 7.1.

The Nominal Data of Generators and Loads

ELEMENT	S_N , MVA	U_N , kV	$\cos\varphi_N$
G1,G2,...,G6	56	11	0.9
G7, G8	78.75	10.5	0.8
LO1	80	20	0.9
LO2	200	20	0.89
LO3	100	20	0.88
LO4	180	20	0.94
LO5	40	20	0.86
LO6	60	20	0.92

Table 7.2.

The Resistance and Reactance Data of Generators

PARAMETER	G1,G2,...,G6	G7, G8
Xd, p.u.	0.77	1.199
X'd, p.u.	0.26	0.224
X ⁽²⁾ , p.u.	0.42	0.186
R ⁽¹⁾ , p.u.	0.01	0.01
R ⁽²⁾ , p.u.	0.02	0.02

Table 7.3.

The Data of Transformers

TRANSFORMER	S _N , MVA	Z, %	X/R
T1, T2, T3, T4, T8	200	11	42.17
T5, T7, T9	125	10	36.15
T6	250	11	45.62
T10	63	11.5	31.49

Table 7.4.

The Data of Specific Impedances, Capacitances and Lengths of Transmission Lines

LINE	Z ₀ ¹ , Ω/km	Z ₀ ⁰ , Ω/km	C ₀ ¹ , nF/km	C ₀ ⁰ , nF/km	L, km
L1	0.059 + 0.326i	0.193 + 0.709i	10.774	7.673	30
L2	0.059 + 0.326i	0.193 + 0.709i	10.774	7.673	90
L3	0.059 + 0.325i	0.174 + 0.858i	10.753	6.100	55
L4	0.059 + 0.325i	0.174 + 0.858i	10.753	6.100	55
L5	0.059 + 0.325i	0.174 + 0.858i	10.753	6.100	35
L6	0.059 + 0.325i	0.174 + 0.858i	10.753	6.100	35
L7	0.059 + 0.326i	0.193 + 0.709i	10.774	7.673	20
L8	0.059 + 0.326i	0.193 + 0.709i	10.774	7.673	50
L9	0.059 + 0.326i	0.193 + 0.709i	10.774	7.673	30
L10	0.059 + 0.326i	0.193 + 0.709i	10.774	7.673	35
L11	0.059 + 0.326i	0.193 + 0.709i	10.774	7.673	40
L12	0.059 + 0.326i	0.193 + 0.709i	10.774	7.673	60

The specific impedance of ZS mutual coupling between parallel lines L3, L4 and L5, L6 is $Z_M^0 = 0.115 + 0.449i$ Ω/km. The potential power limits of randomly generated pre-fault regimes were 0–120 % of the nominal value for the active and reactive power of the loads as well as the active power of the generators, but limits –120–120 % were used for the reactive power of the generators. After random generation of these values, it was tested whether such a power system pre-fault regime could be calculated before proceeding to fault regime calculations. Additionally, the denotation of relays and their corresponding buses (controlled substations) as well as faults and corresponding faulted lines considered in this Thesis can be presented (Tables 7.5 and 7.6).

Table 7.5.

Relays and Their Controlled Buses

RELAY	CONTROLLED BUS
RELAY 1	B10
RELAY 2	B8
RELAY 3	B7
RELAY 4	B17
RELAY 5	B6

Table 7.6.

Faults and Faulted Lines

FAULT	FAULTED LINE
FAULT 1	L5
FAULT 2	L6
FAULT 3	L3
FAULT 4	L4
FAULT 5	L2
FAULT 6	L11
FAULT 7	L12

Considering the potential amount of results to be analysed, it was decided that the characteristics of parameters will be analysed only for faults of RELAY 1, RELAY 2, RELAY 3 (a substation close to large loads, an interconnection substation with little load or generation connected and a substation close to large generation units).

7.2. Results of parameter selection

The results of parameter selection for RELAY 1 installed at substation B10 and corresponding faults FAULT 1, FAULT 2 and FAULT 6 can be presented as an example. Taking into account that for each of these faults the parameter analysis included 12 voltage parameters and 12 current parameters as well as 6 power parameters for each of the connected branches and the fault distance determined by the conventional FL algorithm (a total of 103 parameters), only part of the results used for parameter selection will be shown for L6 when L5 is faulted (Table 7.7). The green highlighter indicates that the parameter in this row has been chosen according to the conservative strategy whereas the yellow one – that the parameter has been chosen according to the opportunistic one. The base values for this line are indicated as $\max(|I_{L6}|)$ or $\max(|S_{L6}|)$. The maximum and minimum differences of a particular parameter are indicated as $\max(|\Delta I|)$, $\max(|\Delta S|)$ and $\min(|\Delta I|)$, $\min(|\Delta S|)$. Re and Im below denotes real and imaginary parts.

Table 7.7.

The Results of Line 6 Current and Apparent Power Sensitivity Analysis for RELAY1 in Case of FAULT1

Parameter	max (I_{L6}), A max ($ S_{L6} $), VA	min (ΔI), A min (ΔS), VA	min (ΔI), % min (ΔS), %	max (ΔI), A max (ΔS), VA	max (ΔI), % max (ΔS), %	Characteristics
$ I^1_{L6} $	1398	0.003	2.15E-04	39.21	2.805	Nonmonotonic, no sensitivity if $R_F > 200 \Omega$
$ I^2_{L6} $		4.975	3.56E-01	39.18	2.803	Nonmonotonic
$ I^0_{L6} $		3.805	2.72E-01	28.98	2.073	Nonmonotonic
$ I_{L6} $		0.0001	7.15E-06	108	7.725	Nonmonotonic, no sensitivity if $R_F > 200 \Omega$
Re (I^1_{L6})		3.543	2.53E-01	21.64	1.548	Monotonic
Im (I^1_{L6})		0	0	38.06	2.722	Nonmonotonic, no sensitivity if $R_F > 100 \Omega$
Re (I^2_{L6})		3.54	2.53E-01	21.48	1.536	Monotonic
Im (I^2_{L6})		0.0001	7.15E-06	37.7	2.697	Nonmonotonic, no sensitivity if $R_F > 100 \Omega$
Re (I^0_{L6})		3.046	2.18E-01	16.03	1.147	Monotonic
Im (I^0_{L6})		0.0001	7.15E-06	27.6	1.974	Nonmonotonic, no sensitivity if $R_F > 100 \Omega$
Re (I_{L6})		10.14	7.25E-01	59.16	4.232	Monotonic
Im (I_{L6})		0.0002	1.43E-05	103.4	7.396	Nonmonotonic, no sensitivity if $R_F > 100 \Omega$
Re (S^1_{L6})		2.12E+08	7.54E+05	3.55E-01	4.45E+06	2.098
Im (S^1_{L6})	7.36E+04		3.47E-02	5.50E+06	2.588	Monotonic
Re (S^2_{L6})	1.46E+04		6.85E-03	9.88E+05	0.465	Monotonic
Im (S^2_{L6})	6.73E+04		3.17E-02	4.54E+06	2.139	Monotonic
Re (S^0_{L6})	415.6		1.96E-04	1.65E+05	0.078	Nonmonotonic, no sensitivity if $R_F > 200 \Omega$
Im (S^0_{L6})	9281		4.37E-03	1.41E+06	0.666	Monotonic

After reviewing the results of the parameter analysis, groups of up to 20 parameters were chosen for both of the strategies. These parameter groups and the ranking of parameters within those groups according to Section 6.1 of this Thesis are presented in Tables 7.8–7.10 (here, “REDI” denotes the existing FL algorithm [143]).

Table 7.8.

The Parameter Groups for RELAY1 According to the Conservative and Opportunistic
Parameter Selection Strategies

RANK	FAULT1		FAULT2		FAULT6	
	Conservative	Opportunistic	Conservative	Opportunistic	Conservative	Opportunistic
1.	$\text{Re}(I_{L6})$	REDI	$\text{Re}(I_{L5})$	REDI	$ I_{L7}^0 $	REDI
2.	$\text{Im}(S_{L6}^1)$	$\text{Im}(I_{L6})$	$\text{Im}(S_{L5}^1)$	$ I_{L5} $	$ I_{L10}^0 $	$ I_{L10} $
3.	$ I_{L7}^0 $	$ I_{L6} $	$ I_{L7}^0 $	$\text{Im}(I_{L5})$	$ I_{L5} $	$ I_{L7} $
4.	$ I_{L10}^0 $	$\text{Re}(I_{L6})$	$ I_{L10}^0 $	$\text{Re}(I_{L5})$	$ I_{L6} $	$\text{Im}(I_{L7})$
5.	$\text{Im}(S_{L6}^2)$	$ I_{L5} $	$\text{Im}(S_{L5}^2)$	$ I_{L6} $	$\text{Re}(I_{L11})$	$ I_{L7}^0 $
6.	$\text{Re}(S_{L6}^1)$	$\text{Im}(I_{L5})$	$\text{Re}(S_{L5}^1)$	$\text{Im}(I_{L6})$	$ I_{L11}^0 $	$ I_{L10}^0 $
7.	$\text{Re}(I_{L5})$	$ I_{L6}^1 $	$\text{Re}(I_{L6})$	$ I_{L5}^1 $	$\text{Re}(I_{L5})$	$\text{Im}(I_{L10})$
8.	$ I_{L11} $	$ I_{L6}^2 $	$ I_{L11} $	$\text{Im}(S_{L5}^1)$	$\text{Re}(I_{L6})$	$\text{Im}(I_{L7}^0)$
9.	$\text{Re}(I_{L6}^1)$	$ I_{L10} $	$\text{Re}(I_{L5}^1)$	$ I_{L5}^2 $	$ I_{L5}^2 $	$\text{Im}(I_{L10}^0)$
10.	$\text{Re}(I_{L6}^2)$	$\text{Im}(I_{L6}^1)$	$\text{Re}(I_{L5}^2)$	$\text{Im}(I_{L5}^1)$	$ I_{L6}^2 $	$ I_{L11} $
11.	$ I_{L5}^0 $	$\text{Im}(I_{L6}^2)$	$ I_{L6}^0 $	$ I_{L7} $	$ I_{L5}^1 $	$\text{Im}(I_{L11})$
12.	$\text{Re}(I_{L10}^0)$	$\text{Im}(S_{L6}^1)$	$\text{Im}(S_{L6}^2)$	$\text{Im}(I_{L5}^2)$	$ I_{L6}^1 $	$ I_{L5} $
13.	$\text{Im}(S_{L5}^2)$	$ I_{L7} $	$\text{Re}(I_{L7}^0)$	$ I_{L10} $	$ I_{L11}^2 $	$ I_{L6} $
14.	$\text{Re}(I_{L6}^0)$	$\text{Im}(I_{L10})$	$ I_{L6}^2 $	$\text{Im}(I_{L7})$	$ I_{L5}^0 $	$\text{Im}(I_{L5})$
15.	$ I_{L5}^2 $	$ I_{L7}^0 $	$\text{Re}(I_{L5}^0)$	$ I_{L7}^0 $	$ I_{L6}^0 $	$\text{Im}(I_{L6})$
16.	$\text{Re}(S_{L5}^1)$	$ I_{L10}^0 $	$\text{Re}(S_{L6}^1)$	$ I_{L10}^0 $	$ U_{B10}^0 $	$\text{Re}(I_{L7})$
17.	$\text{Re}(I_{L11})$	$\text{Im}(I_{L7}^0)$	$\text{Re}(I_{L11})$	$\text{Im}(I_{L10})$	$ U_{B10}^0 $	$\text{Re}(U_{B10})$
18.	$\text{Re}(I_{L5}^0)$	$\text{Im}(I_{L7})$	$\text{Re}(I_{L6}^0)$	$\text{Im}(I_{L7}^0)$	$\text{Re}(I_{L5}^1)$	$ U_{B10} $
19.	$\text{Re}(I_{L5}^2)$	$\text{Im}(I_{L10}^0)$	$\text{Re}(I_{L6}^2)$	$\text{Im}(I_{L10}^0)$	$\text{Re}(I_{L6}^1)$	$\text{Re}(I_{L10})$
20.	$\text{Re}(I_{L5}^1)$	$\text{Im}(S_{L6}^2)$	$\text{Re}(I_{L6}^1)$	$\text{Im}(S_{L5}^2)$	$\text{Re}(I_{L5}^2)$	$\text{Re}(I_{L10}^0)$

Table 7.9.

The Parameter Groups for RELAY2 According to the Conservative and Opportunistic Parameter Selection Strategies

RANK	FAULT1		FAULT2		FAULT3		FAULT4	
	Conservative	Opportunistic	Conservative	Opportunistic	Conservative	Opportunistic	Conservative	Opportunistic
1.	REDI	REDI	REDI	REDI	Re (I_{L4})	REDI	Re (I_{L3})	REDI
2.	Re (I_{L6})	$ I_{L6} $	Re (I_{L5})	$ I_{L5} $	Im (S^0_{T5})	$ I_{L4} $	$ I^0_{T5} $	$ I_{L3} $
3.	$ I_{L5} $	Im (I_{L6})	$ I_{L6} $	Im (I_{L5})	$ I^0_{T5} $	Im (I_{L4})	Im (S^0_{T5})	Im (I_{L3})
4.	$ I^0_{T5} $	Re (I_{L6})	Im (S^1_{L5})	Re (I_{L5})	Re (I_{L3})	$ I_{L3} $	Im (S^1_{L3})	$ I_{L4} $
5.	Im (S^1_{L6})	$ I_{L5} $	Im (S^0_{T5})	$ I^2_{L5} $	Re (S^1_{L4})	Im (I_{L3})	Re (I_{L4})	Re (I_{L3})
6.	Im (S^0_{T5})	Im (I_{L5})	$ I^0_{T5} $	$ I_{L6} $	Im (S^2_{L4})	$ I_{T5} $	Re (S^1_{L3})	Im (I_{L4})
7.	Re (S^1_{L6})	$ I^2_{L6} $	Re (S^1_{L5})	Im (I_{L6})	$ I^0_{L3} $	Re (I_{L4})	Im (S^2_{L3})	$ I_{T5} $
8.	Im (S^2_{L6})	$ I^1_{L6} $	Im (S^2_{L5})	$ I^1_{L5} $	Re (I^2_{L4})	Im (I_{T5})	$ I^0_{L4} $	$ I^0_{T5} $
9.	Re (I_{L5})	$ I_{T5} $	Re (I_{L6})	Im (I^1_{L5})	Im (S^2_{L3})	Im (S^0_{T5})	Re (I^2_{L3})	Im (I_{T5})
10.	Re (I^1_{L6})	Im (I^1_{L6})	$ I_{L3} $	Im (I^2_{L5})	Re (I^1_{L4})	$ I^0_{T5} $	Re (I^1_{L3})	Im (S^0_{T5})
11.	Re (I^2_{L6})	Im (I^2_{L6})	$ I_{L4} $	Im (S^1_{L5})	$ I^2_{L3} $	Im (I^0_{T5})	Im (S^2_{L4})	Im (I^0_{T5})
12.	$ I_{L3} $	Im (I_{T5})	Re (I^1_{L5})	Im (S^0_{T5})	$ I^0_{L5} $	$ I_{L5} $	$ I^2_{L4} $	$ I_{L5} $
13.	$ I_{L4} $	$ I^0_{T5} $	Re (I^2_{L5})	$ I_{T5} $	$ I^0_{L6} $	$ I_{L6} $	$ I^0_{L5} $	$ I_{L6} $
14.	$ I^0_{L5} $	Im (I^0_{T5})	$ I^0_{L6} $	$ I^0_{T5} $	Re (S^1_{L3})	Im (I_{L5})	$ I^0_{L6} $	$ I^0_{L3} $
15.	Re (I^0_{L6})	Im (S^1_{L6})	Re (I^0_{L5})	Im (I_{T5})	Re (I^0_{L4})	Im (I_{L6})	Re (S^1_{L4})	Im (I_{L5})
16.	$ I^1_{L5} $	Im (S^0_{T5})	$ I^1_{L6} $	Im (I^0_{T5})	Re (I^0_{L3})	$ I^2_{L4} $	Re (I^0_{L3})	Im (I_{L6})
17.	$ I^2_{L5} $	$ I^0_{L6} $	$ I^2_{L6} $	Re (S^1_{L5})	$ U^0_{B8} $	Im (I^2_{L4})	Re (I^0_{L4})	Im (I^2_{L3})
18.	Im (S^2_{L5})	Re (S^1_{L6})	Im (S^2_{L6})	$ I^0_{L5} $	Re (I^2_{L3})	Im (I^1_{L4})	$ U^0_{B8} $	Im (S^1_{L3})
19.	Re (S^1_{L5})	Im (I^0_{L6})	Re (S^1_{L6})	Im (S^2_{L5})	Re (I^1_{L3})	Im (S^1_{L4})	Re (I^2_{L4})	Im (I^1_{L3})
20.	Re (I^0_{L5})	Im (S^2_{L6})	$ I^0_{L3} $	Im (I^0_{L5})	Re (I^0_{L5})	$ I^1_{L4} $	Re (I^1_{L4})	$ I^1_{L3} $

Table 7.10.

The Parameter Groups for RELAY3 According to the Conservative and Opportunistic Parameter Selection Strategies

RANK	FAULT3		FAULT4		FAULT5	
	Conservative	Opportunistic	Conservative	Opportunistic	Conservative	Opportunistic
1.	REDI	$ I_{L4} $	REDI	$ I_{L3} $	$ I_{L2} $	$ I_{L3} $
2.	$ I_{L3} $	$\text{Im}(I_{L4})$	$ I_{L4} $	$\text{Im}(I_{L3})$	$\text{Im}(S^2_{L3})$	$ I_{L4} $
3.	$\text{Re}(I_{L4})$	REDI	$\text{Re}(I_{L3})$	REDI	$\text{Im}(S^2_{L4})$	$\text{Im}(I_{L3})$
4.	$ I_{T3} $	$ I_{L3} $	$ I_{T3} $	$ I_{L4} $	$\text{Re}(I_{L3})$	$\text{Im}(I_{L4})$
5.	$ I_{T2} $	$\text{Im}(I_{L3})$	$ I_{T1} $	$\text{Im}(I_{L4})$	$\text{Re}(I_{L4})$	REDI
6.	$ I_{T1} $	$\text{Re}(I_{L4})$	$\text{Re}(I_{L4})$	$\text{Re}(I_{L3})$	$ I_{T3} $	$ I_{L2} $
7.	$\text{Re}(I_{L3})$	$ I_{L2} $	$\text{Im}(S^1_{L3})$	$ I_{L2} $	$ I_{T2} $	$\text{Im}(I_{L2})$
8.	$\text{Im}(S^1_{L4})$	$\text{Im}(I_{L2})$	$\text{Im}(S^2_{L3})$	$\text{Im}(I_{L2})$	$\text{Re}(I_{L2})$	$\text{Im}(S^2_{L3})$
9.	$ I^0_{T2} $	$\text{Im}(I_{T2})$	$ I^0_{T2} $	$\text{Im}(I_{T2})$	$ I^0_{T3} $	$\text{Im}(S^2_{L4})$
10.	$ I^0_{T1} $	$\text{Im}(I_{T1})$	$ I^0_{T1} $	$\text{Im}(I_{T1})$	$ I^0_{T2} $	$ U_{B7} $
11.	$ I^0_{T3} $	$ I_{T3} $	$ I^0_{T3} $	$\text{Im}(I_{T3})$	$ I^0_{T1} $	$\text{Re}(U_{B7})$
12.	$\text{Im}(S^2_{L4})$	$ I_{T2} $	$\text{Re}(S^1_{L3})$	$ U_{B7} $	$ I^0_{L2} $	$\text{Im}(I_{T2})$
13.	$\text{Re}(I_{L2})$	$\text{Im}(I_{T3})$	$\text{Re}(I_{L2})$	$\text{Re}(U_{B7})$	$\text{Re}(I^2_{L3})$	$\text{Im}(I_{T1})$
14.	$\text{Re}(S^1_{L4})$	$ U_{B7} $	$ I^0_{L4} $	$ I_{T3} $	$\text{Re}(I^2_{L4})$	$\text{Im}(I_{T3})$
15.	$ I^0_{L3} $	$\text{Re}(U_{B7})$	$\text{Im}(S^2_{L4})$	$ I_{T2} $	$ I^2_{L2} $	$\text{Re}(I_{L3})$
16.	$\text{Im}(S^2_{L3})$	$ I^2_{L4} $	$ I^1_{L4} $	$ I_{T1} $	$ I^0_{L3} $	$\text{Re}(I_{L4})$
17.	$\text{Re}(I^2_{L4})$	$ I_{T1} $	$ I^2_{L4} $	$ I^2_{L3} $	$ I^0_{L4} $	$ I_{T1} $
18.	$\text{Re}(I^1_{L4})$	$\text{Im}(I^2_{L4})$	$\text{Re}(I^2_{L3})$	$\text{Im}(I^2_{L3})$	$\text{Re}(I^1_{L3})$	$ I_{T3} $
19.	$ I^1_{L3} $	$\text{Im}(I^1_{L4})$	$\text{Re}(I^1_{L3})$	$\text{Im}(I^1_{L3})$	$\text{Re}(I^1_{L4})$	$\text{Im}(S^1_{L3})$
20.	$ I^2_{L3} $	$\text{Re}(I_{L3})$	$\text{Re}(I^0_{L3})$	$\text{Re}(I_{L4})$	$\text{Re}(I^0_{L2})$	$\text{Im}(S^1_{L4})$

Tables 7.8–7.10 show not only the results of parameter analysis and the selection of parameter groups, but also that the selected parameter groups partially overlap. This happened because the ranking of parameters according to the conservative strategy is also performed by the $\max(|\Delta I|)$, $\max(|\Delta S|)$ and $\max(|\Delta U|)$ (for voltage parameters) values, but only after the testing of the additional criteria.

The obtained parameter groups can now be generalized for both strategies in order to predict which parameters would be chosen for other relays. The listed parameters all pertain to the faulted phase or its symmetrical component quantities. For the conservative strategy, the following parameters were chosen in all the fault scenarios:

- $|I^2|$ of the faulted line;
- $|I^0|$ of the faulted line;
- $\text{Re}(I)$ of the faulted line;
- $|I^0|$ of a healthy load branch;
- $|I^0|$ of a healthy generator branch;
- $|I|$ of a healthy generator branch;
- $\text{Re}(I)$ of a healthy single-circuit or double-circuit line in the main transmission ring (L2–L6 and L11, L12).

Other parameters chosen in the tested scenarios were either specific to faults of single or double-circuit lines or they were chosen in some scenarios, but were disregarded in other

scenarios because these parameters did not meet the requirements of the strategy or simply were outperformed by other parameters. Therefore, these parameters will be listed separately for single and double-circuit lines with a note “outperformed” if the parameter met the minimum requirements for conservative strategy, but in some cases it was outperformed when sorted by the values $\max(\Delta y_i)$. A note “insufficient $\min(\Delta y_i)$ ” will be added if the parameter in some of the cases had an insufficient minimal sensitivity $\min(\Delta y_i)$, but it was monotonic. Last, a note “nonmonotonic” will be added if this parameter is nonmonotonic in some scenarios. The described parameters chosen by the conservative strategy in cases of double-circuit line faults were:

- $|I^1|$ of the faulted line, nonmonotonic if the fault is located towards large power sources;
- $\text{Re}(I^1)$ of the faulted line, outperformed;
- $\text{Re}(I^2)$ of the faulted line, outperformed;
- $\text{Re}(I^0)$ of the faulted line;
- $|I|$ of the faulted line, insufficient $\min(\Delta y_i)$;
- $\text{Im}(S^2)$ of the faulted line;
- $\text{Re}(I^1)$ of a healthy parallel line;
- $\text{Re}(I^2)$ of a healthy parallel line;
- $\text{Re}(I^0)$ of a healthy parallel line;
- $\text{Re}(I)$ of a healthy parallel line;
- $\text{Im}(S^1)$ of a healthy parallel line;
- $\text{Re}(S^1)$ of a healthy parallel line;
- $\text{Im}(S^2)$ of a healthy parallel line;
- $\text{Im}(S^0)$ of a healthy load branch, insufficient $\min(\Delta y_i)$;
- $|I|$ of a healthy single-circuit line in the main transmission ring, insufficient $\min(\Delta y_i)$;
- $|I^0|$ of a healthy double-circuit line in the main transmission ring, outperformed;
- REDI, nonmonotonic if the fault is located towards large power sources.

Parameters chosen by the conservative strategy in cases of single-circuit line faults were:

- $\text{Re}(I^0)$ of the faulted line, insufficient $\min(\Delta y_i)$;
- $|I|$ of a healthy load branch, insufficient $\min(\Delta y_i)$;
- $|I^1|$ of a healthy double-circuit line in the main transmission ring, insufficient $\min(\Delta y_i)$;
- $|I^2|$ of a healthy double-circuit line in the main transmission ring, insufficient $\min(\Delta y_i)$;
- $|I^0|$ of a healthy double-circuit line in the main transmission ring;
- $|I|$ of a healthy double-circuit line in the main transmission ring, insufficient $\min(\Delta y_i)$;
- $\text{Re}(I^1)$ of a healthy double-circuit line in the main transmission ring;
- $\text{Re}(I^2)$ of a healthy double-circuit line in the main transmission ring insufficient $\min(\Delta y_i)$;
- $\text{Im}(S^2)$ of a healthy double-circuit line in the main transmission ring, insufficient $\min(\Delta y_i)$;
- REDI, nonmonotonic if the fault is located towards generators (large power sources).

For the opportunistic strategy the following parameters were chosen in all fault scenarios:

- REDI;

- $|I|$ of the faulted line;
- $\text{Im}(I)$ of the faulted line;
- $|I^0|$ of a healthy load branch;
- $|I|$ of a healthy load branch;
- $\text{Im}(I^0)$ of a healthy load branch;
- $\text{Im}(I)$ of a healthy load branch;
- $|I|$ of a healthy generator branch;
- $\text{Im}(I)$ of a healthy generator branch.

Other parameters chosen in the tested scenarios were either specific to faults of single or double-circuit lines or they were chosen in some scenarios, but were disregarded in other scenarios because these parameters were outperformed by different parameters. Therefore these parameters will be listed separately for single and double-circuit lines with a note “outperformed” if the parameter was outperformed when sorted by the values $\max(\Delta y_i)$. Described parameters chosen by the opportunistic strategy in cases of double-circuit line faults were:

- $|I^1|$ of a healthy parallel line, outperformed;
- $|I^2|$ of a healthy parallel line;
- $|I^0|$ of a healthy parallel line, outperformed;
- $|I|$ of a healthy parallel line;
- $\text{Re}(I)$ of a healthy parallel line;
- $\text{Im}(I^1)$ of a healthy parallel line;
- $\text{Im}(I^2)$ of a healthy parallel line;
- $\text{Im}(I^0)$ of a healthy parallel line, outperformed;
- $\text{Im}(I)$ of a healthy parallel line;
- $\text{Im}(S^1)$ of a healthy parallel line, outperformed;
- $\text{Im}(S^2)$ of a healthy parallel line, outperformed;
- $\text{Im}(S^0)$ of a healthy load branch, outperformed;
- $|I|$ of a healthy single-circuit line in the main transmission ring, outperformed;
- $\text{Im}(I)$ of a healthy single-circuit line in the main transmission ring, outperformed.

Parameters chosen by the opportunistic strategy in cases of single-circuit line faults were:

- $\text{Re}(I)$ of a healthy load branch;
- $|I|$ of a healthy double-circuit line in the main transmission ring;
- $\text{Im}(I)$ of a healthy double-circuit line in the main transmission ring;
- $\text{Im}(S^2)$ of a healthy double-circuit line in the main transmission ring, outperformed;
- $\text{Im}(S^1)$ of a healthy double-circuit line in the main transmission ring, outperformed;
- $|U|$ of the faulted line;
- $\text{Re}(U)$ of the faulted line.

Before discussing the testing of the proposed method with the obtained parameter groups, it is possible to briefly analyse the surfaces of the objective function (fitness) created by using them. This analysis will also be limited to RELAY1 faults. In order to evaluate these

surfaces, the values of the objective function were calculated for three points of true α^* and R_F^* ((0.001 p.u.; 0.001 Ω), (0.5 p.u.; 100 Ω), (0.999 p.u.; 200 Ω)). The number of the parameters considered was 20, 10, and 5. The pre-fault regime for the calculations of these surfaces was assumed nominal. When the number of available parameters was decreased the parameters used were the ones with the highest ranking shown in Table 7.8.

The opportunistic strategy produced surfaces with several false minima between fault distances of 0.001 p.u. and 0.1 p.u. and a ravine with more false minima between fault distances of 0.8 p.u. and 1 p.u. starting from fault path resistance of approximately 120 Ω when considering point (0.001 p.u.; 0.001 Ω) for FAULT 1 (Fig. 7.2).

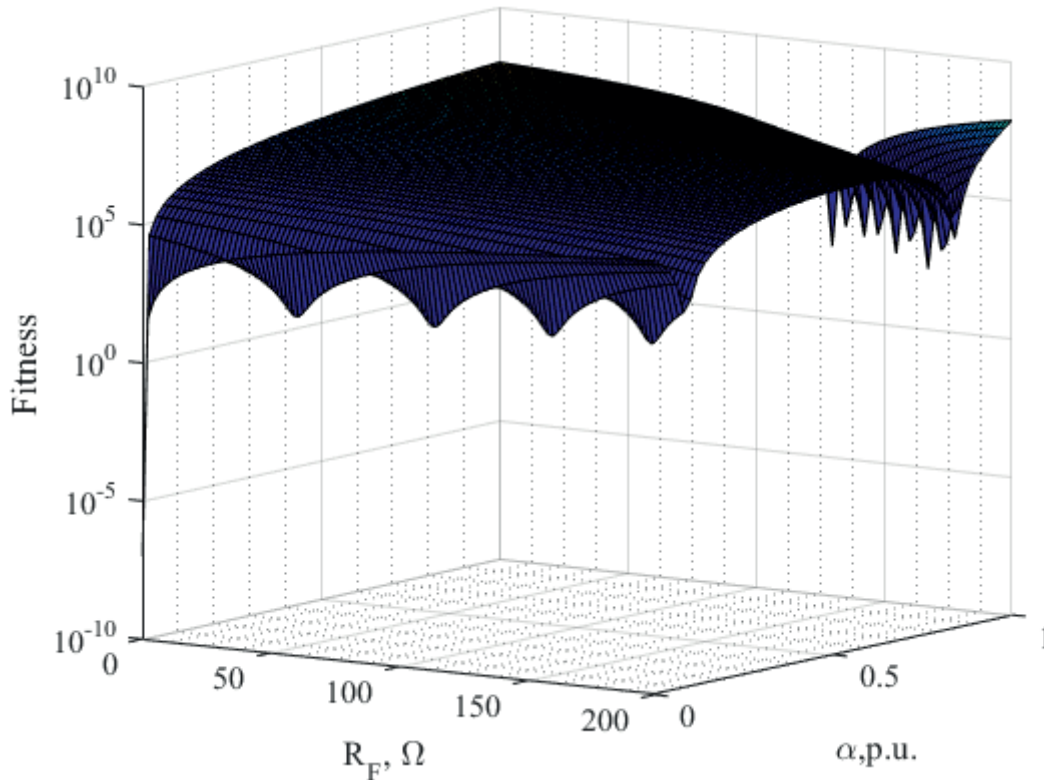


Fig. 7.2. The surface of the objective function (Fitness) for the RELAY1 FAULT1 with a fault distance of 0.001 p.u. and a fault resistance of 0.001 Ω obtained by the opportunistic strategy with 5 parameters.

In case of FAULT2, the situation was the same: insignificant deformations for surfaces of points (0.5 p.u.; 100 Ω), (0.999 p.u.; 200 Ω) and several false minima for the surface of the point (0.001 p.u.; 0.001 Ω). In case of FAULT6, the surface of the point (0.001 p.u.; 0.001 Ω) had multiple false minima for fault distances approximately 0.6–1.0 p.u. if the number of parameters was 10 or less, but the surfaces of the point (0.5 p.u.; 100 Ω) had a wedge form in the proximity of the true global minimum when the parameter group had 20 members, and when this number was decreased, the surface became more distorted (Fig. 7.3).

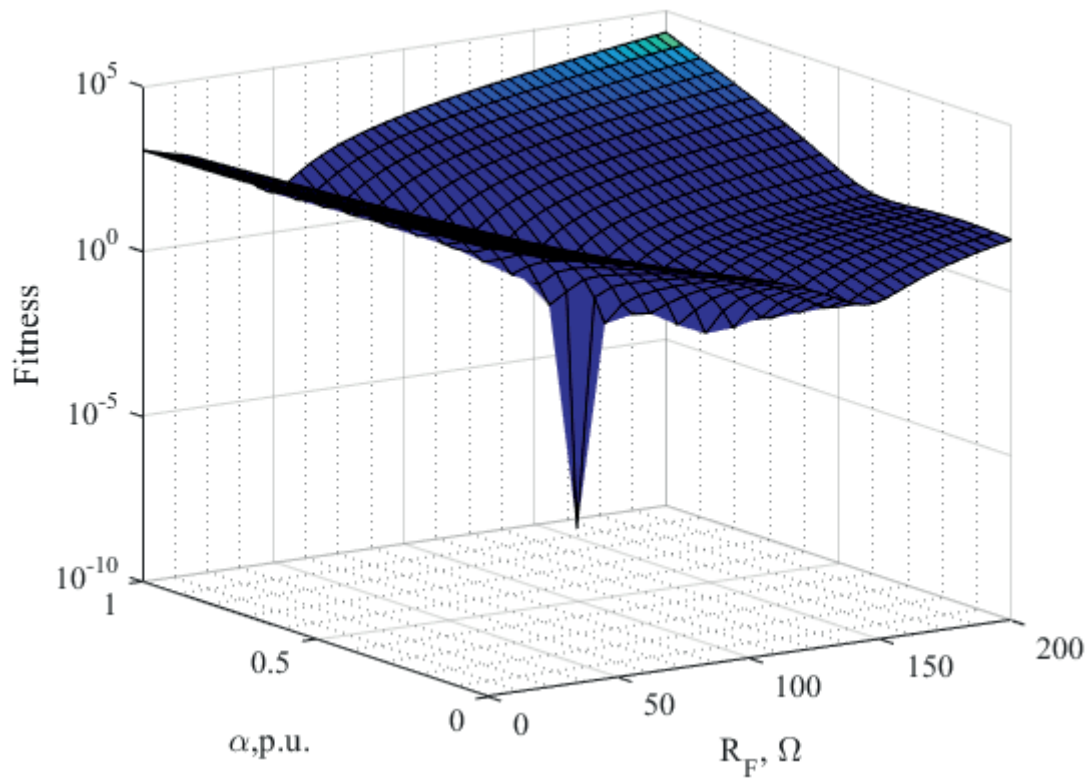


Fig. 7.3. The surface of an objective function (Fitness) for RELAY1 FAULT6 with a fault distance of 0.5 p.u. and a fault resistance of 100 Ω obtained by the opportunistic strategy with 5 parameters.

The conservative strategy in case of FAULT1 had a wedge form around the global minimum of the surface of the point (0.5 p.u.; 100 Ω) with fault distance values remaining fixed around 0.5 p.u., but if the number of parameters was 5 then the surfaces of the point (0.999 p.u.; 200 Ω) had several false minima (Fig. 7.4).

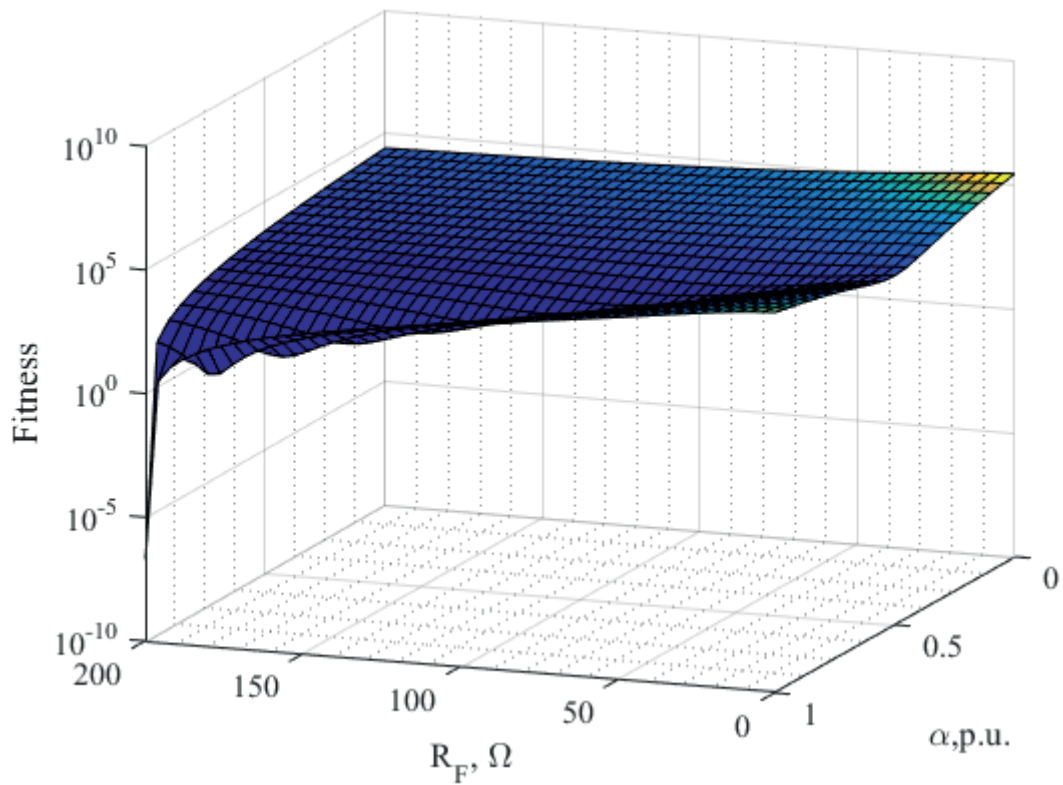


Fig. 7.4. The surface of an objective function (Fitness) for RELAY1 FAULT1 with a fault distance of 0.999 p.u. and a fault resistance of 200 Ω achieved by the conservative strategy with 5 parameters.

As it was with the opportunistic strategy, the surfaces of the conservative strategy for FAULT2 were the same as for FAULT1. However, in case of FAULT6 only the surfaces of the point (0.5 p.u.; 100 Ω) were distorted. In contrast to FAULT1 and FAULT2, here the wedge form was more oriented around a specific fault path resistance interval (approximately 60–140 Ω) and as the number of available parameters was decreased, additional local minima in the wedge materialised (Fig. 7.5).

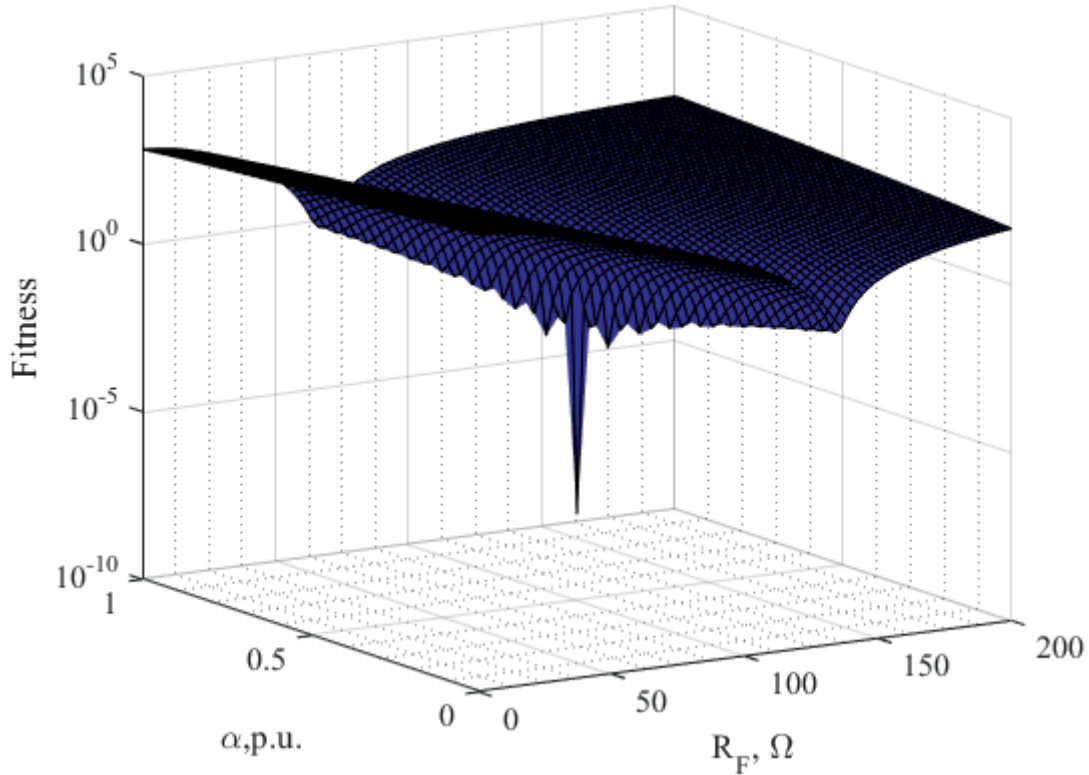


Fig. 7.5. The surface of an objective function (Fitness) for RELAY1 FAULT6 with a fault distance of 0.5 p.u. and a fault resistance of 100 Ω achieved by the conservative strategy with 5 parameters.

First, one can notice that for both strategies at least one of the tested fault points had some distortions in the surface of the objective function, which means that an optimisation algorithm capable of avoiding false extrema is necessary. Second, the analysis with reduction of the number of available parameters has shown that a smaller number of parameters more often yields surfaces with additional false extrema and other form defects. Therefore, it can be suspected that the more parameters are used, the more they cancel out surface distortions characteristic of any one parameter.

7.3. Testing results for the proposed method

In order to evaluate the capabilities of the proposed parameter estimation with GA as the optimisation tool and the described parameter selection strategies, extensive testing was performed. The tests included all of the faults for three relays considered (RELAY1, RELAY2 and RELAY3). These were done for both strategies with 20, 15, 10 and 5 parameters used in the objective function (5.1), and for each of these subcases 1000 tests with randomised pre-fault and fault scenarios were performed. The focus of the testing will be on the estimation of fault regime parameters and the randomised pre-fault regime is assumed to be known. The GA and the settings used were the same as described in Section 5.3 of this Thesis. The parameter groups used were from Tables 7.8–7.10. The maximum and mean values of estimation errors ϵ for fault distance and resistance as well as the mean value of number generations necessary for convergence of the GA (including the number of

generations equivalent to all randomly generated individuals) were determined for each subcase. Additionally, the upper boundaries $\varepsilon_{\alpha B}$ for fault distance estimation errors covering 95 % of the expected values were calculated from numerically obtained cumulative distribution functions. The results are presented in Tables 7.11–7.20.

Table 7.11.

The Results of Testing for RELAY1 FAULT1

STRATEGY	N_{PAR}	max ε_{α} , %	mean ε_{α} , %	$\varepsilon_{\alpha B}$, %	max ε_{RF} , %	mean ε_{RF} , %	mean N_{GEN}
Opportunistic	20	0.787	0.037	0.093	1.722	0.041	1125.9
	15	1.457	0.039	0.102	1.540	0.038	1183.1
	10	0.303	0.035	0.094	2.184	0.044	1252.9
	5	0.768	0.035	0.079	2.168	0.064	1285.5
Conservative	20	0.881	0.036	0.084	4.024	0.058	930.4
	15	1.031	0.034	0.091	40.901	0.133	1280.2
	10	0.772	0.039	0.114	4.888	0.097	989.8
	5	0.848	0.041	0.130	25.885	0.142	1098

Table 7.12.

The Results of Testing for RELAY1 FAULT2

STRATEGY	N_{PAR}	max ε_{α} , %	mean ε_{α} , %	$\varepsilon_{\alpha B}$, %	max ε_{RF} , %	mean ε_{RF} , %	mean N_{GEN}
Opportunistic	20	1.719	0.036	0.086	1.133	0.032	1161.1
	15	1.735	0.038	0.090	4.290	0.041	1072.9
	10	0.849	0.036	0.096	1.349	0.042	1013.5
	5	2.029	0.036	0.090	1.758	0.067	974.5
Conservative	20	0.893	0.033	0.078	49.60	0.149	1078.3
	15	2.220	0.039	0.092	46.178	0.133	1049.6
	10	3.379	0.043	0.101	6.518	0.093	1222.3
	5	1.371	0.041	0.100	33.293	0.129	1446.2

Table 7.13.

The Results of Testing for RELAY1 FAULT6

STRATEGY	N_{PAR}	max ε_{α} , %	mean ε_{α} , %	$\varepsilon_{\alpha B}$, %	max ε_{RF} , %	mean ε_{RF} , %	mean N_{GEN}
Opportunistic	20	2.685	0.085	0.363	0.455	0.030	2764.7
	15	3.641	0.075	0.231	0.764	0.028	2114.1
	10	3.595	0.078	0.262	1.218	0.035	3011.8
	5	5.118	0.076	0.235	1.372	0.049	2863.1
Conservative	20	2.613	0.082	0.309	0.721	0.031	2838.7
	15	3.135	0.094	0.329	0.909	0.035	2436.1
	10	4.024	0.123	0.447	1.204	0.045	4382.9
	5	6.134	0.120	0.424	1.517	0.044	4934.2

Table 7.14.

The Results of Testing for RELAY2 FAULT1

STRATEGY	N_{PAR}	max ε_{α} , %	mean ε_{α} , %	$\varepsilon_{\alpha B}$, %	max ε_{RF} , %	mean ε_{RF} , %	mean N_{GEN}
Opportunistic	20	2.599	0.041	0.106	21.409	0.081	1141.9
	15	1.350	0.040	0.095	3.116	0.047	1227.2
	10	0.699	0.036	0.100	1.381	0.051	869.18
	5	1.470	0.040	0.092	4.983	0.081	1457.3
Conservative	20	1.105	0.036	0.092	3.824	0.068	1085.5
	15	0.604	0.036	0.083	70.867	0.156	1141.0
	10	0.638	0.033	0.084	22.050	0.084	1406.3
	5	0.669	0.038	0.098	2.441	0.067	1218.6

Table 7.15.

The Results of Testing for RELAY2 FAULT2

STRATEGY	N_{PAR}	max ε_{α} , %	mean ε_{α} , %	$\varepsilon_{\alpha B}$, %	max ε_{RF} , %	mean ε_{RF} , %	mean N_{GEN}
Opportunistic	20	1.573	0.038	0.096	1.727	0.048	1024.7
	15	1.198	0.036	0.091	3.484	0.044	1268.6
	10	0.647	0.037	0.107	4.176	0.058	1246.4
	5	1.312	0.042	0.110	3.957	0.114	1820.9
Conservative	20	0.649	0.033	0.077	12.895	0.080	933.70
	15	0.697	0.033	0.086	42.901	0.128	1009.4
	10	0.673	0.034	0.085	32.199	0.094	1209.9
	5	0.474	0.036	0.088	2.180	0.050	1121.1

Table 7.16.

The Results of Testing for RELAY2 FAULT3

STRATEGY	N_{PAR}	max ε_{α} , %	mean ε_{α} , %	$\varepsilon_{\alpha B}$, %	max ε_{RF} , %	mean ε_{RF} , %	mean N_{GEN}
Opportunistic	20	1.674	0.041	0.093	4.887	0.052	1316.8
	15	1.239	0.039	0.107	0.764	0.024	1317.3
	10	1.078	0.038	0.095	2.355	0.036	1303.5
	5	2.023	0.041	0.099	7.576	0.049	1394.3
Conservative	20	0.962	0.040	0.106	1.713	0.026	1484.2
	15	1.373	0.038	0.103	1.523	0.048	1061.3
	10	0.508	0.037	0.100	8.487	0.077	1165.6
	5	0.602	0.040	0.121	0.631	0.039	1184.4

Table 7.17.

The Results of Testing for RELAY2 FAULT4

STRATEGY	N_{PAR}	max ε_{α} , %	mean ε_{α} , %	$\varepsilon_{\alpha B}$, %	max ε_{RF} , %	mean ε_{RF} , %	mean N_{GEN}
Opportunistic	20	2.002	0.041	0.102	1.822	0.031	1245.7
	15	1.574	0.041	0.101	1.108	0.024	1522.7
	10	0.880	0.040	0.103	0.922	0.030	1303.0
	5	3.983	0.038	0.084	2.692	0.055	941.8
Conservative	20	0.844	0.037	0.098	28.147	0.097	1333.9
	15	0.864	0.038	0.098	1.569	0.049	1396.7
	10	2.069	0.040	0.097	14.887	0.082	993.44
	5	6.880	0.049	0.119	23.114	0.065	1713.4

Table 7.18.

The Results of Testing for RELAY3 FAULT3

STRATEGY	N_{PAR}	max ε_{α} , %	mean ε_{α} , %	$\varepsilon_{\alpha B}$, %	max ε_{RF} , %	mean ε_{RF} , %	mean N_{GEN}
Opportunistic	20	3.148	0.039	0.100	6.602	0.027	1277.5
	15	3.020	0.037	0.082	0.586	0.016	997.9
	10	1.495	0.041	0.106	4.048	0.026	1165.9
	5	1.252	0.035	0.079	1.172	0.027	897.1
Conservative	20	0.996	0.031	0.064	6.499	0.062	1089.6
	15	0.847	0.035	0.086	25.562	0.079	958.9
	10	0.730	0.033	0.075	3.381	0.041	1073.4
	5	0.460	0.031	0.080	0.605	0.036	851.82

Table 7.19.

The Results of Testing for RELAY3 FAULT4

STRATEGY	N_{PAR}	max ε_α , %	mean ε_α , %	ε_{aB} , %	max ε_{RF} , %	mean ε_{RF} , %	mean N_{GEN}
Opportunistic	20	1.933	0.039	0.086	0.581	0.022	1147
	15	1.674	0.040	0.098	1.319	0.018	984
	10	0.817	0.035	0.083	0.791	0.021	1094.4
	5	0.760	0.032	0.079	2.212	0.045	982.49
Conservative	20	0.406	0.032	0.082	1.887	0.052	1112.7
	15	0.452	0.032	0.068	5.643	0.053	1045.6
	10	0.902	0.034	0.075	17.915	0.093	1009.5
	5	0.816	0.033	0.073	0.845	0.026	960.1

Table 7.20.

The Results of Testing for RELAY3 FAULT5

STRATEGY	N_{PAR}	max ε_α , %	mean ε_α , %	ε_{aB} , %	max ε_{RF} , %	mean ε_{RF} , %	mean N_{GEN}
Opportunistic	20	1.291	0.049	0.145	1.685	0.043	1738.5
	15	1.986	0.046	0.142	4.569	0.056	1307.3
	10	0.981	0.048	0.142	51.066	0.146	1292.6
	5	3.897	0.055	0.146	2.628	0.067	1793.5
Conservative	20	3.848	0.061	0.202	25.314	0.127	2338.8
	15	2.410	0.066	0.205	21.556	0.135	2321.4
	10	1.549	0.059	0.212	16.460	0.130	2587.7
	5	2.389	0.072	0.248	57.180	0.249	3410.4

First, it is possible to consider how the difference of faults affects the results obtained by the proposed method, using both parameter group selection strategies. One can see from the comparison of Tables 7.11, 7.12, 7.18, 7.19 and Tables 7.13, 7.20 that the maximum and mean values of fault distance estimation error ε_α for faults in a single-circuit line with possible power flow in both directions are larger than for faults in double-circuit lines with possible power flow in both directions. If faults in double-circuit lines are compared according to maximum error of estimated fault distance, it can be noted that faults in the direction of a load result in less error than for faults towards large generation, but in terms of mean errors of the estimated fault distance, the results are similar (Tables 7.11, 7.12, 7.16, 7.17 and Tables 7.14, 7.15, 7.18). When comparing all of the considered faults according to the maximum and mean values of estimated fault path resistance, there is no clear advantage for faults in either single- or double-circuit lines and for the fault directions (towards load or generators). When comparing the mean value of necessary generations, one can notice from the comparison of Tables 7.11, 7.12, 7.18, 7.19 and Tables 7.13, 7.20 that estimation of fault parameters takes more time for faults in single-circuit lines than for faults in double-circuit lines.

Second, results obtained by applying both parameter group selection strategies can be compared between themselves. When considering the maximum and mean values of the fault distance estimation error, the conservative strategy is better for faults towards load in double-circuit lines (Tables 7.14, 7.15, 7.18 and 7.19), for faults in double-circuit lines towards

generators the performance of both strategies differed little (Tables 7.11, 7.12, 7.16 and 7.17), but according to Tables 7.13 and 7.20 for faults in single-circuit lines, the opportunistic strategy outperformed the conservative one. The estimation of fault path resistance was performed better by using the opportunistic strategy as shown by the results of maximum and mean values of the fault path resistance estimation error in Tables 7.11–7.20. According to the mean value of necessary generations for faults in double-circuit lines, both strategies performed similarly with no clear winner in terms of convergence speed (Tables 7.11, 7.12, 7.14–7.19), but for faults in single-circuit lines the opportunistic strategy showed significantly faster convergence (Tables 7.13 and 7.20).

Next, the effects of decreasing number of available measurements on both strategies can be analysed. For the opportunistic strategy a direct increase of maximum errors of fault distance and fault path resistance estimation due to decreased measurement count could be seen for faults in single-circuit lines as indicated by Tables 7.13 and 7.20, but for faults in double-circuit lines towards the load, the opposite can be noticed for maximum errors of fault distance estimation (Tables 7.14, 7.15, 7.18 and 7.19). In other fault cases, both maximum errors of fault distance and fault path resistance estimation varied without a distinct pattern. The mean values of necessary generation count, error of fault distance estimation and error of fault path resistance estimation mostly vary without a distinct pattern. For the conservative strategy, a direct increase in the maximum errors of fault distance and fault path resistance estimation and the mean error of fault path resistance estimation due to decreased measurement count could be seen for FAULT6 results (Table 7.13). The mean error of fault distance estimation mostly varied without a pattern, it also had the highest values when the parameter count was either 5 or 10 indicating that for the fault distance estimation, a larger parameter group is beneficial for this strategy. The mean value of necessary generations was negatively affected for both faults in single-circuit lines, as can be seen from Tables 7.13 and 7.20.

Overall, the performance of the proposed method seems to be most affected by faults in single-circuit lines with possible pre-fault power flow in both directions, especially FAULT6 where both strategies had a case of fault distance estimation error exceeding 5 %, but in a rare case this happened for conservative strategy in case of a fault in a double-circuit line (Table 7.17). However, this mainly indicates that the minimal parameter group size should be between 5 and 10 to ensure that at the most unfavourable conditions the error of fault distance estimate did not exceed 5 %, which in reality should not pose problems as the available parameter count is significantly larger. The calculated boundary values $\varepsilon_{\alpha B}$ containing 95 % of error values not only further confirm the conclusions of the above comparisons, but it also indicates that in almost all cases for double-circuit line faults, the fault distance estimation error will not exceed 0.12 % and for single-circuit line faults 0.45 %.

The different performance of the proposed parameter selection strategies when comparing the faults in single-circuit and double-circuit lines can be demonstrated by distributions of estimation errors. As indicated in Tables 7.11, 7.12 and 7.13 for the opportunistic strategy and 5 available parameters, the mean error of fault distance estimation is larger in case of FAULT6, which can be further illustrated with histograms of estimation errors (Fig. 7.6 and 7.7).

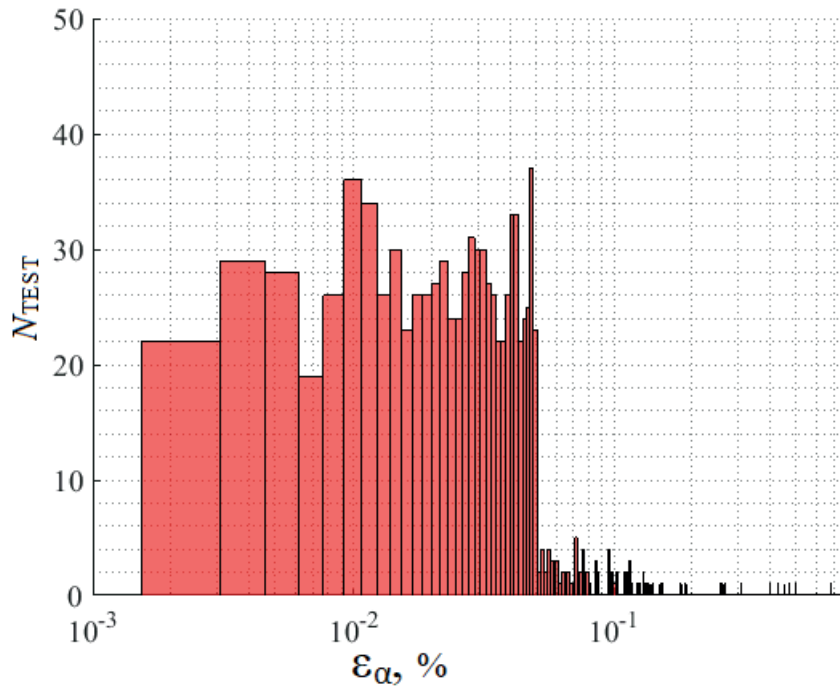


Fig. 7.6. The histogram of fault distance estimation error modulus obtained with opportunistic strategy RELAY1 FAULT1 and parameter count 5.

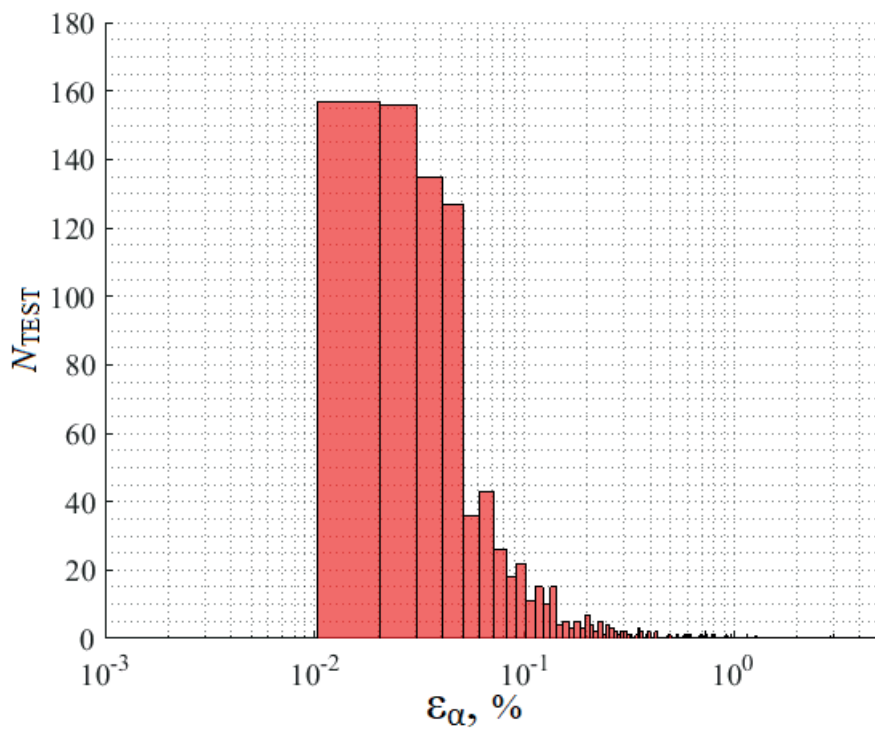


Fig. 7.7. The histogram of fault distance estimation error modulus obtained with opportunistic strategy RELAY1 FAULT6 and parameter count 5.

This in combination with Tables 7.11–7.20 and Fig. 7.6 and 7.7 also shows that in most of the cases, the proposed FL algorithm with the GA achieves a high degree of accuracy. The application of GA resulted in improved performance compared to a modified randomised search. One can see this improvement by comparing the results presented in Section 5.2 (Fig. 5.4 and 5.8) and the results shown by Tables 7.11–7.20 and Fig. 7.6 and 7.7. These

results show that the errors of estimated fault distances have been shifted from mostly between 0.1–1.5 % to mostly between 0.005–0.5 %. The improvement in the speed of parameter estimation is indicated by the significant increase of possible tests performed using the GA. The described improvements should also be partially credited to the more target-oriented parameter selection compared to the initial implementations with the randomised search where the real and imaginary parts of the symmetrical components for voltage and current measurements from the substation were used without any particular analysis of these or other parameters.

In order to compare the performance of the proposed method with the GA with existing FL methods, FL algorithms using one-terminal measurements [143] and two-terminal measurements of NS voltages and currents (from the same terminal as [143]) were tested in the same randomised conditions. The results for all the fault scenarios are presented in Tables 7.21 and 7.22.

Table 7.21.

The Results of Testing of an Existing One-Terminal-Measurement-Based Fault Locator

CASE	max ε_a , %	mean ε_a , %	ε_{aB} , %
RELAY1 FAULT1	169.977	16.679	59.939
RELAY1 FAULT2	157.670	17.754	63.871
RELAY1 FAULT6	939.143	47.575	208.96
RELAY2 FAULT1	106.458	17.609	56.968
RELAY2 FAULT2	114.080	17.042	53.849
RELAY2 FAULT3	383.516	14.160	69.874
RELAY2 FAULT4	430.757	15.742	66.768
RELAY3 FAULT3	5.802	1.573	3.358
RELAY3 FAULT4	7.098	1.649	3.492
RELAY3 FAULT5	72.916	7.930	26.390

Table 7.22.

The Results of the Testing of an Existing Two-Terminal-Measurement-Based Fault Locator

CASE	max ε_a , %	mean ε_a , %	ε_{aB} , %
RELAY1 FAULT1	0.216	0.105	0.198
RELAY1 FAULT2	0.214	0.107	0.199
RELAY1 FAULT6	0.219	0.107	0.200
RELAY2 FAULT1	0.217	0.103	0.196
RELAY2 FAULT2	0.212	0.102	0.196
RELAY2 FAULT3	0.316	0.156	0.293
RELAY2 FAULT4	0.318	0.163	0.298
RELAY3 FAULT3	0.315	0.161	0.292
RELAY3 FAULT4	0.321	0.156	0.295
RELAY3 FAULT5	0.364	0.186	0.345

When comparing the performance of the existing one-terminal-measurement-based FL method with the proposed method, it can be seen that only by the maximum error of the fault distance estimation does the existing method approach the accuracy of the proposed method

in case of RELAY3 FAULT3, but in other cases and according to the mean error and upper boundary for 95 % of error values, it clearly is less accurate than the proposed method (Table 7.21 and Tables 7.11–7.20). The existing one-terminal-measurement-based method had the most difficulties in case of RELAY1 FAULT6 and it tended to perform better if the faults were oriented towards a load centre (Table 7.21), which is similar to the proposed method. If the error of the fault distance estimation was not taken as modulus (as it was for Fig. 7.6 and 7.7), then one can note that the one-terminal-measurement-based method tended to calculate fault distance as being less than the actual distance in case of faults towards generators and more than the actual distance in cases of faults towards a load centre (Fig. 7.8 and 7.9), which could be expected for pre-fault power flows towards the substation or towards the line similarly to the reactance effect for DP.

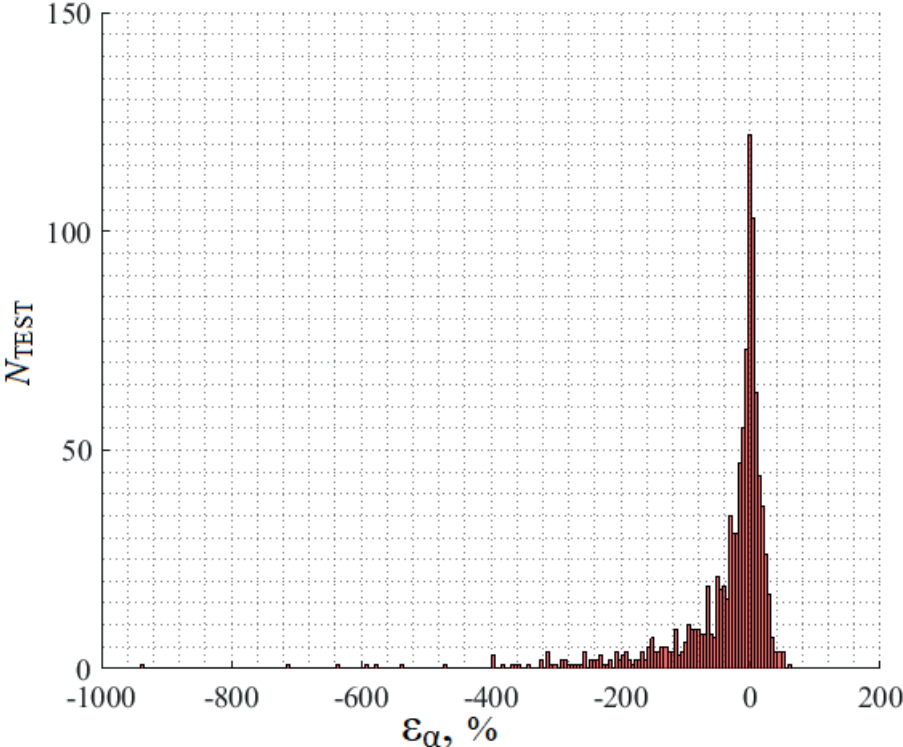


Fig. 7.8. The histogram of fault distance estimation errors obtained by an existing one-terminal-measurement-based fault locator in case of RELAY1 FAULT6.

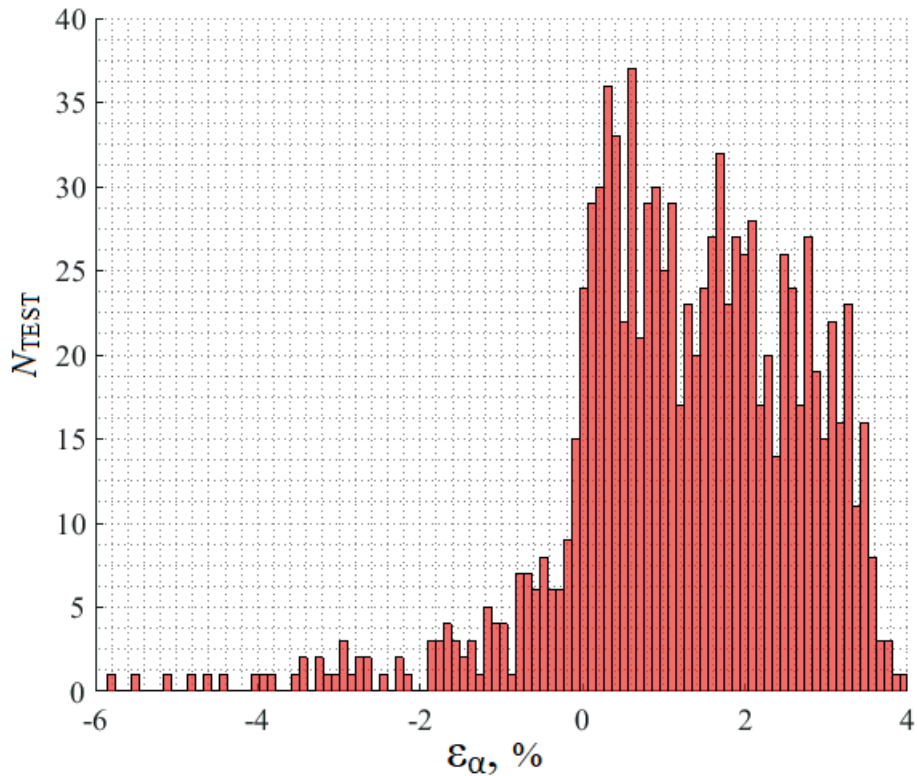


Fig. 7.9. The histogram of fault distance estimation errors obtained by an existing one-terminal-measurement-based fault locator in case of RELAY3 FAULT3.

When comparing the performance of an existing two-terminal-measurement-based FL method with the proposed method (Table 7.22 and Tables 7.11–7.20), it can be seen that the existing method outperforms the proposed method in terms of maximum error of the fault distance estimation. However, in terms of mean values of these errors, the proposed method achieves better results, with the only exception being the case of RELAY1 FAULT6 for the conservative strategy with 5 or 10 parameters. In terms of the upper boundary, for 95 % of error values the proposed method achieved a lower accuracy only for the case of RELAY1 FAULT6, but it performed significantly better for faults in double-circuit lines. This means that the maximum boundary of fault distance estimation errors is lower for the two-terminal-based method, but in most cases the proposed method has a higher concentration of more accurate results as indicated by better results of mean error and upper boundary for most error values. This difference in concentration can also be illustrated by comparison of fault distance estimation error histograms (Fig. 7.6, 7.7 and Fig. 7.10, 7.11). One additional thing to note from the results in Table 7.22 is that the fault distance estimation errors slightly increased for faults closer to generators while there is no clear advantage for a particular fault direction either towards the load centre or towards the generators, which is different from both the proposed method and the existing one-terminal-measurement-based FL method.

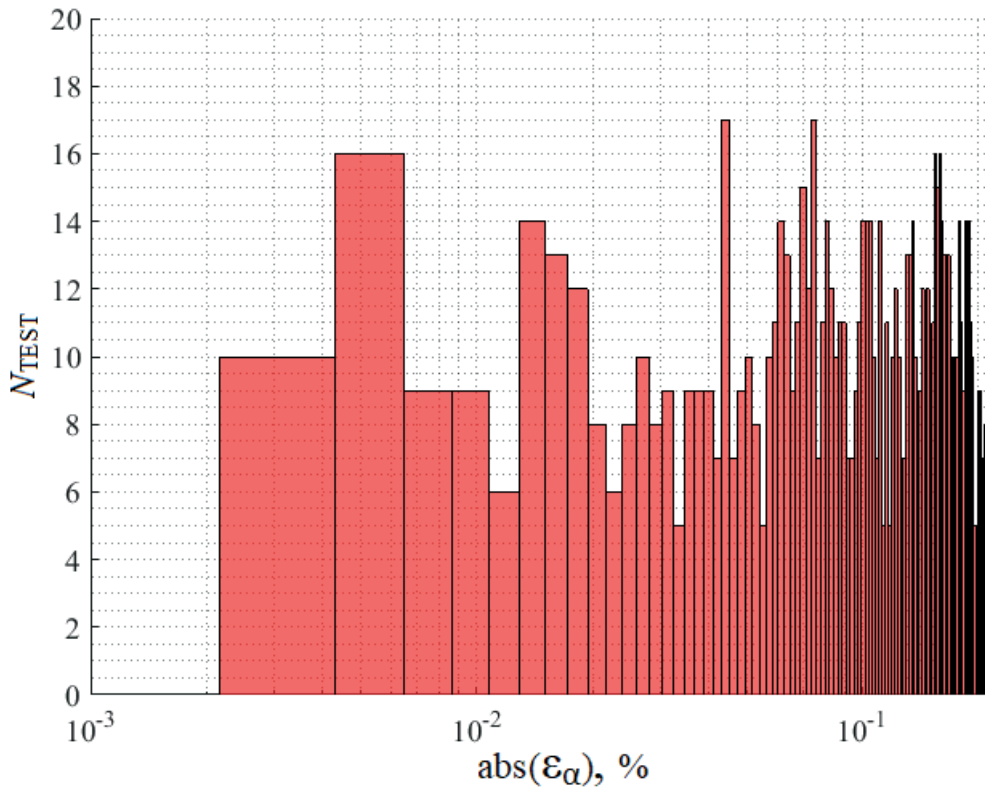


Fig. 7.10. The histogram of fault distance estimation error modulus obtained by an existing two-terminal-measurement-based fault locator in case of RELAY1 FAULT1.

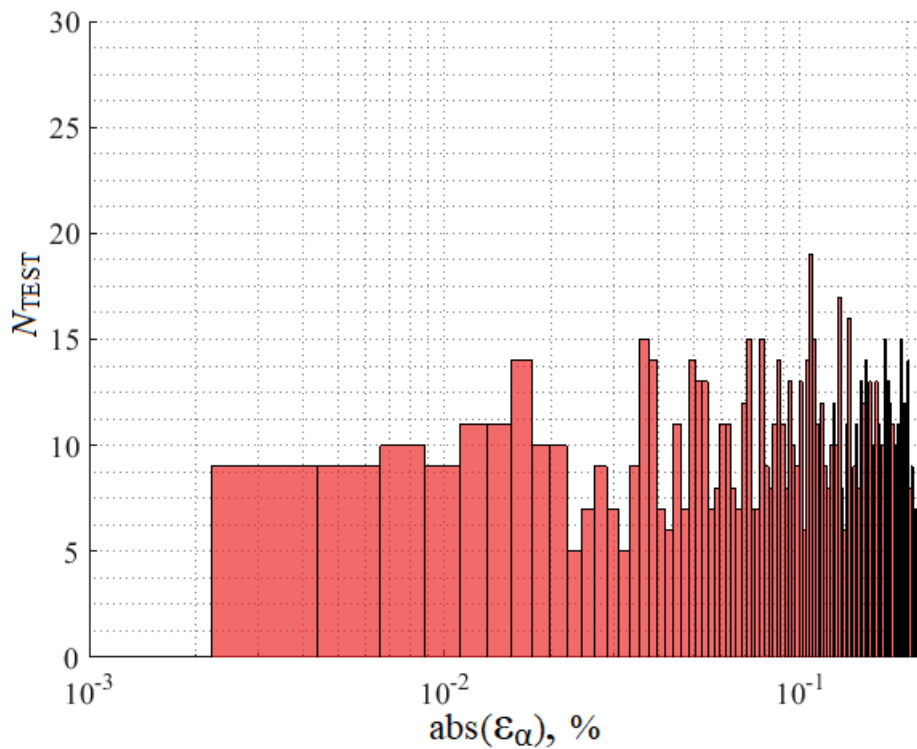


Fig. 7.11. The histogram of fault distance estimation error modulus obtained by an existing two-terminal-measurement-based fault locator in case of RELAY1 FAULT6.

7.4. Conclusions

1. A comparison of the tested parameter selection strategies showed that the conservative strategy performed better or similarly to the opportunistic one for faults in double-circuit lines with possible pre-fault power flow in both directions, but for faults in single-circuit lines the opportunistic strategy was better suited. The comparison of convergence speed according to the generation count also yielded similar results, but in terms of fault path resistance estimation accuracy, the opportunistic strategy outperformed the conservative one.
2. The decrease of available measurements for the objective function has the most noticeable effect on accuracy of fault distance estimation for faults in single-circuit lines, which in general presented the greatest challenge for the proposed method.
3. The updated version of the parameter estimation method using the GA clearly outperformed the existing one-terminal-measurement-based fault locator algorithm.
4. The last version of the proposed method had higher maximum error values than the existing two-terminal-measurement-based FL method using NS quantities, but in terms of mean error and expected concentration of 95 % of fault distance estimation error values, the proposed method mostly outperformed the two-terminal-measurement-based method.

8. APPLICATION OF THE MODEL PARAMETER ESTIMATION AND TOPOLOGICAL MODELLING APPROACH FOR THE DEVELOPMENT OF AN ADAPTIVE SINGLE-POLE AUTOMATIC RECLOSING

Although the main applications of model parameter estimation considered in this Thesis are the DP and FL, this method or its results can be used for other power system automation tasks. One such application developed is an ASPAR. The proposed application uses the topological modelling method both in symmetrical components to model the overall influence of the power system on the one-open-phase regime of the OHTL present during the dead time and in phase coordinates to accurately model interactions between the healthy phases and the disconnected faulted phase. The fault distance estimated by the FL proposed in this Thesis is also used to calculate the adaptive setting used for the developed logic block of the ASPAR.

In HV and EHV networks, SPAR is often used because a disconnection of only the faulted phase decreases the impact of power imbalance and improves the system stability [154], [155]. It is desirable to minimise the dead time of SPAR in order to decrease the time of power imbalance and circulation of significant ZS currents caused by an open-phase regime. However, an excessive decrease in the interruption time may lead to a reignition of an incompletely deionised electric arc channel, which would result in a serious blow to the dynamic stability of the power system and further damage to the switchgear and other system elements. The AR in the case of a permanent fault is undesirable for the same reasons.

8.1. Modelling of high-voltage transmission line in phase coordinates

First, in order to evaluate the possible parameters used for the ASPAR, a model in phase coordinates was developed (Fig. 8.1).

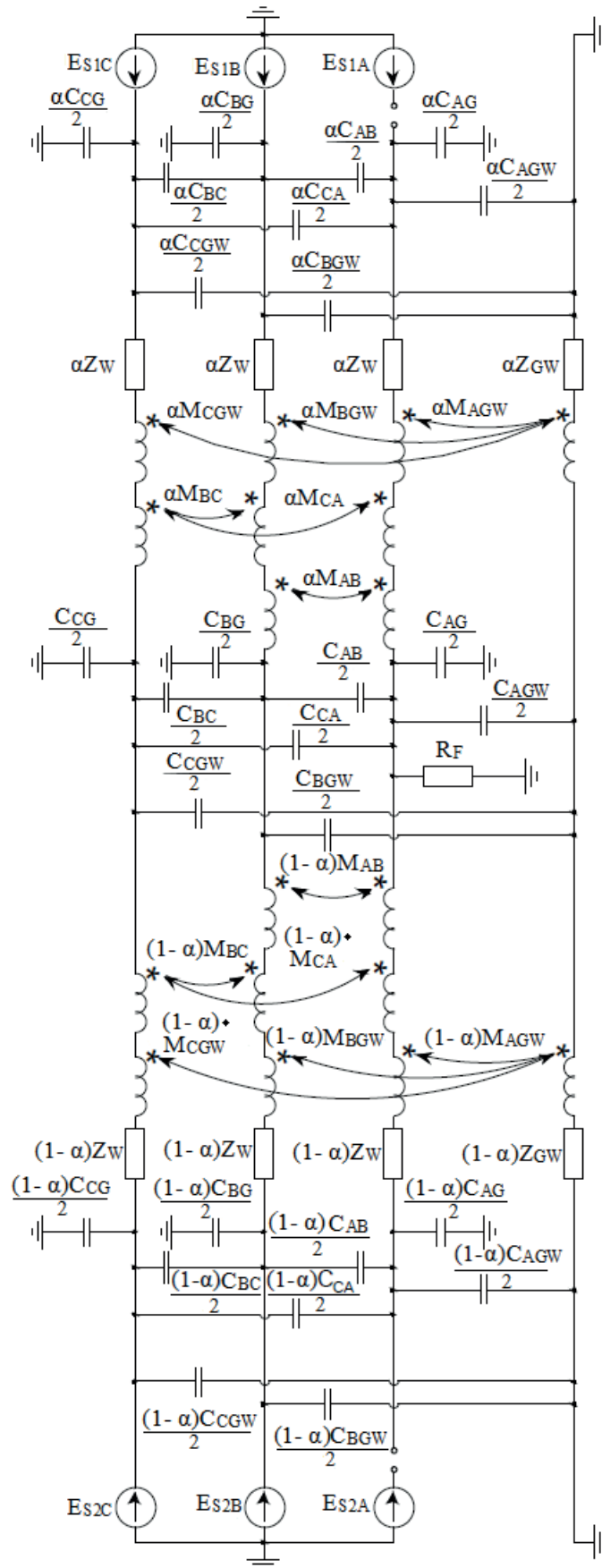


Fig. 8.1. A detailed three-phase line model with a disconnected L-E fault.

The presented model considers the conductor self-impedance Z_W (not to be confused with the PS impedance), the ground (earth) wire impedance Z_{GW} , all of the mutual coupling impedances $Z_{MAB}, Z_{MBC}, Z_{MCA}, Z_{MAGW}, Z_{MBGW}, Z_{MCGW}$ representing $M_{AB}, M_{BC}, M_{CA}, M_{AGW}, M_{BGW}, M_{CGW}$, capacitances between phases C_{AB}, C_{BC}, C_{CA} , between the phases and the earth C_{AG}, C_{BG}, C_{CG} as well as between the phases and the earth (ground) wire $C_{AGW}, C_{BGW}, C_{CGW}$. The self-impedances and mutual impedances can be calculated using equations [156]:

$$Z_W = R_i + 9.88 \cdot 10^{-4} \cdot f + i \left(28.938 \cdot 10^{-4} \cdot f \cdot \lg(D_{eq}/r_{eqi}) \right), \quad (8.1)$$

$$Z_M = 9.88 \cdot 10^{-4} \cdot f + i \left(28.938 \cdot 10^{-4} \cdot f \cdot \lg(D_{eq}/d_{ij}) \right), \quad (8.2)$$

where R_i – the resistance of conductor i , Ω/km ;

f – the voltage frequency, Hz;

i (variable) – an imaginary number ($i = \sqrt{-1}$);

D_{eq} – the equivalent depth of the current flowing in the ground (an average of 930 m), m;

r_{eqi} – the equivalent geometric radius of the conductor i (index), m;

d_{ij} is the distance between the conductors i (index) and j , m.

Capacitances can be calculated by expanding an analytical solution demonstrated in [157] or by using the potential coefficient matrix P , which is a square matrix with elements [158]:

$$P_{ii} = (1/2\pi\epsilon_A) \ln(S_{ii}/r_i) \approx 41.374 \cdot 10^6 \lg(S_{ii}/r_i), \quad (8.3)$$

$$P_{ij} = (1/2\pi\epsilon_A) \ln(S_{ij}/d_{ij}) \approx 41.374 \cdot 10^6 \lg(S_{ij}/d_{ij}), \quad (8.4)$$

where P_{ii} – the potential coefficient of conductor i , km/F;

P_{ij} – the mutual potential coefficient of conductors i and j , km/F;

S_{ii} – the distance between conductor i and its own mirror image in the earth, m;

S_{ij} – the distance between conductor i and the mirror image in the earth of conductor j , m;

r_i – the radius of conductor i , m;

ϵ_A – the absolute permittivity of the air ($\epsilon_A \approx -8.854 \cdot 10^{-9}$ F/km), F/km.

The capacitance matrix, C , is then obtained by an inversion of the potential coefficient matrix ($C = P^{-1}$). However, as shown in [157], to acquire correct capacitive conductivities for use in equivalent circuits, one must subtract the mutual capacitive conductivities to other conductors from the self-capacitances of the conductors (diagonal elements of matrix C). Capacitances and capacitive conductivities are proportional; therefore the subtraction can be performed directly with capacitances. Taking into account that after the inversion of matrix P , non-diagonal elements of matrix C are most often negative, the subtraction is replaced by addition. These considerations provide equations for the capacitance to earth of conductor i and the capacitances between conductors i and j used in equivalent circuits:

$$C_{CiG} = C_{ii} + \sum C_{ij}, \quad (8.5)$$

$$C_{Cij} = |C_{ij}|, \quad (8.6)$$

where C_{CiG} and C_{Cij} – the specific capacitance of conductor i to the earth and the specific capacitance between conductors i and j used in equivalent circuits, F/km;

C_{ii} and C_{ij} – the specific self-capacitance of conductor i and the specific mutual capacitance between conductors i and j from matrix C , F/km.

The disconnected fault considered in Fig. 8.1 had occurred at a distance of α p.u. from the beginning of the line, where the resistance R_F has been connected to the ground representing the equivalent resistance of the electric arc channel. The EMF sources shown are busbar L-E voltages obtained by solving the problem of two simultaneous open-phase faults at both ends of the line for the whole network model. The calculation process for this complex fault is described in Section 3.3. Calculations of such regimes require knowledge of the EMFs and their angles of the actual network generators and the equivalent power system. Considering the relatively high inertia of electromechanical transients, the relative angles of the network generator EMFs inherited from the pre-fault state can be used with an acceptable tolerance. The model in Fig. 8.1 considers a non-transposed line, but transposition can be easily taken into account by extending the model with the same element sections, only reflecting changes due to phase positioning.

Using the described model in phase coordinates and the topological nodal potential method from Chapter 4 of this Thesis, the steady-state line-side voltage of the faulted phase U_F (in the case of Fig. 8.1, the L-E voltage next to Phase A EMF source) was calculated during the dead time for positive and negative pre-fault power flow. The results of the calculations for different fault distances and equivalent fault path resistances up to $1 \text{ M}\Omega$ for a 330 kV OHTL are presented in graphs (Fig. 8.2 and 8.3).

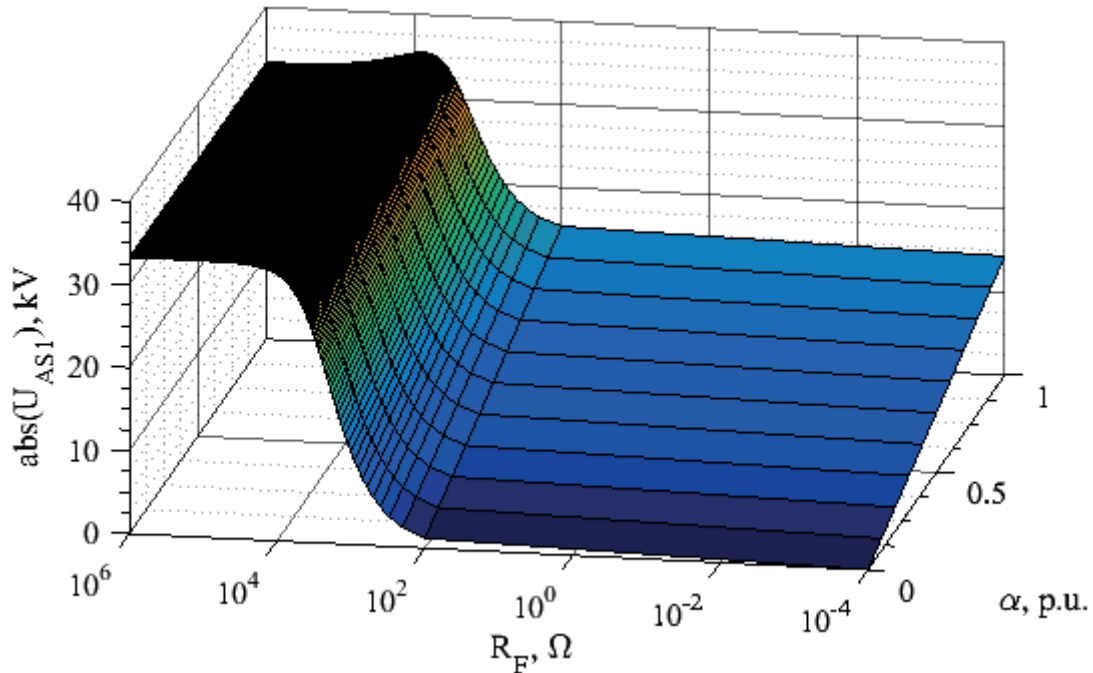


Fig. 8.2. The absolute value of the complex voltage of the disconnected phase depending on the fault distance and the fault path resistance for a positive pre-fault power flow [156].

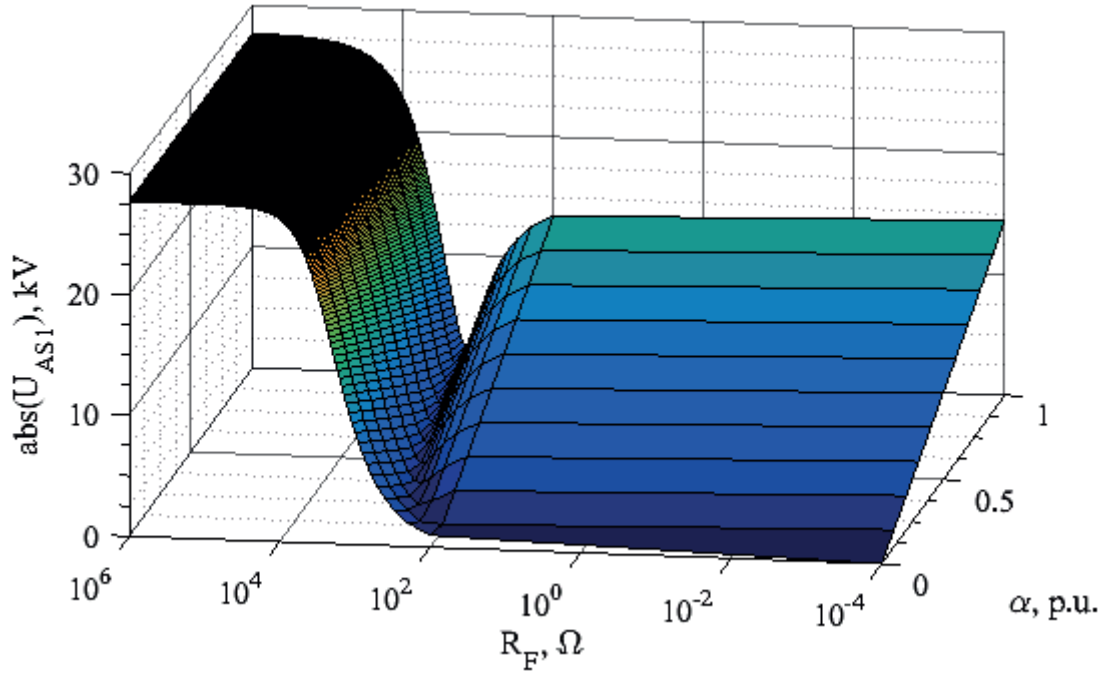


Fig. 8.3. The absolute value of the complex voltage of the disconnected phase depending on the fault distance and the fault path resistance for a negative pre-fault power flow [156].

It can be noted that the graphs presented in Fig. 8.2 and 8.3 show a significantly larger dependence on the fault distance α when the equivalent fault path resistance R_F is between 0Ω and $1\text{--}5 \text{ k}\Omega$. This indicates a larger impact of mutual coupling component U_F^M of fault phase voltage U_F for smaller fault path resistances. When resistance R_F exceeds this value, the impact of the fault distance decreases and a further increase of the faulted phase voltage is more linked to the increase of capacitive component U_F^C of voltage U_F . One can see that the absolute value of the faulted phase voltage stabilises when R_F reaches $10\text{--}15 \text{ k}\Omega$. According to a study about deionisation of HV fault arcs [159] it was considered that a 69 kV L-E voltage could not sustain ionisation of an arc with a resistance of above $50 \text{ k}\Omega$, but in that same paper a more conservative margin of $250 \text{ k}\Omega$ was used to determine deionisation time (for 330 kV it would be even higher). Thus, the absolute value of the phase voltage as a criterion for determining the extinction of fault arc is unreliable and a further analysis is necessary.

Assuming that the currents of the healthy phases are zero, the line model from Fig. 8.1 in reference to voltage $U_F^C \approx U_F$ acts almost as a capacitive voltage divider that determines the voltage by capacitances healthy phases–faulted phase, capacitances phases–earth and equivalent fault path resistance R_F . Increase of the R_F results in changes of ratio $\text{Re}(U_F)/\text{Im}(U_F)$. In most cases there will be a power flow through the healthy phases and an additional rebalancing of the capacitive component and the mutual coupling component, which mostly influences the imaginary part of the faulted phase voltage, can be expected. To illustrate these effects, the dependences of the faulted phase voltage real and imaginary parts on the arc path resistance and the fault distance are presented in graphs (see Fig. 8.4 and 8.5). The graphs of the real and imaginary part for a negative pre-fault power flow have practically

the same form, but the imaginary part curves are shifted to positive values therefore they will be omitted.

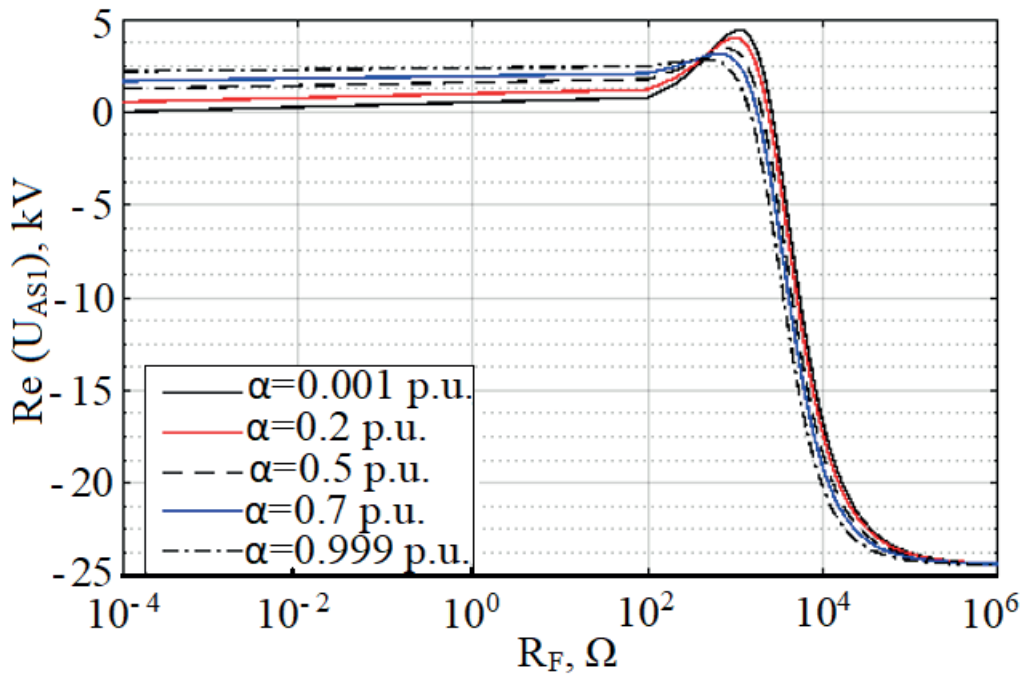


Fig. 8.4. The real part of the complex voltage of the faulted phase as a function of the fault distance and the fault path resistance for a positive pre-fault power flow [156].

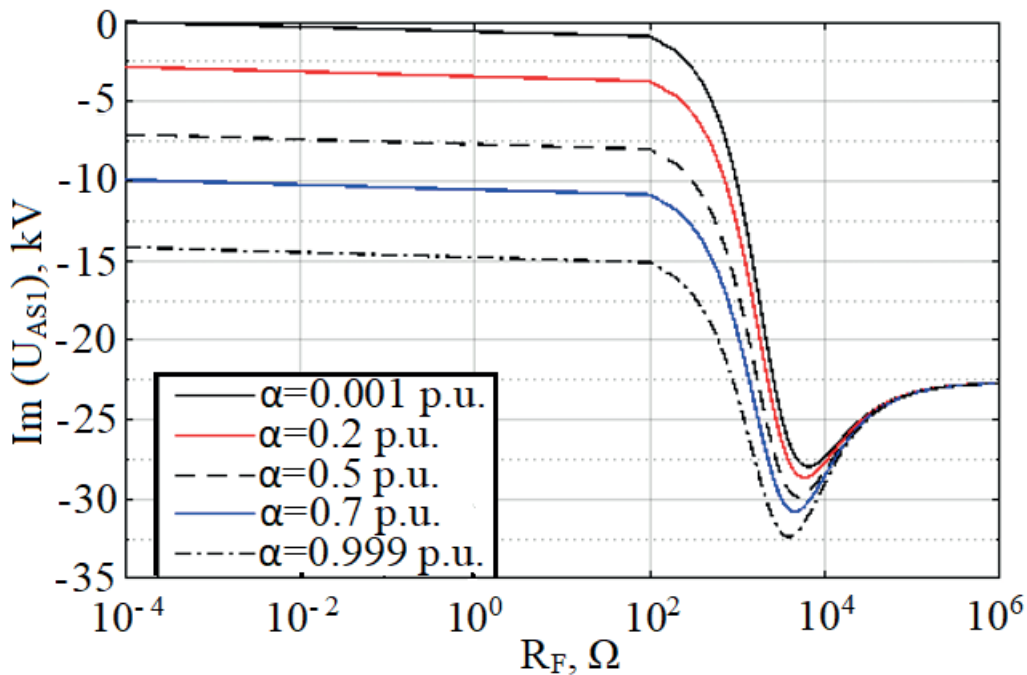


Fig. 8.5. The imaginary part of the complex voltage of the faulted phase as a function of the fault distance and the fault path resistance for a positive pre-fault power flow [156].

One can see that the characteristics of the real part of the faulted phase voltage closely resemble those of the absolute value from Fig. 8.2 with a more uniform dependence and, due to a higher absolute value, it has a larger impact on the RMS value of the faulted phase voltage when R_F approaches a healthy insulation resistance. The real part of the faulted phase

voltage also seems more sensitive to R_F compared to just the RMS value of the voltage. Therefore, a minimum value of the real part of faulted phase voltage could potentially be used as one of the arc extinction indicators, but more importantly, as a blocking mechanism to prevent AR to a permanent fault. The graph of the imaginary part of U_F (Fig. 8.5) shows the expected rebalancing of capacitive voltage component U_F^C and mutual coupling component U_F^M in the 2–10 k Ω section. One can see that the value of $\text{Im}(U_F)$ is not a reliable indicator itself. However, the change of the imaginary part in the section 10 k Ω –1 M Ω is more distinct compared to the real part. This means that at least the stabilisation of the value of the imaginary part can be one of the indicators used to determine arc extinction.

These considerations already provide some indication of possible criteria for an ASPAR algorithm. However, the real process involving a nonlinear arc is much more complicated and a dynamic model of a secondary arc and, if possible, also a primary arc, should be considered.

8.2. Dynamic arc model used for development and testing of the adaptive automatic reclosing method

The secondary arc model used during the dead time is an implementation of the piecewise linear volt-ampere cyclogram (dependence of the voltage gradient on the secondary arc current shown in Fig. 8.6) combined with time-dependent arc reignition.

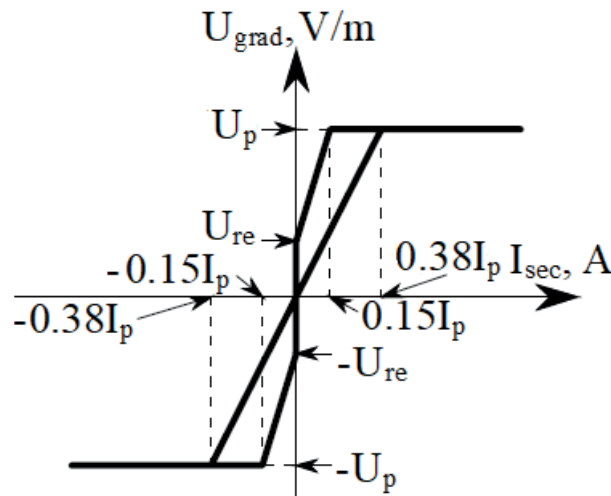


Fig. 8.6. The linearised cyclogram used for a secondary arc model [156].

The secondary arc reignition voltage is calculated and applied during the arc extinctions:

$$U_{re} = (5 + 50T_e)(t - T_e)h(t - T_e), \quad (8.7)$$

where U_{re} – the secondary arc reignition voltage, kV/cm;

T_e – the time from the beginning of the secondary arc till the fault arc extinction (intermediate or final), s;

t – the simulation time, s;

$h(t - T_e)$ – a delayed step function (0, $t < T_e$; 1, $t > T_e$).

The I_p in the cyclogram denotes the secondary arc peak current, which can be determined by the steady-state regime calculation of a disconnected metallic fault, but the peak value of the arc path voltage gradient, U_p , is determined from this current:

$$U_p = 7500I_p^{-0.4}, \quad (8.8)$$

where U_p – the peak value of the arc path voltage gradient, V/m;

I_p – the secondary arc peak current, A.

One of the main reasons why the secondary arc becomes extinguished is the elongation of the arc channel and both the voltage across the arc and the reignition voltage are initially calculated as gradients of the arc length, therefore it is important to describe the elongation process. The simplest approach is to use the linearised version shown in [160]:

$$l_{\text{arc}}/l_{\text{arc0}} = \begin{cases} 1, & t_{\text{sec}} < t_{\text{enl}} \\ 1 + k_{\text{sl}}(t_{\text{sec}} - t_{\text{enl}}), & t_{\text{sec}} \geq t_{\text{enl}} \end{cases}, \quad (8.9)$$

where l_{arc} – the arc length, m;

l_{arc0} – the initial arc length, m;

t_{sec} – the time counted from the beginning of the secondary arc, s;

t_{enl} – the time from the beginning of the secondary arc until the beginning of the arc elongation process, s;

k_{sl} – the slope coefficient defining the rate of increase of the arc length.

The described approach to the depiction of the arc elongation is also used in the case study of this Thesis, with an assumption of the initial arc length l_{arc0} being slightly larger than the insulator length: $l_{\text{arc0}} \approx 1.1l_{\text{ins}}$.

The primary arc (before fault disconnection) model is similar to the secondary arc but the length of the arc channel is assumed to be constant and equal to the initial arc length l_{arc0} . The primary arc cyclogram used in this Thesis is a piecewise linearisation of the volt-ampere cyclogram shown in [161] (Fig. 8.7).

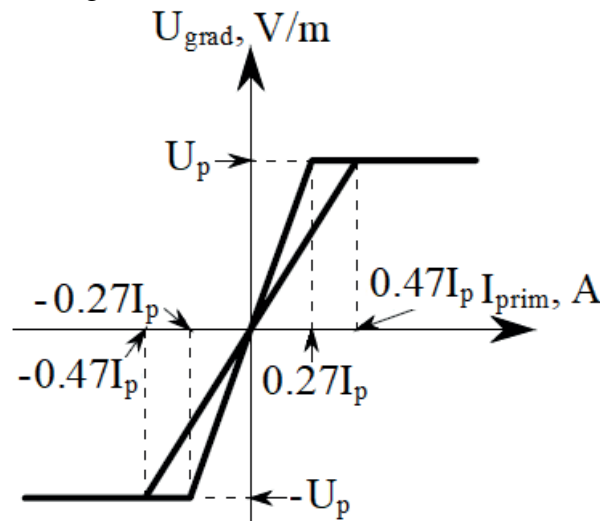


Fig. 8.7. The linearised cyclogram used for a primary arc model.

In the case of a primary arc, the peak voltage gradient, U_p , is assumed to be 1500 V/m, which can be used for arcs with a primary arc peak current I_p between 1.4 kA and 24 kA

[161]. Since the primary arc is stable, the extinction and reignition of this arc are not considered. Both of the described arc models were implemented in MATLAB SimPowerSystems model, where two Thevenin's equivalents of power systems S1 and S2 are connected by two line π -sections representing the parts of the line before and after the fault and two CB groups (CB1A, CB1B, CB1C and CB2A, CB2B, CB2C). Measurements of voltages and currents from both sides of the line were taken with voltage and current sensors (US1A, US1B, US1C, US2A, US2B, US2C, IS1A, IS1B, IS1C, IS2A, IS2B, IS2C). The SPAR block can also be seen controlling CB CB1A (Fig. 8.8). This model was also used for dynamic testing of the proposed ASPAR method.

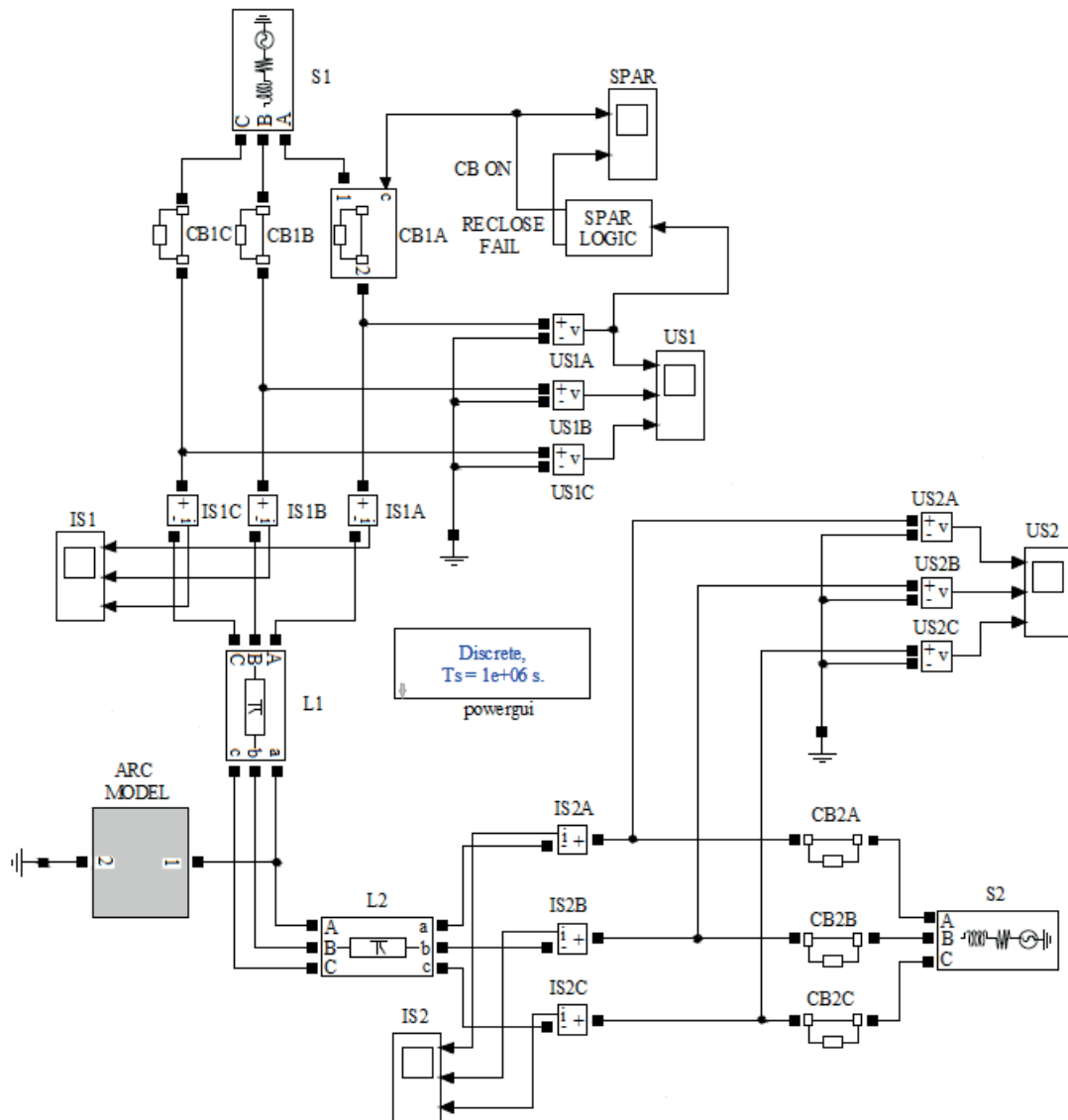


Fig.8.8. The SimPowerSystems model used for the analysis and testing of the proposed method.

The restriking that occurs if the AR command is given while the secondary arc is present or the insulation strength of the arc path is below phase voltage is performed by switching from the secondary arc model to the primary arc model. In order to demonstrate the results of arc modelling, it is possible to show arc voltage and current at the fault point during a successful SPAR (Fig. 8.9). It should be noted that for all of dynamic simulations of fault transients

shown below, the primary arc model is connected 50–100 ms and the secondary arc model – 100 ms after the start of the simulations.

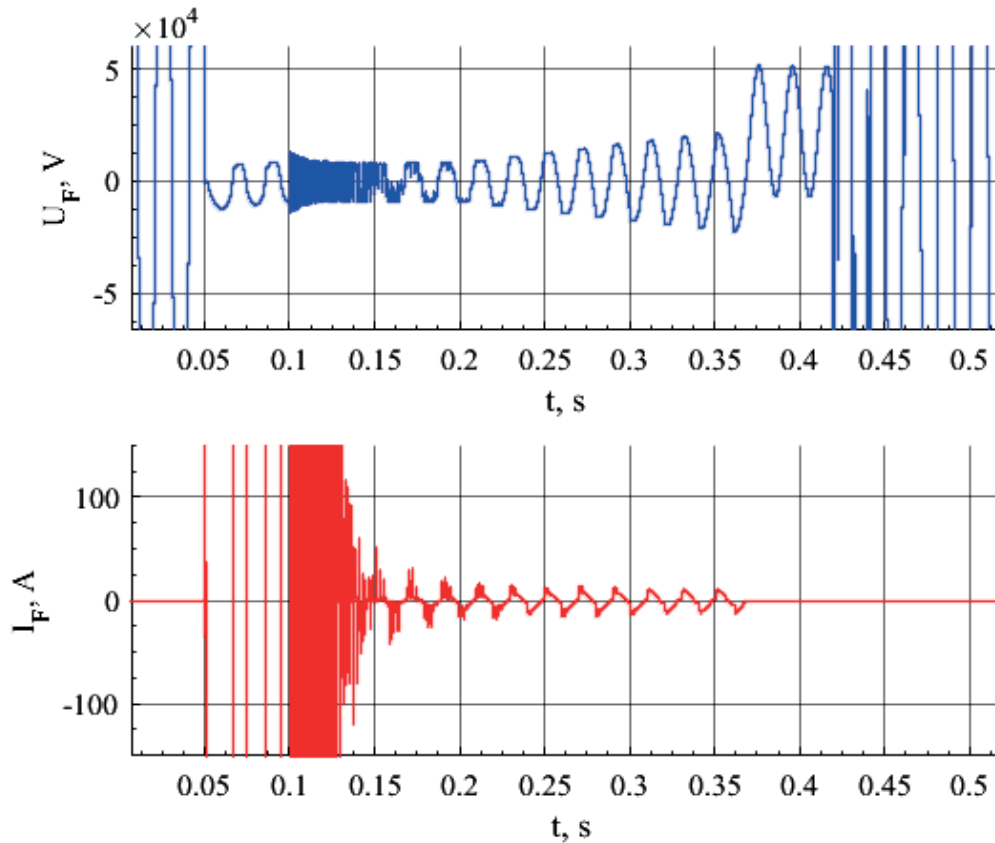


Fig. 8.9. The arc voltage and current at the fault point during a successful SPAR [156].

However, what is more important for the proposed ASPAR algorithm is the line-side voltage at system S1 substation (Fig. 8.10).

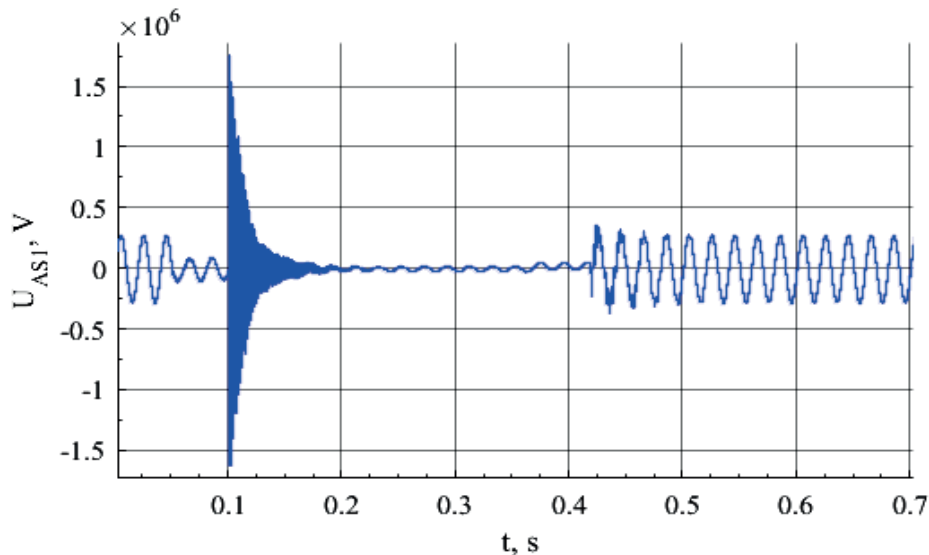


Fig. 8.10. The line-side faulted phase voltage at the system S1 substation during a successful SPAR [156].

As expected, the arc current has higher harmonic distortions created by sudden current increases as instantaneous arc voltage exceeds growing reignition voltage, which are further

increased by the presence of decaying voltage oscillations due to line electromagnetic transients. After arc extinction at approximately 0.369 s (Fig. 8.9), an increase and a DC offset of the fault point voltage can be seen until the CB is switched on (0.42 s).

8.3. The proposed adaptive single pole automatic reclosing method

As one can see from Fig. 8.10, a large overvoltage with high-frequency components is also present after the disconnection of the primary arc current (in reality, this overvoltage would be more limited due to metal oxide varistors but these are more unfavourable conditions, which are useful to test the robustness of the proposed ASPAR algorithm). This overvoltage has little effect after the filtration of the fundamental harmonic, as can be seen by the graph of the real and imaginary part of the line-side faulted phase voltage (Fig. 8.11).

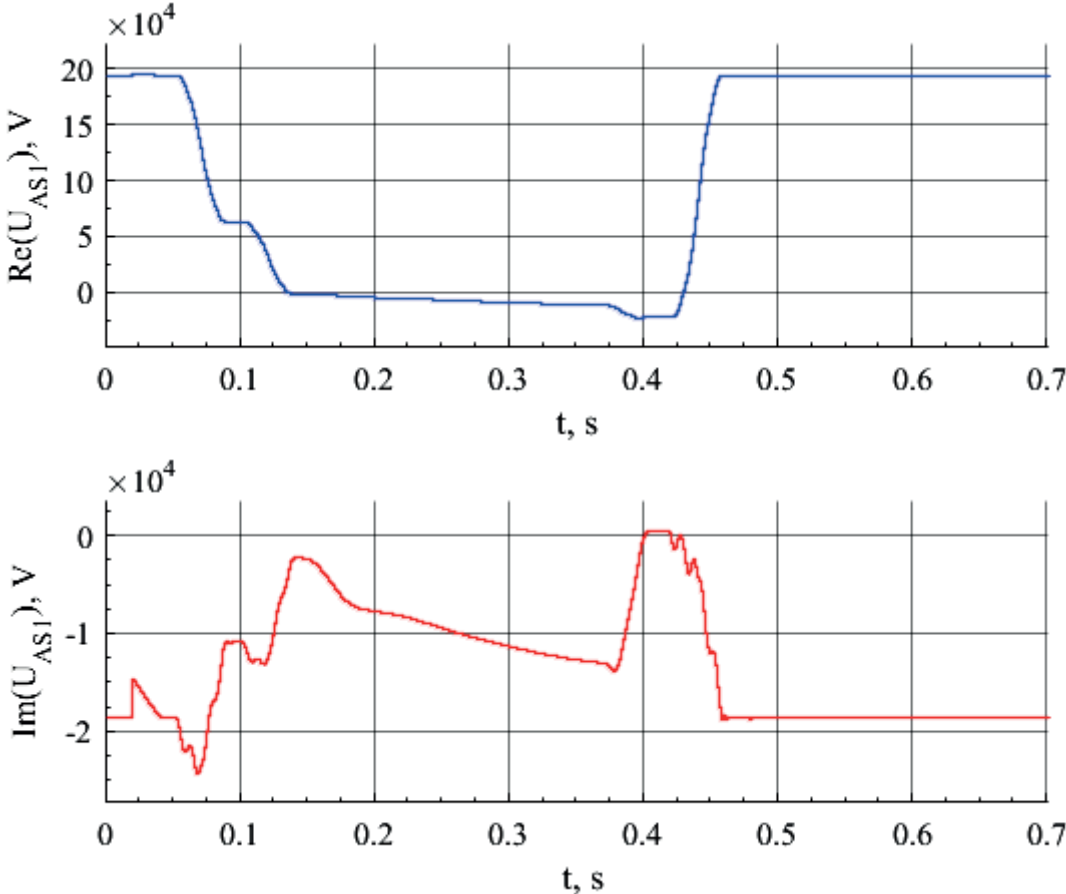


Fig. 8.11. The real and imaginary part of the line-side faulted phase voltage at the system S1 substation during a successful SPAR [156].

The imaginary part graph is more unstable, but both parts indicate that after the arc extinction their values stabilise after a rapid increase (the change after 0.42 s is due to the reclosing of the CB). In order to evaluate the time within which the real and imaginary parts of the faulted phase voltage stabilise, graphs of the absolute values of the discrete derivatives of these signals were obtained (Fig. 8.12).

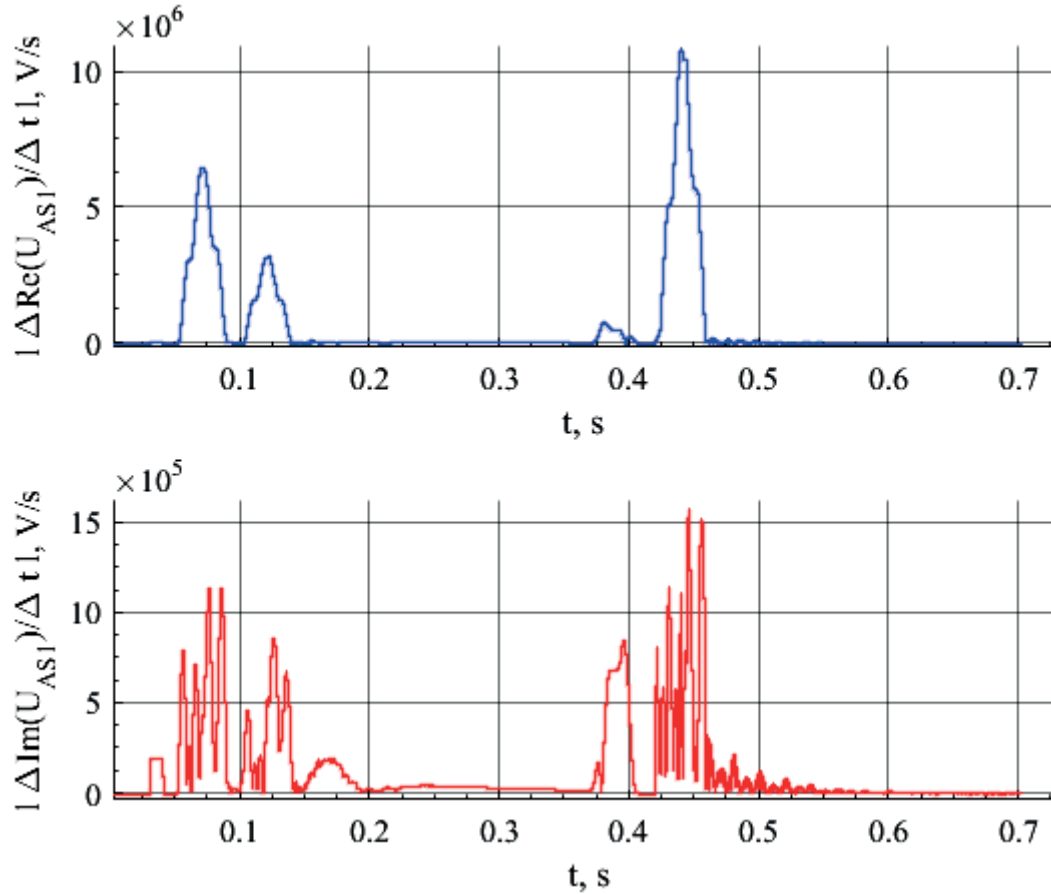


Fig. 8.12. The absolute values of the discrete derivatives of the real and imaginary part of the line-side faulted phase voltage at the system S1 substation during a successful SPAR [156].

The graphs in Fig. 8.12 show that indeed after arc extinction the real and imaginary parts stabilise at their new values at about 0.4 s and, after further consideration, using the minimum value of the derivatives of the real and imaginary part can be regarded as a good precaution against possible intermediate arc extinctions, which would for a short time provide a sufficient value of the real part of the voltage at substation. Based on the above considerations, it can be concluded that using the following criteria: the absolute value of the real part of the faulted phase line-side voltage exceeds a setting $|\text{Re}(U_F)| \geq S_{\text{Re}2}$ and the absolute values of the discrete derivatives of the real and imaginary part of the line-side faulted phase voltage fall below different settings $|\Delta \text{Re}(U_F)/\Delta t| \leq S_{\text{Re}}$, $|\Delta \text{Im}(U_F)/\Delta t| \leq S_{\text{Im}}$, should provide a safe way to detect a stable regime after arc extinction. Setting $S_{\text{Re}2}$ would be calculated as an absolute value of the real part of the faulted phase line-side voltage, using the detailed line model (Fig. 8.1) with online-updated steady-state EMFs and fault path resistance equal to insulation resistance, decreased by a safety coefficient to secure operation in case of measurement errors (here, 90 % of the calculated value was used). Settings S_{Re} and S_{Im} also can be adaptive, for example, defined as percentages (above the noise level of the normal regime) of the current maximum value of these derivatives registered since the beginning of the secondary arc (here, a 5 % setting was applied). The noise level can be decreased by additional filtering of the real and imaginary part signals (in this case, the sliding average filter was applied). After closer examination of Fig. 8.11 and 8.12, one can also

notice that the voltage drop does not occur immediately after the disconnection of the faulted phase (0.1 s) because of the sliding average filter and the line π -section capacitances sustaining the voltage according to the second law of commutation. In such situations, the derivative values are minimal and below the setting for a small time while the condition $|\text{Re}(U_F)| \geq S_{\text{Re}2}$ is also met. Therefore, a simple upper-boundary condition for the RMS value of the faulted phase voltage being below a setting $|U_F| \leq S_{\text{ABS}}$ can be used, where the setting S_{ABS} is obtained by a primary fault regime calculation when the fault is on the other side of the line with a maximum possible fault resistance decreased by a safety margin (if this voltage significantly exceeds setting $S_{\text{Re}2}$, then using values of $(1.5 - 3)S_{\text{Re}2}$ would be more beneficial). Additionally, a start signal, which indicates the open state of CBs is necessary. It should be noted that the proposed ASPAR method is aiming at reducing the reclosing time to a minimum, and the reclosing command from this method should be used for the leading switch reclose (QF1 in Fig. 1.5). This is why the synchronisation is not addressed in this application. In addition to the main criteria of operation, additional time delay Δt_1 is added, which first includes 5–10 ms of switch on delay to further prevent undesirable SPAR operation during intermediate arc extinction or other unexpected short-duration compliance with the operation criteria. Then the signal for SPAR to operate is fixed but the final command given to the CB is delayed by 20 ms to ensure full arc channel deionisation after the extinction of the secondary arc. Based on the analysis of SPAR operation field data shown in [119], the maximal delay after the arc extinction required for secure reclosure for the 330 kV line is approximately 60 ms, but, since the algorithm operates when the regime stabilises after the arc extinction, it was observed that the chosen 20 ms delay is fully adequate. The start signal can also be combined with a significant time delay exceeding possible reclose time Δt_2 to indicate that the ASPAR has failed to operate, which means that the fault is permanent. This indication (RECLOSE FAIL) can be used as an alarm signal if the operation of the healthy phases is critical, or as a disconnection signal for CBs of the healthy phases if it is necessary to avoid damage to transformer neutrals due to significant ZS currents. The described criteria and functions can be implemented into the inner logic diagram of the proposed ASPAR method (Fig. 8.13). Testing of the criterion $|\text{Re}(U_F)| \geq S_{\text{Re}2}$ is performed by a greater-than-or-equal block (GT2), and criteria $|U_F| \leq S_{\text{ABS}}$, $|\Delta \text{Re}(U_F)/\Delta t| \leq S_{\text{Re}}$, $|\Delta \text{Im}(U_F)/\Delta t| \leq S_{\text{Im}}$ are tested by blocks of the same type (GT1, GT4 and GT5). Since all of the discussed criteria need to be met in order to safely perform SPAR, the outputs of these criteria blocks are connected logical AND gates (AND1, AND2, AND3, AND4). When all of the criteria are met, time delays of the block Δt_1 are applied before the activation of output CB ON as described above.

The overall flowchart of the proposed ASPAR method including application of the fault distance estimation, modelling of one-open phase regime of the faulted OHTL and the power system in the symmetrical component coordinates, a detailed three-phase model of the faulted OHTL during the dead time in phase coordinates, calculation of adaptive settings and the above-described inner logic is presented in Fig. 8.14.

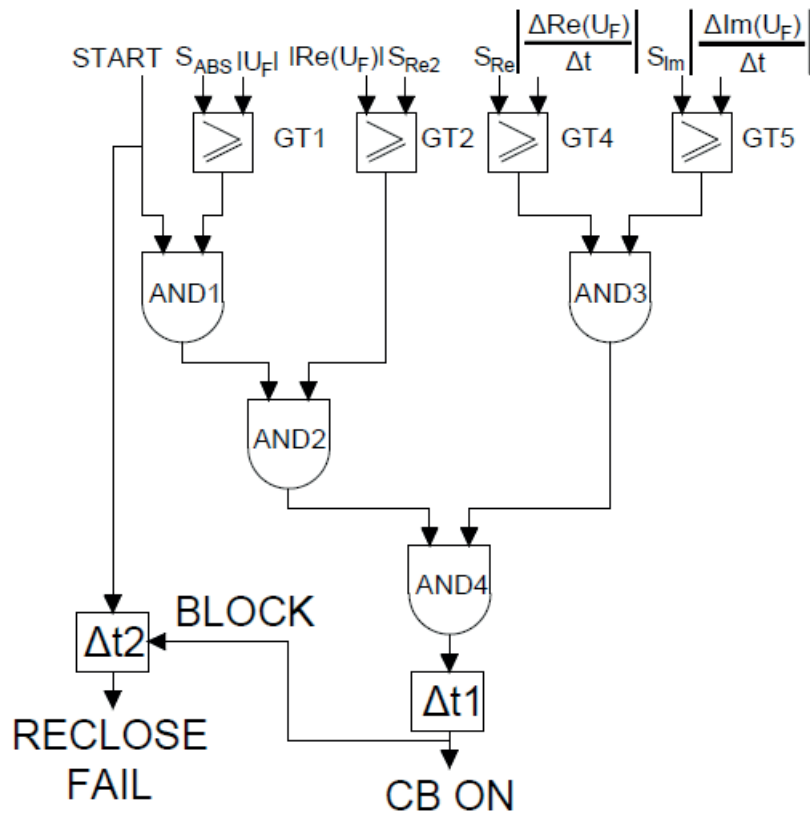


Fig. 8.13. Inner logic diagram of the proposed ASPAR method.

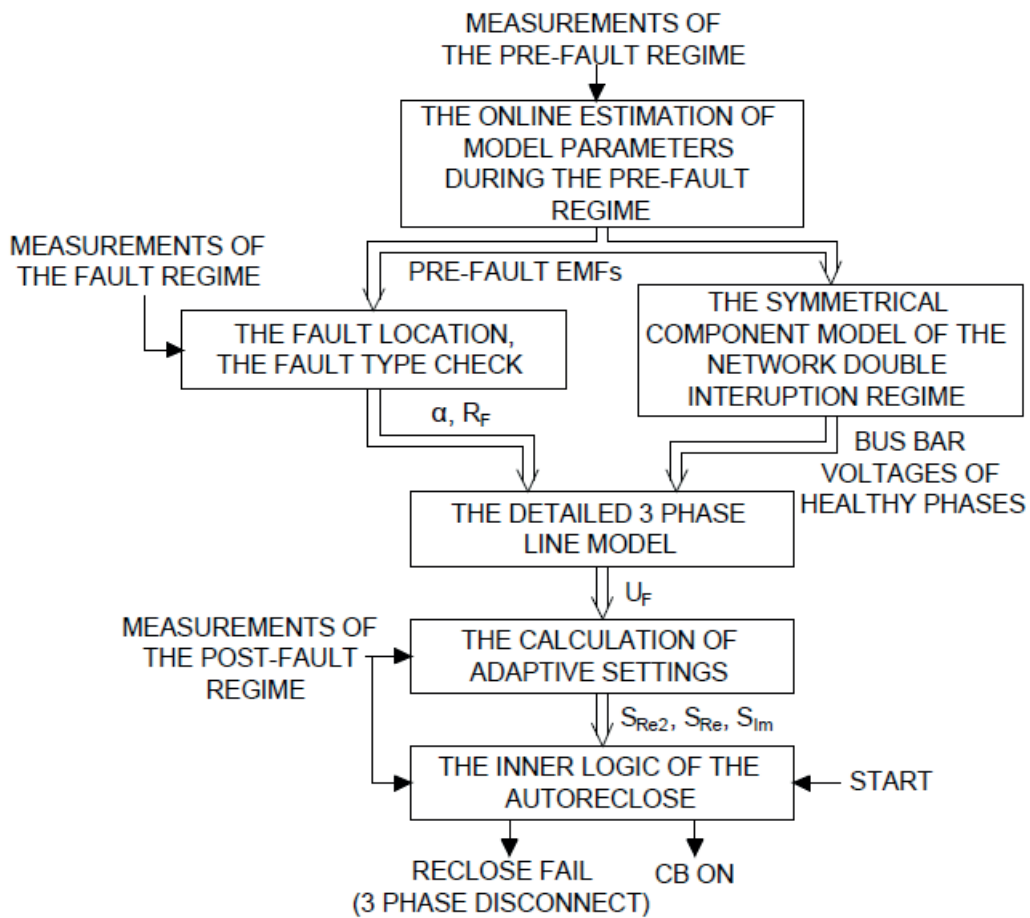


Fig. 8.14. The flowchart of the proposed method.

8.4. Testing of the proposed adaptive automatic reclosing method

The proposed ASPAR method was tested on a 330 kV line, which interconnects two 330 kV systems, S1 and S2, with short-circuit powers of 2 GVA and 1 GVA and X/R ratios of 8 and 6 (Fig. 8.8). The line parameters were calculated based on horizontal phase configuration with two earth wires typical to the Latvian 330 kV transmission grid (for more details see [156]). The testing is focused on the performance of the inner logic of the proposed ASPAR method because the performance of the FL and estimation of the pre-fault regime parameters were demonstrated to be accurate in Chapters 5 and 7 of the Thesis. Therefore, the fault distance and the EMFs for the systems were assumed to be known. As seen from the previous analysis, the fault distance has an insignificant impact on the steady-state value of the real part of the faulted phase line-side voltage and setting S_{Re2} . Because of this, only faults at the beginning, middle and end of the line ($\alpha = 0.001$ p.u.; 0.5 p.u.; 0.999 p.u.) were tested, instead focusing on different arc elongation speeds and time delays before the start of the elongation process. Two pre-fault power flow scenarios were considered by modification of both power system EMFs: a significant positive pre-fault power flow ($E_{S1A} = 1.025e^{i0^\circ}$ p.u.; $E_{S2A} = 1e^{-i20^\circ}$ p.u.) and a negative pre-fault power flow ($E_{S1A} = 1e^{i0^\circ}$ p.u.; $E_{S2A} = 1.025e^{i20^\circ}$ p.u.). The insulator length used for the calculation of the initial arc length is assumed $l_{ins} = 2.7$ m. The absolute steady-state values of the real part of the faulted phase line-side voltage was calculated to be 24371 V and 21819 V for positive and negative power flow directions resulting in settings S_{Re2} having the values of 21934 V and 19637 V. The study network used yields a S_{ABS} close to nominal L-E voltage due to the proximity of both power systems, therefore this setting was simply assumed to be 30 kV (based on the interval mentioned in Section 8.3). First the performance of the proposed method was tested for various transient fault scenarios. The results including the time of arc extinction t_{EXT} , the full deionisation time (when the reignition voltage exceeds the peak value of nominal phase voltage according to (8.7)) – t_{DEION1} –, the full deionisation time considering the maximum statistical necessary time from the moment of the arc extinction (60 ms) – t_{DEION2} –, the moment when the inner logic block AND4 with the 5 ms of switch on delay is triggered, t_{AND4} , the moment when the final output command to reclose the CB is given, $t_{RECLOSE}$, for positive and negative power flows are presented in Fig. 8.15 and 8.16 (for these graphs, zero time corresponds to the beginning of secondary arc).

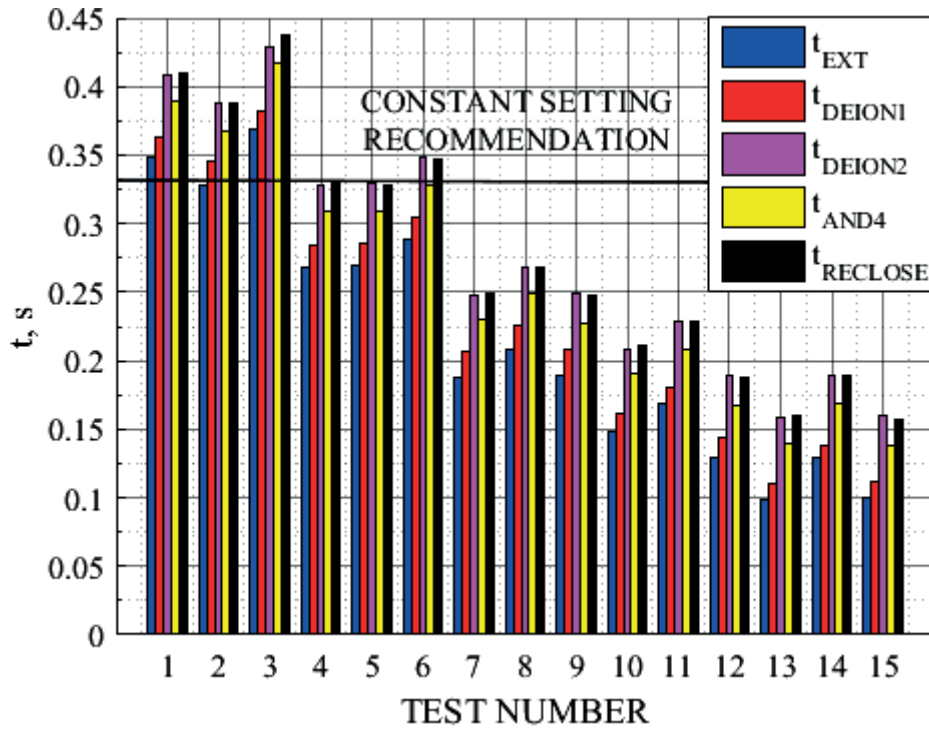


Fig. 8.15. The results of the proposed ASPAR method testing for a positive pre-fault power flow [156].

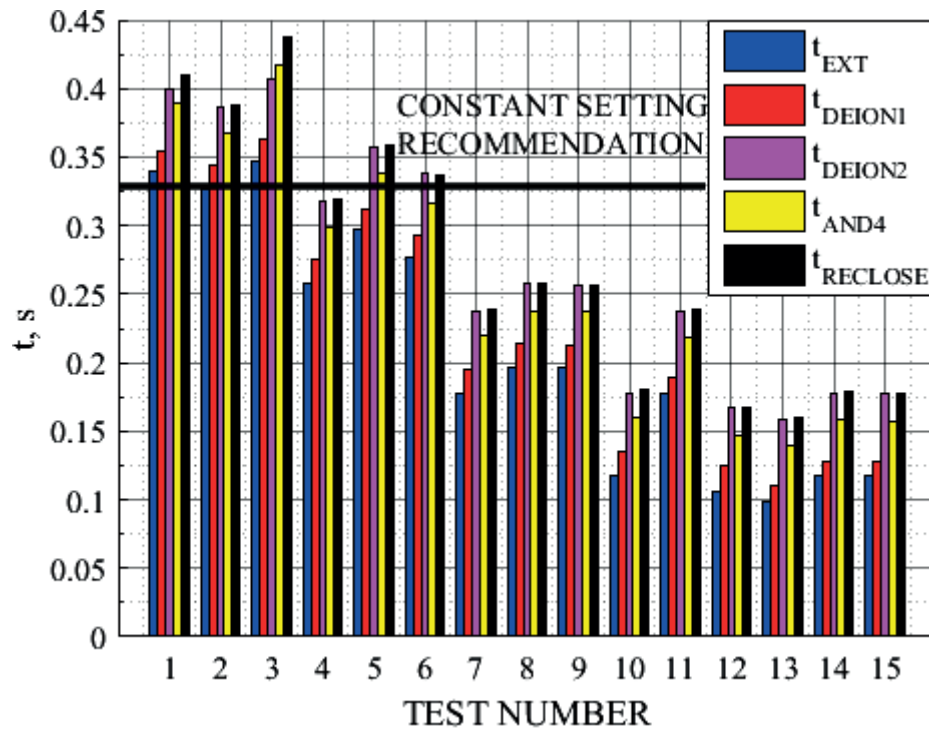


Fig. 8.16. The results of the proposed ASPAR method testing for a negative pre-fault power flow [156].

The constant setting recommendation is given for a comparison with the conventional AR shot method based on the empirical equation for deionisation time given in [162]:

$$t_{\text{deion}} = (1/60)[10.5 + (U_N/34.5)], \quad (8.10)$$

where t_{deion} – the time of full deionisation, s;

U_N – the nominal L-L voltage; kV.

According to (8.10) $t_{deoin} \approx 0.3344$ s for 330 kV voltage level, which is close to the average value of local practice, considering that t_{deion} from table in [163] and other empirical equations varying from 0.3 s up to 0.4 s. First, one can see that the constant setting covers most deionisation scenarios, with the exception of a few scenarios, according to which the arc elongation process began with delays of 100 ms and 200 ms. However, usually this is of little importance since additional delays are often already added for safety reasons or introduced by the CB operation time. However, as can be seen, for rapid arc elongation process scenarios there will be a significant unnecessary time gap between the moment of the actual deionisation and the reclosing command of a conventional AR device. On the other hand, the proposed ASPAR method has changed the time of the output signal, which exceeds the safe deionisation time according to the first approach, t_{DEION1} , and is in most cases is the same as, or exceeds, the statistical safe deionisation time t_{DEION2} , which means that not only were the simulated AR procedures successful, but also the time reserve should be sufficient for deionisation in any case involving a real network. In order to further illustrate the performance of the proposed inner logic and the chosen operation criteria, it is possible to show operation diagrams of separate logic elements (Fig. 8.17 and 8.18) for a scenario of positive power flow also considered in Fig. 8.9–8.12.

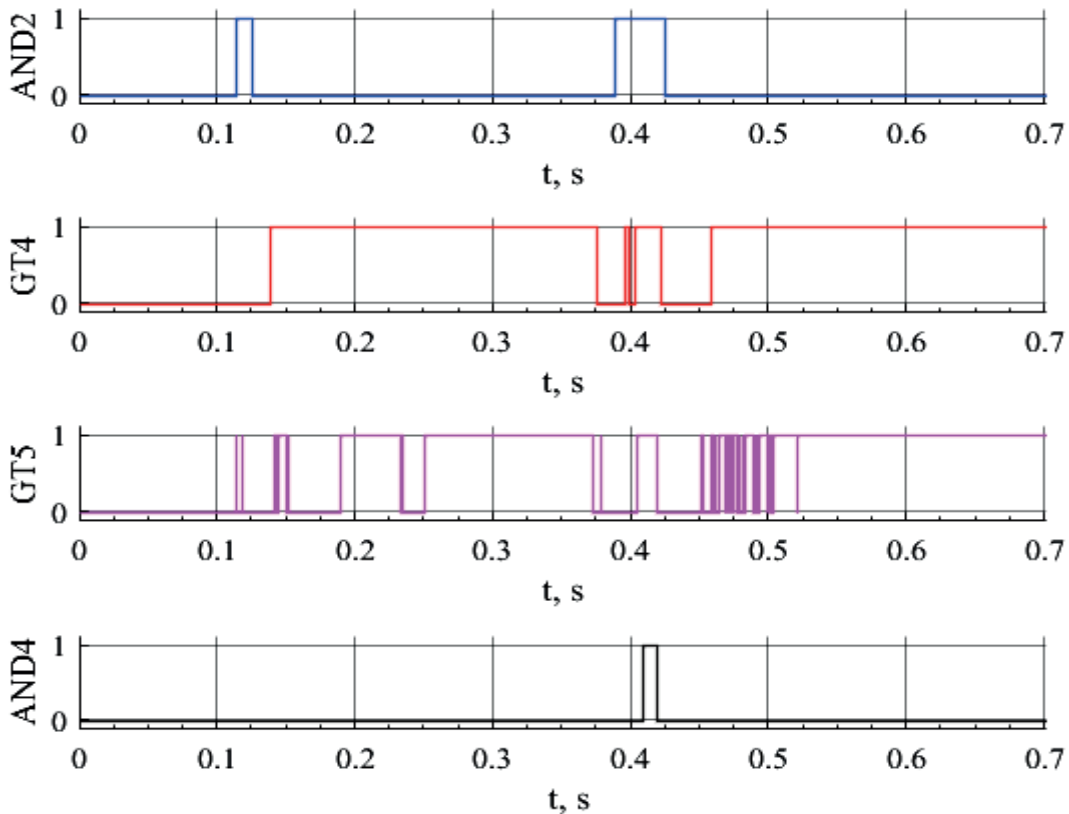


Fig. 8.17. The operation diagram of the inner logic of the proposed ASPAR method for a transient fault [156].

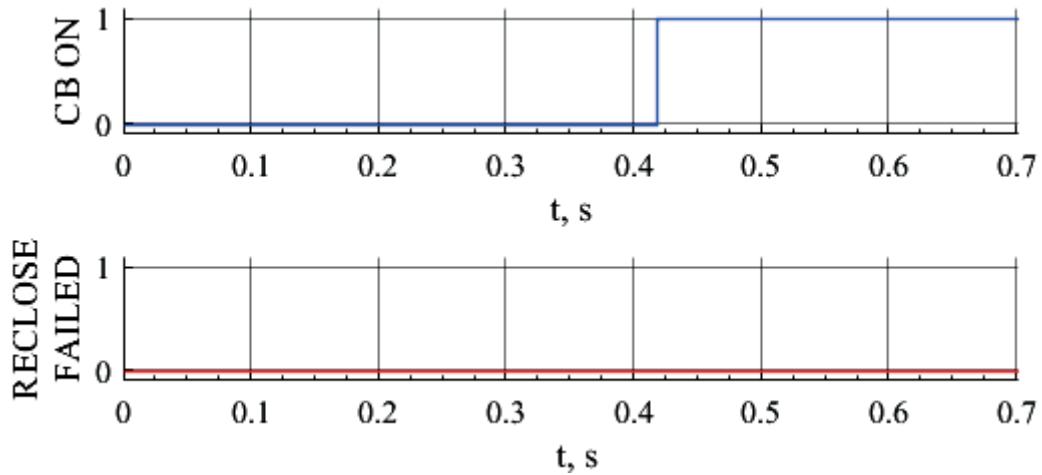


Fig.8.18. The output of the proposed ASPAR method for a transient fault [156].

One can see that during the voltage drop after the disconnection of the fault, the logical AND2 becomes active for a short time but the possible operation is blocked by discrete derivative criteria tests GT4 and GT5. After that, the next time AND2 is active is shortly after the arc extinction at 0.37 s but AND4 is activated at 0.409 s because there is a transient after the extinction of the arc as shown in Fig. 8.11 and therefore GT4 and GT5 are activated later. As a result, the command to reclose the CB was issued 20 ms after the activation of AND4, about 330 ms since the ignition of the secondary arc.

Besides the testing of the operation of the proposed ASPAR method during transient faults, it is also necessary to test its performance in the case of a permanent fault. In order to test the performance of the proposed method in possible unfavourable conditions, it was assumed that this permanent fault would occur at the other side of the line ($\alpha = 0.999$ p.u.) and it would have a high equivalent fault resistance (R_F) in the amount of 5 k Ω , which could represent a partially carbonised fallen tree. The test was performed for both power flow directions and for 1.5 s, while the delay Δt_2 was chosen to be 1 s in order to test the blocking of the reclosing algorithm or indication of a reclosure failure due to a permanent fault. During both tests, the algorithm of the proposed method successfully blocked the operation of the AR. To illustrate the results of these tests, the faulted phase line-side voltage at the system S1 substation and operation diagrams of the test with a positive power flow are presented (Fig. 8.19 –8.21).

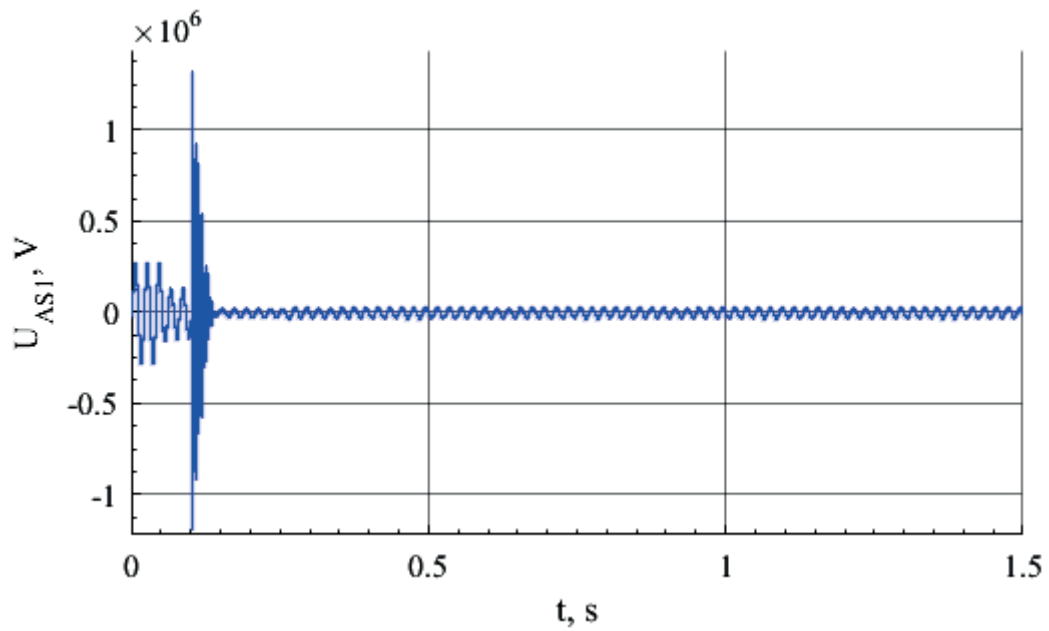


Fig. 8.19. The line-side faulted phase voltage at system S1 substation during a permanent fault with a significant fault path resistance.

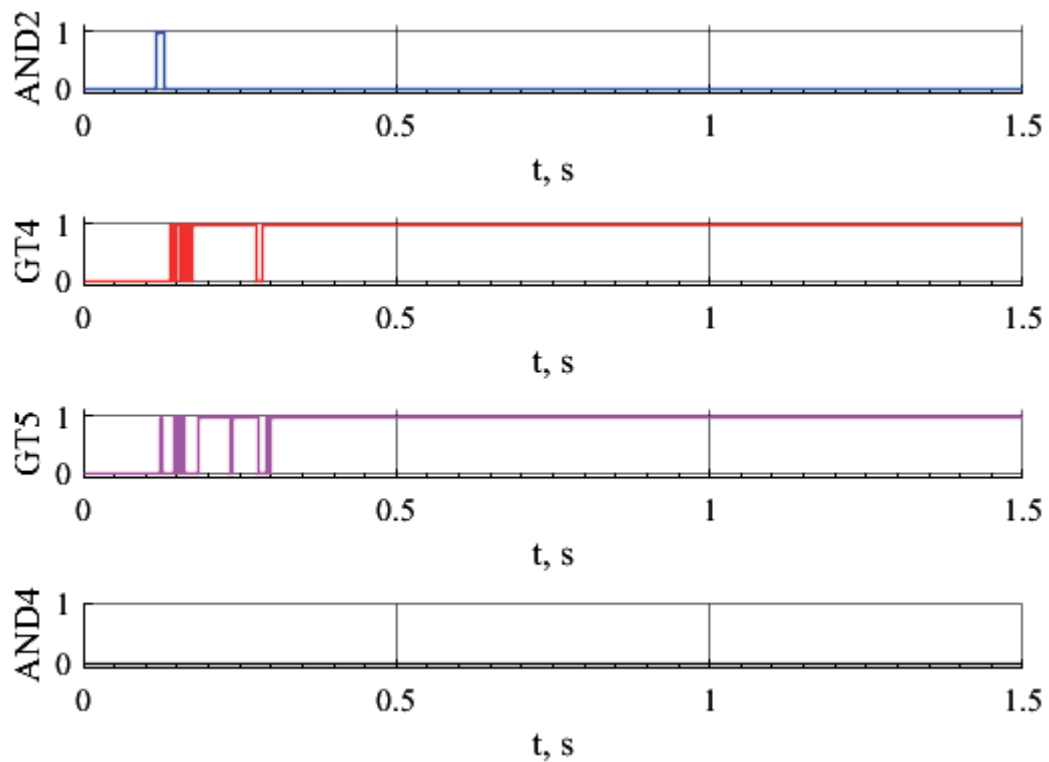


Fig. 8.20. The operation diagram of the inner logic of the proposed ASPAR method during a permanent fault with a significant fault path resistance.

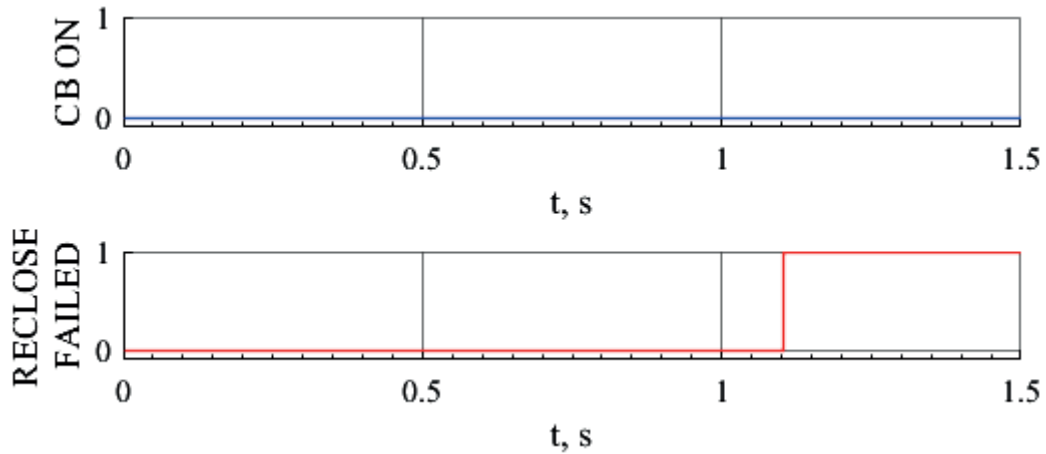


Fig. 8.21. The output of the proposed ASPAR method during a permanent fault with a significant fault path resistance.

On can see from Fig. 8.19 that after the disconnection of the primary fault, the measured voltage stabilises (at about 0.3 s), but an insufficient value of the real part of this voltage is achieved, which is indicated by AND2 remaining deactivated after the initial voltage fall of the secondary arc (Fig. 8.20), as it was expected according to the analysis in Section 8.1. This is why the inner logic was not triggered and, as can be seen from Fig. 8.21, an indication about AR failure to activate was given at 1.1 s (1 s after the ignition of the secondary arc). This means that for permanent faults with an equivalent fault path resistance of up to at least 5 k Ω , the proposed ASPAR method would block operation. According to Fig. 8.4, it could be possible for this method to operate if R_F reached the 10 k Ω limit. However, during permanent faults, which in the Baltic region are often caused by fallen trees, the tree tends to burn through in a short time, sometimes even before the operation of the relay protection [142], and thus cases with the equivalent fault path resistance remaining above the tested magnitude after operation of relay protection are rare.

8.5. Conclusions

1. The proposed model parameter estimation can be applied for other power system automation tasks such as creation of adaptive automation algorithms. This was demonstrated by development of an ASPAR algorithm.
2. The proposed ASPAR algorithm applies topological analysis of a detailed three-phase steady-state line model during the dead time to calculate the adaptive setting, and the results of both parameter estimation stages from the proposed FL algorithm are used as inputs for this model.
3. The implemented dynamic primary and secondary fault arc models allowed confirming the use of the real part of the faulted phase line-side voltage at the substation as a suitable indication for fault arc extinction. The dynamic simulations also resulted in improved safety of proposed ASPAR algorithm with introduction of criteria of discrete derivatives of the real and imaginary parts of the same voltage, which reduces the risk of undesirable

SPAR operations due to an intermittent arcing and provides additional time for the restoration of insulation strength at the fault point.

4. The described ASPAR algorithm testing showed the expected adaptive performance blocking operation for permanent faults and decreased operation times in cases of rapid fault arc elongation and extinction compared with the often-used fixed reclose time method.

CONCLUSIONS

1. The hypothesis of the Doctoral Thesis has been proven: the performance of the tested existing one-terminal-measurement-based FL and DP approaches was impaired when faults had a high fault path resistance and they can be replaced by a technique based on a two-stage estimation of unknown power system model parameters that solves the problem as an optimisation task and expands the available measurements only within the controlled substation.
2. Most often both an apriori optimisation implemented in devices as settings and online optimisation utilised by the control system to generate optimal control operations requires modelling of the power system or its elements to some degree of detail.
3. Some of the automation and protection functions have additional task of estimation of unknown parameters of the power system elements due to lack of measurement data or changes of the system caused by external influences such as faults.
4. Measurements from both terminals of the line provide opportunities for fast and accurate FL, but their operation can be critically affected in case of loss of communication between substations or synchronisation of these measurements.
5. Existing FL methods using one-terminal measurements utilise algorithms that are independent from the influence of the remote-end infeed such as TW methods, or to approximate this influence or errors caused by it using methods such as ANN and Monte-Carlo.
6. Most of research on DP was more oriented towards various implementations of the DP itself in electromechanical, electronic or digital devices.
7. The loss of sensitivity due to the remote-end infeed can be partially compensated with adaptive DP operation regions, but this increases the risk of loss of selectivity.
8. Most ASPAR methods ignore the influence of healthy-phase power flow or they are highly dependent on accurate measurements of higher-harmonic components or DC offset, requiring a higher sampling frequency and resulting in more expensive devices.
9. Fault regimes with multiple simultaneous asymmetries can be modelled by one complex equivalent circuit with electrical interconnections representing one of the asymmetries and iteratively recalculated EMF sources representing the other asymmetries or by interchanging calculation of regimes for two or more of such complex equivalent circuits where each circuit represents different asymmetry with electrical interconnections.
10. Topological modelling of power system equivalent circuits that represent asymmetrical power system regimes combined with the nodal potential (admittance) method in the matrix form result in flexible and easy-to-implement modelling means for computer-based fault analysis and the estimation of unknown power system parameters.
11. The presence of fault path resistance negatively affects the performance of the existing digital DP terminal both for L-L-E and L-E faults, especially in the case of fallen-tree faults, which can result in significant additional time delays.

12. The division of the model parameter estimation into two stages reduces the amount of unknown data that have to be determined after fault inception, thus making the second stage more feasible.
13. The accuracy of the existing digital FL using one-terminal measurements has a high degree of dependence on the pre-fault power flow, especially if it is oriented towards the substation. The proposed applications of parameter estimation for DP and FL do not have this dependence as both the equivalent fault path resistance and the pre-fault loading of the power system are also estimated.
14. The initially tested modification of a randomised search used with the proposed method provided satisfactory results, but it did require significant computation time, which led to the adoption of the GA.
15. One approach to the selection of measured parameters for use in the objective function is to sort them only by their sensitivity to changes in the fault distance. However, it often results in objective functions with surface distortions and false extrema, which increases the risk of inaccurate fault distance estimation.
16. Analysis of measurable parameter curves for different fault distance and resistance values can also be used to obtain parameter groups that would result in fewer distortions in the surface of the objective function and a more distinct global extremum.
17. A comparison of the tested parameter selection strategies showed that the conservative strategy performed better or similarly to the opportunistic one for faults in double-circuit lines with possible pre-fault power flow in both directions, but for faults in single-circuit lines the opportunistic strategy was better suited.
18. The decrease of available measurements for the objective function has the most noticeable effect on accuracy of fault distance estimation for faults in single-circuit lines, which in general presented the greatest challenge for the proposed method.
19. The updated version of the parameter estimation method using the GA clearly outperformed the existing one-terminal-measurement-based fault locator algorithm.
20. The last version of the proposed method had higher maximum error values than the existing two-terminal-measurement-based FL method using NS quantities, but in terms of mean error and expected concentration of 95 % of fault distance estimation error values, the proposed method mostly outperformed the two-terminal-measurement-based method.
21. The proposed model parameter estimation can be applied for other power system automation tasks such as creation of adaptive automation algorithms.
22. The proposed ASPAR algorithm applies topological analysis of a detailed three-phase steady-state line model during the dead time to calculate the adaptive setting, and the results of both parameter estimation stages from the proposed FL algorithm are used as inputs for this model.
23. The implemented dynamic primary and secondary fault arc models allowed to confirm the use of the real part of the faulted phase line-side voltage at the substation as a suitable indication for fault arc extinction. The dynamic simulations also resulted in improved safety of proposed ASPAR algorithm with introduction of criteria of discrete derivatives of the real and imaginary parts of the same voltage, which reduces the risk of undesirable

SPAR operations due to an intermittent arcing and provides additional time for the restoration of insulation strength at the fault point.

24. The described ASPAR algorithm testing showed the expected adaptive performance blocking operation for permanent faults and decreased operation times in cases of rapid fault arc elongation and extinction compared with the often-used fixed reclose time method.

APPENDICES

Appendix 1 A section of MATLAB code for implementation of topological modelling of a L-E short circuit

Appendix 2 A section of MATLAB code for implementation of topological modelling of a two open-phases fault

Appendix 3 An example of MATLAB code for implementation of topological modelling of simultaneous two L-L-E short circuits and a one-open-phase fault

A section of MATLAB code for implementation of topological modelling of a L-E short-circuit

```

%nominal frequency, Hz
fn=50;
%nominal angular frequency, rad/s
Wn=2*pi*fn;
%moment of fault inception, s
tapr=0;
%Impedances, Ohms
%Power system
Zs=1.37+10.94i;
%EMFs of the Power system at the of fault inception tapr, kV
EsA=(Ub/k3)*(cos(Wn*tapr)+sin(Wn*tapr)*1i);
EsB=(EsA*a2)*(cos(Wn*tapr)+sin(Wn*tapr)*1i);
EsC=(EsA*a)*(cos(Wn*tapr)+sin(Wn*tapr)*1i);
%Transformers
Zt=0.085+10.64i;
%Positive-sequence impedance of the OHTL, Ohms/km
Ll=40; %Line length, km
Z1l=(0.235+0.43i)*Ll;
% Zero-sequence impedance of the OHTL, Ohms/km
Z0l=(0.391+1.074i)*Ll;
%Positive-sequence capacity of the OHTL, F
C1l=Ll*8.13e-9;
% Zero-sequence capacity of the OHTL, F
C0l=Ll*4.61e-9;
%Reactive power generated by the OHTL, Mvar
dQc=1.35;
%Impedance of the load, Ohms
Zsl=267.81+129.7i;
%Apparent power of the load, MVA
Ssl=40+19.3729i;
Rpap=0.0001;
%Fault path impedances, ohms
Zka=10;
Zkb=10^6;
Zkc=10^6;
Zkn=0;
%First incidence matrix
% 1 2 3 4 5 6 7 8 9 10 11 12 13 14 15 16 17 18 19 20 21
M=[-1 1 0 0 0 0 0 0 0 0 0 0 0 0 0 0 0 0 0 0 0 %1
    0 -1 1 0 1 0 0 0 0 0 0 0 0 0 0 0 0 0 0 0 0 %2
    0 0 -1 1 0 1 0 0 0 0 0 0 0 0 0 0 0 0 0 0 0 %3
    0 0 0 -1 0 0 1 0 0 0 0 0 0 0 0 0 0 0 0 0 0 %4
    0 0 0 0 0 0 -1 1 0 0 0 -1 -1 0 0 0 0 0 0 0 0 %5
    0 0 0 0 0 0 0 -1 1 0 0 0 0 0 0 0 0 0 0 0 0 %6
    0 0 0 0 0 0 0 0 -1 1 0 1 0 0 0 0 0 0 0 0 0 %7
    0 0 0 0 0 0 0 0 0 -1 1 0 1 0 0 0 0 0 0 0 0 %8
    0 0 0 0 0 0 0 0 0 0 -1 0 0 1 0 0 0 0 0 0 0 %9
    0 0 0 0 0 0 0 0 0 0 0 0 0 -1 1 0 0 0 -1 -1 0 %10
    0 0 0 0 0 0 0 0 0 0 0 0 0 0 -1 1 0 0 0 0 0 %11
    0 0 0 0 0 0 0 0 0 0 0 0 0 0 0 -1 1 0 1 0 0 %12
    0 0 0 0 0 0 0 0 0 0 0 0 0 0 0 0 -1 1 0 1 0 %13
    0 0 0 0 0 0 0 0 0 0 0 0 0 0 0 0 0 -1 0 0 1];%14

```

```

%Branch impedance vector, Ohms
ZZ=[Zs+Zt      %I11
    Rpap      %I21
    Zl1      %I31
    Rpap      %I41
    (2/(Wn*C11*1i)) %I51
    (2/(Wn*C11*1i)) %I61
    Zka      %I71
    Zs+Zt      %I12
    Rpap      %I22
    Zl1      %I32
    Rpap      %I42
    (2/(Wn*C11*1i)) %I52
    (2/(Wn*C11*1i)) %I62
    Zka      %I72
    Zs+Zt      %I10
    Rpap      %I20
    Z0l      %I30
    Rpap      %I40
    (2/(Wn*C0l*1i)) %I50
    (2/(Wn*C0l*1i)) %I60
    Zka+3*Zkn]; %I70
%Branch EMF vector, V
E =[EsA %I11
    0 %I21
    0 %I31
    0 %I41
    0 %I51
    0 %I61
    0 %I71
    0 %I12
    0 %I22
    0 %I32
    0 %I42
    0 %I52
    0 %I62
    0 %I72
    0 %I10
    0 %I20
    0 %I30
    0 %I40
    0 %I50
    0 %I60
    0]; %I70
MS=size(M,1);
ZS=size(M,2);
Z=diag(ZZ);
Mt=M';
for i=1:ZS
    Z1(i,i)=1/Z(i,i);
end
Y=M*Z1*Mt;
B=-M*Z1*E;
disp ('Symmetrical components of Phase A voltage of the nodes of the complex equivalent circuit, kV')
U=Y\B
disp ('Symmetrical components of Phase A current of the branches of the complex equivalent circuit, kA')
Iz=(Z1*(E+Mt*U))

```



```

%Vector of branch EMFs, kV
E=[EgpA %I11
  EgpA %I21
  -EsA %I31
  0 %I41
  0 %I51
  0 %I61
  0 %I71
  0 %I81
  0 %I91
  0 %I101
  0 %ILA1
  0 %I21
  0 %I22
  0 %I32
  0 %I42
  0 %I52
  0 %I62
  0 %I72
  0 %I82
  0 %I92
  0 %I102
  0 %ILA2
  0 %I10
  0 %I20
  0 %I30
  0 %I40
  0 %I50
  0 %I60
  0 %I70
  0 %I80
  0 %I90
  0 %I100
  0]; %ILA0
MS=size(M,1);
ZS=size(M,2);
Z=diag(ZZ);
Mt=M';
for i=1:ZS
  Z1(i,i)=1/Z(i,i);
end
Y=M*Z1*Mt;
B=-M*Z1*E;
Disp ('Symmetrical components of Phase A voltage of the nodes of the complex equivalent circuit, kV')
U=Y\B
disp ('Symmetrical components of Phase A current of the branches of the complex equivalent circuit, kA')
Iz=(Z1*(E+Mt*U))

```

An example of MATLAB code for implementation of topological modelling of simultaneous two L-L-E short circuits and a one-open-phase fault

```

clc;
clear;
%Operator of the symmetrical component method
a=(-1*0.5)+(1i*sqrt(3)/2);
a2=(-1*0.5)-(1i*sqrt(3)/2);
%Element impedances, ohms
Zg1=0.1+62.3i;
Zg2=0.1+49.8i;
Zt1=0.1+30.4i;
Zl11=0.1+14.7i;
Zl10=0.1+51.4i;
Zl21=0.1+33.6i;
Zl20=0.1+117.6i;
Zat=0.1+20.8i;
%L-L Fault path resistances, ohms
ReAB=0.1;
RaAB=0.1;
ReBC=0.1;
RaBC=0.1;
%Given EMFs. kV
Eg=140.5+98.5i;
Es=120.8;

%Complex equivalent circuit for a B-C short-circuit
% 1 2 3 4 5 6 7 8 9 10 11 12 13 14 15 16 17 18
M1=[-1 0 1 0 1 0 0 0 0 0 0 0 0 0 0 0 0 0 %1
     0 0 -1 -1 0 0 0 0 0 0 0 0 0 0 0 0 0 0 %2
     0 -1 0 1 0 1 0 0 0 0 0 0 0 0 0 0 0 0 %3
     0 0 0 0 0 0 -1 0 1 0 1 0 0 0 0 0 0 0 %4
     0 0 0 0 0 0 0 0 -1 -1 0 0 0 0 0 0 0 0 %5
     0 0 0 0 0 0 0 0 -1 0 1 0 1 0 0 0 0 0 %6
     0 0 0 0 0 0 0 0 0 0 0 0 0 -1 0 1 0 1 %7
     0 0 0 0 0 0 0 0 0 0 0 0 0 0 -1 -1 0 0 %8
     0 0 0 0 0 0 0 0 0 0 0 0 0 0 -1 0 1 1 %9
     0 0 0 0 0 -1 0 0 0 0 0 -1 0 0 0 0 0 -1];%10

% Complex equivalent circuit for an open-phase B fault
% 1 2 3 4 5 6 7 8 9 10 11 12 13 14 15 16 17 18
M2=[-1 0 1 0 1 0 0 0 0 0 0 0 0 0 0 0 0 0 %1
     0 0 -1 0 0 0 0 0 -1 0 0 0 0 0 -1 0 0 0 %2
     0 0 0 -1 0 0 0 0 0 -1 0 0 0 0 0 -1 0 0 %3
     0 -1 0 1 0 1 0 0 0 0 0 0 0 0 0 0 0 0 %4
     0 0 0 0 0 0 1 1 0 0 -1 -1 0 0 0 0 0 0 %5
     0 0 0 0 0 0 -1 0 1 0 1 0 0 0 0 0 0 0 %6
     0 0 0 0 0 0 0 -1 0 1 0 1 0 0 0 0 0 0 %7
     0 0 0 0 0 0 0 0 0 0 0 0 0 1 1 0 0 -1 -1 %8
     0 0 0 0 0 0 0 0 0 0 0 0 0 -1 0 1 0 1 0 %9
     0 0 0 0 0 0 0 0 0 0 0 0 0 0 -1 0 1 0 1];%10

```

```

Complex equivalent circuit for a A-B short-circuit
% 1 2 3 4 5 6 7 8 9 10 11 12 13 14 15 16 17 18
M3=[-1 0 1 0 1 0 0 0 0 0 0 0 0 0 0 0 0 0 %1
    0 0 -1 -1 0 0 0 0 0 0 0 0 0 0 0 0 0 0 %2
    0 -1 0 1 0 1 0 0 0 0 0 0 0 0 0 0 0 0 %3
    0 0 0 0 0 0 -1 0 1 0 1 0 0 0 0 0 0 0 %4
    0 0 0 0 0 0 0 0 -1 -1 0 0 0 0 0 0 0 0 %5
    0 0 0 0 0 0 0 -1 0 1 0 1 0 0 0 0 0 0 %6
    0 0 0 0 0 0 0 0 0 0 0 0 0 -1 0 1 0 1 %7
    0 0 0 0 0 0 0 0 0 0 0 0 0 0 0 -1 -1 0 0 %8
    0 0 0 0 0 0 0 0 0 0 0 0 0 0 -1 0 1 0 1 %9
    0 0 0 0 -1 0 0 0 0 0 -1 0 0 0 0 0 -1 0];%10

%transpose of M
Mt1=M1';
Mt2=M2';
Mt3=M3';

%Number of branches and nodes
MS1=size(M1,1);
ZS1=size(M1,2);
MS2=size(M2,1);
ZS2=size(M2,2);
MS3=size(M3,1);
ZS3=size(M3,2);

%branch impedance vector for SC: B-C
ZZ1=[Zg1+Zt1
    Zat
    Zl11
    Zl21
    (RaAB/2)
    (RaBC/2)
    Zg2+Zt1
    Zat
    Zl11
    Zl21
    (RaAB/2)
    (RaBC/2)
    Zt1
    Zat
    Zl10
    Zl20
    ((3*ReAB)+(RaAB/2))
    ((3*ReBC)+(RaBC/2))];

%branch impedance vector OP: B
ZZ2=[Zg1+Zt1
    Zat
    Zl11
    Zl21
    (RaAB/2)
    (RaBC/2)
    Zg2+Zt1
    Zat
    Zl11
    Zl21
    (RaAB/2)
    (RaBC/2)
    Zt1
    Zat
    Zl10
    Zl20
    ((3*ReAB)+(RaAB/2))

```

```

        ((3*ReBC)+(RaBC/2));
%branch impedance vector SC: A-B
ZZ3=[Zg1+Zt1
      Zat
      Zl11
      Zl21
      (RaAB/2)
      (RaBC/2)
      Zg2+Zt1
      Zat
      Zl11
      Zl21
      (RaAB/2)
      (RaBC/2)
      Zt1
      Zat
      Zl10
      Zl20
      ((3*ReAB)+(RaAB/2))
      ((3*ReBC)+(RaBC/2))];
%Inverse of diagonal impedance matrix
Z=0; Z=diag(ZZ1);
for i=1:size(M1,2)
    Z11(i,i)=1/Z(i,i);
end
Z=0; Z=diag(ZZ2);
for i=1:size(M2,2)
    Z21(i,i)=1/Z(i,i);
end
Z=0; Z=diag(ZZ3);
for i=1:size(M3,2)
    Z31(i,i)=1/Z(i,i);
end
%node conductivity matrix
Y1=M1*Z11*Mt1;
Y2=M2*Z21*Mt2;
Y3=M3*Z31*Mt3;
%Inverse Y matrices
Y11=inv(Y1);
Y21=inv(Y2);
Y31=inv(Y3);
%Precision criterion for whole calculation
EPSkrit=0.001;
EPS=10;
%zero step values
UscAB=0;
Uop=0;
%branch EMF vector for first equivalent circuit
E1=[Eg
     Es
     -1*(Uop*a)
     0
     -1*(UscAB*a2)
     0
     0
     0
     0
     -1*(Uop*a2)
     0
     -1*(UscAB*a)
     0

```

```

0
0
-1*(Uop)
0
-1*(UscAB)
0];
%Right side of equation system for first equivalent circuit
B1=-M1*Z11*E1;
%Node voltage vectors for all equivalent circuits
U1=zeros(MS1,1);
U2=zeros(MS2,1);
U3=zeros(MS3,1);
%Step number
N=1;
while EPS>EPSkrit
    EPS1=0;
    EPS2=0;
    EPS3=0;
    %SC11: Phases B-C calculation step
    for i=1:MS1
        Un=0;
        for j=1:MS1
            Un=Un+Y11(i,j)*B1(j);
        end
        T=abs(U1(i)-Un);
        if T>EPS1
            EPS1=T;
        end
        U1(i)=Un;
    end
    EPS1
    %Redefining voltage sources
UscBC=U1(10);
%Redefining EMF source vector for second equivalent circuit
E2=[Eg*a2
    Es*a2
    0
    0
    -1*(UscAB*a)
    -1*(UscBC*a2)
    0
    0
    0
    0
    0
    -1*(UscAB*a2)
    -1*(UscBC*a)
    0
    0
    0
    0
    -1*(UscAB)
    -1*(UscBC)];
B2=-M2*Z21*E2;

```

```

%OP1: Phase B calculation step
for i=1:MS2
    Un=0;
    for j=1:MS2
        Un=Un+Y21(i,j)*B2(j);
    end;
    T=abs(U2(i)-Un);
    if T>EPS2
        EPS2=T;
    end;
    U2(i)=Un;
end;
EPS2
%Redefining voltage sources
Uop=U2(2)-U2(3);
%Redefining EMF source vector for third equivalent circuit
E3=[Eg*a
    Es*a
    -1*(Uop*a2)
    0
    0
    -1*(UscBC*a)
    0
    0
    -1*(Uop*a)
    0
    0
    -1*(UscBC*a2)
    0
    0
    -1*(Uop)
    0
    0
    -1*(UscBC)];
B3=-M3*Z31*E3;
%SC11: Phases A-B calculation step
for i=1:MS3
    Un=0;
    for j=1:MS3
        Un=Un+Y31(i,j)*B3(j);
    end;
    T=abs(U3(i)-Un);
    if T>EPS3
        EPS3=T;
    end;
    U3(i)=Un;
end;
EPS3
%Redefining voltage sources
UscAB=U3(10);
%Redefining EMF source vector for first equivalent circuit
E1=[Eg
    Es
    -1*(Uop*a)
    0
    -1*(UscAB*a2)
    0
    0
    0
    -1*(Uop*a2)

```

```

0
-1*(UscAB*a)
0
0
0
-1*(Uop)
0
-1*(UscAB)
0];
    %Right side of equation system for first equivalent circuit
B1=-M1*Z11*E1;
EPS=max([EPS1 EPS2 EPS3]);
N=N+1;
end;
%calculation of branch currents
Iz1=(Z11*(Mt1*U1+E1));
Iz2=(Z21*(Mt2*U2+E2));
Iz3=(Z31*(Mt3*U3+E3));
disp ('Number of calculation steps')
N
disp ('Symmetrical components of Phase A voltage of the nodes of the complex equivalent circuit, kV')
U1
disp ('Symmetrical components of Phase A current of the branches of the complex equivalent circuit, kA')
Iz1

```

REFERENCES

1. A. Bratlov, I. Puusaar, M. Piironen, R. Stefansson, A. Maklakovs, V. Tarvydas, and others (2019, Feb. 6). *ENTSOE Nordic and Baltic grid disturbance statistics 2017*. ENTSO-E Regional group Nordic. Available from: https://www.fingrid.fi/globalassets/dokumentit/fi/kantaverkko/suomen-sahkojarjestelma/hvac_2017_final_kotisivuille.pdf [Wieved: 6.09.2019 11:30].
2. V. Čuvičins un J. Priedīte. *Vadības sistēmas enerģētikā*. Rīga: RTU Izdevniecība, 2004, 229 lpp. ISBN:9984-32-441-9.
3. Я. Д. Баркан и Л. А. Орехов. *Автоматизация энергосистем: Учебное пособие для студентов вузов*. Москва: Высшая школа, 1981, 271 с.
4. А. Б. Барзам, *Систмная автоматика*. 4-е изд. Москва: Энергоатомиздат, 1989, 446 с. ISBN: 5-283-01024-4.
5. А. М. Федосеев и М. А. Федосеев. *Релейная защита электроэнергетических систем*. 2-е изд. Москва: Энергоатомиздат, 1992, 528 с. ISBN: 5-283-01171-2.
6. Н. И. Овчаренко. *Автоматика электрических станций и электроэнергетических систем: Учебник для вузов*. Москва: Издательство НЦ ЭНАС, 2000, 504 с. ISBN: 5-93196-020-1.
7. J. Gerhards, A. Mahņitko un B. Papkovs. *Energosistēmas vadība, optimizācija un riski*. Rīga: RTU Izdevniecība, 2011, 307 lpp. ISBN:978-9934-10-193-9.
8. M. Bockarjova, A. Sauhats and G. Andersson. Statistical algorithms for fault location on power transmission lines. In: *Proceedings 2005 IEEE Russia Power Tech conference*, St. Petersburg, Russia, 27–30 June 2005. Piscataway: IEEE, 2008, pp. 1–7, ISBN: 978-5-93208-034-4. Available from: DOI: 10.1109/PTC.2005.4524558.
9. M. Bockarjova, A. Dolgicers, and A. Sauhats. Enhancing fault location performance on power transmission lines. In: *Proceedings 2007 IEEE Lausanne Power Tech conference*, Lausanne, Switzerland, 1–5 July 2007. Piscataway: IEEE, 2008, pp. 1123–1128, ISBN: 978-1-4244-2189-3. Available from: DOI: 10.1109/PCT.2007.4538473.
10. A. Sauhats, A. Joņins un M. Bočkarjova. *Augstsprieguma līniju bojājuma vietas noteikšanas algoritmu sintēze*. Rīga: RTU EEF Enerģētikas institūts, 85 lpp. Pieejams: https://www.rtu.lv/writable/public_files/RTU_001.pdf.
11. J. Izykowski. *Fault location on power transmission lines*. Wroclaw: Printing House of Wroclaw University of Technology, 2008, p. 221. ISBN: 978-83-7493-430-5.
12. В. Л. Фабрикант. *Дистанционная защита*. Москва: Высшая школа, 1978, 215 с.
13. Э. М. Шнеерсон. *Цифровая релейная защита*. Москва: Энергоатомиздат, 2007, 549 с. ISBN: 978-5-283-03256-6.
14. G. Ziegler. *Numerical Distance Protection Principles and Applications*. 4th ed., Erlagen: Publicis, 2011, p.419. ISBN: 978-3-89578-381-4.
15. М. А. Беркович, В. А. Гладышев и В. А. Семенов. *Автоматика энергосистем*. Москва: Энергоатомиздат, 1991, 240 с. ISBN: 5-283-01004-X.
16. M. T. Sant and Y. G. Paithankar. Online digital fault locator for overhead transmission line. *Proceedings of the institution of Electrical Engineers*, vol. 126, No. 11, Nov. 1979, pp. 1181–1185. ISSN: 0020-3270. Available from: DOI: 10.1049/piee.1979.0201.
17. T. Takagi, Y. Yamakoshi, M. Yamaura, R. Kondow, and T. Matsushima. Development of a new type fault locator using the one-terminal voltage and current data. *IEEE Transactions on Power Apparatus and Systems*, vol. PAS-101, No. 8, Aug. 1982, pp. 2892–2898. ISSN: 0018-9510. Available from: DOI: 10.1109/TPAS.1982.317615.
18. L. N. Crichton. The distance relay for automatically sectionalizing electrical net works. *Transactions of the American Institute of Electrical Engineers*, vol. XLII, Jan. 1923, pp. 527–537. ISSN: 0096-3860. Available from: DOI: 10.1109/T-AIEE.1923.5060893.

19. L. C. Nicholson. Location of broken insulators and other transmission line troubles. *Transactions of the American Institute of Electrical Engineers*, vol. XXVI, No. 2, Jun. 1907, pp. 1319–1329. ISSN: 0096-3860. Available from: DOI: 10.1109/T-AIEE.1907.4764857.
20. D. Jones and A. T. Johns. Autoreclose-circuit design for large substations using logic sequence switching. *Proceedings of the Institution of Electrical Engineers*, vol. 114, No. 12, Dec. 1967, pp. 1929–1936. ISSN: 0020-3270. Available from: DOI: 10.1049/piee.1967.0367.
21. AIEE Committee Report. Bibliography and summary of fault location methods. *Transactions of the American Institute of Electrical Engineers*. Part III: Power Apparatus and Systems, vol. 74, No. 3, Jan. 1955, pp. 1423–1428. ISSN: 0097-2460. Available from: DOI: 10.1109/AIEEPAS.1955.4499247.
22. T. W. Stringfield, D. J. Marihart, and R. F. Stevens. Fault location methods for Overhead lines. *Transactions of the American Institute of Electrical Engineers*. Part III: Power Apparatus and Systems, vol. 76, No. 4, Apr. 1957, pp. 518–529. ISSN: 0097-2460. Available from: DOI: 10.1109/AIEEPAS.1957.4499601.
23. Megger. *Fault finding solutions*, version MEG-231/mil/3m/11.2003, p. 44. Available from: http://www.unitronics-electric.com/pdf/articulos/FaultFindingBook_AG_en_V03.pdf [viewed 10.07.2019].
24. F. J. Muench and G. A. Wright. Fault indicators: Types, strengths & applications. *IEEE Transactions on Power Apparatus and Systems*, vol. PAS-103, No. 12, Dec. 1984, pp. 3688–3693. ISSN: 0018-9510. Available from: DOI: 10.1109/TPAS.1984.318422.
25. K. Urasawa, K. Kanemaru, S. Toyota, and K. Sugiyama. New fault location system for power transmission lines using composite fiber-optic overhead ground wire (OPGW). *IEEE Transactions on Power Delivery*, vol. 4, No. 4, Oct. 1989, pp. 2005–2011. ISSN: 0885-8977. Available from: DOI: 10.1109/61.35624.
26. S. Jamali, A. Bahmanyar, and H. Borhani-Bahabadi. A fast and accurate fault location method for distribution networks with DG using genetic algorithms. In: *Proceedings 2015 Smart Grid Conference*, Teheran, Iran, 22–23 December 2015. Piscataway: IEEE, 2017, pp. 110–114, ISBN: 978-1-5090-0370-9. Available from: DOI: 10.1109/SGC.2015.7857419.
27. H. O. Cruz and F. B. Leão. Optimal placement of fault indicators using adaptive genetic algorithm. In: *Proceedings 2017 IEEE Power & Energy Society General Meeting*, Chicago, USA, 16 July – 20 July 2017. Piscataway: IEEE, 2018, pp. 1–5, ISBN: 978-1-5386-2213-1. Available from: DOI: 10.1109/PESGM.2017.8273897.
28. P. F. Gale, P. A. Crossley, X. Bingyin, G. Yaozhong, B. J. Cory, and J. R. G. Barker. Fault location based on travelling waves. In: *Proceedings 1993 Fifth International Conference on Developments in Power System Protection*, York, UK, 30 March to 2 April 1993. Piscataway: IEEE, 2002, pp. 54–59, ISBN: 0-85296-559-1.
29. F. F. Roberts. New methods for locating cable faults, particularly on high-frequency cables. *Journal of the Institution of Electrical Engineers- Part III: Radio and Communication Engineering*, vol. 93, No. 26, Nov. 1946, pp. 385–404. Available from: DOI: 10.1049/ji-3-2.1946.0067.
30. R. F. Stevens and T. W. Stringfield. Line-fault locator using fault-generated surges. *Electrical Engineering*, vol. 67, No. 11, Nov. 1948, pp. 1060–1060. ISSN: 0095-9197. Available from: DOI: 10.1109/EE.1948.6444437.
31. R. F. Stevens and T. W. Stringfield. A transmission line fault locator using fault-generated surges. *Transactions of the American Institute of Electrical Engineers*, vol. 67, No. 2, Jan.

- 1948, pp. 1168–1179. ISSN: 0096-3860. Available from: DOI: 10.1109/T-AIEE.1948.5059797.
32. M. Ando, E. O. Schweitzer, and R. A. Baker. Development and field-data evaluation of single-end fault locator for two-terminal HVDC transmission lines-Part 1: Data collection system and field data. *IEEE Transactions on Power Apparatus and Systems*, vol. PAS-104, No. 12, Dec. 1985, pp. 3524–3530. ISSN: 0018-9510. Available from: DOI: 10.1109/TPAS.1985.318905.
 33. M. Ando, E. O. Schweitzer, and R. A. Baker. Development and field-data evaluation of single-end fault locator for two-terminal HVDC transmission lines-Part 2: algorithm and evaluation. *IEEE Transactions on Power Apparatus and Systems*, vol. PAS-104, No. 12, Dec. 1985, pp. 3531–3537. ISSN: 0018-9510. Available from: DOI: 10.1109/TPAS.1985.318906.
 34. A. O. Ibe and B. J. Croy. A travelling wave-based fault locator for two- and three-terminal networks. *IEEE Transactions on Power Apparatus and Systems*, vol. PWRD-1, No. 2, Apr. 1986, pp. 283–288. Available from: ISSN: 0885-8977. DOI: 10.1109/TPWRD.1986.4307961.
 35. H. Lee and A. M. Mousa. GPS travelling wave fault locator systems: investigation into the anomalous measurements related to the lightning strikes. *IEEE Transactions on Power Delivery*, vol. 11, No. 3, Jul. 1996, pp. 1214–1223. ISSN: 0885-8977. Available from: DOI: 10.1109/61.517474.
 36. M. M. Tawfik and M. M. Morcos. A fault locator for transmission lines based on Prony method. In: *Proceedings of 1999 IEEE Power Engineering Society Summer Meeting*, Edmonton, Canada, 18–22 July 1999. Piscataway: IEEE, 2002, pp. 943–947, ISBN: 0-7803-5569-5. Available from: 10.1109/PESS.1999.787443.
 37. Q. Jian, C. Xiangxun, and Z. Jianchao. Travelling wave fault location of transmission line using wavelet transform. In *Proceedings of POWERCON 98. 1998 International Conference on Power System Technology*, Beijing, China, 18–21 August 1998. Piscataway: IEEE, 2002, pp. 533–537, ISBN: 0-7803-4754-4. Available from: DOI: 10.1109/ICPST.1998.729021.
 38. O. Altay, E. Gursoy, A. Font, and O. Kalenderli. Travelling wave fault location on hybrid power lines. In: *Proceedings of 2016 IEEE International Conference on High Voltage Engineering and Application*, Chengdu, China, 19–22 September 2016. Piscataway: IEEE, 2016, pp. 1–4, ISBN: 978-1-5090-0497-3. Available from: DOI: 10.1109/ICHVE.2016.7800719.
 39. A. M. Abeid, H. A. Abd el-Ghany, A. M. Azmy. An advanced travelling-wave fault-location algorithm for simultaneous faults. In: *Proceedings of 2017 Nineteenth International Middle East Power Systems Conference*, Cairo, Egypt, 19–21 December 2017. Piscataway: IEEE, 2018, pp. 747–752, ISBN: 978-1-5386-0991-0. Available from: DOI: 10.1109/MEPCON.2017.8301265.
 40. H. P. Dupuis and W. E. Jacobs. Fault location and relay performance analysis by automatic oscillographs. *Transactions of the American Institute of Electrical Engineers*, vol. 65, No. 7, Jul. 1946, pp. 442–446. ISSN: 0096-3860. Available from: DOI: 10.1109/T-AIEE.1946.5059367.
 41. A. C. Lee. Ground-fault-location indicator. *Transactions of the American Institute of Electrical Engineers. Part III: Power Apparatus and Systems*, vol. 76, No. 3, Apr. 1957, pp. 1370–1372. ISSN: 0097-2460. Available from: DOI: 10.1109/AIEEPAS.1957.4499796.
 42. S. E. Westlin and J. A. Bubenko. An accurate method for fault location on electric power transmission lines. *IFAC Proceedings Volumes*, Melbourne, Australia, 21–25 February

- 1977, vol. 10, No. 1, Feb. 1977, pp. 262–266. Available from: DOI: 10.1016/S1474-6670(17)67067-8.
43. E. O. Schweitzer. Evaluation and development of transmission line fault-locating techniques which use sinusoidal steady-state information. *Computers & Electrical Engineering*, vol. 10, No. 4, 1983, pp. 269–278. ISSN: 0045-7906. Available from: DOI: 10.1016/0045-7906(83)90013-7.
 44. L. Eriksson, M. M. Saha, and G. D. Rockefeller. An accurate fault locator with compensation for apparent reactance in the fault resistance resulting from remote-end infeed. *IEEE Transactions on Power Apparatus and Systems*, vol. PAS-104, No. 2, Feb. 1985, pp. 424–436. ISSN: 0018-9510. Available from: DOI: 10.1109/TPAS.1985.319058.
 45. A. T. Johns, S. Jamali, and S. M. Haden. New accurate transmission line fault location equipment. In: *Proceedings of 1989 Fourth International Conference on Developments in Power Protection*, Edinburgh, UK, 11–13 April 1989. Piscataway: IEEE, 2002, pp. 1–5.
 46. J. A. Jiang, Y. H. Lin, C. W. Liu, J. Z. Yang, and T. M. Too. An adaptive fault locator system for transmission lines. In: *Proceedings of 1999 IEEE Power Engineering Society Summer Meeting*, Edmonton, Canada, 18–22 July 1999. Piscataway: IEEE, 2002, pp. 930–936, ISBN: 0-7803-5569-5. Available from: DOI: 10.1109/PSS.1999.787441.
 47. J. A. Jiang, J. Z. Yang, Y. H. Lin, C. W. Liu, and J. C. Ma. An adaptive PMU based fault detection/location technique for transmission lines. I. Theory and Algorithms, *IEEE Transactions on Power Delivery*, vol. 15, No. 2, Apr. 2000, pp. 486–493. ISSN: 0885-8977. Available from: DOI: 10.1109/61.852973.
 48. J. A. Jiang, Y. H. Lin, J. Z. Yang, T. M. Too, and C. W. Liu. An adaptive PMU based fault detection/location technique for transmission lines. II. PMU implementation and performance evaluation. *IEEE Transactions on Power Delivery*, vol. 15, No. 4, Oct. 2000, pp. 1136–1146. ISSN: 0885-8977. Available from: DOI: 10.1109/61.891494.
 49. M. Joorabian. Artificial neural network based fault locator for EHV transmission system. In: *Proceedings of 2000 10th Mediterranean Electrotechnical Conference*, Lemesos, Cyprus, 29–31 May 2000. Piscataway: IEEE, 2002, pp. 1003–1006, ISBN: 0-7803-6290-X. Available from: DOI: 10.1109/MELCON.2000.879703.
 50. M. M. Saha, K. Wikstrom, J. Izykowski, and E. Rosolowski. New accurate fault location algorithm for parallel lines. In: *Proceedings 2001 Seventh International Conference on Developments in Power System Protection*, Amsterdam, Netherlands, 9–12 April 2001. Piscataway: IEEE, 2002, pp. 407–410, ISBN: 0-85296-732-2. Available from: DOI: 10.1049/cp:20010186.
 51. C. E. M. Pereira and L. C. Zanetta. Optimization algorithm for fault location in transmission lines considering current transformer saturation. *IEEE Transactions Power Delivery*, vol. 20, No. 2, Apr. 2005, pp. 603–608. ISSN: 0885-8977. Available from: DOI: 10.1109/TPWRD.2004.838521.
 52. Z. Jian, Z. HongJun and Q. JiangFeng. A two-terminal fault location algorithm using asynchronous sampling based on genetic algorithm. In: *Proceedings 2011 International Conference on Advanced Power System Automation and Protection*, Beijing, China, 16–20 October 2011. Piscataway: IEEE, 2012, vol. 2, pp. 1513–1516, ISBN: 978-1-4244-9622-8. Available from: DOI: 10.1109/APAP.2011.6180605.
 53. M. G. Davoudi, J. Sadeh, and K. Kamyab. Time domain fault location on transmission lines using genetic algorithm. In: *Proceedings 2012 11th International Conference on Environment and Electrical Engineering*, Venice, Italy, 18–25 May 2012. Piscataway: IEEE, 2012, pp. 1087–1092, ISBN: 978-1-4577-1830-4. Available from: DOI: 10.1109/EEEIC.2012.6221542.
 54. A. S. Ahmed, M. A. Attia, N. M. Hamed, and A. Y. Abdelaziz. Comparison between genetic algorithm and whale optimization algorithm in fault location estimation in power

- systems. In: *Proceedings 2017 Nineteenth International Middle East Power Systems Conference*, Cairo, Egypt, 19–21 December 2017. Piscataway: IEEE, 2018, pp. 631–637, ISBN: 978-1-5386-0991-0. Available from: DOI: 10.1109/MEPCON.2017.8301247.
55. M. Kezunovic and M. Knezev. Selection of optimal fault location algorithm. In: *Proceedings 2008 IEEE Power and Energy Society General Meeting – Conversion and Delivery of Electrical Energy in the 21st Century*, Pittsburg, USA, 20–24 July 2008. Piscataway: IEEE, 2008, pp. 1–5, ISBN: 978-1-4244-1905-0. Available from: DOI: 10.1109/PES.2008.4596775.
 56. A. S. Altaie and J. Asumandu. Fault location using a new control technique, multiple classifier, and artificial neural network. In: *Proceedings 2017 IEEE Texas Power and Energy conference*, College Station, USA, 9–10 February 2017. Piscataway: IEEE, 2017, pp. 1–6, ISBN: 978-1-5090-6618-6. Available from: DOI: 10.1109/TPEC.2017.7868267.
 57. M. Farshad and J. Sadeh. Transmission lines based on k-nearest neighbour algorithm using one-end voltage. *IEEE Transactions Power Delivery*, vol. 27, No. 4, Oct. 2012, pp. 2360–2367. ISSN: 0885-8977. Available from: DOI: 10.1109/TPWRD.2012.2211898.
 58. В. С. Дементьев, В. К. Спиридонов, Г. М. Шалыт. *Определение места повреждения силовых кабельных линий*. Москва: Госэнергоиздат, 1962, 96 с.
 59. А. М. Федосеев. *Релейная защита электрических систем*. Москва: Государственное энергетическое издательство, 1952, 480 с.
 60. W. A. Elmore. *Protective relaying theory and applications*. 2nd edition, New York: Marcel Dekker, 2003, p. 432. ISBN: 978-0824709723.
 61. L. Hewitson, M. Brown, R. Balakrishnan. *Practical Power System Protection*. Oxford: Newnes, 2004, p. 288. ISBN: 0 7506 6397 9.
 62. J. L. Blackburn and J. T. Domin. *Protective Relaying*. 3rd edition, New York: CRC Press, 2006, p. 664. ISBN: 978-1-57444-716-3.
 63. L. N. Crichton. The distance relay for automatically sectionalizing electrical net works. *Transactions of the American Institute of Electrical Engineers*, vol. XLII, Jan. 1923, pp. 527–537. ISSN: 0096-3860. Available from: DOI: 10.1109/T-AIEE.1923.5060893.
 64. H. A. McLaughlin and E. O. Erickson. The impedance relay developments and application. *Transactions of the American Institute of Electrical Engineers*, vol. 47, No.3, Jul. 1928, pp. 776–782. ISSN: 0096-3860. Available from: DOI: 10.1109/T-AIEE.1928.5055053.
 65. L. N. Crichton. High-speed protective relays. *Transactions of the American Institute of Electrical Engineers*, vol. 49, No. 4, Oct. 1930, pp. 1232–1239. ISSN: 0096-3860. Available from: DOI: 10.1109/T-AIEE.1930.5055649.
 66. W. A. Lewis and L. S. Tippet. Fundamental basis for distance relaying. *Electrical Engineering*, vol. 50, No. 6, Jun. 1931, pp. 420–422. ISSN: 0095-9197. Available from: DOI: 10.1109/EE.1931.6430279.
 67. S. L. Goldsborough and R. M. Smith. A new distance ground relay. *Transactions of the American Institute of Electrical Engineers*, vol. 55, No. 6, Jun. 1936, pp. 697–703. ISSN: 0096-3860. Available from: DOI: 10.1109/T-AIEE.1936.5057333.
 68. E. L. Harder, B. E. Lenehan, and S. L. Goldsboroug. A new high-speed distance-type carrier-pilot relay system. *Transactions of the American Institute of Electrical Engineers*, vol. 57, No. 1, Jan. 1938, pp. 5–10. ISSN: 0096-3860. Available from: DOI: 10.1109/T-AIEE.1938.5057729.
 69. L. J. Audlin and A. R. Van C. Warrington. Distance relay protection for subtransmission line made economical. *Electrical Engineering*, vol. 62, No. 9, Sept. 1943, pp. 574–578. ISSN: 0095-9197. Available from: DOI: 10.1109/EE.1943.6435918.

70. W. C. New. Combined phase and ground distance relaying. *Transactions of the American Institute of Electrical Engineers*, vol. 69, No. 1, Jan. 1950, pp. 37–44. ISSN: 0096-3860. Available from: DOI: 10.1109/T-AIEE.1950.5060117.
71. M. A. Bostwick and E. L. Harder. Relay protection of tapped transmission lines. *Transactions of the American Institute of Electrical Engineers*, vol. 62, No. 10, Oct. 1943, pp. 645–650. ISSN: 0096-3860. Available from: DOI: 10.1109/T-AIEE.1943.5058619.
72. S. L. Goldsborough. A distance relay with adjustable phase-angle discrimination. *Transactions of the American Institute of Electrical Engineers*, vol. 63, No. 11, Nov. 1944, pp. 835–838. ISSN: 0096-3860. Available from: DOI: 10.1109/T-AIEE.1944.5058808.
73. E. Clarke. Impedances seen by relays during power swings with and without faults. *Transactions of the American Institute of Electrical Engineers*, vol. 64, No. 6, Jun. 1945, pp. 372–384. ISSN: 0096-3860. Available from: DOI: 10.1109/T-AIEE.1945.5059154.
74. A. R. Van C. Warrington. Graphical method for estimating the performance of distance relays during faults and power swings. *Transactions of the American Institute of Electrical Engineers*, vol. 68, No. 1, Jul. 1949, pp. 608–621. ISSN: 0096-3860. Available from: DOI: 10.1109/T-AIEE.1949.5059984.
75. C. G. Dewey and J. R. McGlynn. A new reactance distance relay. *Transactions of the American Institute of Electrical Engineers*, vol. 67, No. 1, Jan. 1948, pp. 743–746. ISSN: 0096-3860. Available from: DOI: 10.1109/T-AIEE.1948.5059742.
76. F. R. Bergseth. An electronic distance relay using a phase-discrimination principle. *Transactions of the American Institute of Electrical Engineers*, vol. 73, No. 2, Jan. 1954, pp. 1276–1279. ISSN: 0097-2460. Available from: DOI: 10.1109/AIEEPAS.1954.4498958.
77. C. Adamson and L. M. Wedepohl. Power system protection, with particular reference to the application on junction transistors to distance relays. *Proceedings of the IEE – Part A: Power Engineering*, vol. 103, No. 10, Aug. 1956, pp. 379–388. ISSN: 0369-8882. Available from: DOI: 10.1049/pi-a.1956.0106.
78. W. K. Sonnemann and H. W. Lensner. Compensator distance relaying 1. General principles of Operation. *Transactions of the American Institute of Electrical Engineers. Part III: Power Apparatus and Systems*, vol. 77, No. 3, Apr. 1958, pp. 372–382. ISSN: 0097-2460. Available from: DOI: 10.1109/AIEEPAS.1958.4499939.
79. W. E. Rich and H. J. Calhoun. Compensator distance relaying 2. Design and performance. *Transactions of the American Institute of Electrical Engineers. Part III: Power Apparatus and Systems*, vol. 77, No. 3, Apr. 1958, pp. 383–387. ISSN: 0097-2460. Available from: DOI: 10.1109/AIEEPAS.1958.4499940.
80. K. Parthasarathy. Three-system and single-system static distance relays. *Proceedings of the Institution of Electrical Engineers*, vol. 113, No. 4, Apr. 1966, pp. 641–651. ISSN: 0020-3270. Available from: DOI: 10.1049/piee.1966.0104.
81. N. M. Anil Kumar. New approach to distance relays with quadrilateral polar characteristic for e.h.v.-line protection. *Proceedings of the Institution of Electrical Engineers*, vol. 117, No. 10, Oct. 1970, pp. 1986–1992. ISSN: 0020-3270. Available from: DOI: 10.1049/piee.1970.0350.
82. B. J. Mann and I. F. Morrison. Digital calculation of impedance for transmission line protection. *IEEE Transactions on Power Apparatus and Systems*, vol. PAS-90, No. 1, Jan. 1971, pp. 270–279. ISSN: 0018-9510. Available from: DOI: 10.1109/TPAS.1971.292966.
83. G. B. Gilcrest, G. D. Rockefeller, and E. A. Udren. High-speed distance relaying using a digital computer I – System description. *IEEE Transactions on Power Apparatus and Systems*, vol. PAS-91, No. 3, May 1972, pp. 1235–1243. ISSN: 0018-9510. Available from: DOI: 10.1109/TPAS.1972.293482.

84. G. D. Rockefeller and E. A. Udren. High-speed distance relaying using a digital computer II – Test results. *IEEE Transactions on Power Apparatus and Systems*, vol. PAS-91, No. 3, May 1972, pp.1244–1258. ISSN: 0018-9510. Available from: DOI: 10.1109/TPAS.1972.293483.
85. S. P. Patra, S. K. Basu, and S. Choudhuri. Analysis of phase-sequence detector for polyphase distance relay. *Proceedings of the Institution of Electrical Engineers*, vol. 119, No. 10, Oct. 1972, pp.1503–1504. ISSN: 0020-3270. Available from: DOI: 10.1049/piee.1972.0297.
86. V. T. Ingole, M. T. Sant, and Y. G. Paithankar. New technique for quadrilateral distance relay. *Proceedings of the Institution of Electrical Engineers*, vol. 121, No. 6, Jun. 1974, pp. 464–466. ISSN: 0020-3270. Available from: DOI: 10.1049/piee.1974.0112.
87. U. S. Hazra, S. K. Basu, and S. Chowdhuri. Polyphase distance relay by 6-input phase-sequence detector. *Proceedings of the Institution of Electrical Engineers*, vol. 123, No. 10, Oct. 1976, pp. 1017–1020. ISSN: 0020-3270. Available from: DOI: 10.1049/piee.1976.0226.
88. P. G. McLaren and M. A. Redfern. Fourier-series techniques applied to distance protection. *Proceedings of the Institution of Electrical Engineers*, vol. 122, No. 11, Nov. 1975, pp. 1301–1305. ISSN: 0020-3270. Available from: DOI: 10.1049/piee.1975.0316.
89. A. Shanmugasundaram, S. Palanichami, G. Gangadharan, and P. Bhoopathirajan. Development of a static distance relay with conic characteristic for the protection of long transmission lines. *IEE-IERE Proceedings – India*, vol. 14, No. 5, Sep.–Oct. 1976, pp. 192–199. ISSN: 0018-9146. Available from: DOI: 10.1049/iipi.1976.0059.
90. A. T. Johns and A. A. El-Alaily. New distance protective relay with improved coverage for high-resistance earth faults. *Proceedings of the Institution of Electrical Engineers*, vol. 124, No. 4, Apr. 1977, pp. 349–355. ISSN: 0020-3270. DOI: 10.1049/piee.1977.0064.
91. A. G. Phadke, T. Hlibka, M. Ibrahim, and M. G. Adamiak. A microcomputer based symmetrical component distance relay. In: *IEEE Conference Proceedings Power Industry Computer Applications Conference*, Cleveland, USA, 15–19 May 1979. Piscataway: IEEE, 2002, pp. 47–55. Available from: DOI: 10.1109/PICA.1979.720045.
92. P. A. Crossley and P. G. McLaren. Distance protection based on travelling waves. *IEEE Transactions on Power Apparatus and Systems*, vol. PAS-102, No. 9, Sept. 1983, pp. 2971–2983. ISSN: 0018-9510. Available from: DOI: 10.1109/TPAS.1983.318102.
93. Y. Ohura, T. Matsuda, M. Suzuki, F. Andow, Y. Kurosawa, and A. Takeuchi. A digital distance relay using negative sequence current. *IEEE Transactions on Power Delivery*, vol. 5, No. 1, Jan. 1990, pp. 79–84. ISSN: 0885-8977. Available from: DOI: 10.1109/61.107259.
94. Z. Zhizhe and C. Deshu. An adaptive approach in digital distance protection. *IEEE Transactions on Power Delivery*, vol. 6, No. 1, Jan. 1991, pp. 135–142. ISSN: 0885-8977. Available from: DOI: 10.1109/61.103732.
95. Y. Q. Xia, K. K. Li, and A.K. David. Adaptive relay setting for stand-alone digital protection, *IEEE Transactions on Power Delivery*, vol. 9, No. 1, Jan. 1994, pp. 480–491. ISSN: 0885-8977. Available from: DOI: 10.1109/61.277720.
96. P. G. McLaren, G. W. Swift, Z. Zhang, E. Dirks, R. P. Jayasinghe, and I. Fernando. A new positive sequence directional element for numerical distance relays. In: *Proceedings IEEE WESCANEX 95. Communications, Power and Computing conference*, Winnipeg, Canada, 15–16 May 1995. Piscataway: IEEE, 2002, pp. 334-339, ISBN: 0-7803-2725-X. Available from: DOI: 10.1109/WESCAN.1995.494051.
97. S. H. Kang, K. H. Kim, K. R. Cho, and J. K. Park. High speed offset free distance relaying algorithm using multilayer feedforward neural networks. In: *Proceedings of International*

- Conference on Intelligent System Application to Power Systems*, Orlando, USA, 28 January to 2 February 1996. Piscataway: IEEE, 2002, pp. 210–214, ISBN: 0-7803-3115-X. Available from: DOI: 10.1109/ISAP.1996.501070.
98. S. J. Lee and C. C. Liu. Intelligent approach to coordination identification in distance relaying. In: *Proceedings of International Conference on Intelligent System Application to Power Systems*, Orlando, USA, 28 January to 2 February 1996. Piscataway: IEEE, 2002, pp. 62–67, ISBN: 0-7803-3115-X. Available from: DOI: 10.1109/ISAP.1996.501045.
 99. J. P. de Sa, J. Afonso, and R. Rodrigues. A Probabilistic approach to setting distance relays in transmission networks. *IEEE Transactions on Power Delivery*, vol. 12, No. 2, pp. 681–686, Apr. 1997. ISSN: 0885-8977. Available from: DOI: 10.1109/61.584342.
 100. G. Li, S. Zhu, and F. Sui. Adaptive bowl impedance relay. *IEEE Transactions on Power Delivery*, vol. 14, No. 1, Jan. 1999, pp. 142–147. ISSN: 0885-8977. Available from: DOI: 10.1109/61.736705.
 101. A. S. AlFuhaid and M. A. El-Sayed. A recursive least-squares digital distance relaying algorithm. *IEEE Transactions on Power Delivery*, vol. 14, No. 4, Oct. 1999, pp. 1257–1262. ISSN: 0885-8977. Available from: DOI: 10.1109/61.796215.
 102. A. Apostolov. Implementation of a transient energy method for directional detection in numerical distance relays. In: *Proceedings 1999 IEEE Transmission and Distribution Conference*, New Orleans, USA, 11–16 April 1999. Piscataway: IEEE, 2002, pp. 382–387, ISBN: 0-7803-5515-6. Available from: DOI: 10.1109/TDC.1999.755382.
 103. K. K. Li, L. L. Lai, and A. K. David. Stand alone intelligent digital distance relay. *IEEE Transactions on Power Systems*, vol. 15, No. 1, Feb. 2000, pp. 137–142. ISSN: 0885-8950. Available from: DOI: 10.1109/59.852112.
 104. T. Segui, P. Bertrand, M. Guillot, P. Hanchin, and P. Bastard. Fundamental basis for distance relaying with parametrical estimation. *IEEE Transactions on Power Delivery*, vol. 15, No. 2, Apr. 2000, pp. 659–664. ISSN: 0885-8977. Available from: DOI: 10.1109/61.853001.
 105. S. Jamali. A fast adaptive digital distance protection. In: *Proceedings 2001 Seventh International Conference on Developments in Power System Protection (IEE)*, Amsterdam, Netherlands, 9–12 April 2001. Piscataway: IEEE, 2002, pp. 149–152, ISBN: 0-85296-732-2. Available from: DOI: 10.1049/cp:20010122.
 106. C. S. Chen, C. W. Liu, and J. A. Jiang. Application of combined adaptive Fourier filtering technique and fault detector to fast distance protection. *IEEE Transactions on Power Delivery*, vol. 21, No. 2, Apr. 2006, pp. 619–626. ISSN: 0885-8977. Available from: DOI: 10.1109/TPWRD.2005.858808.
 107. M. Bockarjova, A. Sauhats, and G. Andersson. Statistical algorithm for power transmission lines distance protection. In: *Proceedings 2006 Probabilistic Methods Applied to Power Systems conference*, Stockholm, Sweden, 11–15 June 2006. Piscataway: IEEE, 2007, pp. 1–7, ISBN: 978-91-7178-585-5. Available from: DOI: 10.1109/PMAPS.2006.360210.
 108. E. Sorrentino and V. De Andrade. Optimal-probabilistic method to compute the reach settings of distance relays. *IEEE Transactions on Power Delivery*, vol. 26, No. 3, Jul. 2011, pp. 1522–1529. ISSN: 0885-8977. Available from: DOI: 10.1109/TPWRD.2010.2091724.
 109. Z. Song, J. Xin, W. Cong, L. Ding, and Y. Ma. New approach for online fault resistance estimation. In: *Proceedings 2014 IEEE PES Asia-Pacific Power and Energy Engineering conference*, Hong Kong, China, 7–10 December 2014. Piscataway: IEEE, 2015, pp. 1–5, ISBN: 978-1-4799-7537-2. Available from: DOI: 10.1109/APPEEC.2014.7066180.

110. B. Xia, Y. Wang, E. Vazquez, W. Xu, and D. Wong. Estimation of fault resistance using fault record data. *IEEE Transactions Power Delivery*, vol. 30, No. 1, Feb. 2015, pp. 153–160. ISSN: 0885-8977. Available from: DOI: 10.1109/TPWRD.2014.2355041.
111. M. H. Idris, M. S. Ahmad, A. Z. Abdullah, and S. Hardi. Adaptive Mho type distance relaying scheme with fault resistance compensation. In: *Proceedings 2013 IEEE 7th International Power Engineering and Optimization Conference*, Langkawi, Malaysia, 3–4 June 2013. Piscataway: IEEE, 2013, pp. 213–217, ISBN: 978-1-4673-5072-3. Available from: DOI: 10.1109/PEOCO.2013.6564545.
112. K. Jia, T. Bi, W. Li, and Q. Yang. Ground fault distance protection for paralleled transmission lines. *IEEE Transactions on Industry Applications*, vol. 51, No. 6, Nov. – Dec. 2015, pp. 5228–5236. ISSN: 0093-9994. Available from: DOI: 10.1109/TIA.2015.2416243.
113. W. Chen, Z. Hao, J. Guan, Y. Dang, D. Du, and X. Wang. Research on the distance protection performance for untransposed parallel transmission lines based on six-phase parameter information. In: *Proceedings 2016 IEEE 16th International Conference on Environmental and Electrical Engineering*, Florence, Italy, 7–10 June 2016. Piscataway: IEEE, 2016, pp. 1–6, ISBN: 978-1-5090-2321-9. Available from: DOI: 10.1109/EEEIC.2016.7555406.
114. W. Zhang and Y. H. Zhang. Determination of optimal setting parameters of distance relay in transmission system. In: *Proceedings 2015 IEEE Power & Energy Society General Meeting*, Denver, USA, 26–30 July 2015. Piscataway: IEEE, 2015, pp. 1–5, ISBN: 978-1-4673-8040-9. Available from: DOI: 10.1109/PESGM.2015.7285720.
115. M. Washer, J. C. Maun, C. Dzienis, M. Kereit, Y. Yelgin, and J. Blumschein. Precise impedance based fault location algorithm with fault resistance separation. In: *Proceedings 2015 IEEE Eindhoven PowerTech*, Eindhoven, Netherlands, 29–2 July 2015. Piscataway: IEEE, 2015, pp. 1–6, ISBN: 978-1-4799-7693-5. Available from: DOI: 10.1109/PTC.2015.7232595.
116. C. Lozaro, J. P. Marquez, G. Marchesan, and G. C. Junior. Waveform asymmetry of instantaneous current signal based symmetrical fault detection during power swing. *Electric Power Systems Research*, vol. 155, Feb. 2018, pp. 340–349. ISSN: 0378-7796. Available from: <https://doi.org/10.1016/j.epsr.2017.11.005>.
117. S. M. Hashemi and M. S. Pasand. Distance protection during asymmetrical power swings: Challenges and solutions. *IEEE Transactions on Power Delivery*, vol. 33, No. 6, Dec. 2018, pp. 2736–2745. ISSN: 0885-8977. Available from: DOI: 10.1109/TPWRD.2018.2816304.
118. S. Biswas and P. K. Nayak. An unblocking assistance to distance relays protecting TCSC compensated transmission lines during power swing. *International Transactions on Electrical Energy Systems*, vol. 29, No. 8, Apr. 2019, pp. 1–21. ISSN: 2050-7038. Available from: <https://doi.org/10.1002/2050-7038.12034>.
119. Н. Н. Беляков, К. П. Кадомская, М. Л. Левинштейн и др. *Процессы при однофазном автоматическом повторном включении линий высоких напряжений*. Москва: Энергоатомиздат, 1991, 256 с. ISBN: 5-283-01184-4.
120. M. Djuric, Z. Radojevic and K. Zoric. Determination of the arc extinction time on power lines using voltage signals. *ETEP*, vol. 12, No. 6, Nov./Dec. 2002, pp. 415–418. ISSN: 2050-7038. Available from: <https://doi.org/10.1002/etep.4450120605>.
121. D. S. Fitton, R. W. Dunn, R. K. Aggarwal, A. T. Johns, and A. Bennett. Design and implementation of an adaptive single pole autoreclosure technique for transmission lines using artificial neural networks. *IEEE Transactions on Power Delivery*, vol. 11, No. 2, Apr. 1996, pp. 748–756. ISSN: 0885-8977. Available from: DOI: 10.1109/61.489331.

122. S. P. Ahn, C. H. Kim, R. K. Aggarwal, and A. T. Johns. An alternative approach to adaptive single pole auto-reclosing in high voltage transmission systems based on variable dead time control. *IEEE Transactions on Power Delivery*, vol. 16, No. 4, Oct. 2001, pp. 676–686. ISSN: 0885-8977. Available from: DOI: 10.1109/61.956756.
123. P. Upadhyay, L. Heistrene, and S. Chandrasekaran. Design and implementation of adaptive autoreclosure for EHV transmission line. In: *Proceedings 2016 International Conference on Microelectronics, Computing and Communications (MircoCom)*, Durgapur, India, 23–25 January 2016. Piscataway: IEEE, 2016, pp. 1–6, ISBN: 978-1-4673-6622-9. Available from: DOI: 10.1109/MircoCom.2016.7522588.
124. B. Mahamedi. An adaptive single-pole auto-reclosing function. In: *Proceedings 2012 06th Power Systems Protection & Control Conference (PSPC06)*, Teheran, Iran, 3 January 2012. Teheran: Iranian Association of Electrical & Electronics Engineers, 2012, pp. 1–5. Available from: http://www.ipaps.ir/files/archive/6/Arc6_259.pdf [viewed 10.09.2019].
125. K. M. C. Dantas, W. L. A. Neves, and D. Fernandes. An Approach for controlled reclosing of shunt-compensated transmission lines. *IEEE Transactions on Power Delivery*, vol. 29, No. 3, Jun. 2014, pp. 1203–1211. ISSN: 1932-5517. Available from: DOI: 10.1109/TPWRD.2013.2289394.
126. X. Luo, C. Huang, Y. Jiang, and S. Guo. An adaptive three-phase reclosure scheme for shunt reactor-compensated transmission lines based on the change of current spectrum. *Elsevier Electric Power Systems Research*, vol. 158, May 2018, pp. 184–194. ISSN: 0378-7796. Available from: <https://doi.org/10.1016/j.epsr.2018.01.011>.
127. B. Papkovs, I. Zicmane, *Elektromagnētiskie pārejas procesi elektriskās sistēmās*. Rīga: RTU Izdevniecība, 2007, 306 lpp. ISBN 978-9984-32-3.
128. G. I. Atabekov. *The Relay protection of High Voltage Networks*, London: Pergamon Press, 1960, p. 576.
129. С. А. Ульянов. Электромагнитные переходные процессы в электрических системах. Москва: Энергия, 1970, 520 с.
130. A. Dolgicers and I. Zalitis. Numerical calculation method for symmetrical component analysis of multiple simultaneous asymmetrical faults. In: *Proceedings 2017 IEEE 58th International Scientific Conference on Power and Electrical Engineering of Riga Technical University*, Riga, Latvia, 12–13 October 2017. Piscataway: IEEE, 2017, pp. 1–7, ISBN: 978-1-5386-3847-7. Available from: DOI: 10.1109/RTUCON.2017.8124748.
131. E. Clarke. *Circuit analysis of A-C power systems*, New York: Wiley, 1943, p. 936.
132. Л. А. Бессонов. *Теоретические основы электротехники. Электрические цепи: Учебник для электротехнических, энергетических, приборостроительных специальностей вузов. 9-е изд.* Москва: Высшая школа, 1996, 638 с. ISBN: 5-06-002160-2.
133. A. Agarwal and J. H. Lang. *Foundations of analog and electronic circuits*, San Francisco: Morgan Kaufmann Publishers, 2005, p. 1008. ISBN: 1-55860-735-8.
134. A. Dolgicers and J. Kozadajevs. Phase plane usage for convergence analysis of Seidel method applied for network analysis. In: *Proceedings 2014 IEEE 2nd Workshop on Advances in Information, Electronic and Electrical Engineering*, Vilnius, Lithuania, 28–29 November 2014. Piscataway: IEEE, 2015, pp. 1–6, ISBN: 978-1-4799-7122-0. Available from: DOI: 10.1109/AIEEE.2014.7020321.
135. А. А. Самарский, А. В. Гулин. *Введение в численные методы*. Москва: Наука, 1987, 286 с.
136. S. C. Chapra and R. P. Canale. *Numerical methods for engineers*. 6th ed., London: McGraw-Hill Higher Education, 2010, p. 960.

137. В. И. Крылов, Н. С. Скобля. *Методы приближенного преобразования Фурье и обращения преобразования Лапласа. Справочная книга.* Москва: Наука, 1974, 224 с.
138. Б. А. Калабеков, В. Ю. Лапидус, В. М. Малафеев. *Методы автоматизированного расчета электронных схем в технике связи.* Москва: Радио и связь, 1990, 272 с. ISBN:5-256-00674-6.
139. W. Lu, X. Du, J. Ding, and X. Wang. Modal parameter identification based on fast Fourier transform and Hilbert Huang transform. In: *Proceedings 2012 2nd International Conference on Consumer Electronics, Communications and Networks*, Yichang, China, 21–23 April 2012. Piscataway: IEEE, 2012, pp. 2703–2706, ISBN: 978-1-4577-1414-6. Available from: DOI: 10.1109/CECNet.2012.6201909.
140. P. Taklaja, R. Oidram, J. Niitsoo, and I. Palu. Causes of indefinite faults in Estonian 110 kV overhead power grid. *Oil Shale*, vol. 30, No. 2S, 2013, pp. 225–243. ISSN: 0208-189X. Available from: DOI: 10.3176/oil.2013.2S.04.
141. S. Šeikins. *Pārejas pretestības ietekme uz distances aizsardzību.* Maģistra darbs, Rīga: RTU, 2014, 72. lpp.
142. I. Zalitis, A. Dolgicers, and J. Kozadajevs. Experimental testing of distance protection performance in transient fault path resistance environment. In: *Proceedings 2017 5th IEEE Workshop on Advances in Information, Electronic and Electrical Engineering*, Riga, Latvia, 24–25 November 2017. Piscataway: IEEE, 2018, pp. 1–6, ISBN: 978-1-5386-4138-5. Available from: DOI: 10.1109/AIEEE.2017.8270526.
143. M. Silarajs, A. Utans, L. Leite, and A. Sauhats. Multifunction relay protection device for power transmission lines LIDA. In: *Proceedings 2007 The 2nd International conference on Electrical and Control Technologies*, Kaunas, Lithuania, 3–4 May 2007. Kaunas: Kaunas University Of Technology, 2007, pp. 120–125, ISBN: 978-1-6343-9796-4. Available from: <http://www.proceedings.com/25048.html> [viewed 10.09.2019].
144. I. Zalitis, A. Dolgicers, J. Kozadajevs. A distance protection based on the estimation of system model parameters. In: *Proceedings 2017 IEEE Manchester PowerTech*, Manchester, UK, 18–22 June 2017. Piscataway: IEEE, 2017, pp. 1–6, ISBN: 978-1-5090-4238-8. Available from: DOI: 10.1109/PTC.2017.7981277.
145. I. Zalitis, A. Dolgicers, J. Kozadajevs. A power transmission line fault locator based on the estimation of system model parameters. In: *Proceedings 2017 IEEE International Conference on Environment and Electrical Engineering*, Milan, Italy, 6–9 June 2017. Piscataway: IEEE, 2017, pp. 1–6, ISBN: 978-1-5386-3918-4. Available from: DOI: 10.1109/EEEIC.2017.7977459.
146. S. S. Geramian, H. A. Abyane, and K. Mazlumi. Determination of optimal PMU placement for fault location using genetic algorithm. In: *Proceedings 2008 13th International Conference on Harmonics and Quality of Power*, Wollongong, Australia, 28 September to 1 October 2008. Piscataway: IEEE, 2008, pp. 1–5, ISBN: 978-1-4244-1771-1. Available from: DOI: 10.1109/ICHQP.2008.4668810.
147. L. He, K. Jia, and Z. Fan. The immune genetic algorithm in fault diagnosis of modern power system. In: *Proceedings 2010 2nd International Conference on Education Technology and Computer*, Shanghai, China, 22–24 June 2010. Piscataway: IEEE, 2010, pp. 26–29, ISBN: 978-1-4244-6367-1. Available from: DOI: 10.1109/ICETC.2010.5529742.
148. Л. А. Гладков, В. В. Курейчик, В. М. Курейчик. *Генетические алгоритмы. Учебное пособие.* 2-е изд. Москва: Физматлит, 2006, 320 с. ISBN: 5-9221-0510-8
149. Т. В. Панченко. *Генетические алгоритмы. Учебно-методическое пособие.* Астрахань: АГУ, 2007, 87 с. ISBN: 5-88200-913-8.
150. I. Plummer. *Asymmetry in distribution systems: causes, harmful effects and remedies.* M. Sc. Eng. thesis, Dept. Electrical and Computer Engineering, Louisiana State University

- and Agricultural and Mechanical College, Louisiana, 2011, p. 130. Available from: https://digitalcommons.lsu.edu/cgi/viewcontent.cgi?article=2489&context=gradschool_theses [viewed 12.09.2019].
151. Нормы качества электрической энергии в системах электроснабжения общего назначения, ГОСТ 32144-2013, Март 2013, 20 с. Доступно: <https://www.elec.ru/files/2014/05/06/GOST-32144-2013-Elektricheskaja-energija.pdf>.
 152. C. Preve. *Protection of electrical networks*, London: ISTE Ltd., 2006, p. 508. ISBN: 978-1-905209-06-4.
 153. D. P. Kothari and I. J. Nagrath. *Modern Power System Analysis*, New Delhi: Tata McGraw Hill Education Private Limited, 3rd. ed., 2009, p. 694. ISBN: 978-0-07-049489-3.
 154. T. W. Wilcox and R. A. Hore. Single-phase autoreclose on the 330 kV Kariba transmission System. In: *Proceedings 1962 AIEE Summer General Meeting conference*, Denver, USA, 17–22 June 1962, pp. 999–1006.
 155. IEEE Committee. IEEE Committee report: Single phase tripping auto reclosing of transmission lines. *IEEE Transactions Power Delivery*, vol. 7, Jan. 1992, pp. 182–192. ISSN: 0885-8977. Available from: DOI: 10.1109/61.108906.
 156. I. Zalitis, A. Dolgicers, J. Kozadajevs. An adaptive single-pole automatic reclosing method for uncompensated high-voltage transmission lines. *Electric Power Systems Research*, vol. 166, Jan. 2019, pp. 210–222. ISSN: 0378-7796. Available from: <https://doi.org/10.1016/j.epsr.2018.10.012>.
 157. C. F. Wagner, R. D. Evans. *Symmetrical components as applied to the analysis of unbalanced electrical circuits*. 1st ed., New York: McGraw-Hill, p. 437, 1933.
 158. E. R. Bussy, N. M. Ljumb, and A. C. Britten. Effect of ADLash optical fibre cable on corona inception gradient and electric fields around the earth wire of the Apollo-Cahora Bassa HVDC transmission line. In: *Proceedings 2004 IEEE AFRICON. 7th Africon Conference*, Gaborone, Botswana, 15–17 September 2004. Piscataway: IEEE, 2005, pp. 607–612, ISBN: 0-7803-8605-1. Available from: DOI: 10.1109/AFRICON.2004.1406751.
 159. E. J. Harrington and E. C. Starr. Deionization Time of High-Voltage Fault-Arc Paths. *AIEE Transactions*, vol. 68, No. 2, Jul. 1949, pp. 997–1004. ISSN: 0096-3860. Available from: DOI: 10.1109/T-AIEE.1949.5060041.
 160. A. T. Johns and A. M. Al-Rawi. Digital simulation of EHV systems under secondary arcing conditions associated with single-pole autoreclosure. *IEE Proceedings C-Generation, Transmission and Distribution*, vol. 129, No. 2, Mar. 1982, pp. 49–58. ISSN: 0143-7046. Available from: DOI: 10.1049/ip-c.1982.0009.
 161. A. T. Johns, R. K. Aggarwal, and Y. H. Song. Improved techniques for modelling fault arcs on faulted EHV transmission systems. *IEE Proceedings C-Generation, Transmission and Distribution*, vol. 141, No. 2, Mar. 1994, pp. 148–154. ISSN: 1350-2360. Available from: DOI: 10.1049/ip-gtd:19949869.
 162. A. Pereira, F. Perez-Yauli, F. L. Quilumba. Three-phase recloser time delays determination in 138 kV and 46 kV lines of the Empresa Electrica Quito. In: *Proceedings 2017 IEE Second Ecuador Technical Chapters Meeting (ETCM)*, Gaborone, Botswana, 16–20 October 2017. Piscataway: IEEE, 2018, pp. 1–6, ISBN: 978-1-5386-3895-8. Available from: DOI: 10.1109/ETCM.2017.8247514.
 163. *Network Protection & Automation Guide*, May 2011 ed., France: Alstom Grid, 2011, p. 508. Available from: <http://rpa.energy.mn/wp-content/uploads/2016/07/network-protection-and-automation-guide-book.pdf> [viewed 01.10.2019].